AD-A075 378 UNITED TECHNOLOGIES RESEARCH CENTER EAST HARTFORD CONN F/G 1/3
INVESTIGATION OF THE AIRFLOW AT ROCKET TRAJECTORY AND WIND SENS--ETC(U)
SEP 79 R B TAYLOR, A J LANDGREBE DAAG29-77-C-0013
UNCLASSIFIED UTRC-R79-912985-5 ARO-14277.1-E NL

1 OF 3
AD A075378

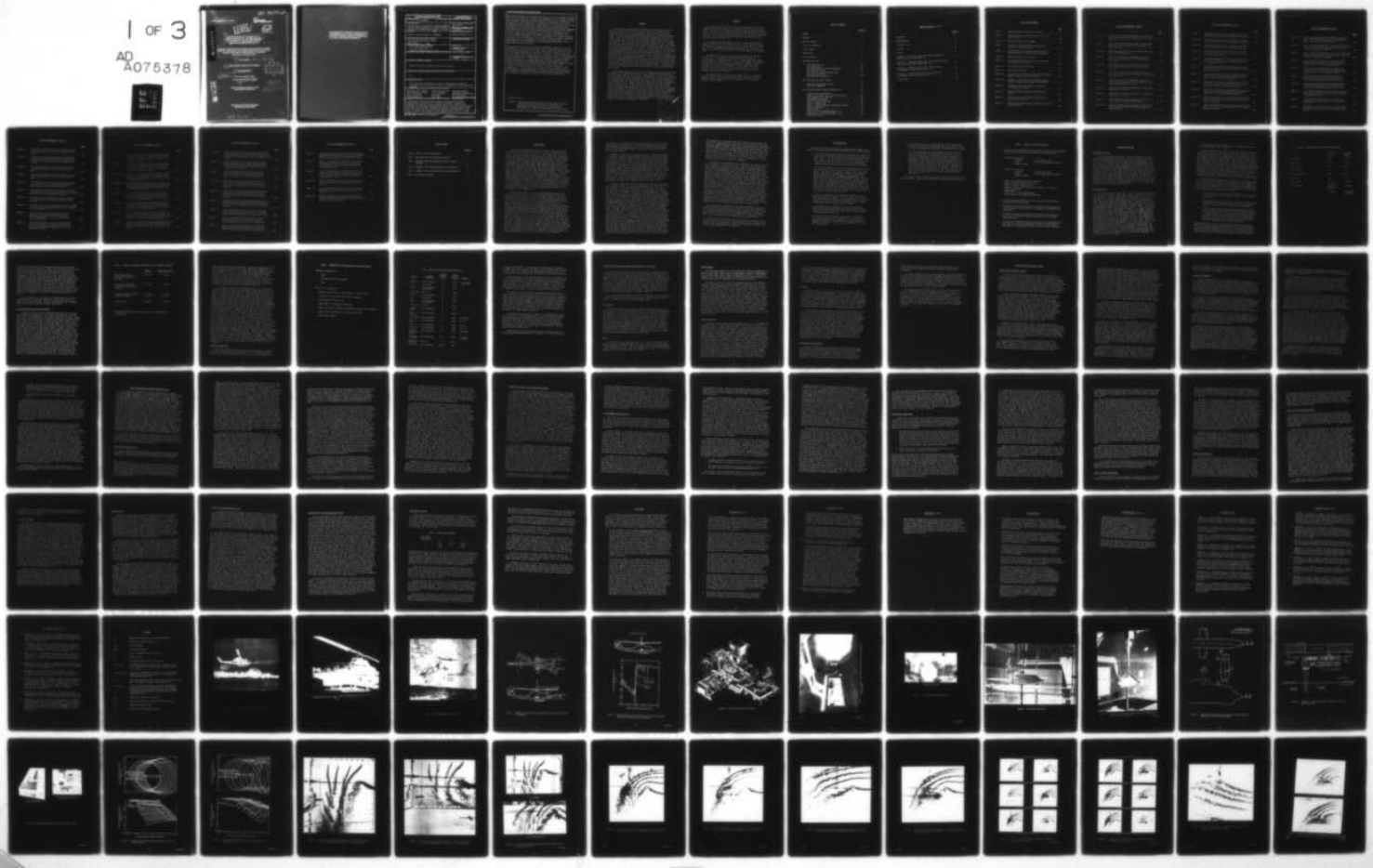

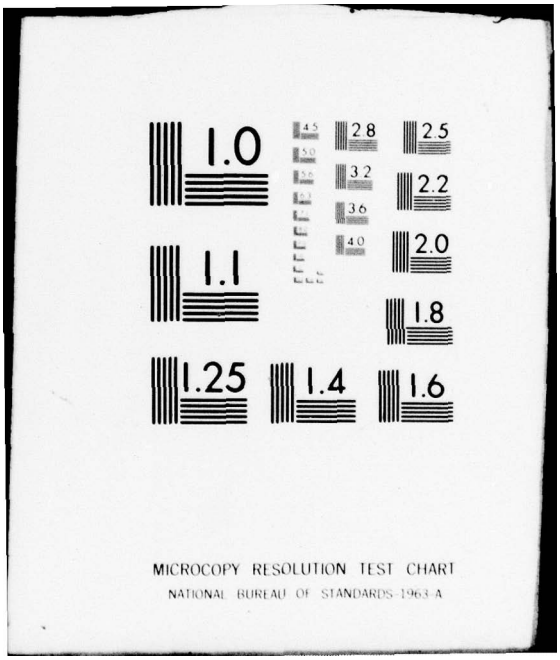
1.0
1.1
1.25
1.4
1.6
1.8
2.0
2.2
2.5
2.8
3.2
3.6
4.0
4.5
5.0
MICROCOPY RESOLUTION TEST CHART
NATIONAL BUREAU OF STANDARDS-1963-A

ARO 14277.1-E

(14) UTRC R79-912985-5

UNITED TECHNOLOGIES

LEVEL II

AD A075378

(6) INVESTIGATION OF THE AIRFLOW AT ROCKET TRAJECTORY AND WIND SENSOR LOCATIONS OF A MODEL HELICOPTER SIMULATING LOW SPEED FLIGHT.

Application of Model Helicopter Testing, Laser Velocimetry, and Rotor Wake Flow Visualization to Investigate the Aerodynamic Interference at Rocket Trajectories and Wind Sensors of a Helicopter Operating in Low Speed Flight.

(9) Final Report. May 77-Sep 79

(10) Robert B. Taylor and Anton J. Landgrebe

(11) September 1979

(12) 233

U.S. Army Research Office

Contract No. DAAG29-77-C-0013 (15)

United Technologies Research Center
East Hartford, Connecticut

(18) ARO

(19) 14277.1-E

APPROVED FOR PUBLIC RELEASE;
DISTRIBUTION UNLIMITED

409 252

JOB

THE FINDINGS IN THIS REPORT ARE NOT TO BE CONSTRUED AS AN OFFICIAL DEPARTMENT OF THE ARMY POSITION, UNLESS SO DESIGNATED BY OTHER AUTHORIZED DOCUMENTS.

SECURITY CLASSIFICATION OF THIS PAGE (When Data Entered)

REPORT DOCUMENTATION PAGE

READ INSTRUCTIONS BEFORE COMPLETING FORM

1. REPORT NUMBER: R79-912985-5	2. GOVT ACCESSION NO.
3. RECIPIENT'S CATALOG NUMBER	
4. TITLE (and Subtitle): INVESTIGATION OF THE AIRFLOW AT ROCKET TRAJECTORY AND WIND SENSOR LOCATIONS OF A MODEL HELICOPTER SIMULATING LOW SPEED FLIGHT (Subtitle on reverse side)	5. TYPE OF REPORT & PERIOD COVERED: Final Report, May 1977- September 1979
	6. PERFORMING ORG. REPORT NUMBER: R79-912985-5
7. AUTHOR(s): Robert B. Taylor and Anton J. Landgrebe	8. CONTRACT OR GRANT NUMBER(s): DAAG29-77-C-0013
9. PERFORMING ORGANIZATION NAME AND ADDRESS: United Technolgies Research Center, Silver Lane, East Hartford, CT. 06108	10. PROGRAM ELEMENT, PROJECT, TASK AREA & WORK UNIT NUMBERS
11. CONTROLLING OFFICE NAME AND ADDRESS: U. S. Army Research Office, Post Office Box 12211, Research Triangle Park, NC 27709	12. REPORT DATE: September 1979
	13. NUMBER OF PAGES: 229
14. MONITORING AGENCY NAME & ADDRESS(if different from Controlling Office)	15. SECURITY CLASS. (of this report): Unclassified
	15a. DECLASSIFICATION/DOWNGRADING SCHEDULE: NA

16. DISTRIBUTION STATEMENT (of this Report)

Approved for public release; distribution unlimited.

17. DISTRIBUTION STATEMENT (of the abstract entered in Block 20, if different from Report)

NA

18. SUPPLEMENTARY NOTES

The findings in this report are not to be construed as an official Department of the Army position, unless so designated by other authorized documents.

19. KEY WORDS (Continue on reverse side if necessary and identify by block number)

Helicopter Rotor Airflow	Rocket Trajectories	Induced Velocities
Model Helicopter Testing	2.75 In. Rockets	Aerodynamic Interference
Laser Velocimetry	Wind Sensor	AH-1G Helicopter
Flow Visualization	Rotor Wake	Low Speed Helicopter Flight
		Ground Effect

20. ABSTRACT (Continue on reverse side if necessary and identify by block number)

An experimental investigation was conducted to determine the airflow characteristics in the vicinity of a model helicopter to determine the aerodynamic interference at representative rocket trajectories and wind sensor locations of an Army AH-1G helicopter operating in low speed forward flight. Laser velocimetry and flow visualization techniques were applied in a wind tunnel to provide flow velocity and wake geometry data for use in a rocket

DD FORM 1 JAN 73 1473 EDITION OF 1 NOV 65 IS OBSOLETE

Unclassified

SECURITY CLASSIFICATION OF THIS PAGE (When Data Entered)

aeroballistics analysis, correlation with theory, and for a systematic determination of the influence of the helicopter components (rotor, fuselage, and wing) and significant operating condition parameters (flight speed, flight direction, ground effect, gross weight, and aircraft/rocket attitude) on the airflow influencing rocket trajectories. In addition, the flow velocities at potential locations for a fire control wind sensor mounted on the helicopter were determined to evaluate potential wind sensor locations for accurately measuring flow velocities at the low flight speeds required in accordance with current terrain flying/rocket firing tactics. This research investigation also served to demonstrate advanced experimental techniques and provide rotor wake and airflow information, which will contribute to the general technology associated with the application of model rotor testing,to achieve an improved understanding of the aerodynamics of helicopter low speed flight. In particular, initial flow information on blade-vortex interaction for low speed conditions were acquired.

Time-averaged values of two flow velocity components, measured with a laser velocimeter, are presented for the model test configurations and conditions. Also, the peak-to-peak values and cyclic time-variant flow velocities, related to blade azimuth position, are presented for points on a rocket trajectory for the reference AH-1G configuration and conditions. Predicted wake geometries and flow velocities are compared with the test data and used for interpretation of the airflow results. A most significant finding for low speed forward flight conditions is the notable reduction in the time variation of flow velocities (peak-to-peak amplitude) at points on the rocket trajectory compared to tip vortex induced flow velocities near the blade tip and, also, compared to theoretical predictions and hover test results from two prior investigations. For the AH-1G, the phasing of the blade azimuth and tip vortex travel is synchronized such as to produce a blade-vortex intersection which results in a diffusion of each tip vortex and an associated decrease in the unsteady aerodynamic interference at the rocket trajectories.

4. SUB-TITLE (Cont'd)

Subtitle: Application of Model Helicopter Testing, Laser Velocimetry, and Rotor Wake Flow Visualization to Investigate the Aerodynamic Interference at Rocket Trajectories and Wind Sensors of a Helicopter Operating in Low Speed Flight.

SUMMARY

An experimental investigation was conducted to determine the airflow characteristics in the vicinity of a model helicopter to determine the aerodynamic interference at representative rocket trajectories and wind sensor locations of an Army AH-1G helicopter operating in low speed forward flight. Laser velocimetry and flow visualization techniques were applied in a wind tunnel to provide flow velocity and wake geometry data for use in a rocket aeroballistics analysis, correlation with theory, and for a systematic determination of the influence of the helicopter components (rotor, fuselage, and wing) and significant operating condition parameters (flight speed, flight/wind direction, ground effect, gross weight, and aircraft/rocket attitude) on the airflow influencing rocket trajectories. In addition, the flow velocities at potential locations for a fire control wind sensor mounted on the helicopter were determined to evaluate potential wind sensor locations for accurately measuring flow velocities at the low flight speeds required in accordance with current terrain flying/rocket firing tactics. This research investigation also served to demonstrate advanced experimental techniques and provide rotor wake and airflow information, which will contribute to the general technology associated with the application of model rotor testing to achieve an improved understanding of the aerodynamics of helicopter low speed flight. In particular, initial flow information on blade-vortex interaction for low speed conditions was acquired.

Time-average values of two flow velocity components, measured with a laser velocimeter, are presented for the model test configurations and conditions. Also, the peak-to-peak values and cyclic time-variant flow velocities, related to blade azimuth position, are presented for points on a rocket trajectory for the reference AH-1G configuration and conditions. Predicted wake geometrics and flow velocities are compared with the test data and used for interpretation of the airflow results. A most significant finding for low speed forward flight conditions is the notable reduction in the time variation of flow velocities (peak-to-peak amplitude) at points on the rocket trajectory compared to tip vortex induced flow velocities near the blade tip and, also, compared to theoretical predictions and hover test results from two prior investigations. For the AH-1G, the phasing of the blade azimuth and tip vortex travel is synchronized such as to produce a blade-vortex intersection which results in a diffusion of each tip vortex and an associated decrease in the unsteady aerodynamic interference at the rocket trajectories.

FOREWORD

This report is the third of a series resulting from three contracts provided by the Dept. of Army to the United Technologies Research Center (UTRC). The first report "Prediction of Rotor Wake Induced Flow Along the Rocket Trajectories of an Army AH-1G Helicopter" was published in March 1975 (Ref. 15). The second report "Investigation of the Airflow of a Hovering Model Helicopter at Rocket Trajectory and Wind Sensor Locations" was published in July 1977 (Ref. 23).

This investigation was sponsored by the U.S. Army Research Office, Research Triangle Park, North Carolina, under Contract DAAG29-77-C-0013. Supplementary funding for the contract was provided by the MICOM, AMRDL (Ft. Eustis) and ARRADCOM (Picatinny Arsenal) branches of the Dept. of Army. The contract was initiated in May 1977 and completed in September 1979.

The Army contract monitor was Dr. Robert Singleton of the Army Research Office. The interest and project support provided by Dr. Singleton, Mr. Saul Wasserman of the U.S. Army Armament R&D Command and Mr. Robert W. Bergman of the U.S. Army Missile Command is gratefully acknowledged. Also acknowledged is the support provided at UTRC by Dr. John C. Bennett, Jr., Mr. Thomas Murrin, Miss Donna Hess, and personnel of the UTRC Test Facilities Section of UTRC. Dr. Bennett provided the laser velocimeter support and Mr. Murrin was the test engineer during the test program.

The program manager for the contract was Mr. Anton J. Landgrebe, Supervisor, Rotary Wing Technology Group, UTRC. Mr. Robert B. Taylor, Research Engineer, Rotary Wing Technology Group, was the principal engineer for the contract.

TABLE OF CONTENTS

TABLE OF CONTENTS (Cont'd)

LIST OF ILLUSTRATIONS

LIST OF ILLUSTRATIONS (Cont'd)

LIST OF ILLUSTRATIONS (Cont'd)

LIST OF ILLUSTRATIONS (Cont'd)

LIST OF ILLUSTRATIONS (Cont'd)

LIST OF ILLUSTRATIONS (Cont'd)

LIST OF ILLUSTRATIONS (Cont'd)

LIST OF ILLUSTRATIONS (Cont'd)

LIST OF TABLES

INTRODUCTION

The accurate determination of the flow field in the vicinity of a helicopter is required when a helicopter is used as a weapons platform. Since a free-flight projectile such as a rocket, when fired from a helicopter, initially travels at a speed which is the same order of magnitude as the flow velocities, the flow field induced by the rotor wake system can have a significant effect on the rocket trajectory. This can necessitate some form of aiming compensation or special firing techniques -- particularly at the low helicopter flight speeds at which rockets are to be fired in accordance with current Army nap-of-the-earth, tactical concepts. The shortage of information on helicopter airflow and its influence on free flight rockets for the purpose of achieving an effective fire control is a major concern of the Army, as stated in Ref. 1. Current Army doctrine calls for employment of helicopters such as the AH-1, AAH, and UTTAS in hover, pop-up, and terrain flying modes. The requirement for investigation of rocket aerodynamic interference for helicopters operating in such modes and recommendations for such investigation are well documented in the Army Missile Command memo (Ref. 1), included herein as Appendix A. The requirement is also discussed in the Proceedings of the Conference on the Effects of Helicopter Downwash on Free Projectiles (Ref. 2), particularly in the presentations of Army representatives Marner (Ref. 3), Morse (Ref. 4), and Bergman (Ref. 5).

To assess the influence of the rotor/wake flowfield on the flight path of a 2.75 inch rocket fired from the Army AH-1G helicopter (Figs. 1 through 3) when hovering or flying at low forward speeds, an analytical investigation was completed in 1975 at the United Technologies Research Center, UTRC (formerly the United Aircraft Research Laboratories), to predict the induced flow velocities at the rocket trajectories (Fig. 4). UTRC computer analyses which have the capability to calculate tip vortex geometry and rotor wake induced velocities were used to calculate the time-averaged and time-varying (instantaneous) induced flow velocities along the rocket trajectories for helicopter flight speeds of 0, 15, and 30 kts. Descriptions of these analyses and their application and validation are contained in Refs. 6 to 14. The results of the analytical investigation have been reported in Ref. 15 in a report entitled "Prediction of Rotor Wake Induced Flow Velocities Along the Rocket Trajectories of an Army AH-1G Helicopter". Sample results were presented on August 12, 1975 at the Conference on the Effects of Helicopter Downwash on Free Projectiles organized by the U.S. Army Aviation Systems Command. The paper for this presentation, entitled "Rotor Wake Induced Flow Along Helicopter Rocket Trajectories" (Ref. 16), is included herein as Appendix B. The induced velocity results from this investigation have been used by Wasserman in a trajectory analysis at the Picatinny Arsenal to predict the influence of the aerodynamic

interference of the rotor wake on rocket trajectories (Ref. 17). It was concluded that this influence is significant and must be compensated for when establishing aiming techniques. This conclusion has been substantiated in Army flight tests such as those reported for the UH-1 and the AH-1 in Refs. 18 and 19.

Although the analytical investigation provided a significant amount of information regarding induced velocities along the AH-1G rocket trajectories, it was limited in scope to three forward flight conditions, and the interference effects of the fuselage, wing, and ground on the predicted velocities were not included. It was concluded that model helicopter testing should be conducted to provide systematic experimental data for correlation, investigation of other operating conditions and neglected interference effects, and determination of wind sensor locations. It was thus suggested that the model hovering and wind tunnel facilities, and experimental flow measurement and visualization techniques, available at UTRC, be used to measure the flow velocities and wake boundaries in the regions of the rocket trajectories and potential wind sensor locations. Descriptions of UTRC prior experience with similar model testing and experimental techniques are contained in Refs. 6, 7 and 20 to 22.

A contract (DAAA21-76-C-0151) was awarded to UTRC by the Army (Picatinny Arsenal) in March 1976 to use the UTRC model rotor hover test facility to conduct such an investigation for the hover mode of operation. This contract was completed in June 1977 with the delivery of a final report (Ref. 23). The Summary, Conclusions, and Recommendations from Ref. 23 and the Scope of Work for this contract are presented herein in Appendix C. This investigation was conducted to determine the airflow characteristics in the vicinity of a model helicopter to determine representative flow velocities at the rocket trajectory and wind sensor locations of a hovering Army AH-1G "Cobra" helicopter. Laser velocimetry and flow visualization techniques were applied to provide flow velocity and wake geometry data for correlation with theory and for a systematic determination of the total and separate influence of each of the aircraft components (rotor, fuselage, and wing), and significant operating condition parameters (rotor thrust, tip speed, and ground effect) on the airflow influencing rocket trajectories. In addition, the flow velocities at potential locations for a fire control system wind sensor, mounted on the aircraft, were determined to assist in identifying wind sensor locations for accurately measuring flow velocities at hover. Time-average and peak-to-peak values of flow velocity components, measured with a laser velocimeter (LV), were compared for the hovering model test configurations and conditions. Also, the cyclic time-variant flow velocities, related to blade azimuth position, were presented for points on a rocket trajectory for the reference model AH-1G configuration and condition. The measured model flow velocities were scaled to representative full-scale values, and the applicability of scaling procedures to rotor thrust and tip speed variations

was demonstrated. Rotor wake theory was applied to selected model and full-scale configurations and conditions. The predicted flow velocities generally compared favorably with LV test data and were used in combination with wake geometry data for interpretation of the airflow results. The location of the hovering rotor wake (particularly the tip vortices at the wake boundary) relative to the rocket trajectories and wind sensors was shown to be a major determinant of their flow velocities. A sample comparison of the measured and predicted time-average flow velocities for the hovering condition is presented in Fig. 5. A complete list of the findings from Ref. 23 is presented in Appendix C.

Following the experimental hover investigation, the subject wind tunnel investigation, reported herein, was conducted for the Army Research Office (ARO) with supplementary funding support from MICOM, AMRDL (now Applied Technology Laboratory, Army Research and Technology Laboratories, Ft. Eustis), and ARRADCOM branches of the Army. The wind tunnel investigation was conducted to provide information for the low aircraft flight speeds of interest in accordance with current rocket firing tactics. Consistent with the hover test, combined model rotor-fuselage-wing testing, application of laser velocimeter techniques to measure flow velocities, and application of flow visualization techniques to determine wake geometry were conducted for a model configuration approximately representative of the Army AH-1G (Cobra). As will be presented, the results of the experimental program provide velocity and wake geometry data for correlation with theory and for a systematic determination of the total and separate influence of each of the aircraft components (rotor, fuselage, and wing) and significant parameters (flight speed, flight direction, ground effect, gross weight, and aircraft attitude) on the airflow influencing rocket trajectories. Also, the flow velocities at potential locations for a wind sensor mounted on the aircraft were determined to assist in solving the problem of accurately measuring flow velocities at the low aircraft flight speeds required in accordance with current rocket firing tactics.

It is noted that, in addition to the rocket application, the use of a laser velocimeter to measure flow velocities at low flight speeds and the evaluation of computer analyses for predicting such velocities is useful in demonstrating techniques for determining helicopter aerodynamic characteristics required in other investigations of interest to the Army (e.g., those associated with low speed, terrain flying missions).

The objectives of this wind tunnel test program are presented in the following section of this report. In following sections, a description of the test, the flow visualization results, the flow velocity results, conclusions, and recommendations are presented.

TEST OBJECTIVES

Test data were acquired, prepared in graphical form, compared, and analyzed in accordance with the following specific objectives and subtasks:

1. To provide representative flow velocity distributions along rocket trajectories of the AH-1G helicopter by appropriately scaling the model results. The velocity data shall provide information for use in rocket trajectory analyses to assess the influence of the aerodynamic interference on the accuracy of the AH-1G weapons systems and similar weapons systems of future Army helicopters.

2. To assess the influence of the helicopter components (rotor, fuselage, and wing) on interference velocities at the rocket trajectories. The separate and combined influence of the components shall be analyzed to determine their relative significance. These results will provide fundamental information for determining whether or not it would be advantageous to move the location of a rocket launch point relative to the fuselage and stub-wing. Also, the experimental data for the separate components shall provide independent data for correlation with theory. The requirement for including the fuselage and wing interference capability in the computer analysis for predicting rocket flow velocities shall be assessed (fuselage and wing effects were neglected in the results reported in Ref. 15).

3. To assess the influence of the experimental variations of the operating condition parameters. The test data for the variations in forward flight speed, rearward flight speed, cross wind, ground effect, thrust coefficient (representing gross weight), and helicopter/rocket attitude shall be compared.

4. To perform an initial evaluation of theory by comparing the scaled experimental wake geometry and velocity results with the predicted full-scale AH-1G helicopter results from the analytical study reported in Ref. 15.

5. To identify the most desirable locations for a wind sensor. The test data at the potential wind sensor locations shall be compared and analyzed. Two components of velocity shall be analyzed to determine flow direction and magnitude in the fore-aft vertical plane.

6. To assess the influence of canopy design on rocket interference velocities and wind sensor locations. The velocity data for the two canopy configurations (round and flat-sided) shall be compared.

7. To provide aerodynamic data which demonstrates the results of laser velocimeter and flow visualization techniques of general interest for application to other Army research programs. The combination of model helicopter and wind tunnel testing with performance, flow velocity, and wake geometry measurements shall demonstrate a unique capability for other investigations such as those involving low speed and nap-of-the-earth operation and related blade-vortex interaction. The ability to determine both the time-average and time history of individual components of flow velocity and relate them to the rotor operating conditions and associated wake geometry (tip vortex positions) shall be demonstrated.

The specific objectives associated with each type of test data are presented in Table 1. Ample data were obtained to comply with each objective.

TABLE 1. SPECIFIC TEST DATA OBJECTIVES

1. To measure time averaged horizontal and vertical flow velocity components along the rocket trajectory to determine the following effects:

   . Effect of - rotor only
   - fuselage — at 15 kts full scale
   - wing — (also time-dependent velocities)
   - modified canopy

   . Effect of - rotor only
   - fuselage — at 30 kts full scale
   - wing — (also time-dependent velocities)
   - modified canopy

   . Effect of low airspeed (10 kts full scale)
   . Effect of change in thrust coefficient
   . Effect of rocket launch position
   . Effect of rocket trajectory attitude (relative to rotor disc)
   . Effect of crosswind
   . Ground effect
   . Effect of tail wind/rearward flight
   . Ground effect in tail wind/rearward flight

2. To measure time averaged horizontal and vertical flow velocities at selected wind sensor locations.

3. To measure instantaneous horizontal and vertical flow velocities at selected rocket trajectory points to investigate time dependent flow interference.

4. To measure instantaneous horizontal and vertical flow velocities in the vicinity of the rotor disk and wake boundary to study blade/vortex interaction.

5. To obtain flow visualization data (using smoke still photography and motion picture strobe cinematography) for selected configurations and conditions representing the primary effects listed in objective 1.

DESCRIPTION OF TEST

WIND TUNNEL FACILITY

The test program was conducted in the 18 ft octagonal test section of the UTRC Large Subsonic Wind Tunnel. This closed return tunnel is 18 ft in height and width and has a speed range of approximately 5 kts to 175 kts. An illustration of the wind tunnel and photographs of the test section are shown in Figs. 6, 7, and 8. An overhead support structure in the test section supports the model rotor system so that it is positioned laterally on the centerline of the tunnel with the rotor center 10.27 ft from the tunnel floor. The vertical positioning was chosen to minimize tunnel floor and wall effects and at the same time provide maximum coverage of the rotor wake by the LV system. As shown in Fig. 7, a portion of the tunnel wall on the control room side is composed of glass windows to allow the LV beams to enter the test section. The glass windows are 5 ft high by 12 ft long and allow the LV focal point to traverse 1.4 rotor radii up and downstream and +.25, -.75 rotor radii above and below the rotor center, respectively.

HELICOPTER MODEL

The helicopter model shown in Fig. 9 used to simulate the Army AH-1G helicopter is composed of 2 major parts: the fuselage and the rotor system. The model is shown installed in the wind tunnel in Fig. 10. An existing 1/8 scale AH-1G fuselage model was loaned by the Government from the Bell Helicopter Company and provided to UTRC for the test program. The fuselage model has removable wings, and provisions were made to interchange a square-sided canopy and a rounded canopy. The fuselage is supported underneath the model rotor by means of a strut extending up from the tunnel floor. The fuselage is fixed for zero angle between a waterline and the freestream velocity. Yawing of the model to simulate crosswinds or tailwinds is accomplished by manually rotating the fuselage model on the strut to the desired yaw angle and then tightening the retaining fixtures. The rotor test rig is mounted to an overhead support structure as shown in Fig. 10 and has a 90 Hp electric drive motor with a belt-type transmission connected to the rotor shaft. Rotor thrust is measured with a strain gaged load cell to within 2% accuracy and rotor torque is measured by means of a strain gage bending beam. For consistency with the hover test results reported in Ref. 23, the same rotor hub and blades used in the hover test were utilized in this test. The model rotor is two bladed, articulated in flapping, and rigid in lag. Collective pitch and rotor shaft angle are set manually, and there are no provisions for cyclic pitch.

The primary model rotor design values are compared with those of the full-scale AH-1G rotor in Table 2.

Although the model rotor values do not exactly duplicate the full-scale values, they are regarded to be sufficiently close so as not to significantly compromise the accomplishment of the objectives of the experimental program. The rotor parameters of most significance to this test (number of blades, solidity ratio, aspect ratio, and taper ratio) were identically or very closely scaled. The effects of the relatively small differences in twist and airfoil sections, indicated in Table 2 on the rotor wake and flow velocities were minimized through test operation at full-scale thrust coefficient. The use of an available hub with flapping articulation rather than a teetering hub is, in itself, of little consequence for low speed forward flight as long as the full scale control angle is maintained during the wind tunnel testing. This was ensured during the test by adjusting shaft tilt to provide a near zero (slightly propelling) control angle as in the AH-1G in low speed flight.

The available AH-1G fuselage model was 1/8th full-scale size. The ratio of the model rotor diameter to the full-scale rotor diameter was 1/9.26. Although the resulting rotor-fuselage scaling was somewhat inconsistent (the fuselage was 14 percent too large), the anticipated effect of this inconsistency, on the data to be measured, was anticipated to be small when the following were considered:

1. The contribution of the fuselage interference to the velocities at rocket trajectory points is small compared to the influence of the rotor.

2. The narrow width of the AH-1G (only 7 percent of the rotor diameter) results in a scaling inaccuracy of the model fuselage width of less than 2 percent of the model rotor diameter.

3. The model fuselage was positioned under the model rotor such that the primary distances for rotor/fuselage flow interference at rocket trajectories and wind sensor locations were scaled to be consistent with full-scale AH-1G values. Considering the importance of the rotor as the flow velocity producing device, the primary distances selected were measured relative to the rotor hub center and scaled to the rotor radius.

Regarding the above, several scaling selections should be mentioned. First, the fuselage was positioned relative to the rotor hub such that the vertical distance between the canopy roof (at the pylon junction) and the rotor was appropriately scaled to the full-scale value (0.18 R). This was important for both canopy interference on the flow at rocket

TABLE 2. MODEL AND FULL-SCALE ROTOR DESIGN VALUES

	Full-Scale AH-1G	Available Model
Rotor Radius, R	22 ft.	28.5 in.
Blade Chord, c	27 in.	2.94 in.
Aspect Ratio	9.78	9.69
Number of Blades	2	2
Rotor Solidity Ratio	0.0651	0.0657
Taper Ratio	1.0	1.0
Linear Twist	-10 deg	-8 deg
Airfoil Section	modified NACA 0009	NACA 0012
Hub	Teetering	Articulated (flapping)

trajectory locations beneath the canopy and for selected wind sensor locations aside of the top of the canopy. The hub was moved forward over the fuselage to better simulate the full-scale nose-to-hub distance (0.65 R) (The forward portion of the fuselage was of importance for this rocket trajectory, wind sensor test.) This scaling was slightly compromised to 0.70 R to prevent the hub center from moving forward of the pylon. Model stub wings were specially designed to be scaled to the rotor. Following fabrication, they were mounted on the fuselage such that their relative position to the rotor hub was scaled equivalent to that of the full-scale wing to rotor position. In addition to being sized and positioned correctly for the rotor flow field, scaling the wings to the rotor permitted rocket trajectory locations relative to the wing to be representative of full-scale and correctly positioned in the flow field. A summary of the primary scaling values are presented in Table 3.

It is noted that the rotor-diameter-to-tunnel-span ratio (1:4) is sufficiently small to minimize tunnel wall floor and ceiling effects. Also, for the in-ground-effect testing, the ground plane had a leading edge splitter plate to minimize boundary layer growth.

TEST CONFIGURATIONS AND TEST CONDITIONS

The major portion of the test program was performed with the model in the reference configuration. The reference configuration consisted of the rotor, the fuselage with a flat-sided canopy, and the wing. Changes of the model from the reference configuration were made to determine parametric effects of the fuselage, the wing, and a modified canopy. Two (2) reference operating conditions were selected based on a thrust coefficient representative of the AH-1G gross weight (9500 lbs) and two (2) nominal advance ratios (tunnel flow velocity/rotor tip speed) of approximately 0.034 and 0.068. These advance ratios correspond to the 15 and 30 kts flight speeds of the full-scale AH-1G conditions analyzed and reported in Ref. 15. A tip speed (373 fps) equivalent to one-half of the full-scale AH-1G tip speed was selected. The reduced tip speed was chosen based on structural considerations for the available model blades. The tip speed selection was justified on the basis that both theoretical and experimental results have shown the validity of linear scaling of flow velocities with tip speed for constant thrust coefficient. Good examples of the experimental validity are shown in the hover test report (Ref. 23). To retain the appropriate advance ratio scaling, the wind tunnel free-stream velocities (7.5 and 15 kts) were also set at one-half the simulated full-scale flight speeds. The shaft angle for the reference conditions was 2 degrees (upstream blade tip down). This selection was based on the requirement to maintain a near zero tip path plane angle to

TABLE 3. SCALING OF RELATIVE POSITIONS OF ROTOR, FUSELAGE, AND WING

	Model*	Full-Scale AH-1G*
Canopy Roof to Rotor (Vertical Positioning of Fuselage)	$z = -0.18$	$z = -0.18$
Nose to Rotor Hub Center (Horizontal Positioning of Fuselage)	$x = 0.70$	$x = 0.65$
Wing Trailing Edge (At Root) to Rotor Hub Center	$x = -0.06$ $z = -0.37$	$x = -0.06$ $z = -0.37$
Wing Semi-Span	$y = \pm 0.23$	$y = \pm 0.23$

*All values are scaled to the rotor radius (i.e., nondimensionalized by R).

closely simulate AH-1G low speed flight. At full scale speeds of 15 and 30 kts it will be shown later that blade longitudinal flapping was 1.2 and 1.8 degrees, respectively. Therefore the 2 degree shaft tilt selection provided the required slightly propelling tip-path-plane angles (0.8 and 0.2 deg). The selected reference launch position is No. 4, located at the most outboard wing station on the right side of the fuselage. The selected reference launch angle is 7 deg. Table 4 summarizes the reference model configuration and reference test conditions. A summary of all combinations of test configurations and test conditions for which LV data were acquired is presented in Table 5.

The reference configuration, the isolated rotor, the rotor-fuselage combination without the wing, and the modified canopy configuration were tested at thereference test conditions. Variations from the reference conditions to simulate aircraft velocity, flight (or wind) direction, gross weight, attitude variation, and ground effect were tested as follows. In addition to the two (2) reference flight speeds (15 and 30 kts), a third simulated forward flight speed (10 kts) and a 15 kt simulated rearward flight speed were tested for the reference configuration. An independent variation of thrust coefficient was tested for the reference configuration. An independent variation of the relative attitude of the rocket trajectory to the aircraft was simulated by varying the model rotor attitude for the reference configuration. A change in trajectory angle relative to the rotor disk from the reference 7° angle was simulated by increasing the rotor shaft angle to -4° from -2°. This provided an effective trajectory angle relative to the rotor of 9°. The crosswind conditions were simulated by yawing the model $\pm 30°$ with respect to the free stream velocity which was maintained at 15 kt full scale. To simulate the tail wind (or rearward flight) condition, the fuselage model was rotated 180° so that the nose pointed downstream. Since the reference No. 4 rocket launch position was now blocked by the fuselage from the LV beams, the No. 1 launch position was used for acquiring LV data. This is the launch position on the left side of the fuselage corresponding to the No. 4 launch position on the right side of the fuselage. In addition to the No. 4 launcher, data for an inboard launcher (No. 3) was acquired for forward flight. To simulate a ground effect condition, a ground plane was installed in the tunnel at a height of .75R below the rotor center. This corresponds to a skid height on the AH-1G of about 3.5 feet above the ground. The reference configuration was tested in-ground effect (IGE) for forward flight and rearward flight/tailwind conditions.

TEST DATA ACQUISITION

Rotor instrumentation consisted of a rotor thrust load cell, longitudinal and lateral vibration pickups mounted to the rotor shaft housing (fixed system) for safety monitoring, and blade root flapping measured by

TABLE 4. REFERENCE TEST CONFIGURATION AND TEST CONDITIONS

Reference Configuration

- Rotor
- Fuselage with flat sided canopy
- Wing

Reference Test Conditions

Forward speed = 7.5 kts, 15 kts (scaled to 15 and 30 kts)

Tip speed = 373 fps (1/2 of full scale tip speed)

Fuselage angle of attack = 0°

Shaft angle = -2° (upstream blade down)

Thrust coefficient = .00472 (corresponding to AH-1G G.W. of 9200 lbs)

Rocket launch position No. 4 (outboard, right side)

Rocket launch angle = 7°

TABLE 5. SUMMARY OF TEST CONDITIONS AND TEST CONFIGURATIONS

Objective	Model Configuration	Airspeed Full Scale (kts)	Thrust Coefficient (±2%)	Comments
Reference	Rotor-Fuselage-Wing	30	.00472	No. 4 launcher $h/R=\infty$, $\alpha_s=-2°$
Wing	Rotor-Fuselage	30	.00472	
Canopy	Rotor-Fuselage-Wing-Modified Canopy	30	.00472	
Isolated Rotor	Rotor only	30	.00472	
Reference	Rotor-Fuselage-Wing	15	.00472	
Wing	Rotor-Fuselage	15	.00472	
Canopy	Rotor-Fuselage-Wing-Modified Canopy	15	.00472	
Isolated Rotor	Rotor only	15	.00472	
Alternate airspeed	Rotor-Fuselage-Wing	10	.00472	
Thrust Coefficient	Rotor-Fuselage-Wing	15	.00435	
Launch Position	Rotor-Fuselage-Wing	15	.00472	No.3 launcher
Trajectory Angle	Rotor-Fuselage-Wing	15	.00472	$\alpha_s = -4°$
Crosswind	Rotor-Fuselage-Wing	15	.00472	yaw = $\pm 30°$
Ground effect	Rotor-Fuselage-Wing	15	.00489	$h/_R = .75$
Tail wind (or Rearward Flight)	Rotor-Fuselage-Wing	-15	.00472	No.1 launcher
Ground effect in tail wind	Rotor-Fuselage-Wing	-15	.00489	No.1 launcher $h/_R = .75$
Blade-Vortex Interaction	Rotor only	15	.00472	
Wind sensors	Rotor-Fuselage-Wing	15 and 30	.00472	

an angular potentiometer. A motion picture camera was also continually throughout the test to monitor the model so that the model could be viewed on a TV screen in the control room. The motion picture was also used in conjunction with high intensity strobe lighting to track the rotor blades.

As shown in Ref. 23, the flow velocities at points on the rocket trajectories are dependent on the relative position of the rotor wake boundary to the trajectory points. In order to determine the wake boundaries to assist in analysis of the velocity data and to compare with theoretical wake boundaries, flow visualization data were acquired. Smoke patterns indicating the rotor wake in the vicinity of the rocket trajectories were recorded on film for most of the test configurations and conditions.

Flow velocity data were acquired by traversing the focal point of a laser velocimeter to selected points along rocket trajectories. Velocity points for the various configurations were selected to provide comparative data at trajectory points of primary interest such as between the rocket launch point and the wake boundary. Considering the blockage of the fuselage, velocity data were primarily acquired for the rocket trajectories on the side of the model accessible to the laser velocimeter equipment. Consistent with the results presented in Ref. 23, emphasis was placed on the rocket trajectory nearest the laser velocimeter (most starboard trajectory for the forward flight condition).

To provide flow velocity data to assist in the determination of induced flow velocities and desired locations for a wind sensor for measuring flight speed, velocity measurements were taken at several potential wind sensor locations. The vertical component of velocity and the component in the direction of the tunnel flow velocity were measured at three points in the region of the nose and cabin of the model fuselage at the simulated 15 and 30 kt flight speeds. The locations of the wind sensor points are shown in Fig. 11.

A description of the laser velocimeter used in this test and the associated data acquisition system is presented in the following section.

DESCRIPTION OF LASER VELOCIMETER AND DATA ACQUISITION SYSTEM

This section describes the laser velocimeter (LV) and data acquisition system installed in the UTRC 18-ft Subsonic Wind Tunnel. The laser velocimeter (LV) measures the velocity of particles in the flow field and uses the Doppler shift of light scattered by the moving particles to determine particle velocity. Since the particles are traveling with the fluid flow, the flow velocity is also determined. The Doppler shift frequency is the difference between the frequency of incident light and scattered light. The use a of monochromatic coherent light source makes it possible to determine the frequency and wavelength of the incident light so that the Doppler shift and hence the particle velocity can be determined. A more thorough discussion of basic LV principles and theory is included in Ref. 23.

The laser velocimeter system consists of 5 subsystems: the installation, the laser, sending and receiving electro-optics, signal processors, and a seeder. A short description of each subsystem follows.

Installation

The basic LV system is housed in the area between the wind tunnel test section and the control room, as shown in Fig. 12. A window system measuring 5 ft high by 12 ft long is installed on the LV side of the test section to allow passage of the LV beams into the test section. The laser with optics shown in Fig. 13 is secured to a table that is mounted on tracks so that it can traverse the entire length of the windows (12 ft) in the test section. The traverse of the LV system is operated from inside the control room so that the longitudinal streamwise location of the LV focal point is remotely controlled. The table holding the LV system also incorporates a jack-screw scissors support arrangement that raises or lowers the table so that the vertical location of the LV focal point is remotely controlled. The lateral location of the LV focal point is set by the zoom lens in the optics system, which is also operated remotely from the control room.

Laser

The laser used is a 4 watt Argon-Ion laser. Two colors are used, 5145 Angstroms (green) and 4880 Angstroms (blue), to provide velocity measurements in two orthogonal directions. These are normally the freestream and vertical velocity components relative to the wind tunnel test section. The total power available for these two color lines is 1.4 watts.

Electro-Optics

This subsystem contains all of the optical and electrical components required to emit laser light, focus the laser beams to cross at the measurement point (focal volume), collect light scattered from a particle in the focal volume, project the received light on a photomultiplier tube, and amplify the voltage signals from the photomultiplier for signal processing.

The optics consist of a three lens scanning system for zoom capability designed to maintain constant angles between the laser beams over the entire scanning distance (approximately 6.5 to 18 ft) and three mirrors required to turn the laser beams and scattered light through three right angles to provide compactness of the system. This is shown clearly in Fig. 12. The optics send three beams that are focused on the focal volume: one blue and one green beam and a blue-green beam. Both the blue and green beams have been frequency-shifted by a Bragg cell module before leaving the optics. The known frequency shift allows a zero velocity offset in the voltage signal so that positive and negative velocities may be discerned. This step is required because the Doppler signal transmits only frequency increment information without the sign of the increment. As light is scattered off of particles moving through the focal volume, the optics receive light in the back-scatter mode. Blue and green light are separated by filters and then focused on separate photomultiplier tubes. The collected light energy is converted into an electrical voltage signal for both the blue and green signals and then sent to the signal processors.

Signal Processors

The purpose of the signal processors shown in Fig. 13 is to transform the electrical signals received from the photomultiplier tubes into a velocity. To accomplish this, two counter processors (one for each velocity component) were directly connected to a PDP 11/40 computer to perform the signal processing tasks as well as the data reduction and storage tasks. The counter processors amplify and filter the signals, validate the Doppler frequency samples, and finally compute the Doppler frequency. The processors are interfaced with the PDP 11/40 computer and the data are transferred into the computer. Each piece of data transferred is flagged with clocktime and rotor revolution time so that the blade azimuth position at the time the data were taken can be determined. Once the data have been stored in the computer, the possibilities for data reduction and analysis are numerous. The emphasis in the present test was first on time-average velocities, and secondly on time-dependent velocities. Thus, the computer was used to organize the data and calculate the time averaged velocity and RMS value for a rotor revolution as well as the time dependent velocities that are a function of blade azimuth. For the on-line data reduction, the data were grouped azimuthally into 10 degree increments so that all data fell into 36 separate bins for 360 degrees of azimuth. The mean

velocity for each azimuth bin were calculated on-line for both the vertical and horizontal velocity components and then plotted on-line as a function of azimuth. In addition the time-average and RMS values were displayed on-line. Generally, 500 data samples (500 seedant particle measurements) per velocity channel were taken for each data point and all of these data were stored on magnetic disc for any further data reduction or analysis. For selected data points the complete time histories showing the proper velocity/blade azimuth combination for all 500 samples were plotted.

Seeding

Artificial seeding was introduced into the flow to provide particles following the airflow for LV measurement. Atomized mineral oil was used as a seedant and was pressure injected into the flow by means of nozzles which were attached to an upstream traversing smoke rake used for smoke flow visualization. The smoke rake is connected to a pulley system in the upstream portion of the test section. The pulley system provides remote positioning of the rake, both vertically and laterally, in the test section. This provided the capability to inject seedant into the flow at the best location for passage through the focal volume to achieve optimal signal response.

Another type of seeding system was also used for some portions of the test. In this system, seedant was injected into the flow downstream of the test section so that the seedant particles had to travel the tunnel circuit before entering the test section for possible velocity measurement by the LV. This sytem has the advantage in theory of providing a homogenous seedant-air volume due to mixing around the circuit so that every differential flow volume contains an equal number of seedant particles. The disadvantage of this seeding technique is that it is difficult to seed a large volume tunnel. Experience with this technique showed that a more even azimuthal distribution of data samples were obtained, which indicated more homogenous seeding, but the signal-to-noise ratio was lower and the data rate was also lower. The upstream seeding system with localized seeding provided good quality data after obtaining a certain level of experience and practice in positioning the upstream seeding rake, and was used for most of the test points.

DATA REDUCTION AND ANALYSIS

Measured data consisted of rotor thrust, flow visualization photographic data, velocity measurement point locations, and velocity component data. The rotor thrust data was reduced to coefficient form. The flow visualization data was analyzed to determine the forward wake boundary and tip vortex coordinates in the vicinity of the rocket trajectories. All flow velocity data were reduced to time-average form.

Selected flow velocity data were reduced to provide time histories of velocity with rotor azimuth position as averaged over several rotor revolutions.

The laser velocimeter system is a two-component system and measures the v_x and v_z velocity components in the wind tunnel freestream (horizontal) direction and the vertical direction, respectively. Thus, data for these two components were measured and analyzed. Although the lateral flow velocity component was not measured, its omission is not critical to the objectives of this test program because its magnitude is significantly lower than the other two components for most all of the conditions tested.

The experimental wake geometry and flow velocity results were prepared in graphical form and then compared and analyzed to assess the influence of the model helicopter components (fuselage and wing) and the experimental variations of the operating condition parameters. The experimental wake and velocity results for the model were scaled and compared with those of the predicted full-scale AH-1G helicopter results from the analytical study reported in Ref. 15. Also, the most desirable location for a wind sensor were identified from the data at the measured locations.

SMOKE FLOW VISUALIZATION RESULTS

In this section, the flow visualization results obtained from injecting smoke into the flow are presented. The flow visualization of the forward wake boundary and its location with respect to the rocket trajectory were especially helpful for interpreting the laser velocimeter flow velocity results presented in the next section. To assist in the interpretation of and comparison with the forthcoming flow visualization results, the tip vortex geometry patterns for the 15 and 30 kt flight conditions as predicted by the UTRC Rotor Wake Geometry Analysis are repeated from Ref. 15 in Figs. 14 and 15. These sample wake patterns apply to the rotor azimuth position indicated.

A remotely controlled moveable smoke rake was used to inject smoke into the flow upstream of the model. The rake consisted of a series of nozzles spaced about 8 in. apart on a vertical wire. The smoke rake could be moved vertically or horizontally so that the smoke filaments covered a section of a vertical plane in the test section. The recording equipment consisted of 16 mm motion picture movies and 70 mm still photographs. A system of strobe lights were connected to the camera triggering systems by an electronic time delay system. Using a 1/rev signal from the rotor as a reference, the electronic delay system triggered both the light strobes and the cameras when the rotor was in the desired azimuthal position. Strobing and photographing at 2/rev could also be accomplished so that the vortex trail from one rotor blade could be superimposed onto that for the other rotor blade. Sample smoke flow visualization photographs are shown in Figs. 16 to 26.

Figures 16 to 18 include results for the hover condition from Ref. 23. The smoke in the vertical plane creates a two-dimen-sional cross section of the rotor wake in which the vortex sheet cross sections are indicated by the discontinuities in the smoke filaments passing through the inner region of the rotor wake, and the cross sections of the tip vortices in the wake boundary appear as circles. The center of each circle normally contains little smoke which indicates high centrifugal pumping present in the vortex centers attributable to the vortex circulation.

Figure 18 shows a comparison of the rotor wake for hover and low speed forward flight at 7.5 kts model scale (15 kts full-scale). The hover wake is symmetrical so that, except for the small fuselage influence, a cross section at any azimuth is representative of the rotor wake. For the forward flight case the wake is convected downstream. These

photographs are good examples of the tip vortices and also the inboard wake described above. The fundamental difference observed between hover and low speed forward flight is the location of the forward rotor wake. In hover, tip vortices in the wake boundary are convected downward whereas in low speed forward flight the tip vortices travel inboard and slightly above the rotor and are then convected down through the rotor disc. This difference in the wake geometry is fundamental to the results of this test and will be discussed in detail later. Figures 19 to 22 show additional flow visualization photographs for low speed forward flight at 10, 15 and 30 kts (full scale). A comparison of Figs. 19, 20 and 21 shows the change in the rotor wake as airspeed increases from 10 kts to 30 kts. The wake angle increases with airspeed but the location of the wake boundary near the blade tip retains essentially the same previously mentioned characteristic for all three airspeeds. Figure 22 shows the 15 kt rotor wake for the reference configuration with the fuselage. The wake is nearly the same as for the isolated rotor wake shown in Fig. 20 for the same airspeed.

The important characteristic for all three airspeeds for the isolated rotor and the reference configuration with the fuselage is the location of the forward rotor wake near the rotor disc. Figures 23 and 24 show the location of the tip vortices in the rotor wake when the rotor blade is slightly before, at, and after 180 degrees azimuth. Figure 23 is for the scaled 10 kt condition and Fig. 24 is for the 15 kt condition. Note that the phasing of the passing blade and the tip vortices is such to cause a close passage or even an intersection between the vortex and the blade at 180 degrees azimuth.

Figure 25 is an example of the rotor wake near the blade tip on the advancing side of the rotor disc. Instead of placing the smoke filaments in the 0°-180° azimuth plane, as in the previous figures, the smoke filaments were moved outboard to pass over the advancing blade tip near 90 degrees azimuth. Figure 23 shows how the wake rolls up at the blade tip into a concentrated vortex. The upper two smoke filaments indicate how the airflow is convected in the wake. Another important feature shown is the large change in velocity gradients (magnitude and direction) as air is entrained into the wake. Following the two middle filaments from the upstream position, the air rises up and then curves over into the rotor wake, indicating the highly three-dimensional character of the rotor flow field.

Flow visualization of the rotor wake in-ground-effect for low speed forward flight, and also for rearward flight (or a simulated tailwind), is shown in Fig. 26. The important characteristic shown in this figure is the change in the forward rotor wake. Instead of being convected downstream as in the out-of-ground effect condition, the forward rotor wake rolls up in front of the fuselage nose, creating a large ground

vortex. The diameter of the ground vortex is roughly the distance from the rotor to the ground. The effects of the ground vortex will be discussed more fully in the Flow Velocity Results.

ROTOR WAKE BOUNDARIES

The rotor wake boundary in the 0-180 degree azimuth vertical plane can be mapped by plotting the center of each vortex. The distance between each tip vortex cross section in the wake boundary represents time equivalent to 180° of rotor azimuth for the two-bladed rotor and therefore every other tip vortex emanates from the same blade. Since both rotor blades are creating the same lift and have the same tip vortex strength at a given azimuth, the locus of tip vortices can be thought of as the time history of a helical tip vortex as it is convected downward.

The locus of tip vortices forming the forward wake boundary in the 0-180° azimuth vertical plane were plotted for various model configurations and test conditions. The wake boundaries for the isolated rotor and the reference configuration (rotor, fuselage with wing and flat sided canopy) are shown in Fig. 27 for the 15 kt reference conditon. The location of each tip vortex in the wake, when the rotor blades are in the 0-180° azimuthal position, is denoted by the circular arrow which also denotes vortex circulation direction.

Counting the newly formed tip vortex, there are 4 tip vortex cross sections on the rotor wake boundary by the time the wake boundary crosses the rocket trajectory. Up near the rotor disc plane, the wake boundaries for the isolated rotor and the reference configuration with the fuselage are nearly the same. This indicates that the presence of the AH-1G fuselage has a small effect on the wake boundary near the rotor disc.

After the tip vortex is formed by the rotor blade at 180° azimuth it travels downstream above and then down through the rotor disc near 80 percent radius. Because the rotor blades are in the 0-180° position only twice per revolution, it could be possible for the tip vortices to pass down through the rotor disc between blades and not be in close proximity to a rotor blade approaching the 180° azimuth position. However, as shown in the figure by the circular arrows denoting tip vortices, the tip vortex from the retreating blade crosses the rotor disc close to that instant in time when the advancing blade is at 180° azimuth. The result is a blade-vortex intersection, and the blade absorbs energy from and thereby diffuses the vortex. An indication of the magnitude of the vortex diffusion is evident in the time histories of the instantaneous flow velocities that will be discussed later. It suffices to say at this

point that the vortex intersection has important implications, not only relating to the impact on rocket trajectories but also to helicopter loads and vibration in low speed flight.

The wake boundary down near the rocket trajectory is slightly affected by the fuselage. For the isolated rotor, the wake boundary crosses the trajectory at x_T =.4 compared to a crossing point of x_T = .43 for the reference configuration with the fuselage. Since the thrust coefficient and therefore the momentum flux is the same for the isolated rotor and the reference configuration, some expansion of the wake boundary as well as wake acceleration could be expected for the reference configuration to compensate for the flow blockage due to the fuselage.

Figure 27 also shows the wake angle calculated from simple momentum theory. This line defines the forward part of the skewed cylinder of air to which momentum is imparted by the rotor for the 15 kt condition. Therefore this line can be thought of as a pseudo momentum wake boundary characterized by a straight line emanating from the forward part of the rotor disc. This does not accurately represent the curving of the actual wake above and then down through the rotor disc. However, down near the rocket trajectory the momentum wake angle is similar to the measured wake boundary.

The rotor wake boundaries for the isolated rotor and the reference configuration are shown in Fig. 28 for the 30 kt reference conditon. Up near the rotor disc plane, the wake boundaries for the isolated rotor and reference configuration are nearly the same and also retain the fundamental characteristics observed for the 15 kt condition whereby the wake travels radially above the tip path plane and then passes down through the rotor disc. Also the phasing between the tip vortices and the advancing blade is such that a blade vortex intersection occurs which again results in an impact on the tip vortex from the preceding blade by the blade at 180 deg azimuth. After passing down through the rotor disc, the 30 kt wake boundary is displaced downstream at the rocket trajectory relative to the 15 kt condition, and therefore crosses the trajectory much closer to the launch point. For the reference configuration, the rotor wake expands slightly in the vicinity of the rocket trajectory relative to the isolated rotor due to fuselage blockage, and the crossing point on the trajectory moves slightly outward to x_T = .08. For air speeds above 30 kts, the wake boundary passes behind the launch point and the entire rocket trajectory is in free air.

Comparing the predicted and measured tip vortex geometry along the forward wake boundary for the 15 and 30 kt conditions, the following is observed. (For 15 kts, Fig. 14 predicted results are compared with Fig. 27 test results; for 30 kts, Fig. 15 predicted results are compared with Fig. 28 test results.)

1. The wake contraction in the downstream direction is predicted resulting in accurate predictions of the point where the forward wake boundary (tip vortices) crosses the rocket trajectory (x_T = 0.4 and x_T = 0 for 15 and 30 kts, respectively).

2. The blade-vortex intersection is predicted for both flight speeds.

Additional flow visualization data were taken for the AH-1G at 10 kts and the wake boundary results for this condition are shown in Fig. 29. The wake boundaries for the isolated rotor and the reference configuration have the familiar characteristics observed at 15 and 30 kts. The tip vortices still travel above the rotor disc as they emanate from the blade at 180° azimuth and are intersected by the advancing rotor blade 1/2 rev later as they pass down through the rotor disc. The fuselage has the same small characteristic effect on the wake boundaries near the rocket trajectory that was observed at 15 and 30 kts. The rotor wake expands slightly due presence of the fuselage and the wake boundary crosses the trajectory at x_T = .55 compared to x_T = .5 for the isolated rotor.

The wake boundary results shown in Figs. 27 to 29, showing the blade-vortex intersection, are among the most important results uncovered during this test because they not only impact directly on the influence of the wake velocity on the rocket flight paths, but also because it is a phenomenon that affects other critical aspects of low speed helicopter flight such as blade loads, helicopter vibration, noise and handling qualities. It is important to observe that the blade-vortex intersection occurs over a wide range of low airspeeds and that airspeed range is still unbounded experimentally, except for the hover condition. Sensitivity of the blade-vortex intersection to tip path plane angle is not entirely known, but certainly there is a highly propelling tip path plane angle (approaching the propeller mode) for which the wake boundary passes entirely below the rotor disc. Likewise there is probably an autorotating condition that keeps the wake boundary above the rotor disc. In between these two extremes are the normal propelling and braking modes of operation at low speed. The range of tip path plane angle covered in the tests (0 to 3° forward) included simulation of the AH-1G in steady, unaccelerated flight, and therefore the shaft angle range required to reach these two extremes is not known. However, the tip path plane angle range covered during the test essentially covers the practical range that would be used on a full scale helicopter in low speed flight so the results presented do have meaning from a practical viewpoint.

One other point of interest is that the results shown in Figs. 27 to 29 are for a 2-bladed rotor and the wake geometry would be different for rotor systems with more blades.

FLOW VELOCITY RESULTS (LASER VELOCIMETER DATA)

In this section the flow velocity results obtained from the laser velocimeter data are presented. For the conditions tested and discussed herein, two orthogonal components of velocity are shown: v_x and v_z, which are the horizontal and vertical velocity components in the wind axis system.[1] The major portion of the data to be presented is in time-average form such that the flow velocities are averaged over all blade azimuth positions. In addition, the mean instantaneous flow velocities at each azimuth that describe a periodic time history with blade azimuth position will also be presented for the reference configurations at the reference test conditions. With the exception of some wind sensor results and blade-vortex interaction results, all of the LV data results will be shown as a function of position along the rocket trajectory. As previously mentioned, this is the distance along the x_T axis with the origin being the rocket launch point. Hence, when plotted in this manner, the results will show the change in time-average horizontal and vertical flow velocity components that a rocket encounters as it travels from the launch point along the trajectory to the target. No data are plotted along the trajectory at distances from the launch point greater than 1.4 radii since at this point the rocket is nearly unaffected by the rotor wake. A complete set of plots of time-average velocity data for each test configuration and condition, with each data point indicated, is presented in Appendix D. The figures referred to in this section contain faired curves from the Appendix D plots.

As previously mentioned, the test plan was formatted in terms of achieving test objectives. The results presented and discussed in this section are formatted in the same manner. Following a presentation of the baseline results for the isolated rotor configuration, the data results that achieve each of the objectives in Table 5 are compared and discussed.

ISOLATED ROTOR CONFIGURATION

Figures 30 and 31 show the measured time average vertical and horizontal flow velocity components along the rocket trajectory for the isolated rotor configuration. The tunnel speed is 7.5 kts to simulate low speed forward

---

[1]The positive sign conventions for the flow velocity components are upstream (opposite to the freestream velocity direction) for v_x and up in the vertical direction for v_z. Note that the measured flow velocities in the horizontal and vertical directions, v_x and v_z, presented in this report are in the wind axes as opposed to the rocket trajectory axes, v_{xT} and v_{zT}, used in Refs. 15 and 16 (and Appendix B). Also, v_x, as defined in this report, includes the freestream velocity, -V.

flight of the AH-1G at 15 kts. Both vertical and horizontal velocities have fundamental identifiable characteristics along the trajectory. At the rocket launch point (x_T = 0) the rocket is subjected to a strong downward and rearward flow velocity due to the rotor downwash. With respect to the rocket trajectory the total flow velocity vector in the x-z plane makes an angle of 50 degrees with the inclined rocket trajectory (as will be shown in Figs. 32 and 33) and the velocity magnitude is 60 fps. As the rocket travels along the trajectory from the launch point it encounters an abrupt change in the flow velocities (stronger for the vertical component) as the rotor wake boundary is approached. The steepest gradient of vertical velocity occurs near x_T = 0.4 which identifies the location of the wake boundary. This definition of the wake boundary crossing point on the rocket trajectory agrees well with the crossing point defined by the flow visualization results in Fig. 27 and the predicted wake geometry of Fig. 14. Also, as expected, this region of steep velocity gradient corresponding to the wake boundary has been displaced downstream on the rocket trajectory relative to the hovering rotor results (x_T = 0.73) shown in Fig. 5. On the rocket trajectory ahead of the wake boundary the vertical velocity is much smaller (slight upwash) and the horizontal velocity has decelerated to below freestream velocity but still retains the free stream direction. By the time the rocket has traveled 1.4 radii along the trajectory the vertical flow velocity is near zero and the horizontal flow velocity is within 85 percent of the free stream velocity. Hence, the largest changes and rates of change of flow velocities have occurred within 1.4 radii, and therefore this is the x_T range along the rocket trajectory where the rotor wake has the largest influence on the rocket flight path.

A vector plot of the flow velocities along the trajectory in Fig. 32 provides a good pictorial representation of the influence of the rotor wake. The figure shows a profile of the AH-1G from the wing forward. The rocket trajectory is shown, and the flow velocities obtained from LV measurements are plotted vectorially along the trajectory so that the magnitude and direction of the flow can be seen. The wake boundary, obtained from the flow visualization results shown previously in Fig. 27, is also presented here. Referring to Fig. 32, ahead of the wake boundary the flow vectors show the slight upwash and deceleration as the boundary is approached. The large increase in flow velocity is seen as the boundary is crossed and the flow simultaneously aligns with the angle of the wake boundary. The inboard flow is evident from the nearly constant magnitude flow velocities, and the direction of the inboard flow remains parallel to the wake boundary. Figure 33 summarizes the influence of the rotor wake average velocities by depicting the magnitude of the flow velocity and the angle at which it acts with respect to the rocket trajectory. It is noted that the momentum induced velocity for this condition is 32 fps; and when combined with the freestream velocity, the resultant velocity is 51 fps. The largest flow velocities (60 fps) combine with the largest flow angles (-50 deg) near the rocket launch point. Since the rocket flight velocities are lowest at the

launch point this would seem to be the area of greatest influence of the rotor wake on the rocket flight path. Negative flow angles will create negative angles of attack on the rocket and the rocket fins. For an initial rocket launch velocity of 100 fps, the angle of attack of the rocket is -19 deg and the dynamic pressure is approximately 26. Hence the rocket would experience a downward force due to pressure drag and a nose up pitching moment about its center of gravity due to the downward aerodynamic force acting on the tail fins.

Predictions of the rotor wake flow velocities for the AH-1G in low speed forward flight were made using the UTRC Rotorcraft Wake Analysis under contract DAAA21-74-C-0195 and are reported in Ref. 15 and summarized in Ref. 16 which is included herein as Appendix B. The isolated rotor flow velocity predictions for the 15 kt reference condition are compared to the test results in Figs. 34 and 35. The test results are taken directly from Figs. 30 and 31. The theory correctly predicts the magnitude and gradient of the vertical flow velocity along the trajectory as the wake boundary is approached from upstream. The peak vertical velocity for the inboard wake is also correctly predicted. However the theory predicts a greater decrease in the inboard wake flow velocities as the launch point is approached. Referring to the theory-test correlation in Fig. 35 for the horizontal velocity, the theory correctly predicts the magnitude and gradient of the horizontal velocity as the wake boundary is approached from upstream. However, peak time-average horizontal velocity is over-predicted by a factor of 2 and the gradient of this velocity component in the inboard wake region is over-predicted. The noted discrepancies are mainly attributed to what is considered to be the most significant finding of this test program; the diffusion of the circulation strength of the tip vortices following their intersection with the blade opposite to the one from which each was emitted. This vortex diffusion shown in the previous Flow Visualization section, results in flow mixing effects and related wake geometry changes which were not modeled in the UTRC Rotorcraft Wake Analysis used for the Ref. 15 predictions. These results identify the requirement for a more detailed investigation of the blade-vortex intersection phenomenon for refinement of current rotor flow field and airloads analyses.

It is recognized that the actual flow interference at the rocket is dependent on the instantaneous flow velocity corresponding to the instant of time the rocket passes each point along its trajectory. The instantaneous velocity is time (blade azimuth) dependent, and thus should be considered as well as the time-averaged velocity. However, due to the vortex diffusion phenomenon due to blade-vortex intersection mentioned above, it will be shown in a later section that the time dependent flow increments at the rocket trajectory are smaller than anticipated, and the influence of the time average flow is the primary consideration.

The previous results were for the first AH-1G reference condition at 15 kts. The results to be presented next are for the second reference condition

at 30 kts. Figures 36 and 37 show the time average vertical and horizontal flow velocity components, respectively. Both flow velocity components along the trajectory have similar characteristics to that seen at 15 kts except that the wake boundary now crosses the trajectory at or behind the launch point. This is characterized by the absence of peak horizontal and vertical velocities to indicate the inboard wake flow. This agrees with the flow visualization results in Fig. 28 and the predicted wake geometry of Fig. 15 which show the wake boundary crossing the trajectory at the launch point.

Other than this important difference in wake boundary crossing points between the 15 kt and 30 kt conditions, the trend of the flow velocities along the trajectory are as would be expected. As the rocket travels along the trajectory from the launch point, the vertical component decreases nearly linearly to zero at $x_T = 1.0$. The horizontal component of velocity also decreases to about half of the free stream value at $x_T = 0.3$ due to blockage by the rotor wake. As the distance along the trajectory is further increased, the presence of the rotor wake has less influence and the horizontal component approaches 95 percent of the free stream velocity at $x_T = 1.4$. Figure 38 summarizes the influence of the rotor wake average velocities for the 30 kt condition. As in Fig. 33, the magnitude of the flow velocity and the flow angle with respect to the rocket trajectory are shown. It is noted that the momentum-induced velocity for this condition is 24 fps, and when combined with the freestream velocity, the resultant velocity is 56 fps. As for the 15 kt condition, the largest flow velocities combine with the largest flow angles at the launch point. Thus, this is the region of largest influence of the rotor wake on the rocket flight path. For an initial rocket velocity of 100 fps at the launch point, the angle of attack on the rocket and the fins is -8 degrees and the dynamic pressure is 30 psf, compared to -18 degrees and 28 psf for the 15 kt condition. Therefore, it could be argued that the influence of the rotor wake at the launch point is about half as severe for the 30 kt condition since the aerodynamic angle of attack on the rocket fins is half that for the 15 kt condition (with only a slight increase in dynamic pressure). Also the rocket fin drag could be expected to be as much as 4 times higher for the 15 kt condition than for the 30 kt condition due to stall effects for the larger negative angle of attack. The rate of change of flow angle and flow velocity are also less severe for the 30 kt condition as the rocket travels along the trajectory. These rate effects could be important factors influencing rocket pitching oscillations generally characterized as "fish tailing" motions.

In summary, for the 30 kt condition the rotor wake influence on rocket trajectories would be expected to be less than half of that at 15 kts. The main reasons for this decreased sensitivity are the passing of the rotor wake boundary at or behind the launch point, a smaller aerodynamic angle of attack at the launch point and reduced rates of changes of wake velocity and flow angle as the rocket travels along the trajectory.

EFFECTS OF FUSELAGE, WING, AND MODIFIED CANOPY

In this section, the individual effects of the fuselage, the wing, and the modified canopy on the time-average flow velocities are shown by comparing results for the different model configurations with the previously presented results for the isolated rotor. For the AH-1G at 15 kts the effect of the fuselage is shown in Figs. 39 and 40 for the vertical and horizontal flow velocities, respectively. Referring to Figs. 39 and 40, the primary impact of the fuselage is to move the rotor wake boundary forward to about $x_T = 0.5$ on the rocket trajectory compared to 0.4 for the isolated rotor. The magnitude of the peak flow velocity has slightly increased to 62 fps compared to 60 fps for the isolated rotor. These two results are expected based upon the blockage effect of the fuselage on the rotor downwash. To satisfy continuity and conservation of momentum, the wake velocities will increase and the wake diameter will expand to accommodate the same mass flow rate (same thrust coefficient) with reduced area due to fuselage blockage. This result agrees with the expansion of the wake boundary with the fuselage presence as observed in the flow visualization results. Additional data results are shown in Figs. 39 and 40 for the effects of the wing and the effect of modifying the canopy from the flatsided configuration to the rounded configuration. The addition of the wing has a small effect on flow velocities. The change in the canopy configuration has nearly no effect on the flow velocities. In summary, it is evident that the effects of the fuselage and particularly changes in the fuselage configuration (stub-wings, canopy) at 15 kts have only a small influence on flow velocities so that the major impact of the rotor wake on the rocket along the trajectory is represented by the isolated rotor results. It follows that, although the presence of the fuselage has some influence, the flight condition rather than the aircraft configuration is the prime factor affecting the rocket aerodynamics interference.

The effect of the fuselage, wing, and modified canopy on time-average flow velocities are shown in Figs. 41 and 42 for the second reference condition at 30 kts. In these figures, the results for the different fuselage configurations are compared with the isolated rotor results. The effects of the fuselage are nearly the same as those at 15 kts. The fuselage provides rotor wake blockage so that the wake boundary moves forward slightly, as was observed in the flow visualization results, and the maximum time-average vertical velocity increases from 30 fps to 40 fps at the launch point. However, this launch point value is still only two-thirds of the value at 15 kts. Therefore, the conclusion drawn from the isolated rotor results, that the influence of the rotor wake for the 15 kts condition is more severe than at 30 kts, also applies for the rotor plus fuselage configuration. It is also clear that changes in the fuselage configuration (addition of wing or change in canopy) have only a small impact on flow velocities.

Additional data were taken for the AH-1G at 10 kts to further study changes in flow velocities with forward speed. Data were obtained for the

reference configuration (rotor and fuselage, wing and flat sided canopy) at this airspeed and are shown in Figs. 43 and 44. As expected, the wake boundary is farther forward for the 10 kt condition than at 15 kts and is approaching the position of the hovering rotor wake boundary. This can be seen more clearly in Fig. 45 which shows the magnitude of the average flow velocity and the flow angle for the 10 kt condition. The magnitude of flow velocity is similar to that for 15 kts, but the flow angle is larger for the 10 kt condition and reaches its peak farther out on the trajectory. From these results, it can be concluded that the overall impact of the rotor flow field on rocket flight paths at 10 kts is similar to that at 15 kts except that the peak vertical velocities occur slightly farther along on the trajectory (about x_T = 0.6) for the 10 kt condition.

TIME DEPENDENT FLOW VELOCITIES

The flow velocity results presented up to this point are time-averaged over many rotor revolutions such that periodic changes in flow velocities that occur every one-half rotor revolution for a two-bladed rotor are averaged out. The results presented in this section will concentrate on the periodic changes in the flow velocities that a rocket will encounter as it travels along the trajectory.

Periodic changes in the flow velocities at a fixed point in space are caused by the passing of tip vortices along the wake boundary and the inboard vortex sheets. This can be envisioned by referral to the tip vortex plots of Figs. 27, 28, and 29. The Biot-Savart Law states that the velocity induced at a point in space by a vortex is directly proportional to the vortex circulation strength and inversely proportional to the distance between the point and the vortex. For a fixed point on the rocket trajectory, the horizontal and vertical distances from the point to all vortex segments change periodically as the vortices travel down the wake. Each vortex segment is most influential when it is nearest the point on the trajectory. For a 2-bladed rotor, the minimum distance condition occurs twice per revolution for both the tip vortices and the inboard vortex sheets (not necessarily in phase).

An example of the laser velocimeter data for the time variation of horizontal and vertical flow velocities for one rotor revolution is shown in Fig. 46. Each data point shown in this figure represents a laser velocimeter measurement of the velocity of one seedant particle (data for 500 particles were normally acquired per flow field point). It is noted that the measurements are made over many rotor revolutions until the prescribed number of seedant particle measurements are acquired. The faired curves in Fig. 46 thus represent at each azimuth the mean of the instantaneous flow velocities. The model configuration for Fig. 46 is the fuselage with wing and flat sided canopy

for the AH-1G at 15 kts. Both the vertical and horizontal velocity components exhibit at $x_T = 0.2$ on the trajectory the expected 2 per rev periodic variation, and the horizontal component shows the largest time variation for this particular point.

A measure of the time variation is the peak-to-peak value which is the maximum minus the minimum value occuring in one period. The peak-to-peak values of the flow velocities along the trajectory from the launch point to $x_T = 1.4$ are shown in Figs. 47 and 48 for the AH-1G at 15 kts. Data for different model configurations are shown on these figures and are distinguished by different symbols. The most evident characteristic is the local maximum of the peak-to-peak vertical velocity occuring at $x_T = 0.5$ (Fig. 47). The results from Figs. 39 and 40 showed that the forward wake boundary is located near $x_T = 0.5$ on the trajectory so it can be concluded that, as expected, the largest periodic fluctuations in the flow velocities on the rocket trajectory occur near the wake boundary. For points on the trajectory outside the wake, the peak to peak horizontal and vertical velocities rapidly approach zero exponentially. Inside the wake the peak-to-peak velocities reach a residual level near the launch point. A comparison of data for the two different model configurations indicates that the presence of the fuselage has a small impact on the peak-to-peak velocities. The differences in the vertical and horizontal peak-to-peak velocity variations along the rocket trajectory are believed to be primarily due to the wake orientation which causes the tip vortices to be more influential on the vertical component, and the inboard vortex sheets to be more influential on the horizontal component.

The most predominant result evident in the data of Figs. 47 and 48 is the large reduction in peak-to-peak amplitudes at the rocket trajectory relative to those predicted in the Ref. 15 investigation. For example, at the intersection of the rocket trajectory and the wake boundary, measured peak-to-peak amplitudes are several times less than the predicted values. This is attributable to the blade-vortex intersection effects which cause a drastic decrease in vortex circulation strength in the wake boundary and hence a proportional decrease in peak-to-peak velocities along the rocket trajectory. The vortex diffusion was not represented in the Rotorcraft Wake Analysis. The two clues supporting the occurrence of this effect are:

1. The marked decrease in peak-to-peak velocities at 15 kts in Figs. 47 and 48 compared to that measured in hover as reported in Ref. 23.

2. The blade-vortex intersection and resulting diffuse tip vortex cross sections evident in the flow visualization data (Fig. 24).

With respect to the decreased peak-to-peak velocities, the hover results in Ref. 23 showed values on the order of 60 fps full scale where the wake

boundary crossed the rocket trajectory, whereas the maximum value from Figs. 47 and 48 is 25 fps. Figure 49 compares the rotor wake boundaries for hover, 15 kts and 30 kts as determined from flow visualization. The hover wake boundary proceeds immediately downward from the blade tip while the forward flight wake boundaries travel above the tip path plane and then proceed downward through the rotor disc. The phasing of the tip vortices in the wake boundary for the tested 2-bladed rotor is such that, when it reaches an azimuth of approximately 180 deg, an advancing blade intersects a vortex as it travels down through the rotor disc for both 15 kt and 30 kt conditions. The vortex intersection is believed to result in a dissipation of energy from the vortex, and therefore results in reduced vortex strength. For hover, no vortex intersection occurs and any decrease in vortex strength can be attributed primarily to viscous decay. It is thus clear that the flow influence on a rocket as it travels along the trajectory is different in hover than in low speed forward flight. In hover, the peak-to-peak velocities are of the same order as the time-averaged flow velocities. Therefore, the aerodynamic impact of the flow velocities on the rocket could be minimized by proper phasing between rotor blade position and rocket firing. In forward flight at 15 kts, the maximum peak-to-peak velocities are about half of the maximum time average velocities, and therefore, the maximum aerodynamic impact is not only reduced but also phasing of rocket firing with rotor blade position becomes much less important.

The peak-to-peak vertical and horizontal flow velocities along the trajectory for the AH-1G at 30 kts are shown in Figs. 50 and 51, respectively. The trend results for the 30 kt condition are similar to the results for the 15 kt condition: the presence of the fuselage has a small impact, the maximum peak-to-peak value is about 25 fps, and the peak-to-peak velocities decrease exponentially as the rocket travels along the rocket trajectory. As shown in Fig. 28, the wake boundary crosses the trajectory near the launch point, so the maximum peak-to-peak velocities that can be expected to occur are those shown at the launch point ($x_T = 0$). The maximum peak-to-peak velocities are roughly the same for the 15 kt and 30 kt conditions. Figure 28 also shows that the 30 kt wake boundary intersects with the tip path plane, and the phasing of the tip vortices is such that a blade intersects the preceding blade's vortex at the upstream blade position (180 deg). These flow visualization results indicate that the blade-vortex intersection phenomenon is occurring at 15 and 30 kts, and the reduced peak-to-peak velocities at the rocket trajectory demonstrate the impact of the phenomenon in both cases. Just as for the 15 kt condition, the time-averaged velocities dominate for the 30 kt condition; and therefore, phasing of rocket firing with blade position is less important than for hover. Of the three flight conditions considered it is felt that the 30 kt condition minimizes the aerodynamic impact of flow velocities on rockets. The hover condition is the most critical because of the large peak-to-peak velocities and the larger duration of the rocket in the wake. The 30 kt condition has the smallest time-averaged and peak-to-peak velocities.

Thus, the nature of the aerodynamic influence on the rocket flight path between hover and forward flight is different. In hover, the influence of phasing of the rocket firing time within the blade/wake passage interval may be important due to the high peak-to-peak velocities encountered. If the flow interference is significant, random excursions in the rocket flight paths could result without a firing time control. For low speed forward flight conditions with vortex diffusion resulting from blade-vortex intersection, the time-averaged flow velocities dominate, and more constant variations in the rocket flight path from the intended trajectory are anticipated. Corrective aiming compensation should thus be more effective for such conditions.

BLADE/VORTEX INTERACTION

A brief study of the blade/vortex interaction was performed by taking LV data points close to the rotor tip path plane in addition to the rocket trajectories. The area of concentration was slightly above the tip path pane at outer points along the 180 deg azimuth line of the rotor. Obtaining time history LV data in this region to investigate blade/vortex interaction is considered important for two basic reasons:

1. The peak-to-peak velocities along the rocket trajectory, shown earlier, are much lower than expected. Since the flow visualization results indicated a blade/vortex intersection in this region as the rotor wake passed down through the rotor disc, obtaining LV data above the rotor before the blade/vortex intersection occurs would indicate the original strength of the tip vortex and also to what extent it was dissipated by the blade intersection. This could help explain quantitatively the low peak-to-peak velocities along the rocket trajectory.

2. Blade-vortex interactions have important influences on helicopter noise, performance, stresses, and vibrations.

The LV data to study blade/vortex interaction were obtained at simulated forward speeds of 10 and 15 kts. For both conditions, the model configuration was the isolated rotor, and the thrust coefficient was set at the reference value for steady level flight of the AH-1G helicopter. For the 10 kt condition, the rotor shaft tilt was four degrees forward, and for the 15 kt condition, the rotor shaft tilt was two degrees forward. The 15 kt condition is more realistic of low speed flight since the tip path plane resulting from the two degree shaft tilt is nearly level which provides a low propulsive force as required in low speed flight. The -4 degree shaft angle was tested at 10 kts to explore whether or not the blade-vortex intersection could be eliminated by increased rotor tilt to redirect the initial vortex travel beneath the rotor. The blade-vortex intersection persisted.

Referring first to the 15 kt condition, the time history velocities in the vertical and horizontal directions are shown in Fig. 52 for one rotor revolution. The LV focal point was positioned 1.5 inches (0.05 R) above the rotor blade and one inch (0.035 R) in from the blade tip (when the blade is in the 180 degree azimuth position). This point proved difficult to obtain due to difficulty in acquiring a uniform azimuthal (time) distribution of LV seedant particles. The data point was repeated many times, and the results shown in Fig. 52 are synthesized from the repeated data points. The most obvious result of this figure is the large peak-to-peak velocities for both the vertical and horizontal components. The peak-to-peak velocity components are on the order of 40-60 fps compared to maximum periodic velocities along the rocket trajectory of 25 fps (Fig. 47). This result indicates that, between the time the tip vortex is newly formed and the time it crosses the rocket trajectory, the tip vortex circulation strength is decreased substantially. Furthermore, there is no assurance that the periodic velocities shown in Fig. 52 are the largest that occur since the LV point is only one flow field point and the tip vortex may pass above or below the point as it emanates from the blade tip. The initial vortex strength could be higher, and the percentage reduction of peak-to-peak velocities at the rocket trajectory due to vortex dissipation could be even greater.

The tip vortex dissipation is believed to be due to the interaction of the rotor blade with the tip vortex. Previously in the flow visualization results, it was shown that the forward rotor wake passes up above and then down through the rotor disc plane. It was also shown that the phasing between the blade passing the 180 degree azimuth and the path of the tip vortices down through the disc plane was such that the rotor blade came quite close to and even impacted the tip vortex. This is the phenomenon that is believed to cause this large reduction in periodic velocities along the rocket trajectory.

Figure 53 compares the flow velocity time histories as the LV focal point is moved above the rotor (1.5 inches above) along the 180 degree azimuth line. Considering the 28.5 in. rotor radius, the range of data points is 2 inches inboard of the blade tip to 0.25 inches outboard of the blade tip. The periodic velocity grows as the focal point moves inboard. This is seen most clearly in the vertical component.

Apparently, the proximity between the LV point and the passing tip vortices increases as the LV point is moved inboard from the blade tip. The most inboard point shown is 2 inches in from the blade tip, and the peak-to-peak vertical velocities indicate that there may be further growth for points even further inboard. These results are quantitative substantiation of the differences in the rotor wake between hover and low speed forward flight. The hover results in Ref. 23 showed that LV points above and inboard of the blade tip exhibit less periodic velocity than at the blade tip. This is due to the immediate downward movement of the newly formed tip vortex. In contrast, for

low speed flight, these results show that the forward rotor wake travels downstream slightly above or nearly in the rotor disc plane before trailing downward. Therefore, the maximum periodic velocities occur slightly inboard of the blade tip.

The periodic velocities presented in Figs. 52 and 53 definitely show a much larger peak-to-peak variation than those measured along the rocket trajectory, and the difference is attributed to blade-vortex interaction. The maximum tip vortex periodic velocities before intersection with the rotor blade are not known for certain because there is no guarantee that a tip vortex passes directly over any of the LV focal points selected. The results for Fig. 54 are believed to be closer to this situation. The flight condition for Fig. 54 simulates the AH-1G at 10 kts with four degrees of forward shaft tilt, compared to 15 kts with two degrees of forward shaft tilt for Figs. 52 and 53. The LV focal point is one inch inboard of the blade tip when the blade is in the 180 degree azimuth position, and the vertical displacement of the LV focal point above the rotor tip path plane was about 3 inches compared to 1.5 inches for the previous figures. Apparently, this combination of forward speed and tip path plane angle was favorable for positioning the LV focal point close to the path of the tip vortex as it emanates from the blade tip. The peak-to-peak velocities shown in Fig. 54 are about 100 fps, the largest experienced during the test, and the nature of the velocity time history (particularly the vertical velocity) has a spike characteristic typical of a close vortex passage. The overall conclusion to be drawn from this figure is that the peak-to-peak velocities are four times larger than those experienced along the rocket trajectory, so this quantifies to a certain extent the influence of the blade vortex interaction responsible for the periodic flow velocity reduction at the rocket trajectory.

Additional substantiating LV data from two other operating conditions are presented in Figs. 55 and 56. LV data are presented for a point directly above and close to the passing blade tip (Fig. 55) and a point on the rocket trajectory in the immediate vicinity of the wake boundary (Fig. 56). The contrast in velocity distributions representative of the tip vortex influence before and after blade-vortex intersection is further evidence of the vortex diffusion associated with blade-vortex interaction.

It is concluded that for the 2-bladed AH-1G rotor, the phasing of the blade azimuth and tip vortex travel is synchronized such as to result in a diffusion of the tip vortex core and an associated decrease in its local induction strength in the region of the rocket trajectories.

EFFECT OF THRUST COEFFICIENT

A change in the rotor thrust coefficient was made at the 15 kt reference condition to determine the resulting effect on time-averaged flow velocities

along the rocket trajectory. Rotor thrust was decreased by approximately 8 percent (C_T = 0.00435 vs 0.00472) at 15 kts for the reference configuration, and the flow velocity results are shown in Figs. 57 and 58. In these figures the flow velocity data for the reference thrust and reduced thrust conditions are compared.

The impact of decreased thrust is strongest at the wake boundary for the time-averaged vertical velocity and in the inboard wake region for the horizontal velocity. The steep gradient of vertical velocity along the trajectory has moved toward the launch point, which indicates that the wake boundary has moved inboard. The peak time-averaged vertical velocity has decreased by 5 percent and the horizontal velocity across the inboard wake has increased by 10 percent, which indicates that the flow angle has changed. These changes with decreased thrust are shown more clearly in Fig. 59 which compares the magnitude of the flow velocity and the flow angle for the reference thrust and reduced thrust conditions. The large gradient of flow angle locates the wake boundary crossing point on the trajectory, and the flow angle comparison shows that it has moved toward the launch point by 0.10R with reduced thrust. This result is expected for a rotor in forward flight with near zero tip path plane angle since the vertical velocity component is fundamentally the rotor induced velocity, and by decreasing thrust the induced velocity is also reduced so that the rotor wake will be inclined further back.

Although these changes in the wake characteristics with rotor thrust are of interest for understanding the rotor wake characteristics, the impact of these thrust induced changes in the flow velocities on rocket flight paths are probably small. Moving the wake boundary crossing point on the rocket trajectory inboard by 0.10R should have little effect on the rockets particularly if the peak vertical velocity is reduced by only 5 percent. Therefore the effect of flow velocities on rocket trajectories for 10 percent reduced thrust condition is not anticipated to be much different from that for the reference thrust condition.

EFFECT OF LAUNCH POINT

The bulk of the LV flow velocity data are for the No. 4 launch position, which is the outermost launch point on the starboard wing located at y = .22R as shown in Fig. 4. To determine if the flow velocities along the rocket trajectories change from launch point to launch point, LV flow velocity data were taken for the 15 kt reference condition along the rocket trajectory for the No. 3 launch position, located on the starboard wing at y = 0.16R. The blockage of the LV beams by the fuselage prevented obtaining LV data for the two port side launch points. Comparisons between flow velocity results along the trajectory for the No. 3 and No. 4 launch positions are shown in Figs. 60 and 61 for the 15 kt reference condition and reference configuration. Figure

60 shows effectively no change in the vertical flow velocity component between No. 3 and No. 4 trajectories, and the horizontal velocity results in Fig. 61 show a 5 fps increase along the No. 3 trajectory in the region of the inboard wake. Overall, the change in flow velocities between the No. 3 and No. 4 trajectories is small, so that the influence of the rotor wake on rocket flights would be essentially the same for both the No. 3 and No. 4 starboard trajectories for low-speed flight.

EFFECT OF ROCKET TRAJECTORY ANGLE

The effect of rocket trajectory angle relative to the rotor disc was simulated by varying the rotor shaft tilt angle from the reference position by two degrees. Tilting of the rotor shaft changes the rotor tip path plane angle and hence changes the relative positioning of the rotor and rotor wake to the rocket trajectory. This testing was done with the rotor only, so the two degree change in shaft tilt should closely simulate a two degree change in trajectory angle.

Figures 62 and 63 show the time-averaged full scale vertical and horizontal velocities for the two rotor shaft tilt positions. The 2 degree forward shaft tilt results are for the reference condition with a 7 degree trajectory angle relative to the rotor. The four degree forward shaft tilt results in a 2 degree change in rocket trajectory angle relative to the rotor from 7 degrees to 9 degrees. The data in Figs. 62 and 63 show that the simulated two degree variation in trajectory angle changed the vertical and horizontal flow velocity components. As the shaft tilt was increased to simulate a larger nose up rocket trajectory angle, the maximum vertical velocity component decreased, and the maximum horizontal velocity component increased. This indicates a change in the rotor wake angle relative to the rocket trajectory as expected. In Fig. 64 the magnitude of the flow velocity and the flow angle for both shaft tilt conditions are shown. These results indicate that the magnitude of the flow velocity was essentially unaffected, but the flow angle was largely affected over the inboard wake and also upstream of the rotor wake. However, the change in flow angle is much larger than expected. Over the inboard wake region, a two degree change in shaft tilt changed the flow angle by 15 degrees whereas a nearly equal tradeoff was expected. The reason for the large change in flow angle is not known. The change in flow angle over the inboard wake and also upstream of the rotor wake is unreasonably large for a 2 degree change in shaft angle. It is reasonable to expect a nearly equal tradeoff between shaft angle change and flow angle change for this test condition so the results presented are suspect. Particularly suspect are the data for the -4 degree shaft angle considering that the vertical velocity component data in Fig. 64 indicates a residual velocity value (10 fps) at $x_T = 1.4$.

In summary, test results for a change in rotor shaft tilt indicate that increasing the rocket trajectory angle will decrease the velocity component

perpendicular to the rocket flight path which is beneficial; however, the size of the decrease is unexplicably larger than expected, and additional data is required to check the results.

EFFECT OF CROSSWIND

The effect of cross wind was simulated by yawing the model fuselage to the left and right by 30 degrees. This simulated an effective crosswind velocity component equivalent to 50 percent of the total freestream velocity. Figures 65 and 66 show the flow velocity results at the No. 4 rocket trajectory for the crosswind condition at 15 kts. In each figure the left and right yaw results are compared with the zero yaw results previously presented in Figs. 39 and 40. The results in Fig. 65 show that the vertical flow velocities for both yaw conditions are close to the zero yaw condition. These changes in the vertical flow velocities with model yaw are small, as expected, since at these low airspeeds the vertical time-averaged induced velocities are roughly independent of azimuth location. The horizontal flow velocities in Fig. 66 show little variation from the baseline for the negative yaw condition in which the starboard side is open to the freestream. However, a moderate increase in horizontal velocity is evident near the wake boundary for the positive yaw condition for which the starboard side is blocked by the freestream. At least part of this horizontal flow acceleration can be attributed to the lifting characteristics of the fuselage when yawed. When yawed positively the starboard side of the fuselage acts as the upper surface of an airfoil, and the horizontal flow will be accelerated as a net side force on the fuselage is created. It is noted that, although the LV data were acquired along the rocket trajectory locations yawed with the model, the measured horizontal flow component remained in the freestream direction (direction of wind tunnel flow) due to the laser velocimeter component restriction.

Figure 67 summarizes the influence of crosswinds on the flow velocity magnitude and flow angle at the trajectory. The peak flow velocity magnitude for the positive yaw condition has increased by 10 fps over the baseline and the wake boundary has also moved outward by about 0.1R, but these are relatively small changes from the baseline. These results show that the induced effects of the flow velocities are small, so that the main difference between a forward flight condition and a crosswind condition will be the increasing size of the sideward component of the total flow velocity (which is normal to the rocket trajectory) as the helicopter is yawed.

GROUND EFFECT

Testing was performed with a wind tunnel spanning ground plane installed in the tunnel to simulate ground effect in low speed flight. The vertical distance from the rotor center to the ground plane was set at 0.75R which corresponds to a skid height of 3.5 ft above the ground. LV measurements were taken along the rocket trajectory for the reference configuration at the 15 kt condition, and a vector plot of the measured flow velocities is shown in Fig. 68. With the aid of two points taken below the trajectory, the flow vectors show the turning of the airflow due to the ground vortex. Instead of the forward wake trailing downstream under the fuselage, the wake impinges on the ground and then turns upstream. This confirms the flow recirculation (ground vortex) ahead of the aircraft in ground effect observed in the flow visualization results (Fig. 26) that were previously discussed.

Figures 69 and 70 show the vertical and horizontal flow velocity components for the in-ground-effect condition (IGE) and compare them with the reference out-of-ground effect (OGE) results. In Fig. 69, the peak time average vertical velocity at the rocket trajectory for IGE has not changed from the reference OGE. The gradient of velocity along the trajectory differs from that for the OGE condition. In Fig. 70, the character of the IGE horizontal velocity along the trajectory has completely changed from the reference OGE results. In ground effect, the largest horizontal velocities on the trajectory occur ahead of the wake boundary reflecting the roll up of the rotor wake ahead of the aircraft into a "ground vortex", whereas the OGE results show flow deceleration in the same region.

The horizontal flow acceleration inside the wake boundary is not as large for IGE compared to OGE. This characteristic would tend to make the wake impinge on the ground at a steeper flow angle and also move outward the wake boundary crossing point on the trajectory. This is shown more clearly in Fig. 71 which shows the flow angle and the flow velocity magnitude for the IGE condition compared to the OGE condition. The translation of the flow angle gradient outward by about 0.25R for IGE indicates that the wake boundary crossing point on the trajectory has also move outward and the maximum flow angle is also greater for IGE. With respect to the magnitude of the flow velocity, the IGE results have the same characteristic as the OGE results except that the variation of time-averaged velocity along the trajectory is about half that for OGE. From these results, the influence of flow velocities on the rocket trajectories due to ground effect is difficult to ascertain. From a peak time-average flow velocity viewpoint, there is little difference between IGE and OGE; but the duration of the large flow velocities along the trajectory is greater for IGE. The importance of each of these flow characteristics remains to be determined through application of an aeroballistics analysis.

EFFECT OF TAILWIND/REARWARD FLIGHT

A tailwind was simulated by yawing the model 180 degrees in the tunnel so that the fuselage tail pointed upstream. This also simulated a 15 kt rearward flight condition. Flow velocities were measured along the trajectory for the outermost launch point on the port wing (No. 1 launcher) for the 15 kt condition, and a vector plot of the measured flow velocities is shown on the left side of Fig. 72. To provide a more complete flow picture in Fig. 72, the flow velocity vectors for the 15 kt forward flight condition are shown for the No. 4 trajectory pointing upstream so that an approximation to the total rotor wake can be visualized. These are shown on the trajectory on the right side of Fig. 72.

The rocket trajectory in a tailwind (or rearward flight) is that shown on the left side of Fig. 72. The uniform flow of the inboard wake passes just aft of the wing and the low momentum core of the rotor wake due to the non-lifting portion of the rotor radius (the aerodynamic blade root cutout is at 0.20R) crosses the trajectory just at the launch point and extends along the trajectory to about $x_T = 0.4$. The notable characteristic of the flow in this region is the absence of vertical velocity since no vertical momentum has been imparted directly to the flow. Also, the inboard vortex sheets from the blades induce a retarding upflow in this region. The orientation of the flow vectors near the launch point in Fig. 72 even suggest a slight upflow and a strong downstream horizontal velocity. The inboard wake crosses the trajectory from $x_T = 0.4$ to about $x_T = 1.0$. At $x_T = 1.0$, the vertical velocity decreases sharply which indicates that the wake boundary has been crossed. The separate vertical and horizontal velocity measurements for the tailwind condition are compared with the forward flight flow velocities in Figs. 73 and 74. For the vertical velocity, the most important result is the region of near zero velocity near the launch point which was observed by the vector orientation in the previous figure. Since the rocket velocity is lowest at the launch point, minimizing the vertical velocity at the launch point is beneficial for reducing rotor wake influence. Therefore the tailwind condition is advantageous from this viewpoint. However, the obvious disadvantage is the double gradient of vertical velocity along the trajectory in the tailwind compared to the single gradient for the reference forward flight condition. The double gradient would create an oscillation in the angle of attack on the rocket which could possibly have as strong an influence on the rocket flight path as high vertical velocity at the launch point. For the tailwind/rearward flight condition, the horizontal velocity component is in the same direction as the rocket flight direction (v_x is negative in the freestream velocity direction). The flow direction for tailwind thus differs from the forward flight situation where the horizontal flow direction is opposite to the rocket direction.

GROUND EFFECT IN TAILWIND/REARWARD FLIGHT

The tailwind/rearward flight condition was also simulated with the ground plane installed so that flow velocities along the trajectory could be measured in a 15 kt tailwind with the helicopter hovering in-ground-effect (IGE). Testing was performed with the same model height above the ground plane previously used in the forward flight testing (3.5 ft skid height for the AH-1G). Figure 75 shows the velocity vectors for the tailwind IGE condition. Comparing these results with those shown in Fig. 72 for the tailwind OGE condition, two differences are apparent. First, the low momentum wake region (due to the non-lifting portion of the rotor radius inboard of the cut-out) extends farther along the trajectory for IGE than for OGE. For IGE, this low vertical velocity region extends nearly to the nose of the aircraft. The importance of the reduced vertical velocity is that it decreases the aerodynamic angle of attack acting on the rocket due to the wake flow velocities. Extending this region from the launch point where the rocket axial velocity is lowest will reduce wake effects on the rocket flight path. The second difference noted is the change in wake angle not only for the inboard wake region, but also for points on the trajectory downstream of the wake boundary. The flow angle for IGE is significantly less than for OGE since the ground inhibits the vertical flow and redirects the rotor wake downstream. This effectively decreases the vertical velocity and increases the horizontal velocity. This result is shown more clearly in Figs. 76 and 77 which present the separate velocity components along the trajectory for the IGE and OGE tailwind conditions. The region of low vertical velocity previously observed in the velocity vector plot (Fig. 75) is shown in Fig. 76 to extend to about $x_T = 0.6$ on the trajectory. The decrease in peak vertical velocity due to deflection by the ground previously observed is significant (25 fps) and amounts to about one-third of the peak time-averaged vertical velocity for the OGE tailwind condition. Figure 77 shows the effect of the ground on the horizontal velocity. The ground displaces the wake further downstream where the horizontal velocity increases. At $x_T = 1.0$ the increase over the OGE results is about 30 fps. Similar to OGE, the horizontal velocity component is in the same direction as the rocket flight direction.

Just as for the tailwind OGE condition, it is difficult to ascertain the impact of the flow velocities on rocket flight paths for a tailwind in-ground-effect. The magnitude of flow velocity and the range of flow angles along the trajectory are close to the reference forward flight condition. Therefore, any differences in how the flow velocities affect the rocket flight paths will be due to the particular combination of flow velocity magnitude and flow angle and also due to the rate at which they change along the trajectory. The impact of these effects should be determined by analytical simulation of the rocket dynamic response to the experimental flow field.

WIND SENSOR LOCATION

Flow velocity data were obtained at three potential wind sensor locations near the fuselage for the 15 kt and 30 kt conditions. As shown in Fig. 5, one sensor location is near the top of the canopy, and two sensor locations are in front of the fuselage nose. The blocking of the LV beams by the fuselage prevented obtaining LV wind sensor data at other locations on the port side of the fuselage. Table 6 presents the coordinates of the wind sensor locations as measured from the rotor hub center.

TABLE 6. WIND SENSOR LOCATIONS

Wind Sensor Location No.	x	y	z
1	0.27	0.133	-0.185
2	0.77	0	-0.40
3	0.835	0	-0.40

The perfect wind sensor is described as one that exactly measures the freestream velocity for all flight conditions. Because of the influence of the fuselage on the airflow, and also because of the induced velocity field of the rotor, the airflow around the fuselage is not freestream velocity and is also affected by flight condition. Therefore, the best practical wind sensor location could be described as that which can be accurately calibrated to give the freestream velocity, and be insensitive to changes in the fuselage configuration.

Figures 78 and 79 show vector plots of time-averaged airflow velocities measured at the wind sensor locations for 15 kts and 30 kts, respectively. Data for the two canopy configurations (reference flat-sided and rounded) are shown. In addition, some results in-ground-effect (IGE) for the 15 kt condition are also shown. To provide a reference, the freestream velocity vector with correct length scale is also shown.

The most obvious result in the figures is that the velocities measured at the canopy wind sensor point are larger than freestream due to the rotor induced flow and the velocities measured in front of the fuselage are less than freestream due to fuselage blockage. The effect of the canopy is most pronounced at 30 kts for the wind sensor locations in front of the fuselage, and is larger than expected.

One other interesting result is shown in Fig. 78 for the in-ground-effect condition at 15 kts. The flow velocity vectors at the wind sensor locations ahead of the fuselage nose are pointing down and upstream and are also much larger in magnitude than the freestream velocity. These velocity vectors are

the result of the large ground vortex ahead of the fuselage that was observed and discussed in the flow visualization section. It is obvious that these two wind sensor locations would be useless for low speed IGE flight conditions.

The potential for calibrating the horizontal component of the wind sensor velocities is shown in Fig. 80. The horizontal components of the measured flow velocities are plotted versus the freestream velocity for both canopy configurations. The perfect sensor measurement would lie on the 45 degree line shown.

For the reference flat-sided canopy, the results for wind sensors 2 and 3 have nearly the correct slope with airspeed so that the calibrated correction is approximately a constant bias. Of the three wind sensors, the No. 3 location has the closest slope and has a -13 fps bias.

Caution should be used when interpreting the results for wind sensor 1. This wind sensor location is immersed in the rotor wake at both the 15 kt and 30 kt conditions, as shown previously in Figs. 27 and 28. At a flight speed of approximately 40 kts, the forward wake boundary will be at this wind sensor point, and for higher speeds, the wind sensor point will be outside of the rotor wake. Thus, large variations of the horizontal velocity component can be expected at wind sensor 1 at this low speed range. In fact, the variation between 15 kts and 30 kts is probably not at all linear, as drawn in Fig. 80.

Results for the modified canopy are markedly different than for the reference flat-sided canopy. For the wind sensors ahead of the fuselage, the sensitivity with airspeed is significantly changed so that the correction is a slope differential plus a constant bias.

In summary, wind sensors at any of the three wind sensor locations tested cannot be used for low-speed flight to measure the freestream velocity directly. Significant deviations from freestream velocity were measured at all three locations. For the reference flat-sided canopy, the No. 3 wind sensor location is best, except for IGE conditions, where it is useless due to the ground vortex.

CONCLUSIONS

The following conclusions are based on the application of model test results to a full-scale helicopter in low speed flight. Where specific values are indicated, they are representative of the full-scale AH-1G helicopter. Each conclusion listed below either supplements or further substantiates the conclusions from the earlier theoretical investigation (Ref. 15) and the experimental model helicopter hover investigation (Ref. 23) which are included herein as Appendices B and C, respectively.

1. The wake boundaries and the measured time-averaged flow velocities along the rocket trajectories are generally similar to those predicted by the UTRC Wake Geometry Analysis and Rotorcraft Wake Analysis for low speed forward flight. As the rocket moves from its launch position, the imposed time-average flow velocites are large until the wake boundary is crossed. As the rocket moves beyond the rotor wake, the induced flow velocity decreases abruptly and becomes insignificant within a distance of one rotor diameter from the launch position. The intersection of the wake boundary and the rocket trajectory approaches the launch point with increasing flight speed and moves from a distance of 75 percent of the rotor radius for hover to about 40 percent at 15 kts and to the launch point at 30 kts. Beyond 30 kts, the wake induced flow velocities are insignificant due to the location of the forward wake boundary aft of the rocket launch point.

2. A significant finding is the notable reduction in the time variation of flow velocities (peak-to-peak amplitude) at points on the trajectory, and in particular where the tip vortices in the wake boundary cross the trajectory, compared to theoretical predictions, the hover test results, and LV measurements of the local tip vortex induced velocity near the blade tip. This is primarily attributed to the aerodynamic interaction of the blade with the preceding blades' tip vortex resulting from the occurrence of a blade vortex intersection. For the 2-bladed AH-1G rotor in low speed forward flight (not hover), the tip vortex initially moves above the rotor, and the phasing of the blade and tip vortex as it travels down through the rotor disc is synchronized such that a blade-vortex intersection consistently occurs at a blade azimuth above the rocket trajectories. This results in a diffusion of the tip vortex core and an associated significant decrease in its local induction strength in the region of the rocket trajectories. Thus, the nature of the aerodynamic influence on the rocket flight path between hover and forward flight is different. In hover, the influence of phasing of the rocket firing time within the blade/wake passage interval may be important due to the high peak-to-peak velocities encountered. If

the flow interference is significant, random excursions in the rocket flight paths could result without a firing time control. For low speed forward flight conditions, with vortex diffusion resulting from blade-vortex intersection, the time-averaged flow velocities dominate, and more constant variations in the rocket flight path from the intended trajectory are anticipated. Corrective aiming compenstion should thus be more effective for such conditions.

3. The occurrence of the forward flight blade-vortex intersection and the location of the crossing point of the forward wake boundary (tip vortices) and the rocket trajectory was accurately predicted by the UTRC Wake Geometry Analysis. Accurate prediction of the reduced peak-to-peak flow velocities at the rocket will require representation of the vortex diffusion associated with the blade-vortex intersection in the UTRC Rotorcraft Wake Analysis. In addition to the rocket problem, the blade-vortex interaction phenomemon presents significant implications for the prediction of airflow velocities for helicopter low speed performance, handling qualities, vibrations, and noise.

4. The application of laser velocimetry to measure model rotor airflow for low speed flight conditions was successful. LV proved to be a valuable technique for acquiring both the time-average and time variation of flow velocity components at rocket trajectory and wind sensor locations inside and outside of the rotor wake. The total and separate influence of each of the aircraft components (rotor, fuselage, modified canopy, and wing), and significant operating condition parameters (rotor thrust, wind direction, and ground effect) on the airflow influencing rocket trajectories were successfully measured. LV also proved useful for identifying wake features and investigating blade-vortex interaction.

5. Flow visualization techniques (smoke) were valuable for the tested low speed flight conditions to identify wake geometry (tip vortices and in-board vortex sheets), wake stability, and vortex core characteristics in the vicinity of the rotor, rocket trajectory and wind sensor locations. The influence of flight speed, the fuselage, modified canopy, thrust level, flight/wind direction, and ground effect on wake geometry, determined from analysis of the flow visualization data, were useful for interpretation of the flow velocity data.

6. For forward flight conditions, the influence of the fuselage and particularly changes in the fuselage configuration (stub-wings, canopy) on the rocket trajectory airflow were generally small.

The fuselage produces an expected wake expansion which moves the rotor wake boundary forward on the rocket trajectory (approximately 10 percent of the rotor radius) in low speed flight. Although the presence of the fuselage has some influence in low speed forward flight, the flight condition rather than the aircraft configuration is the primary factor affecting the rocket aerodynamic interference.

7. In low speed forward flight, the effect of thrust (gross weight) increment primarily results in a wake skew angle change which reorients the wake boundary relative to the rocket trajectory. At 15 kts an 8 percent decrease in thrust coefficient produced a movement of the wake boundary and associated high flow velocity region 10 percent of the rotor radius toward the launch point.

8. Differences in the airflow at inboard and outboard rocket trajectories are small in low speed forward flight.

9. As anticipated, the ground effect, crosswind and tail wind conditions are very influential for the flow velocities at the rocket trajectories in low speed flight. For ground effect conditions, the decreased flow velocities in the inboard wake region, the relocation of the wake boundary, and the presence of the observed upstream ground vortex all contribute to a considerable change in the flow velocity distribution along the rocket trajectories. For crosswind conditions, the flow velocity distribution is primarily influenced by the relocation of the intersection of the wake boundary and rocket trajectory and the reorientation of the freestream flow to the rocket trajectory direction. For tail wind conditions, the reversal of the inclination and orientation of the wake relative to the rocket trajectory results in locating the central, low momentum region of the rotor wake at and ahead of the launch point on the rocket trajectory. This and the relocated wake boundary produce a considerable variation in the airflow at the rocket trajectory. Combining tail wind and ground effect extends the low momentum region farther along the trajectory. The flow impact on the rocket trajectory, for tail wind conditions, may be less severe due to the resulting decreased vertical flow velocities near the launch point where its flight velocity is lowest.

10. Due to rotor wake and fuselage aerodynamic interference, wind sensors at the locations tested (ahead of the fuselage nose

CONCLUSIONS (Cont'd)

and laterally extended from the top of the cockpit canopy) cannot be used to directly measure the freestream velocity for low speed flight. Of those tested, the best calibrated wind sensor location is the farthest from the fuselage nose (15 percent of the rotor radius), except for in-ground-effect conditions, where it is useless due to the ground vortex. However, this location is unsatisfactory in hovering flight due to its proximity to the rotor wake boundary, and thus a further distance from the fuselage nose is desirable.

RECOMMENDATIONS

1. The effect of the rotor wake induced velocities determined in this investigation on the rocket trajectories should be calculated using the Army rocket dynamic response analysis. From this analysis, the deviations of the rocket trajectories can be determined, and the degree of accuracy required of the induced effects for rocket trajectory calculations would be established.

2. Analysis of the time-varient flow velocity data to present and interpret the results for all configurations and conditions relative to rotor azimuth position was beyond the scope of the investigation reported herein. The results of the above recommended aeroballistics investigation should be used to assess the requirement for additional data in the time history format.

3. Flow velocity data for full-scale aircraft should be acquired, at least for a limited number of flow field points and test conditions, to compare with the model test data and to determine the relative flow unsteadiness between full-scale operation and model testing in a controlled environment.

4. Due to the larger than expected and unexplicable effects for the rotor disc/rocket trajectory angle variation and the influence of the rounded canopy on the wind sensor measurements, it is recommended that conclusions not be made for these effects without additional data.

5. The model testing, laser velocimetry, and flow visualization techniques, as demonstrated in combination in this investigation for the specific rocket/wind sensor application, are recommended for use in a more general investigation of rotor aerodynamics and associated performance. In addition to further defining fundamental characteristics, such an experimental program would provide comprehensive data for validation of rotor airloads theory and the further generalization of the aerodynamics and performance of helicopters operating in low speed and nap-of-the-earth flight.

6. A future detailed investigation, using the experimental procedures identified during this test program, has a potential technological application for acquiring a fundamental understanding of the blade-vortex interaction phenomenon which, in addition to aerodynamic interference, can influence rotor performance, handling qualities, vibrations, and noise.

RECOMMENDATIONS (Cont'd)

7. Considering the favorable correlation of the wake geometry theory (UTRC Rotor Wake Geometry Analysis) for the isolated rotor in low speed flight, and the usefulness of the air flow theory (UTRC Rotorcraft Wake Analysis) for interpretation of the model data for full-scale aircraft, it is recommended that analytical refinements be included to improve the scope and accuracy of the analyses. Recommended refinements include provisions for ground effect, maneuvers, and fuselage aerodynamic interference. Wake modeling refinements, particularly for the vortex diffusion associated with the blade-vortex intersection phenomemon, should be incorporated as guiding experimental data become available.

8. Application and evaluation of the demonstrated experimental techniques and rotor wake theory for other aircraft (for example, AAH and UTTAS) over a wide range of operating conditions, and generalization of the predicted flow velocities is recommended.

LITERATURE CITED

1. Ragano, F. P. and R. Bergman: Helicopter Air Flow Analysis at Hover and Low Air Speeds, Memo from U.S. Army Missile Command to the U.S. Army Aviation Systems Command, April 21, 1975. (Enclosed as Appendix A).

2. Proceedings of the Conference on the Effects of Helicopter Downwash on Free Projectiles, U.S. Army Aviation Systems Command, St. Louis, Missouri, November 1975.

3. Marner, G. R.: The Effects of Helicopter Downwash on Free Projectiles, Introduction and Assessment of the Problem, Proceedings of the Conference on the Efffects of Helicopter Downwash on Free Projectiles, November 1975.

4. Morse, H. A.: Some Practical Aspects of Rotor Wake Effects on Rocket Accuracy, Proceedings of the Conference on the Effects of Helicopter Downwash on Free Projectiles, November 1975.

5. Bergman, R.: Interaction of Air Flow and Helicopter Characteristics on the 2.75 Inch Rocket System, Proceedings of the Conference on the Effects of Helicopter Downwash on Free Projectiles, November 1975.

6. Landgrebe, A. J.: An Analytical and Experimental Investigation of Helicopter Rotor Hover Performance and Wake Geometry Characteristics, United Aircraft Research Laboratories; USAAMRDL Technical Report 71-24, Eustis Directorate, U.S. Army Air Mobility Research and Development Laboratory, Fort Eustis, Virginia, June 1971, AD728835.

7. Landgrebe, A. J.: The Wake Geometry of a Hovering Helicopter Rotor and Its Influence on Rotor Performance, Journal of the American Helicopter Society, Vol. 17, No. 4, October 1972. (Also preprint No. 620, 28th Annual National Forum of the American Helicopter Society, May 1972.)

8. Landgrebe, A.J.: An Analytical Method for Predicting Rotor Wake Geometry; Journal of the American Helicopter Society, Vol. 14, No. 4, October 1969. (Also, AIAA Paper No. 69-196, AIAA/AHS VTOL Research, Design and Operations Meeting, Atlanta, Georgia, February 1969.)

LITERATURE CITED (Cont'd)

9. Landgrebe, A. J., and M. C. Cheney: Rotor Wakes - Key to Performance Prediction, AGARD-CP-111, AGARD Conference Proceedings No. 111 on Aerodynamics of Rotary Wings, Fluid Dynamics Panel Specialists Meeting, September 1972. (Also, paper presented at the Symposium on Status of Testing and Modeling Techniques for V/STOL Aircraft, Mideast Region of the American Helicopter Society, October 1972.)

10. Landgrebe, A. J., and E. D. Bellinger: An Investigation of the Quantitative Applicability of Model Helicopter Rotor Wake Patterns Obtained From a Water Tunnel, United Aircraft Research Laboratories; USAAMRDL Technical Report 71-69, Eustis Directorate, U.S. Army Air Mobility Research and Development Laboratory, Fort Eustis, Virginia, December 1971, AD739946.

11. Clark, D. R., and A. J. Landgrebe: Wake Boundary Layer Effects in Helicopter Rotor Aerodynamics, AIAA Paper No. 71-581, AIAA 4th Fluid and Plasma Dynamics Conference, Palo Alto, California, June 21-23, 1971.

12. Landgrebe, A. J., and T. A. Egolf: Rotorcraft Wake Analysis for the Prediction of Induced Velocities, United Technologies Research Center, USAAMRDL Technical Report 75-45, U.S. Army Air Mobility Research and Development Laboratory, Fort Eustis, Virginia, January 1976.

13. Landgrebe, A. J. and T. A. Egolf: Prediction of Helicopter Induced Flow Velocities Using the Rotorcraft Wake Analysis. Proceedings of the 32nd Annual National Forum of the American Helicopter Society, March 1975.

14. Landgrebe, A. J., R. Moffitt, and D. R. Clark: Aerodynamic Technology for Advanced Rotorcraft. Journal of the American Helicopter Society, Part I: Vol. 22, No. 2, April 1977; Part II: Vol. 22, No. 3, July 1977.

15. Landgrebe, A. J. and T. A. Egolf: Prediction of Rotor Wake Induced Flow Velocities Along the Rocket Trajectories of an Army AH-1G Helicopter, United Aircraft Research Laboratories, Picatinny Arsenal Technical Report 4797, U.S. Army Picatinny Arsenal, Dover, New Jersey, March 1975.

LITERATURE CITED (Cont'd)

16. Landgrebe, A. J. and T. A. Egolf: Rotor Wake Induced Flow Along Helicopter Rocket Trajectories, Proceedings of the Conference on the Effects of Helicopter Downwash on Free Projectiles, November 1975. (Enclosed as Appendix B).

17. Wasserman, S. and R. Yeller: Preliminary Analysis of the Effect of Calculated Downwash Distributions on the Flight Performance of the 2.75 Inch Rocket, Proceedings of the Conference on the Effects of Helicopter Downwash on Free Projectiles, November 1975.

18. Jenkins, B. Z.: The Perturbed Flow Environment About Helicopters and Its Effect on Free Rockets, Proceedings of the Conference on the Effects of Helicopter Downwash on Free Projectiles, November 1975.

19. Boirun, B. H. and E. E. Bailes: AH-1G Helicopter Flow Field Survey, Proceedings of the Conference on the Effects of Helicopter Downwash on Free Projectiles, November 1975.

20. Landgrebe, A. J., and B. V. Johnson: Measurement of Model Helicopter Rotor Flow Velocities with a Laser Doppler Velocimeter, Jl. American Helicopter Society, Vol. 19, No. 3, July 1974.

21. Landgrebe, A. J., and E. D. Bellinger: Experimental Investigation of Model Variable-Geometry and OGEE Tip Rotors, Prepared by United Aircraft Research Laboratories for the Langley Research Center, NASA, NASA CR-2275, February 1974. (Paper with Same Title: AHS Paper No. 703, 29th Annual National Forum of the American Helicopter Society, May 1973.)

22. Landgrebe, A. J., and E. D. Bellinger: A Systematic Study of Helicopter Rotor Stall Using Model Rotors, AHS Paper No. 804, 30th Annual National Forum of the American Helicopter Society, May 1974.

23. Landgrebe, A. J. and J. C. Bennett: Investigation of the Airflow of a Hovering Model Helicopter at Rocket Trajectory and Wind Sensor Locations, United Technologies Research Center Contractor Report No. R77-912573-15 (Prepared for Dept. Army, ARADCOM), July 1977. (Summary, Scope of Work, Conclusions and Recommendations enclosed as Appendix C.)

GLOSSARY

C_T	Rotor thrust coefficient, rotor thrust/$\rho\pi R^2(\Omega R)^2$
h	Height of rotor above ground, ft
IGE	In-ground-effect
OGE	Out-of-ground-effect
r	Radial coordinate from rotor center, ft
R	Rotor radius, ft
V	Freestream velocity, kts or fps as noted
v_x, v_y, v_z	Horizontal and vertical flow velocity components in the x, y, z coordinate axis system, same sign convention as x, y, z; fps
v_{x_T}, v_{y_T}, v_{z_T}	Flow velocity components in rocket trajectory coordinate system (x_T, y_T, z_T); sign convention is consistent with coordinate definition, fps
x, y, z	Hub centered wind axis system coordinates nondimensionalized by R, left-handed coordinate system (see Fig. 4)
x_T, y_T, z_T	Rocket trajectory axis system coordinates nondimensionalized by R, centered at intersection of axis of rocket launch positions and fuselage centerline, left handed coordinate system with positive x_T in direction of rocket travel (see Fig. 4)
α_S	Shaft angle, positive nose up, deg
γ	Rocket launch attitude, positive upward rotation, deg
ψ	Blade azimuth angle, deg
Ω	Rotor rotational frequency, rad/sec

Figure 1. AH-1G Helicopter Firing 2.75 In. Rockets.

Figure 2. Forward Section of AH-1G Helicopter With 2.75 In. Rocket Launcher.

Figure 3. AH-1 Helicopter with Flat Canopy.

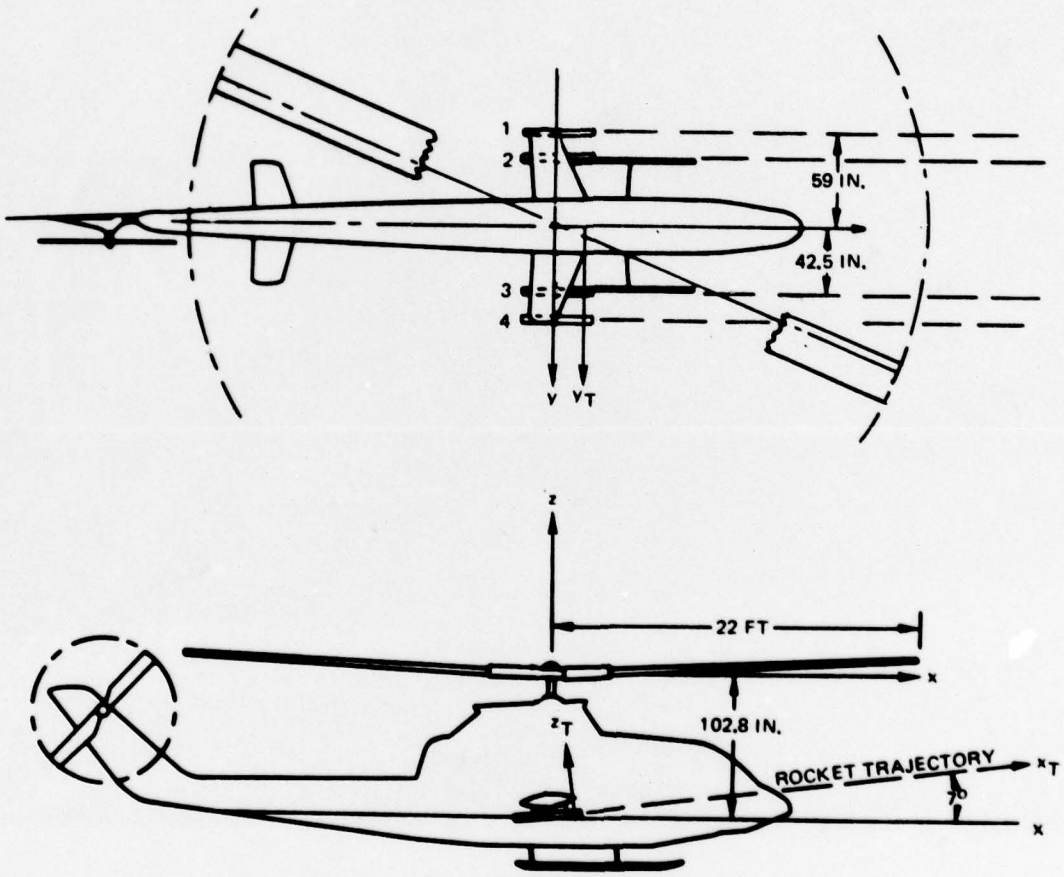

Figure 4. Schematic of AH-1G Helicopter Showing Rocket Trajectories and Axis Systems.

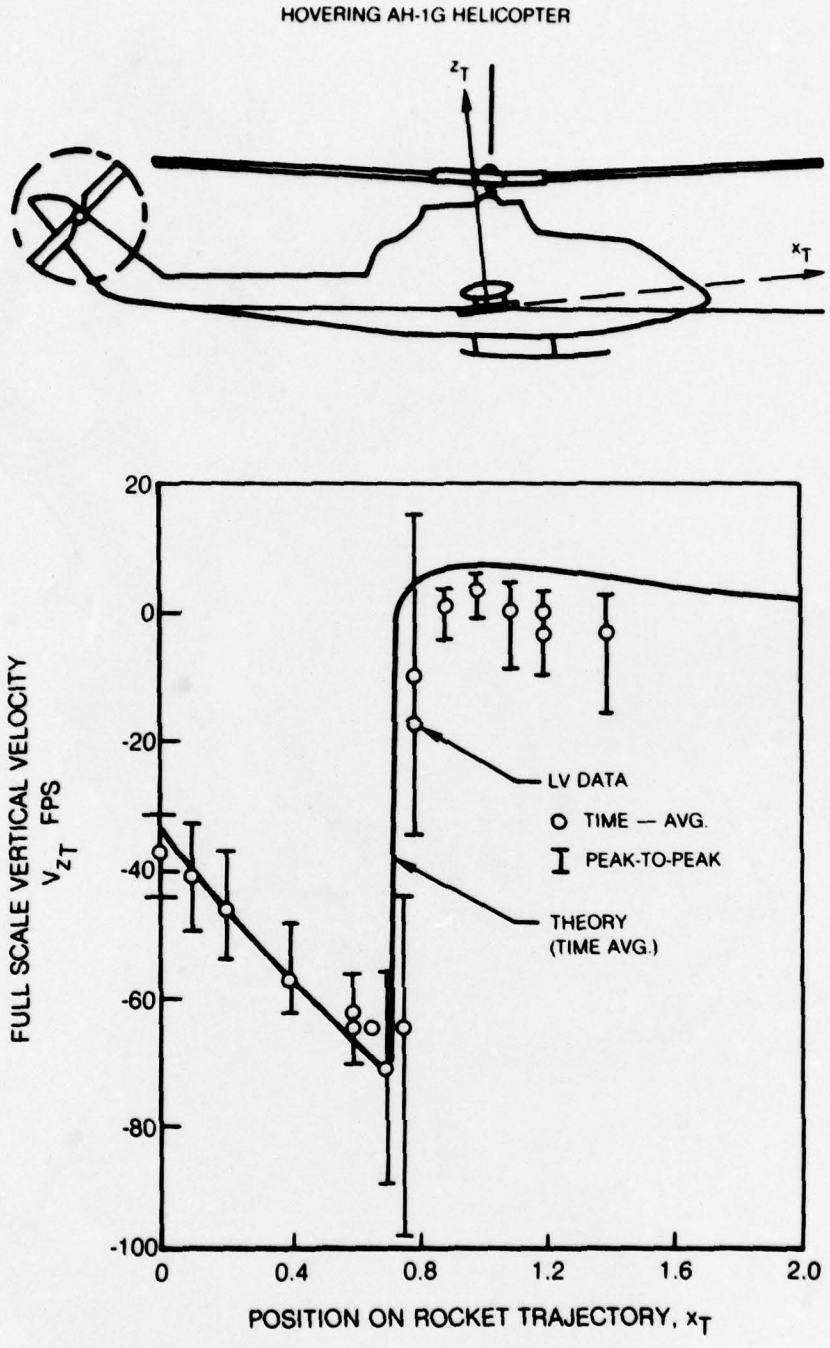

Figure 5. Sample Measured and Predicted Flow Velocities at Rocket Trajectory of Hovering AH-1G Helicopter.

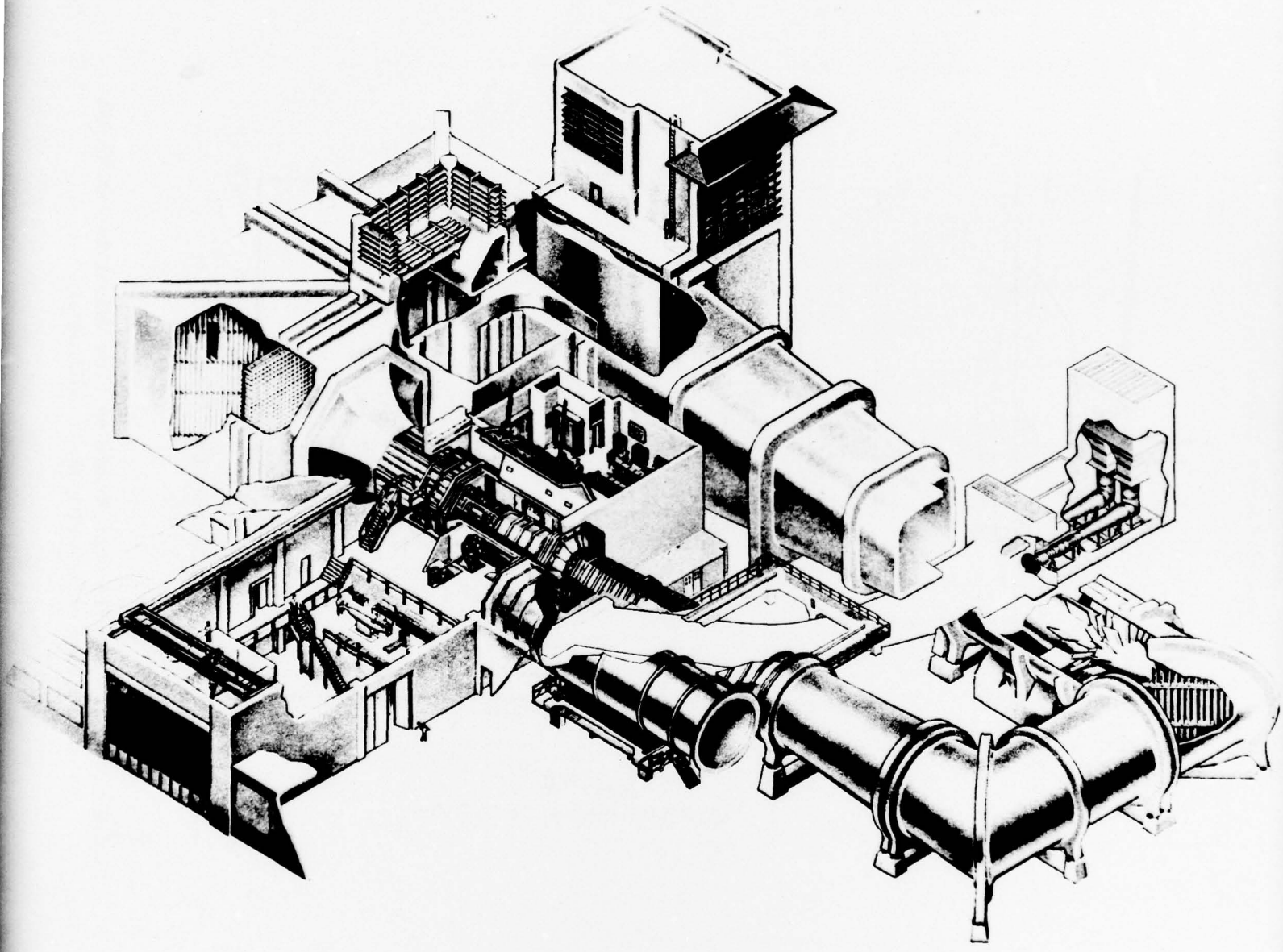

Figure 6. UTRC Large Subsonic Wind Tunnel.

77-350-A

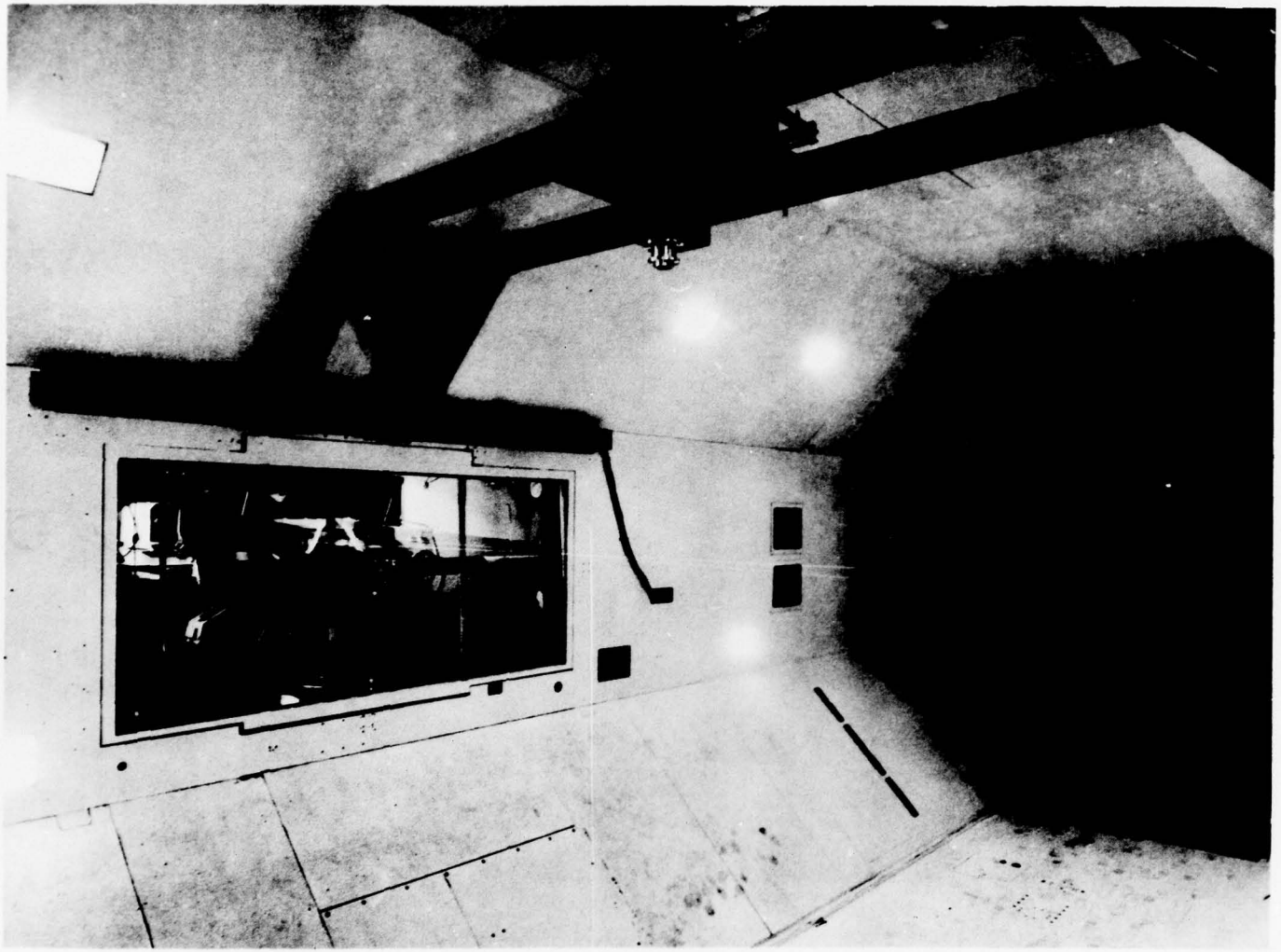

79-09-33-95

Figure 7. 18-ft Main Wind Tunnel Test Section with Window Installation for LV System.

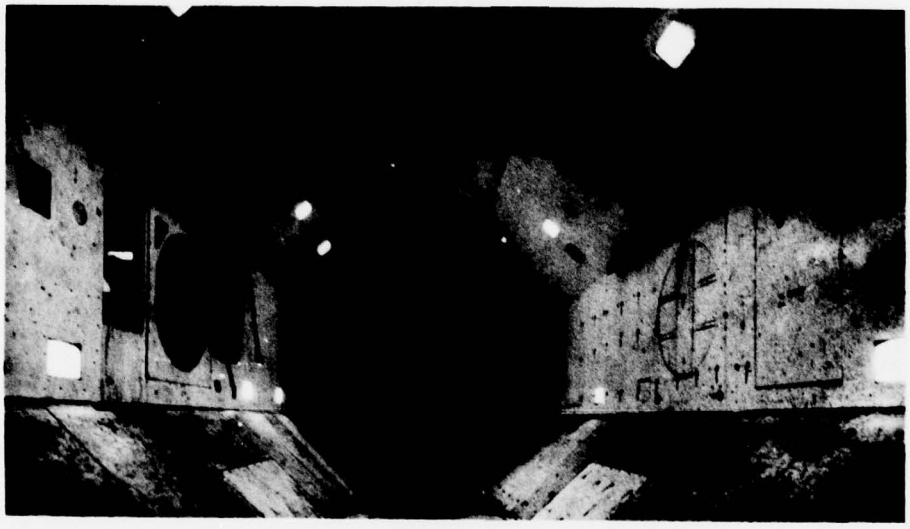

TUNNEL TEST SECTION

Figure 8. 18-ft Wind Tunnel Test Section.

79-09-33-96a

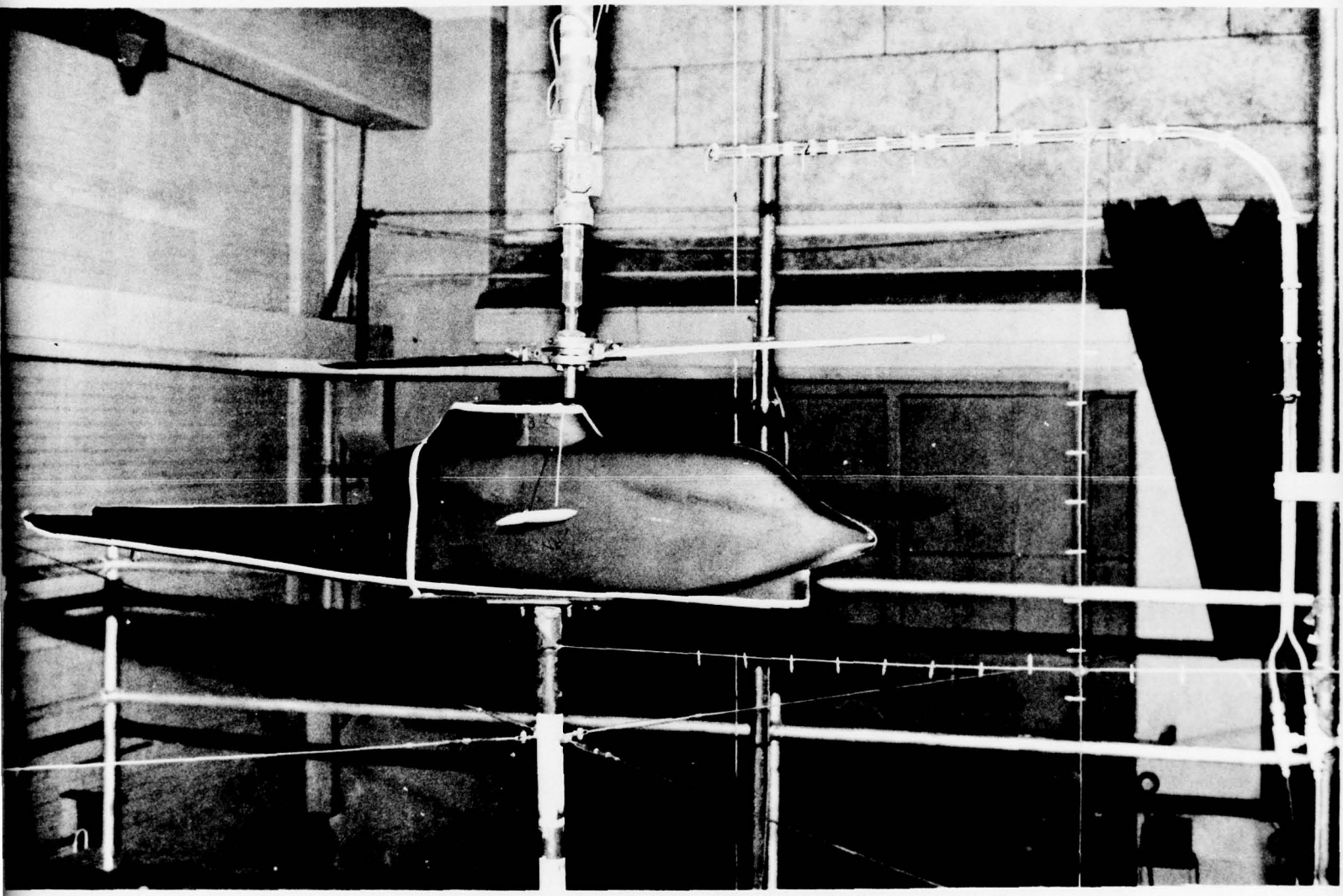

Figure 9. AH-1G Model Helicopter.

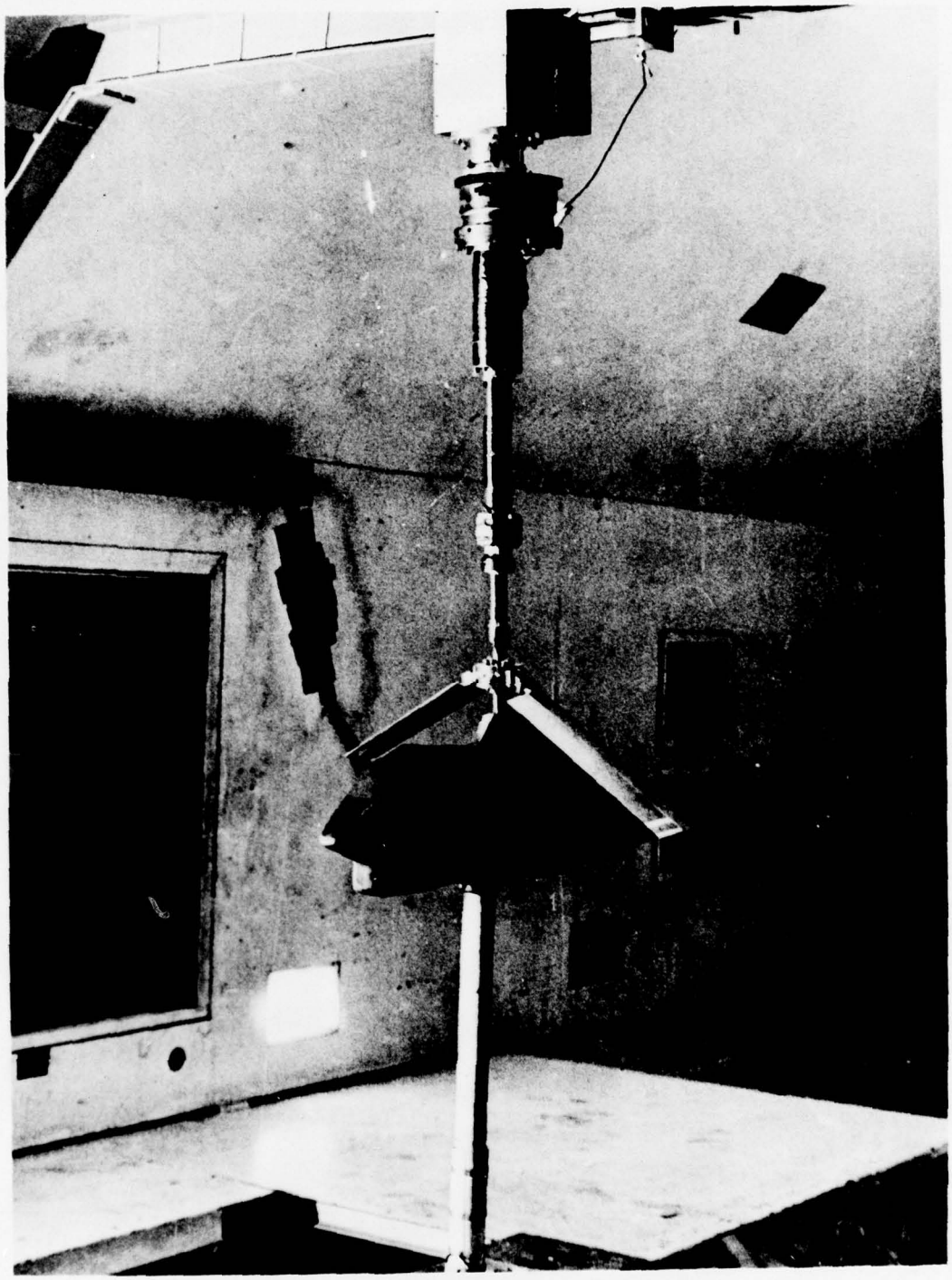

Figure 10. Installation of Wind Tunnel Model Showing Overhead Support Structure for Rotor Test Rig.

79-09-33-94

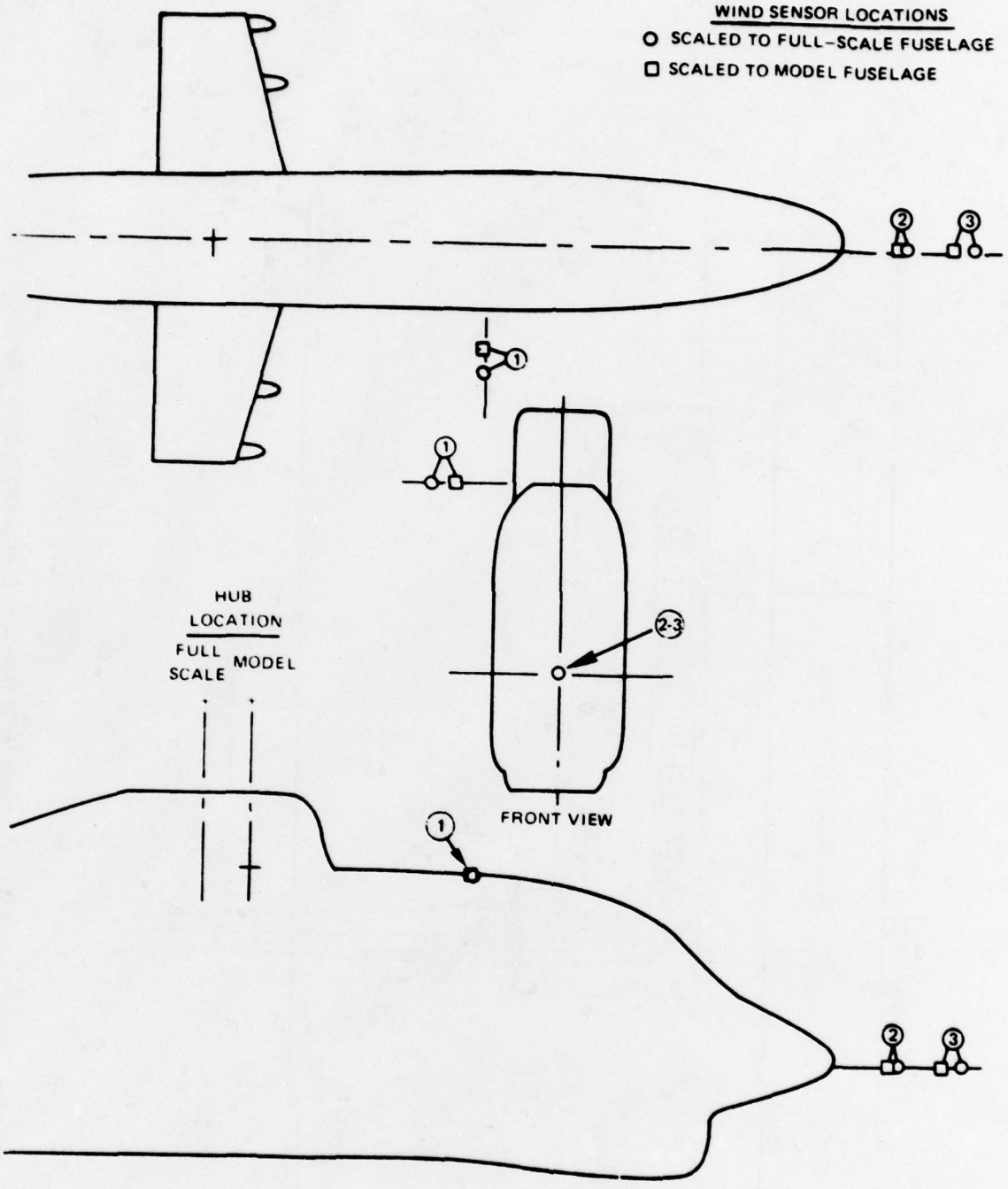

Figure 11. Schematic of Test Wind Sensor Locations Scaled Relative to Model and Full-Scale AH-1G Fuselage.

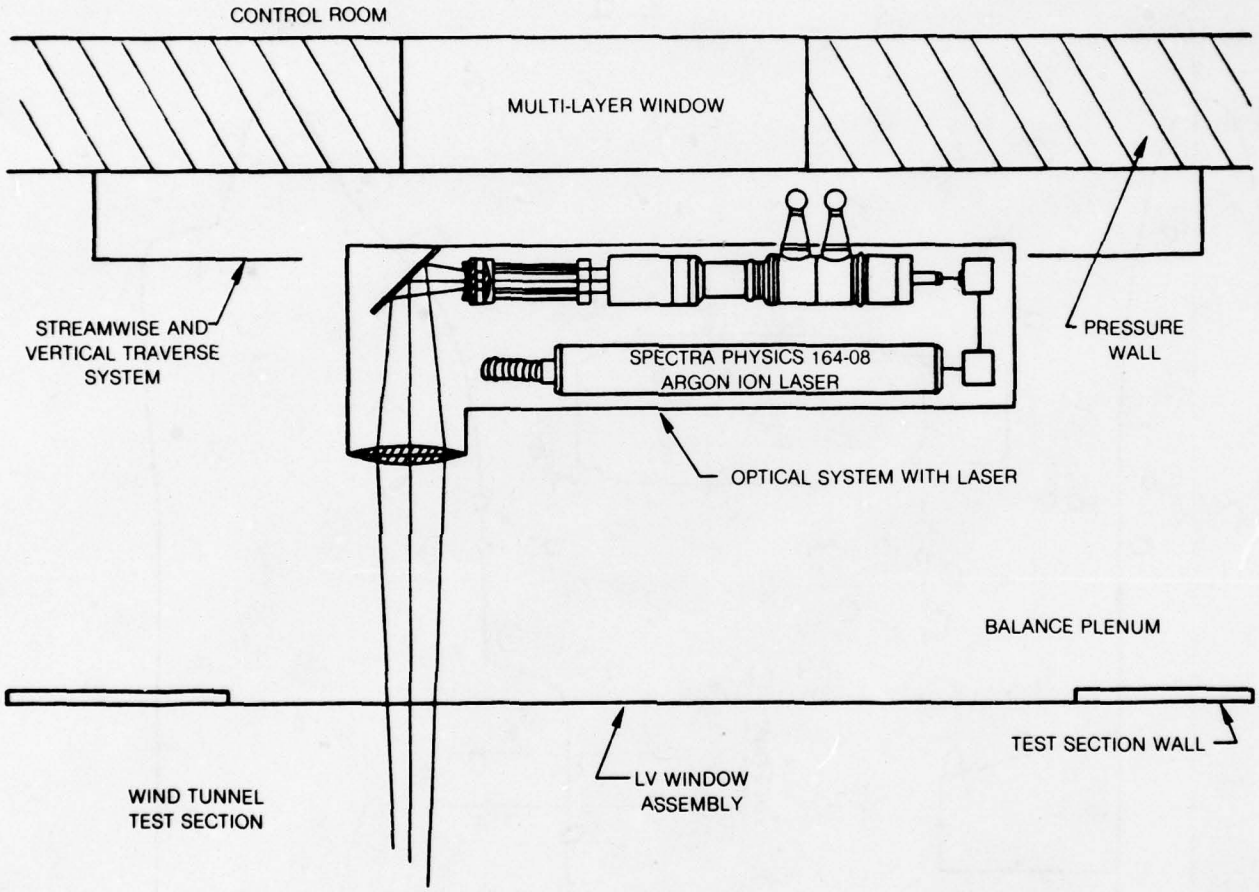

Figure 12. Schematic of Laser Velocimeter Installation in 18-ft Main Wind Tunnel.

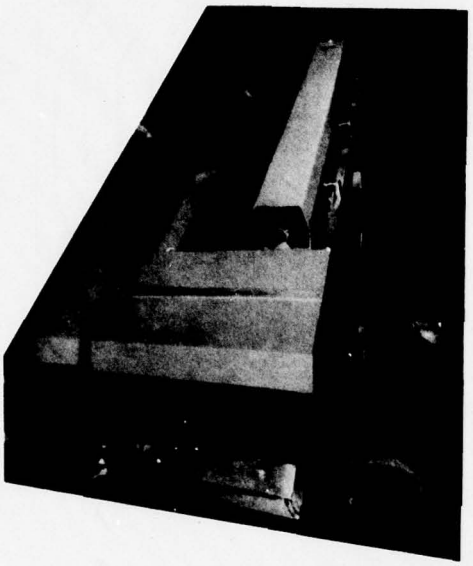

LASER VELOCIMETER

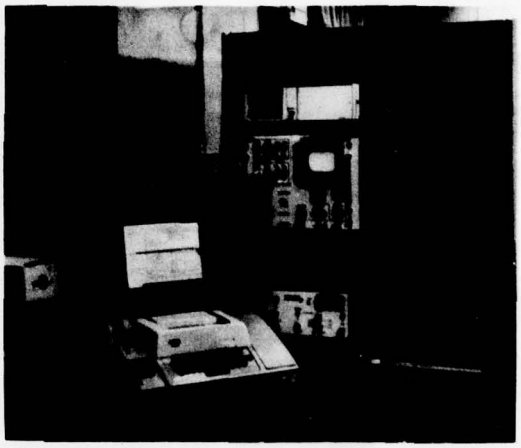

DATA ACQUISITION SYSTEM

Figure 13. Laser Velocimeter System for UTRC 18-ft Wind Tunnel.

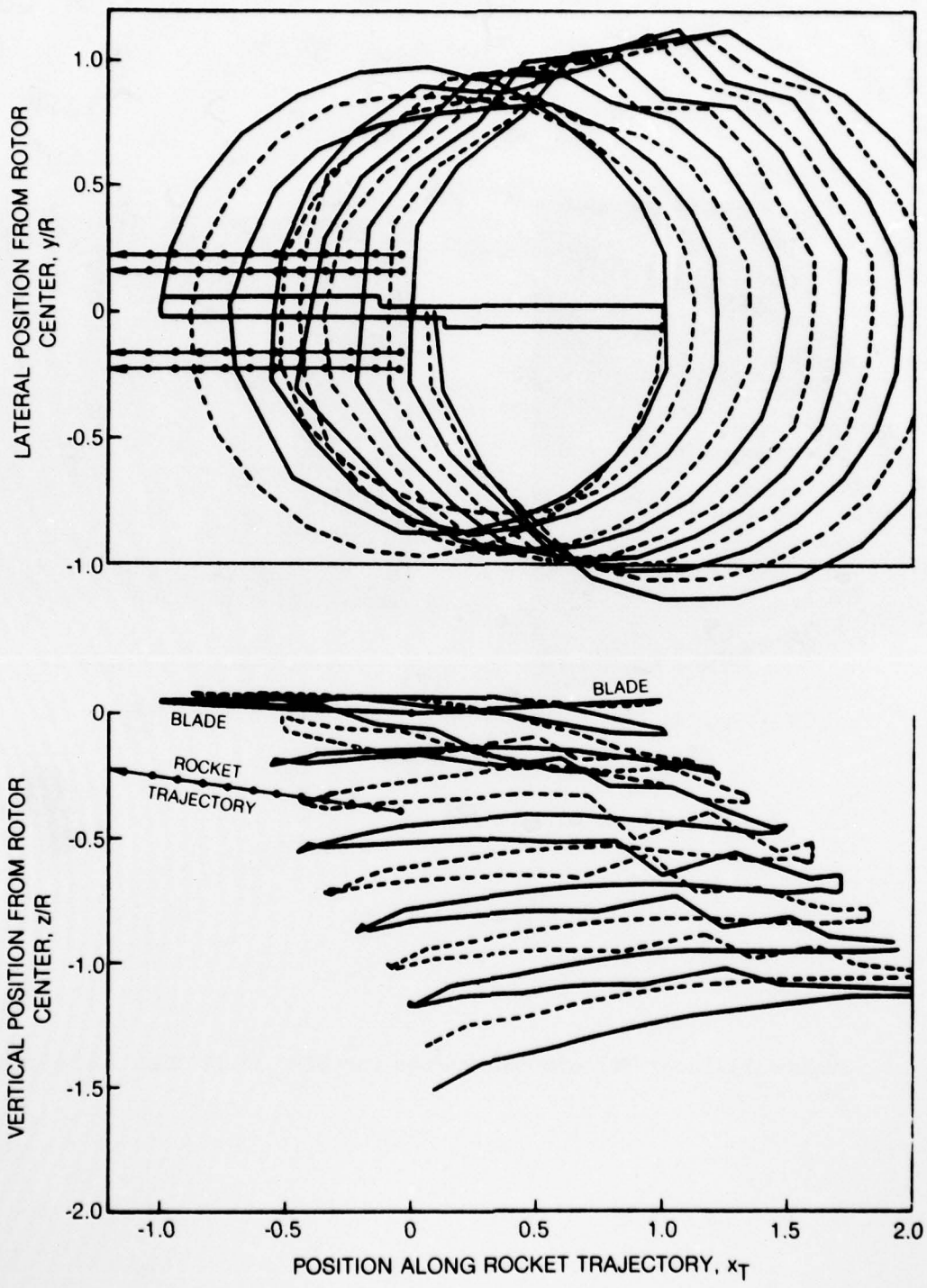

Figure 14. Predicted Tip Vortex Geometry (Analytical) for 15 kt Flight Condition.

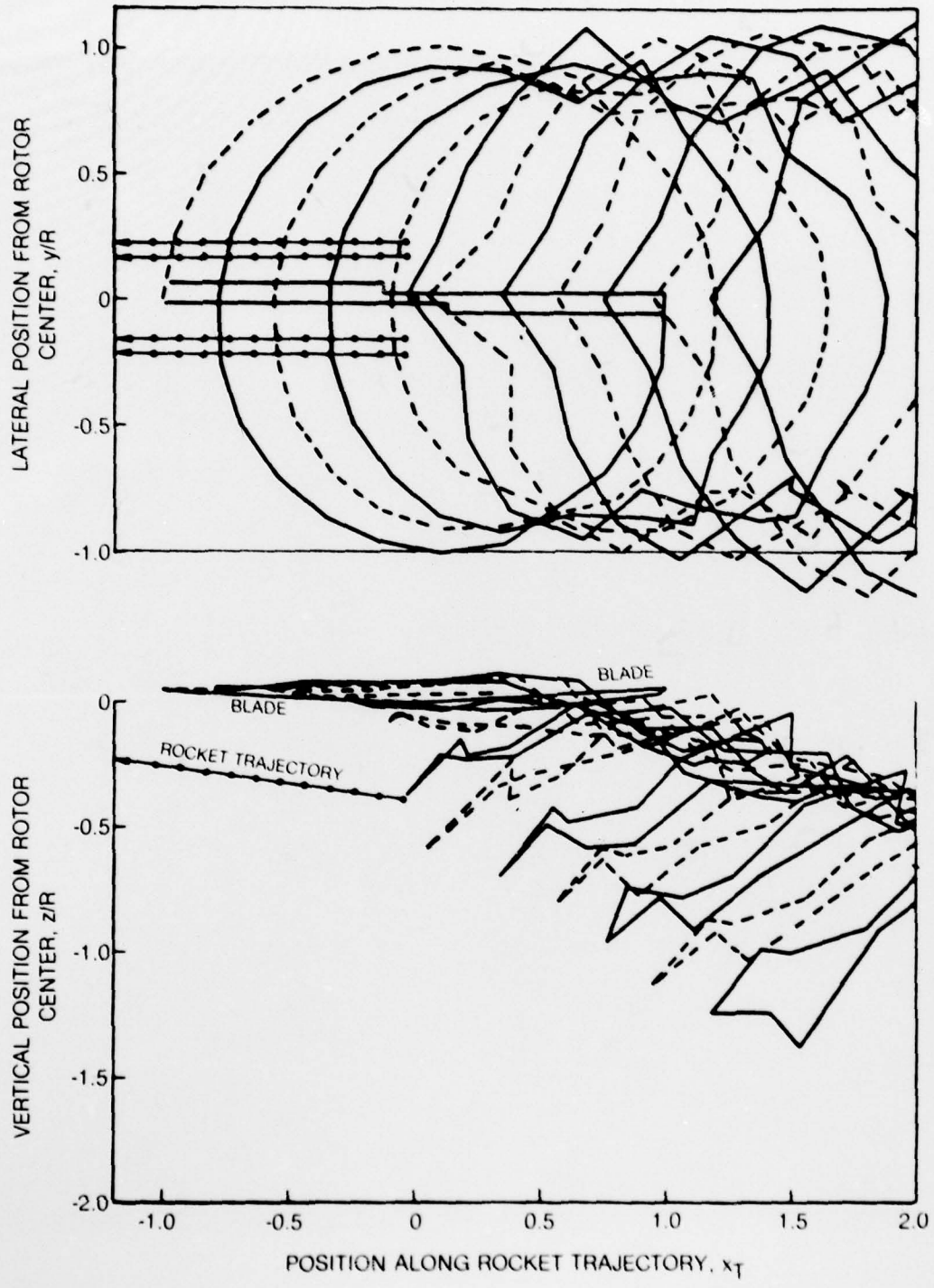

Figure 15. Predicted Tip Vortex Geometry (Analytical) for 30 kt Flight Condition.

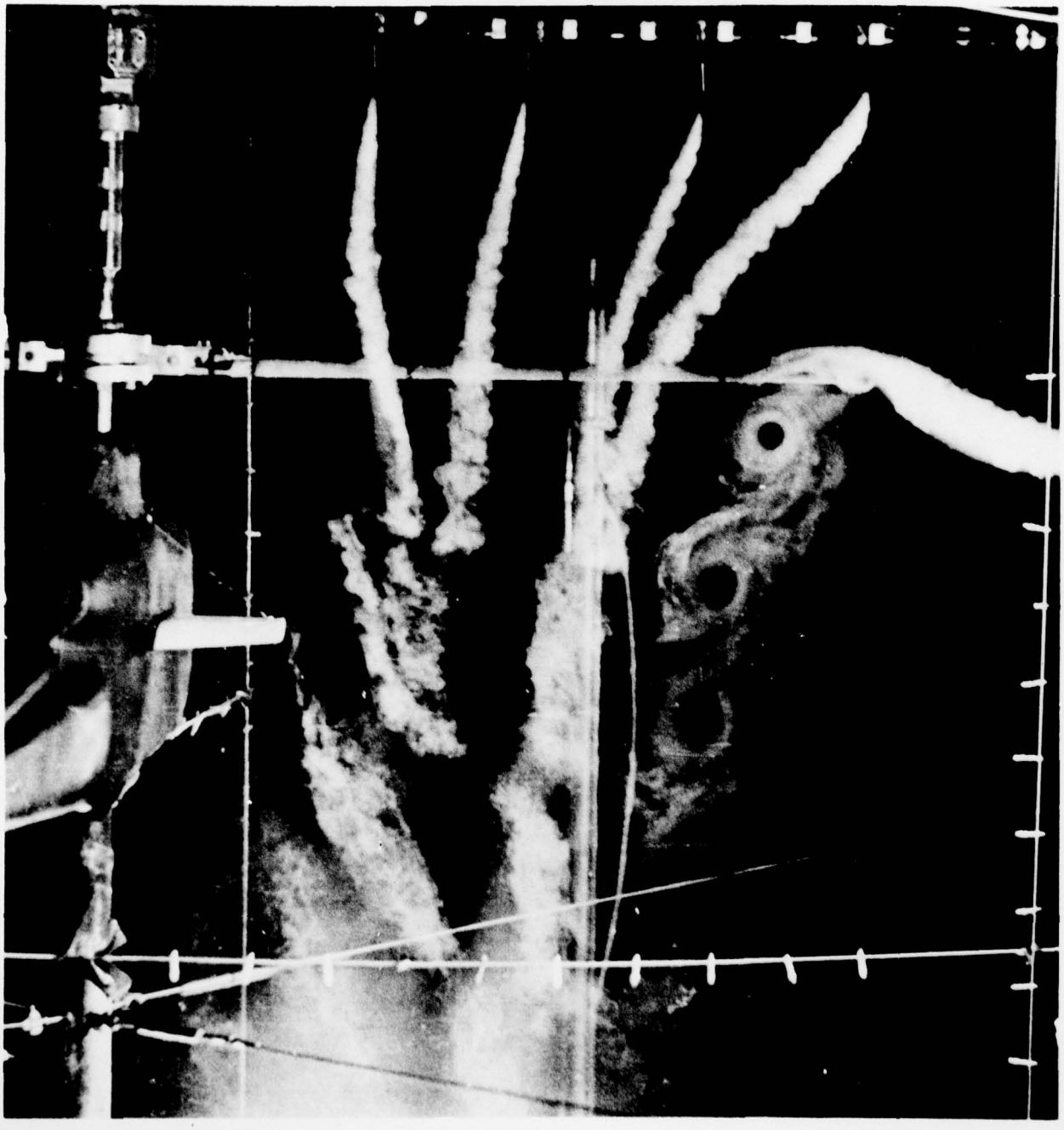

Figure 16. Smoke Flow Visualization Photograph of a Wake Cross Section for the Reference Configuration in the Hover Condition.

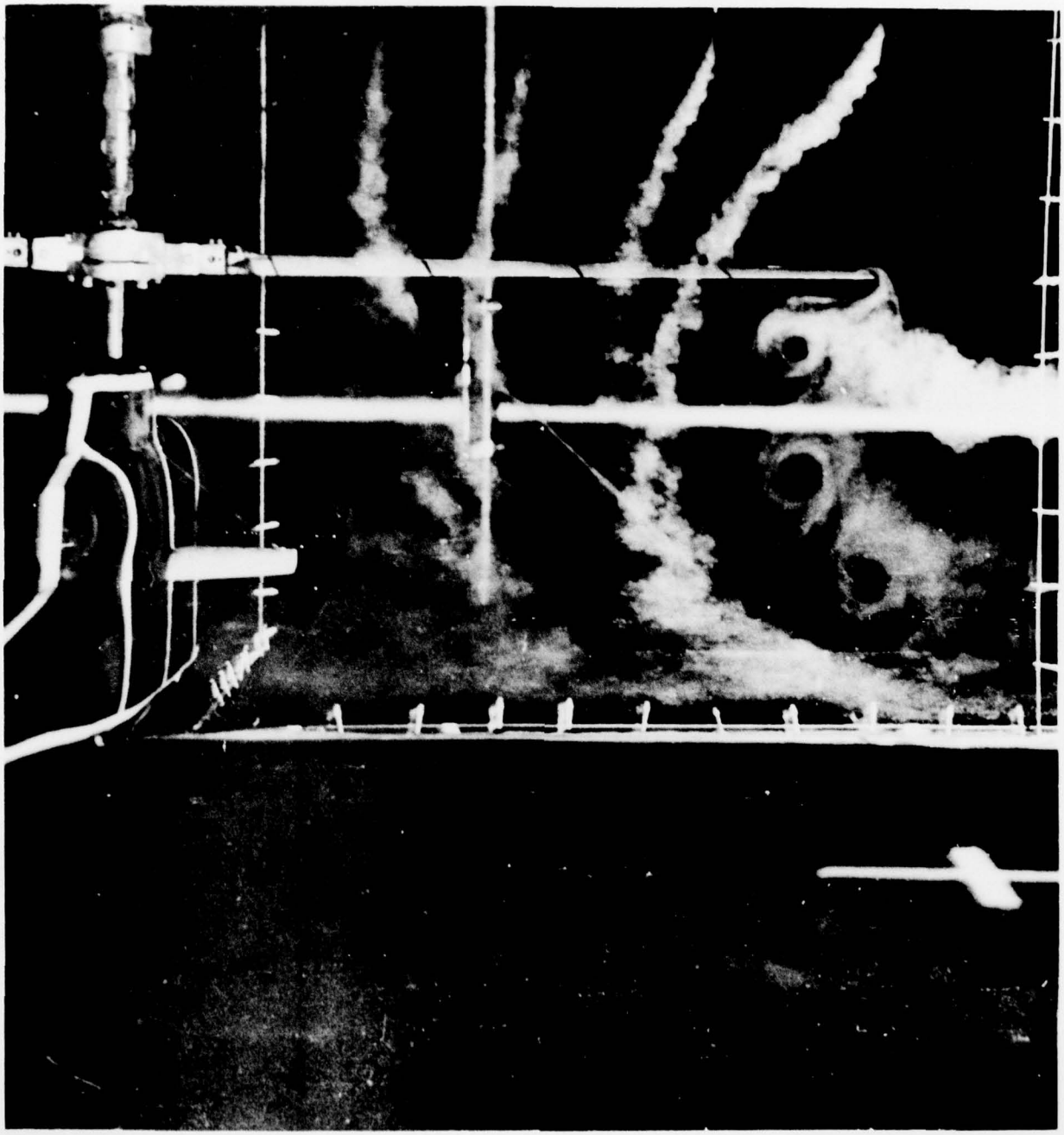

Figure 17. Smoke Flow Visualization Photograph of a Wake Cross Section for the In-Ground-Effect (Skid Height = 0) Hover Condition.

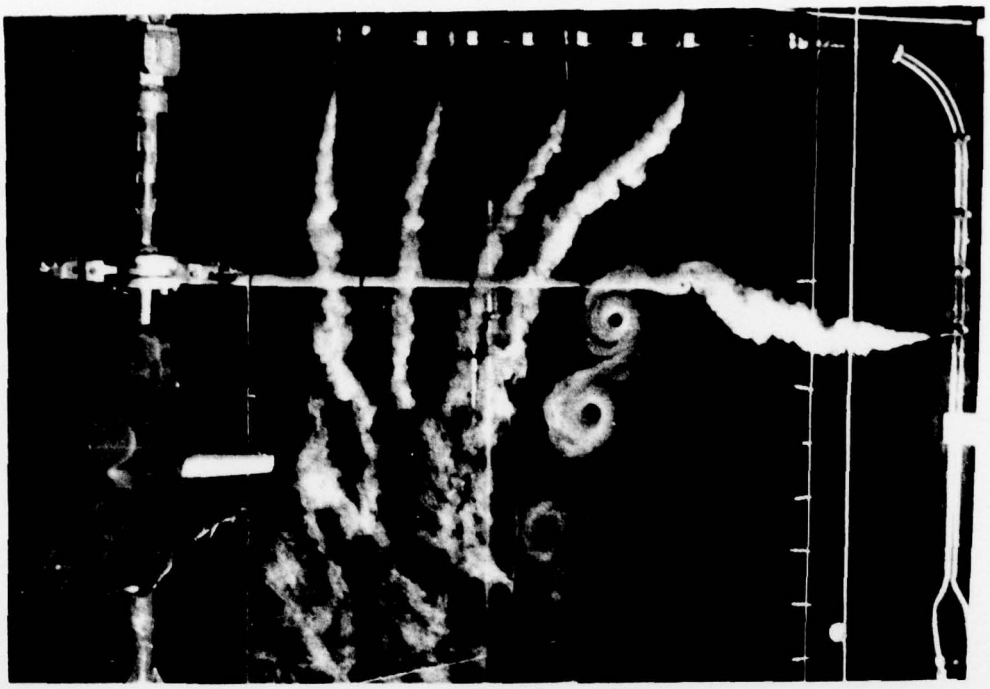

V = 0 (HOVER)

V = 7.5 KTS SCALED TO 15 KTS

Figure 18. Smoke Flow Visualization of Rotor Wake for Hover and Low Speed Forward Flight.

79-09-33-93

V = 5 KTS SCALED TO 10 KTS

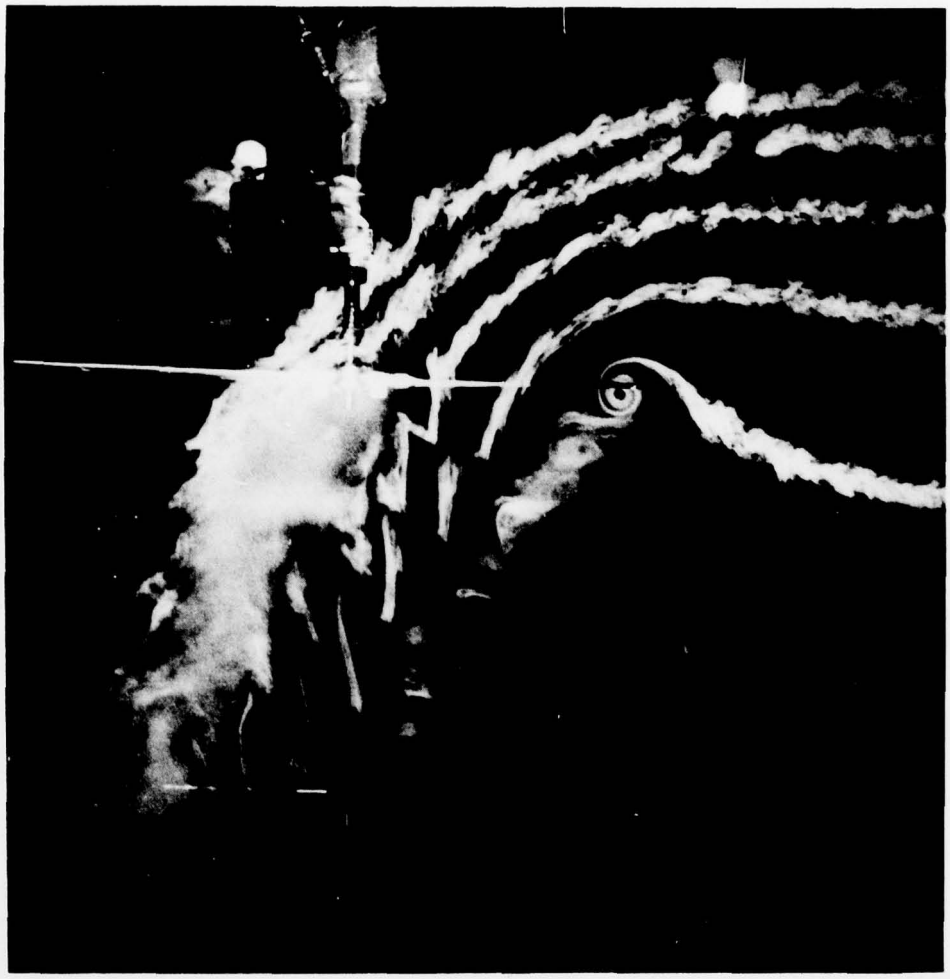

Figure 19. Smoke Flow Visualization Photograph of Wake Cross Section for Isolated Rotor in Low Speed Flight (v = 10 kts).

79-431

79-09-33-86

V = 7.5 KTS SCALED TO 15 KTS

Figure 20. Smoke Flow Visualization Photograph of Wake Cross Section for Isolated Rotor in Low Speed Flight (v = 15 kts).

79-422

79-09-33-87

V = 15 KTS SCALED TO 30 KTS

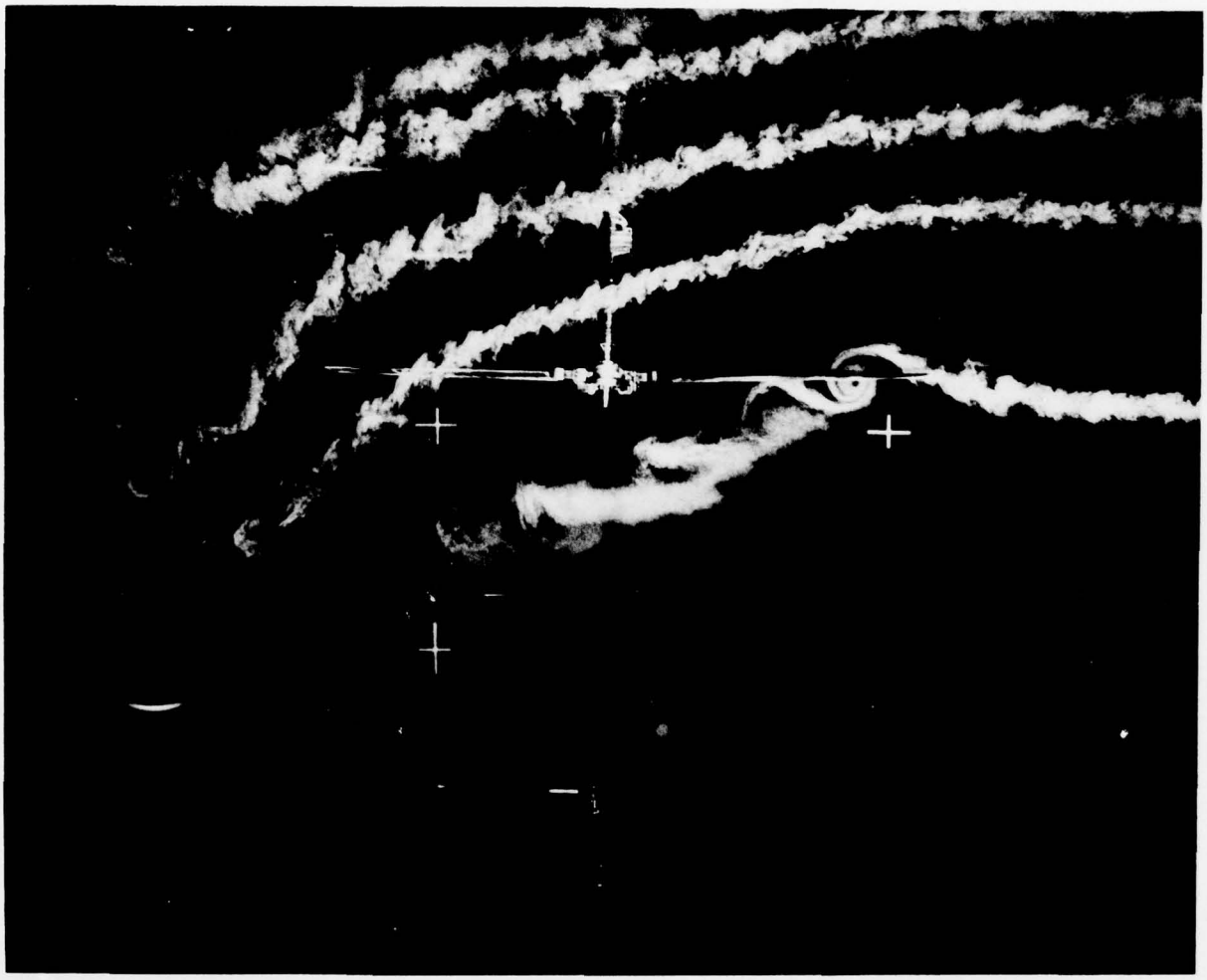

Figure 21. Smoke Flow Visualization Photograph of Wake Cross Section for Isolated Rotor in Low Speed Forward Flight (v = 30 kts).

79-493

79-09-33-89

V = 7.5 KTS SCALED TO 15 KTS

Figure 22. Smoke Flow Visualization Photograph of Wake Cross Section for Rotor-Fuselage-Wing Configuration in Low Speed Forward Flight (v = 15 kts).

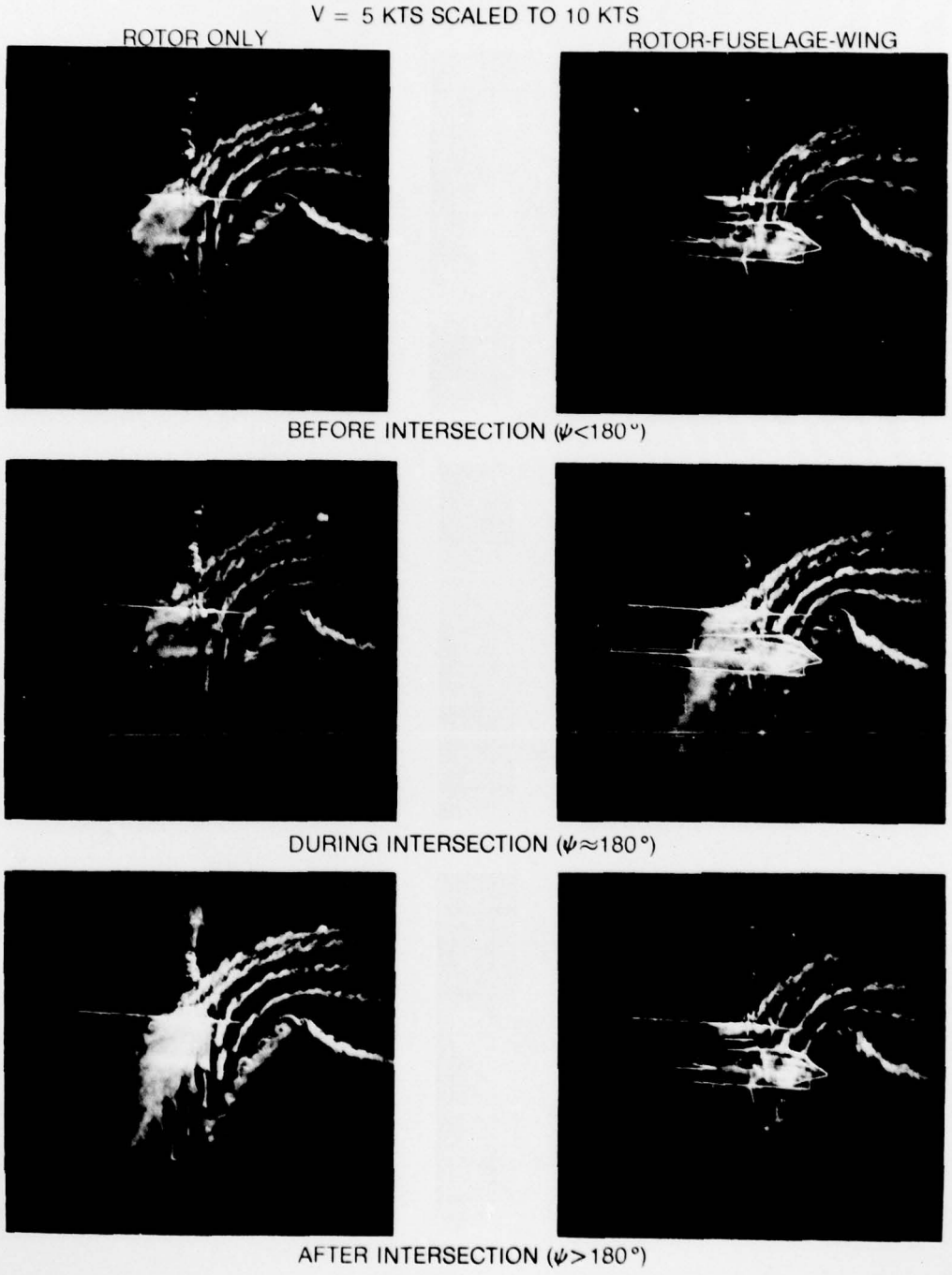

Figure 23. Smoke Flow Visualization Photographs of Blade-Vortex Interaction (v = 10 kts).

79-09-33-91

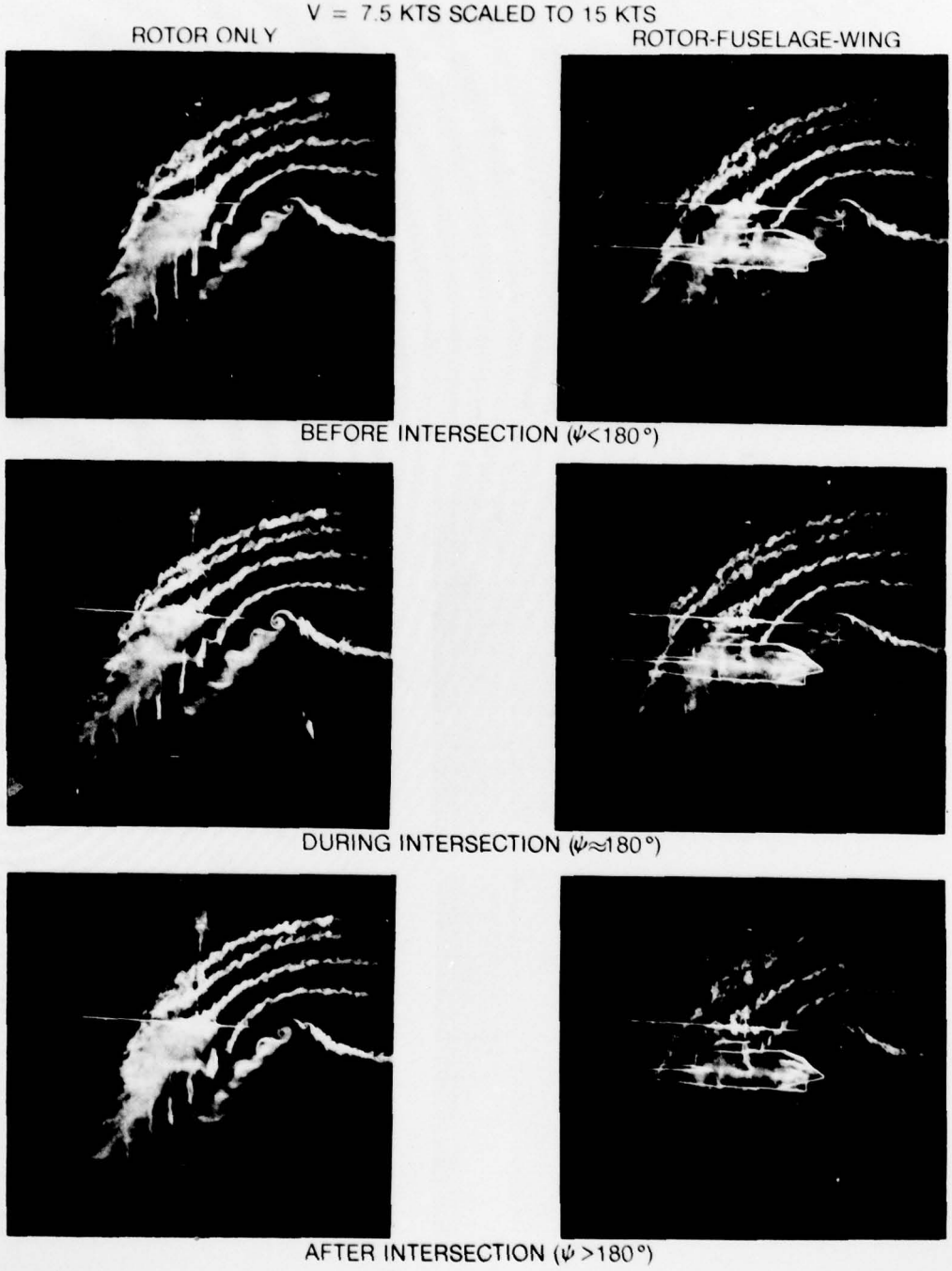

Figure 24. Smoke Flow Visualization Photographs of Blade-Vortex Interaction (v = 15 kts).

79-09-33-92

V = 7.5 KTS SCALED TO 15 KTS

Figure 25. Smoke Flow Visualization Photograph of Roll-up of Lateral Wake in Low Speed Forward Flight.

79-09-33-90

79-438-439

7.5 KTS SCALED TO 15 KTS

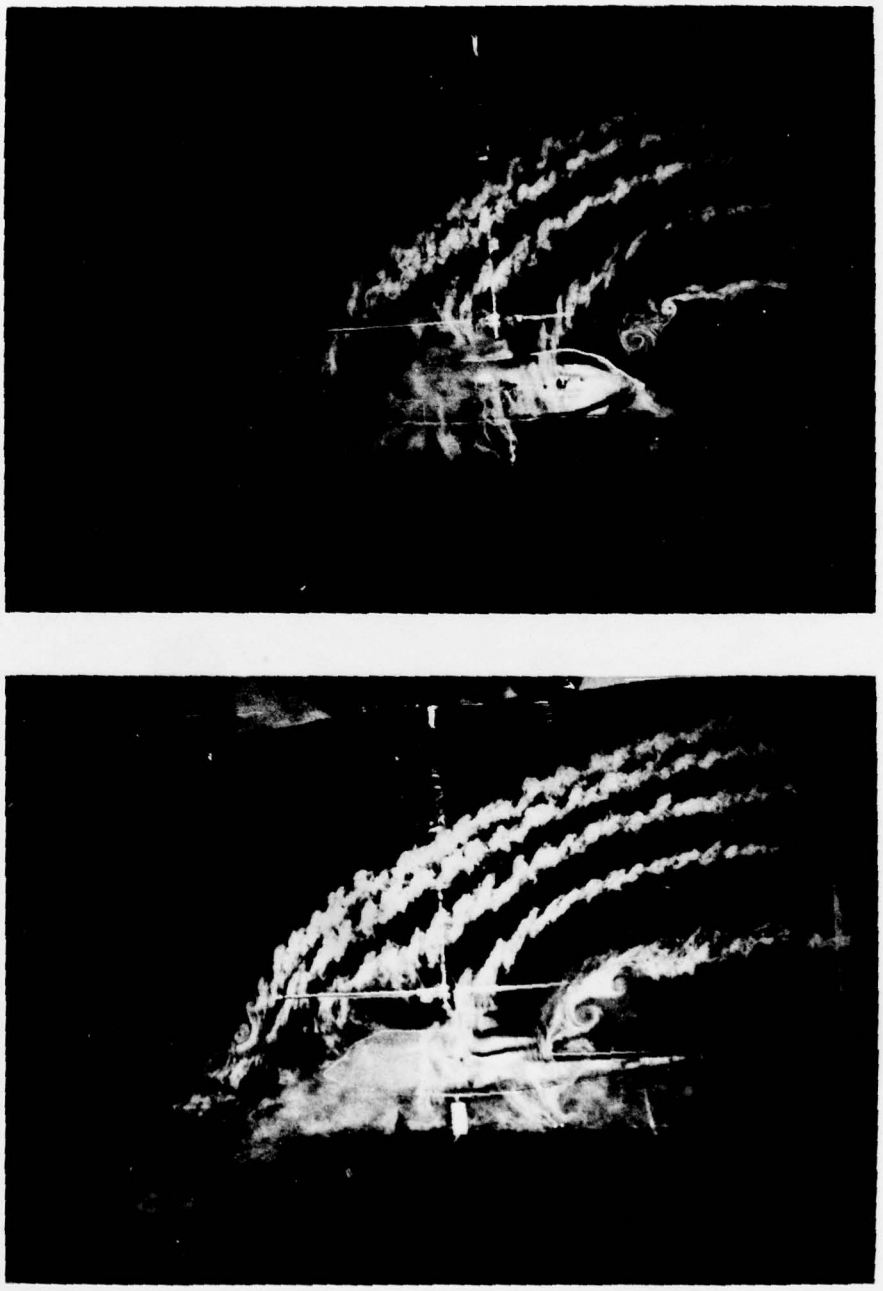

Figure 26. Smoke Flow Visualization Photographs of Wake Cross Section In-Ground-Effect for Low Speed Forward and Rearward Flight.

79-291
79-324

79-09-33-85

AD-A075 378 UNITED TECHNOLOGIES RESEARCH CENTER EAST HARTFORD CONN F/G 1/3
INVESTIGATION OF THE AIRFLOW AT ROCKET TRAJECTORY AND WIND SENS--ETC(U)
SEP 79 R B TAYLOR, A J LANDGREBE DAAG29-77-C-0013
UNCLASSIFIED UTRC-R79-912985-5 ARO-14277.1-E NL

2 OF 3
AD A075378

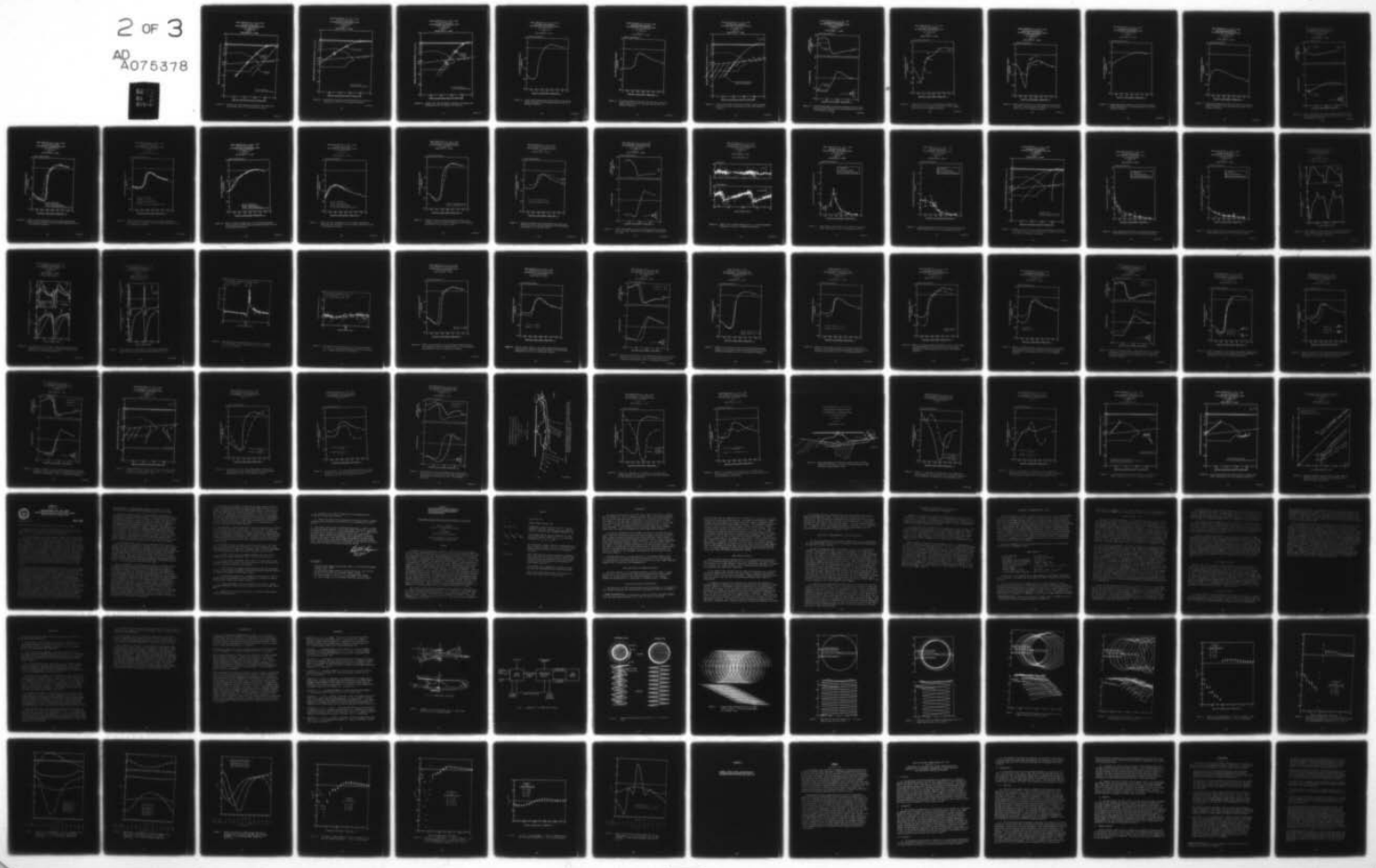

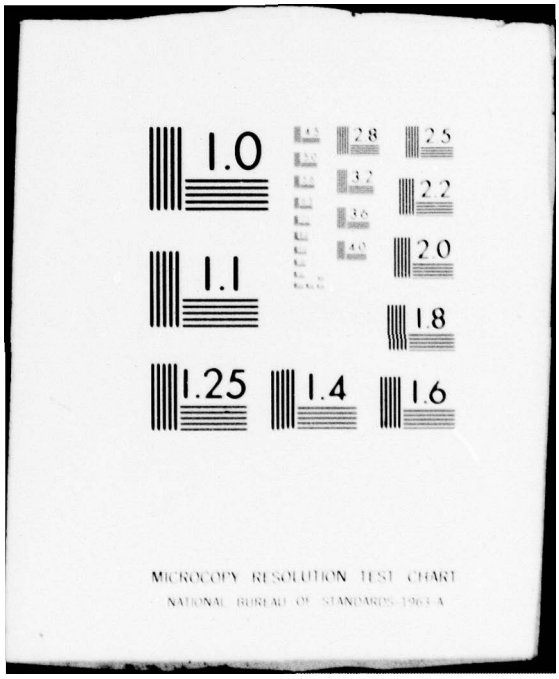
1.0
1.1
1.25
1.4
1.6
2.8
3.2
3.6
4.0
2.5
2.2
2.0
1.8
MICROCOPY RESOLUTION TEST CHART
NATIONAL BUREAU OF STANDARDS-1963-A

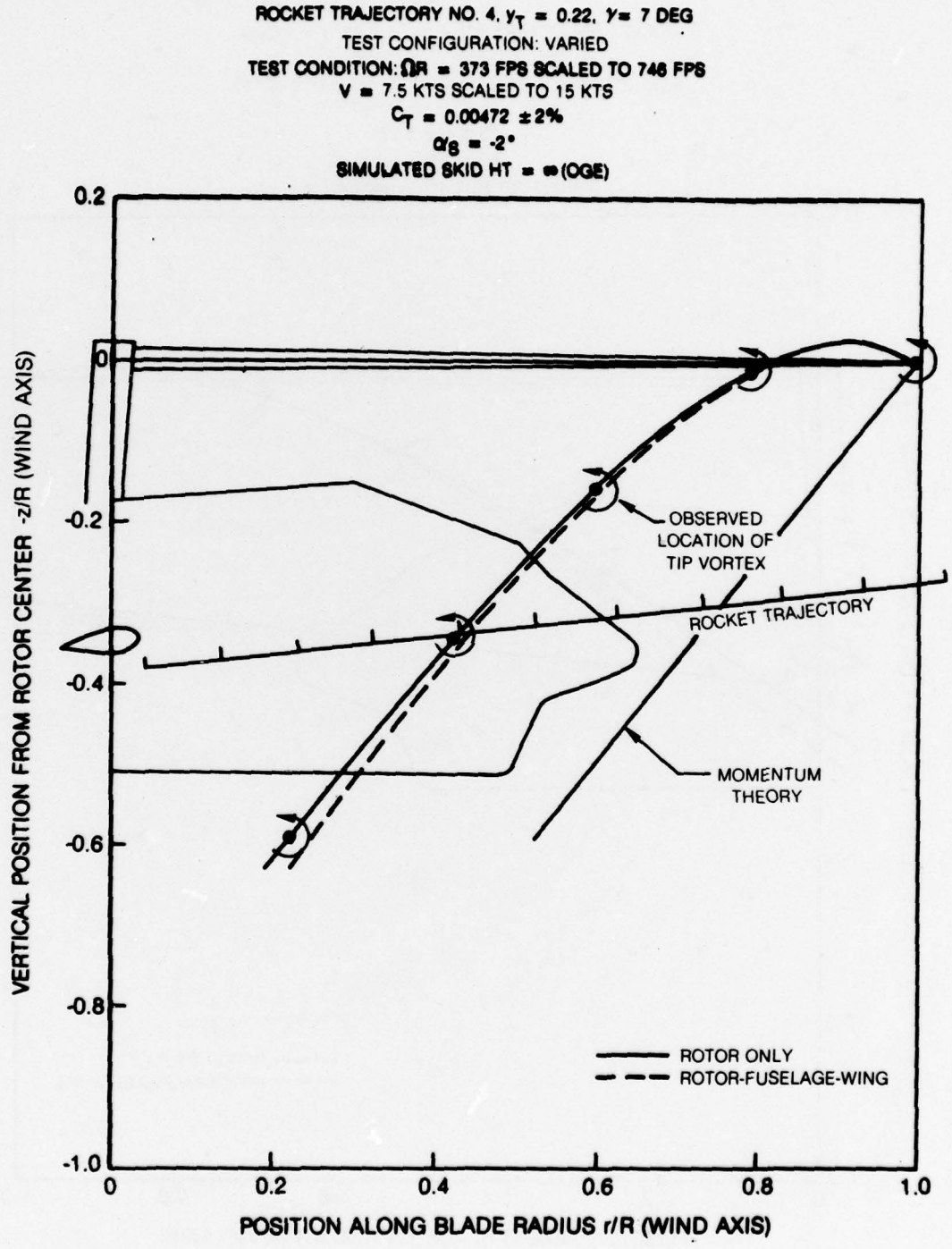

Figure 27. Forward Rotor Wake Boundaries Determined from Smoke Flow Visualization for the 15 kt Reference Condition.

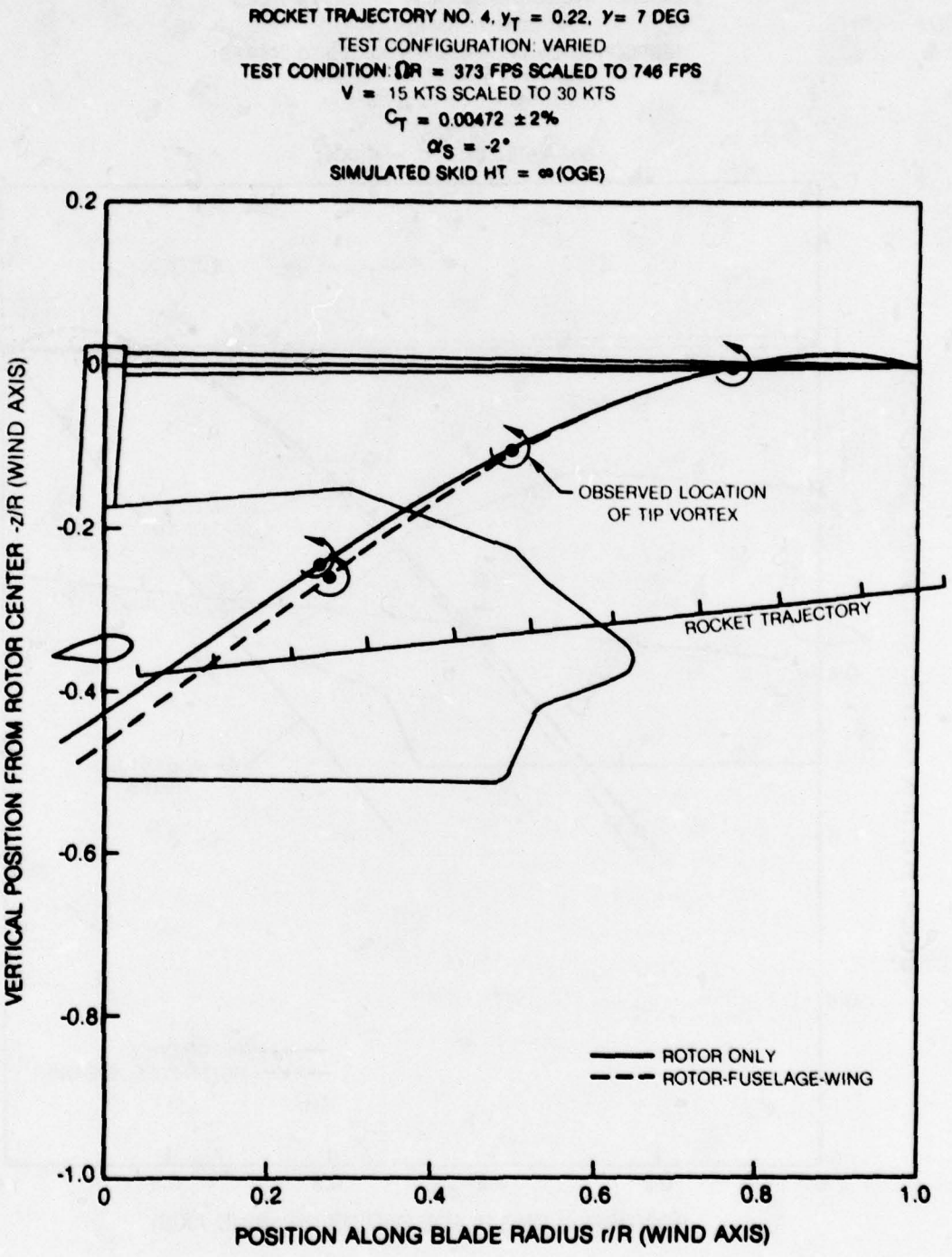

Figure 28. Forward Rotor Wake Boundaries Determined from Smoke Flow Visualization for the 30 kt Reference Condition.

79-09-33-71

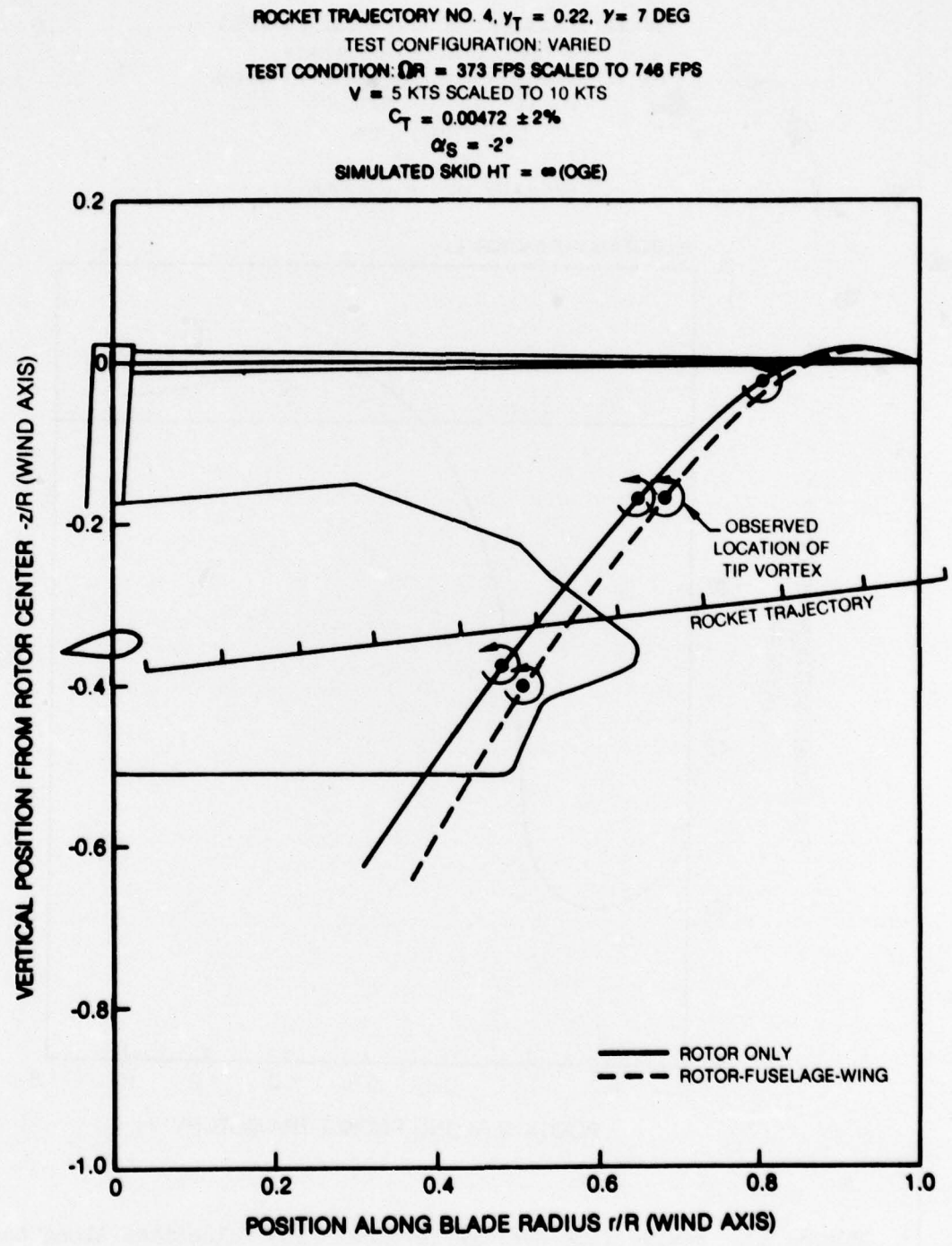

Figure 29. Forward Rotor Wake Boundaries Determined from Smoke Flow Visualization for the Scaled 10 kt Condition.

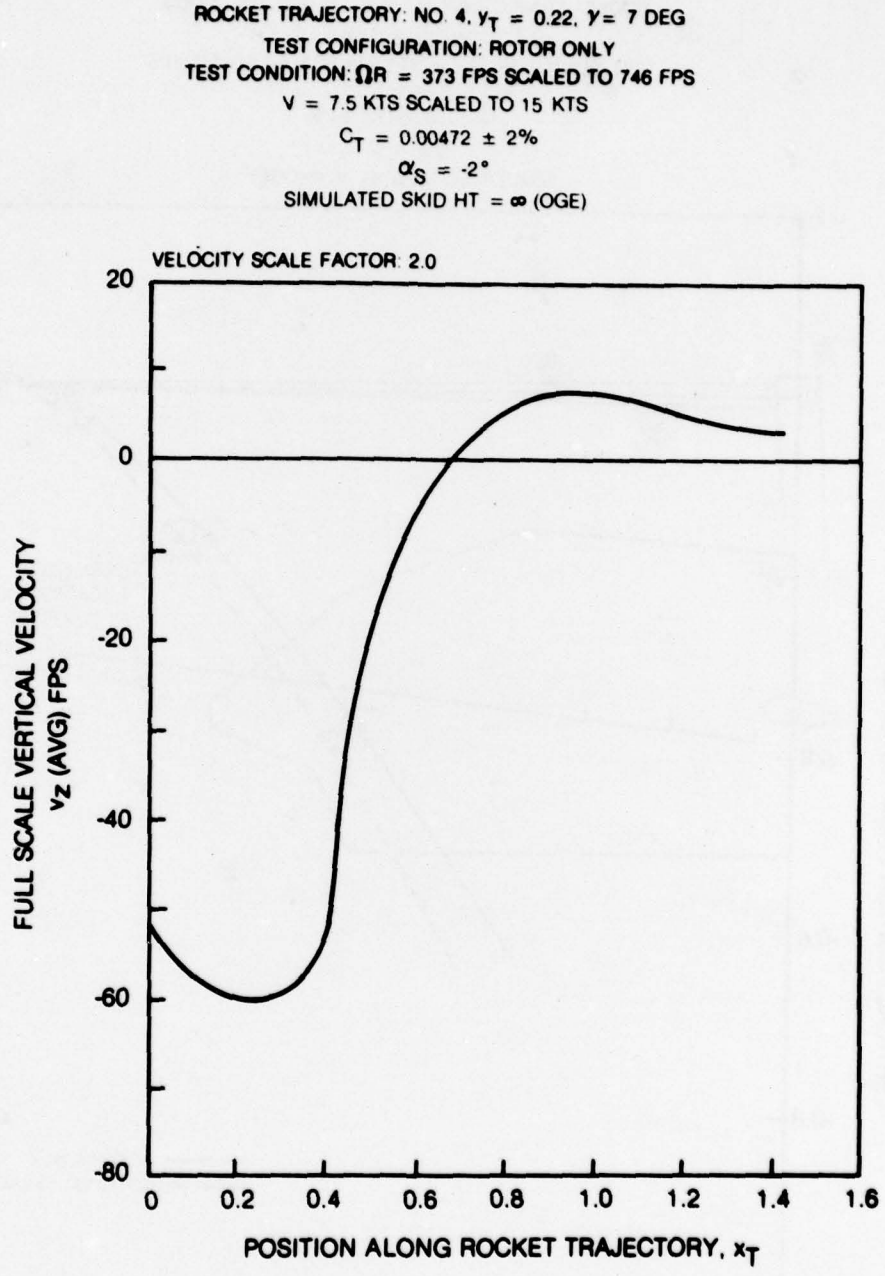

Figure 30. Scaled Time-Average Vertical Flow Velocities Along the Rocket Trajectory for the Isolated Rotor at the 15 kt Reference Condition.

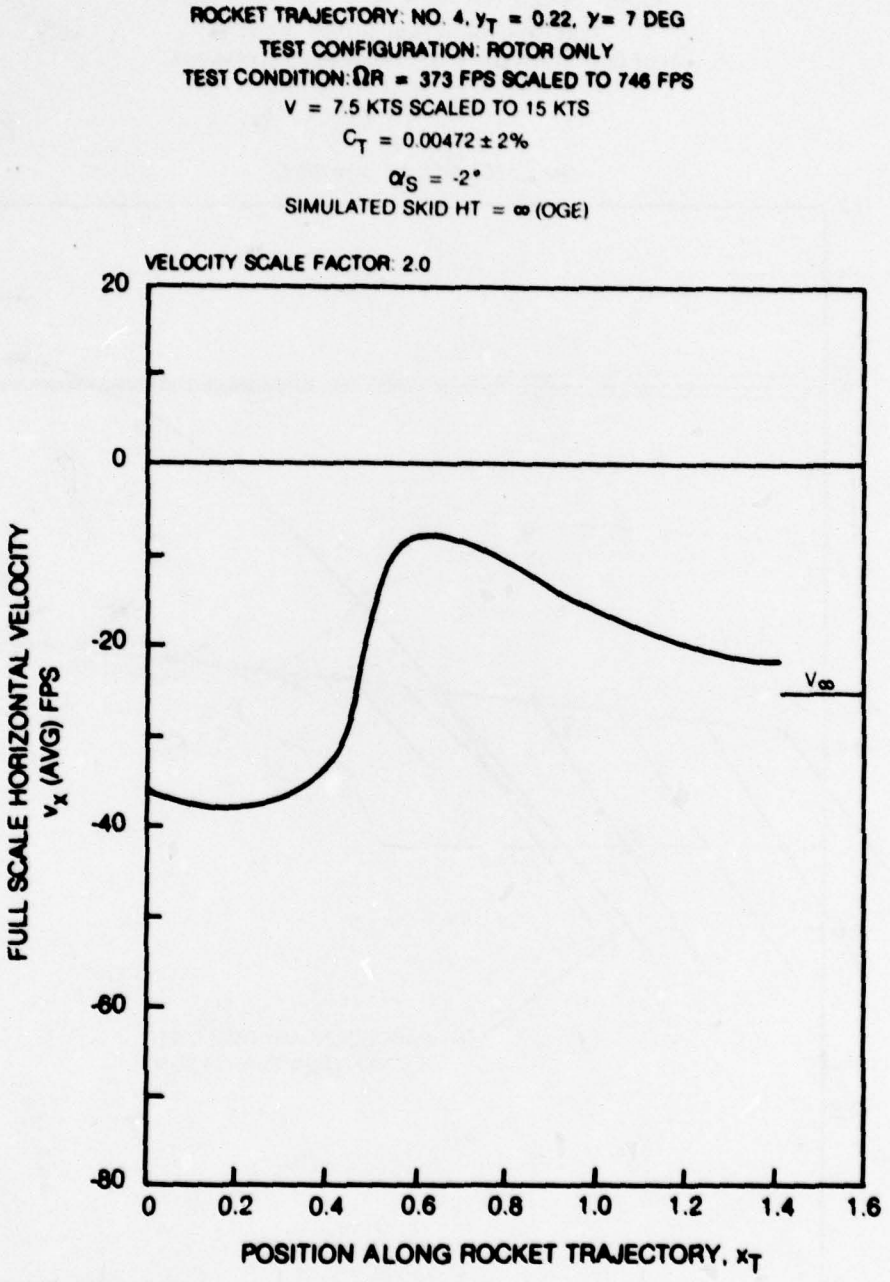

Figure 31. Scaled Time-Average Horizontal Flow Velocities Along the Rocket Trajectory for the Isolated Rotor at the 15 kt Reference Condition.

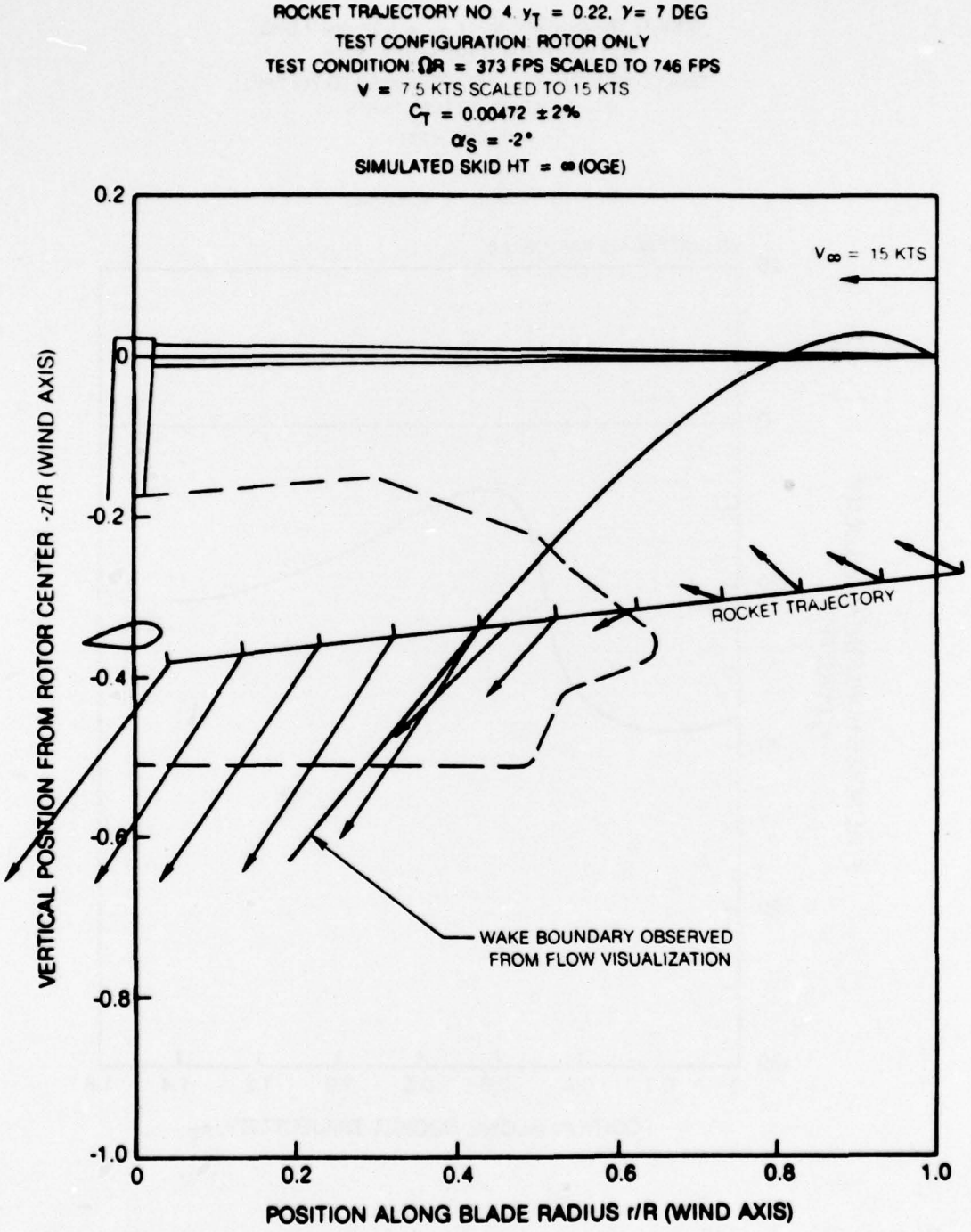

Figure 32. Scaled Time-Average Flow Velocity Vectors Along the Rocket Trajectory for the Isolated Rotor at the 15 kt Reference Condition.

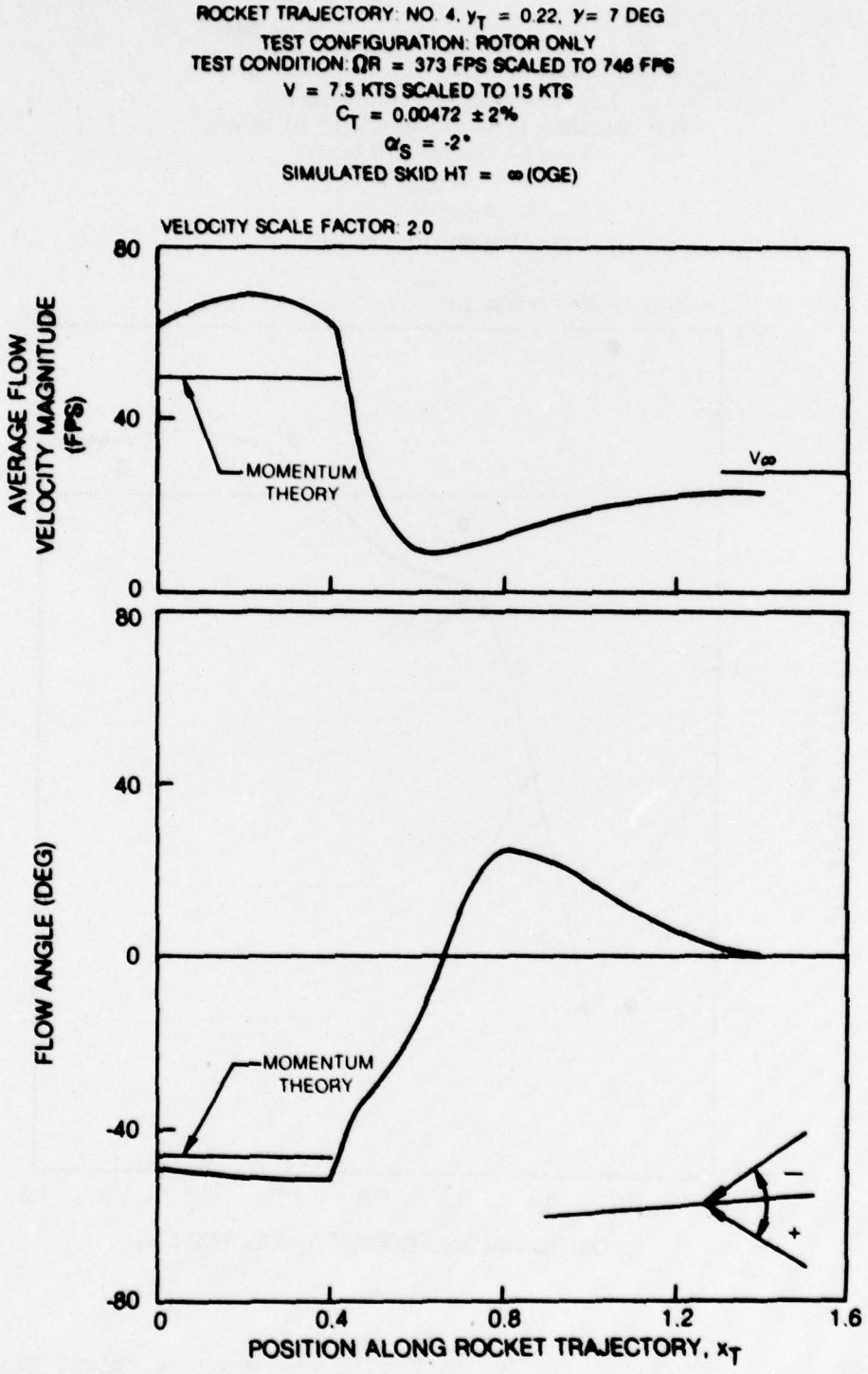

Figure 33. Scaled Time-Average Flow Velocity Magnitude and Flow Angle Along the Rocket Trajectory for the Isolated Rotor at the 15 kt Reference Condition.

79-09-33-61

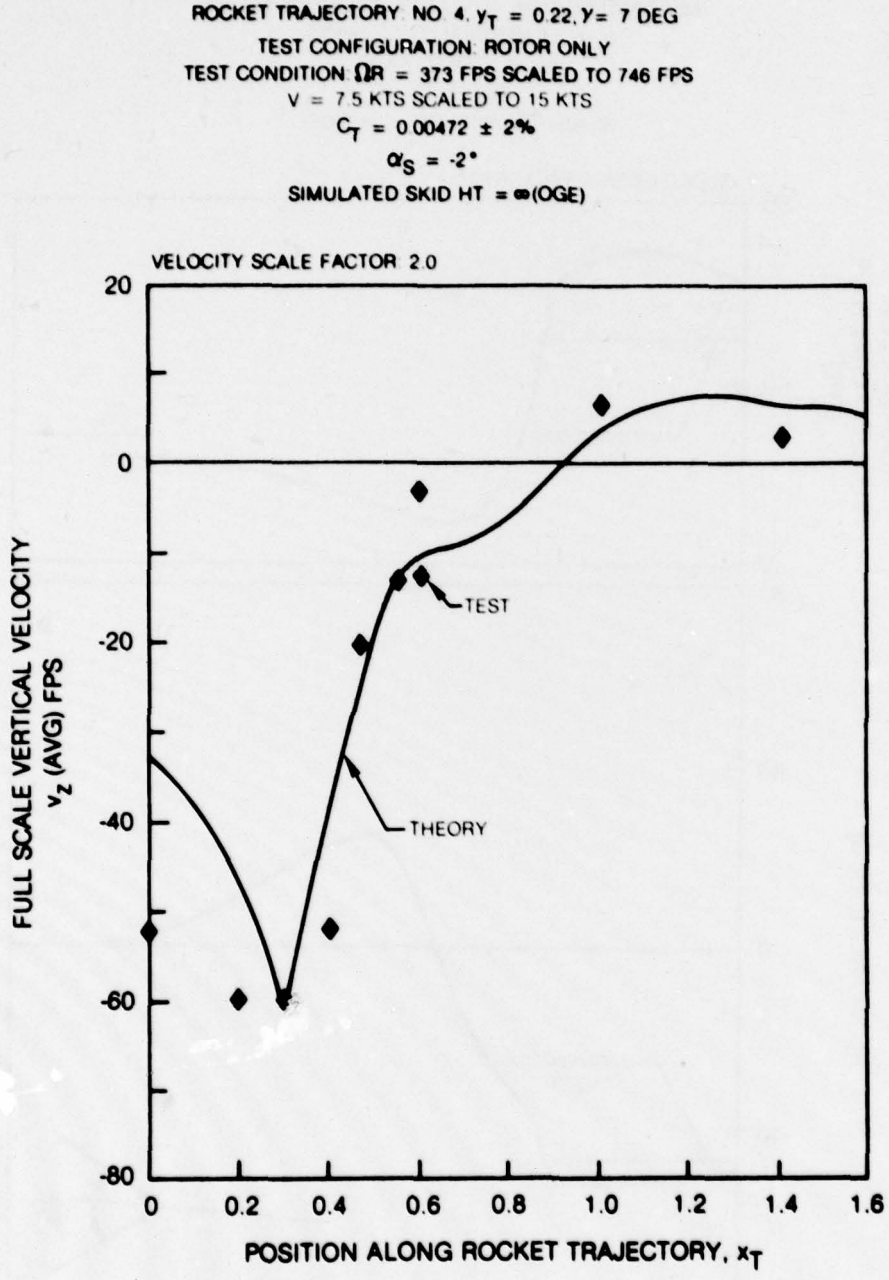

Figure 34. Theory-Test Correlation of Time-Average Vertical Flow Velocities Along the Rocket Trajectory for the Isolated Rotor at the 15 kt Reference Condition.

79-09-33-78

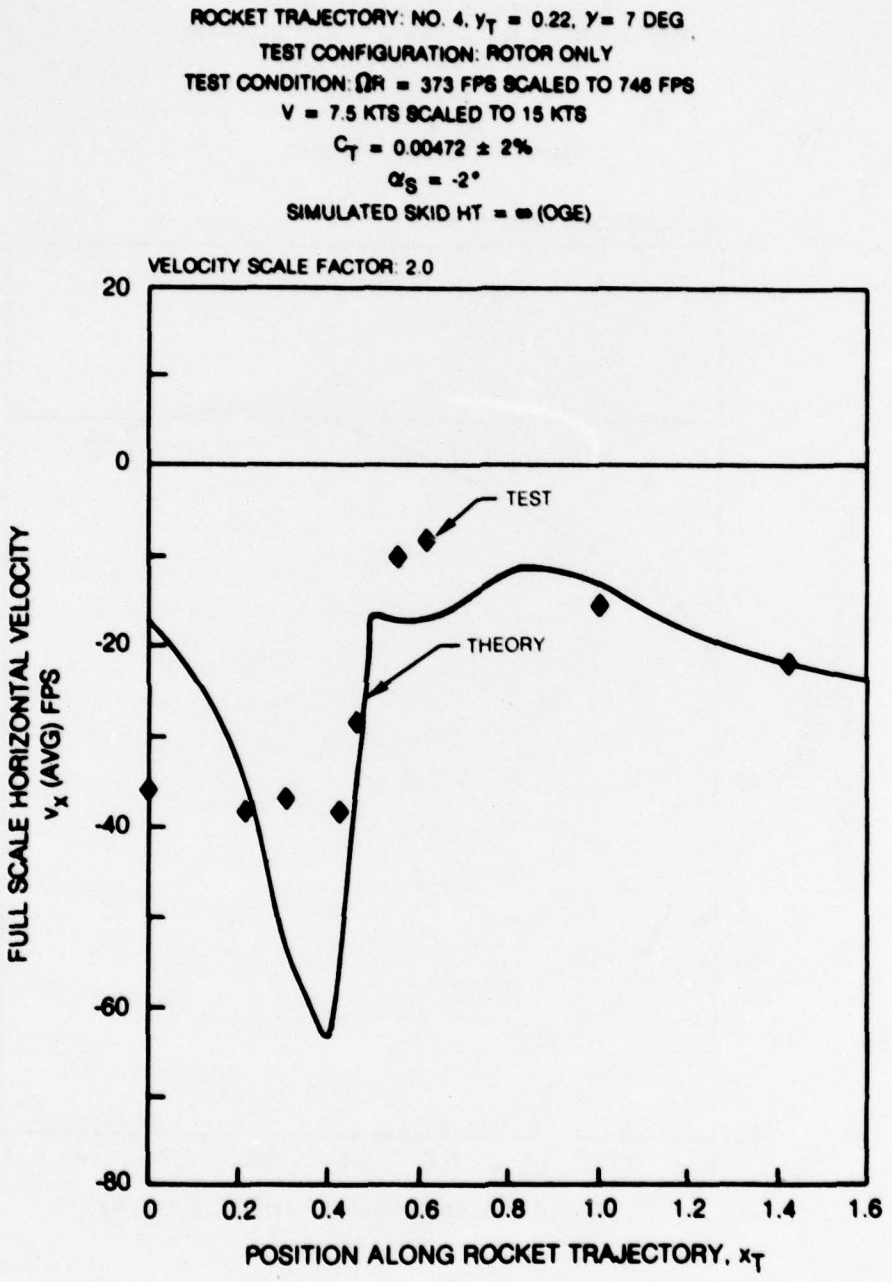

Figure 35. Theory-Test Correlation of Time-Average Horizontal Flow Velocities Along the Rocket Trajectory for the Isolated Rotor at the 15 kt Reference Condition.

79-09-33-79

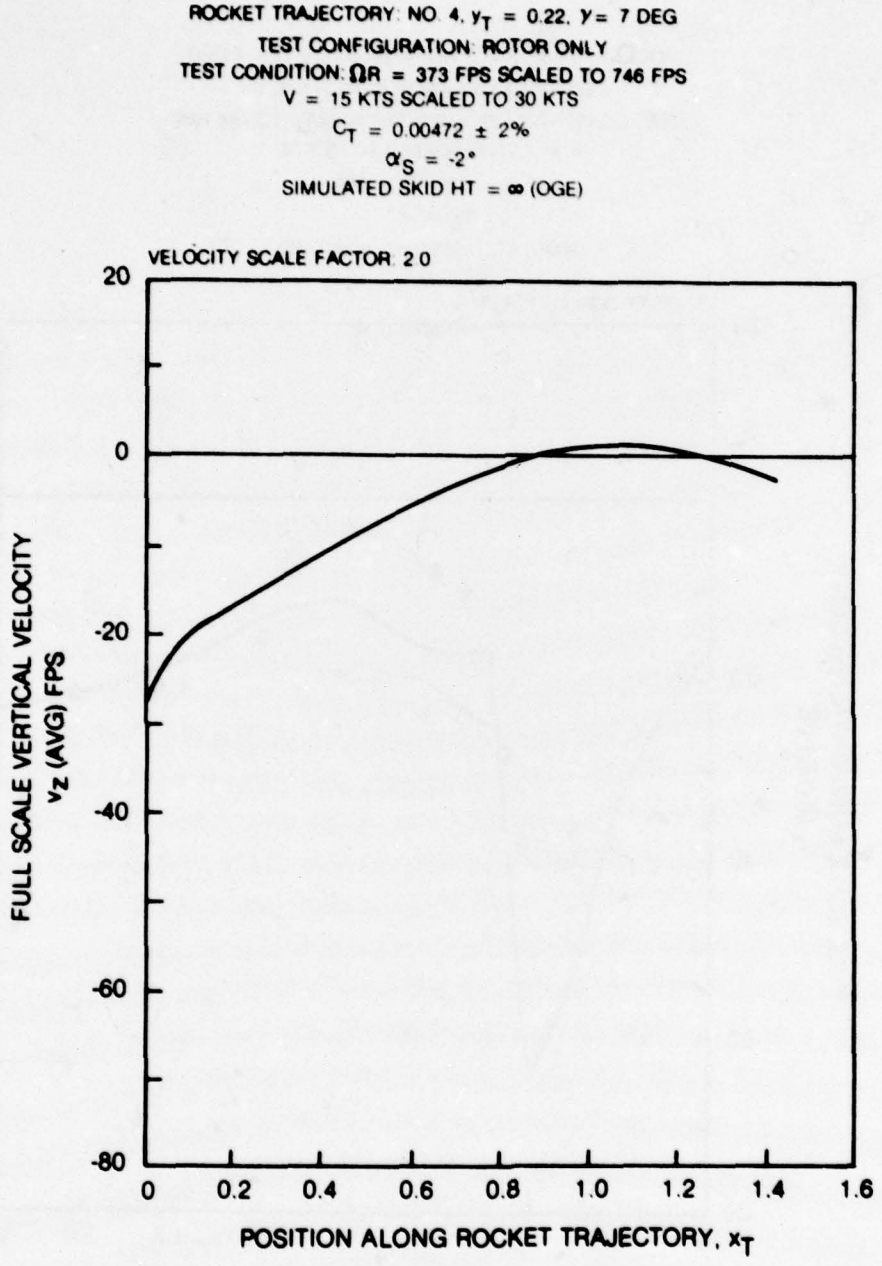

Figure 36. Scaled Time-Average Vertical Flow Velocities Along the Rocket Trajectory for the Isolated Rotor at the 30 kt Reference Condition.

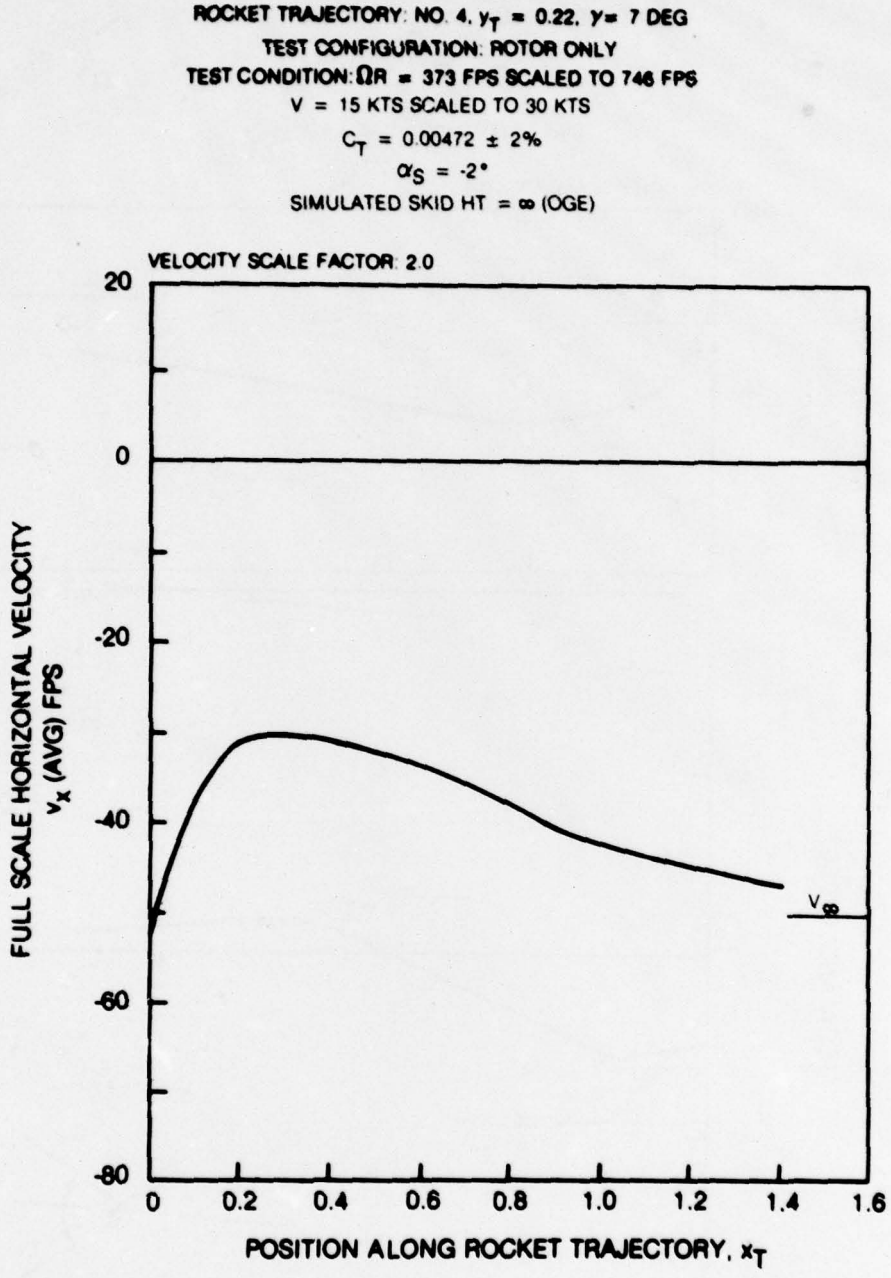

Figure 37. Scaled Time-Average Horizontal Flow Velocities Along the Rocket Trajectory for the Isolated Rotor at the 30 kt Reference Condition.

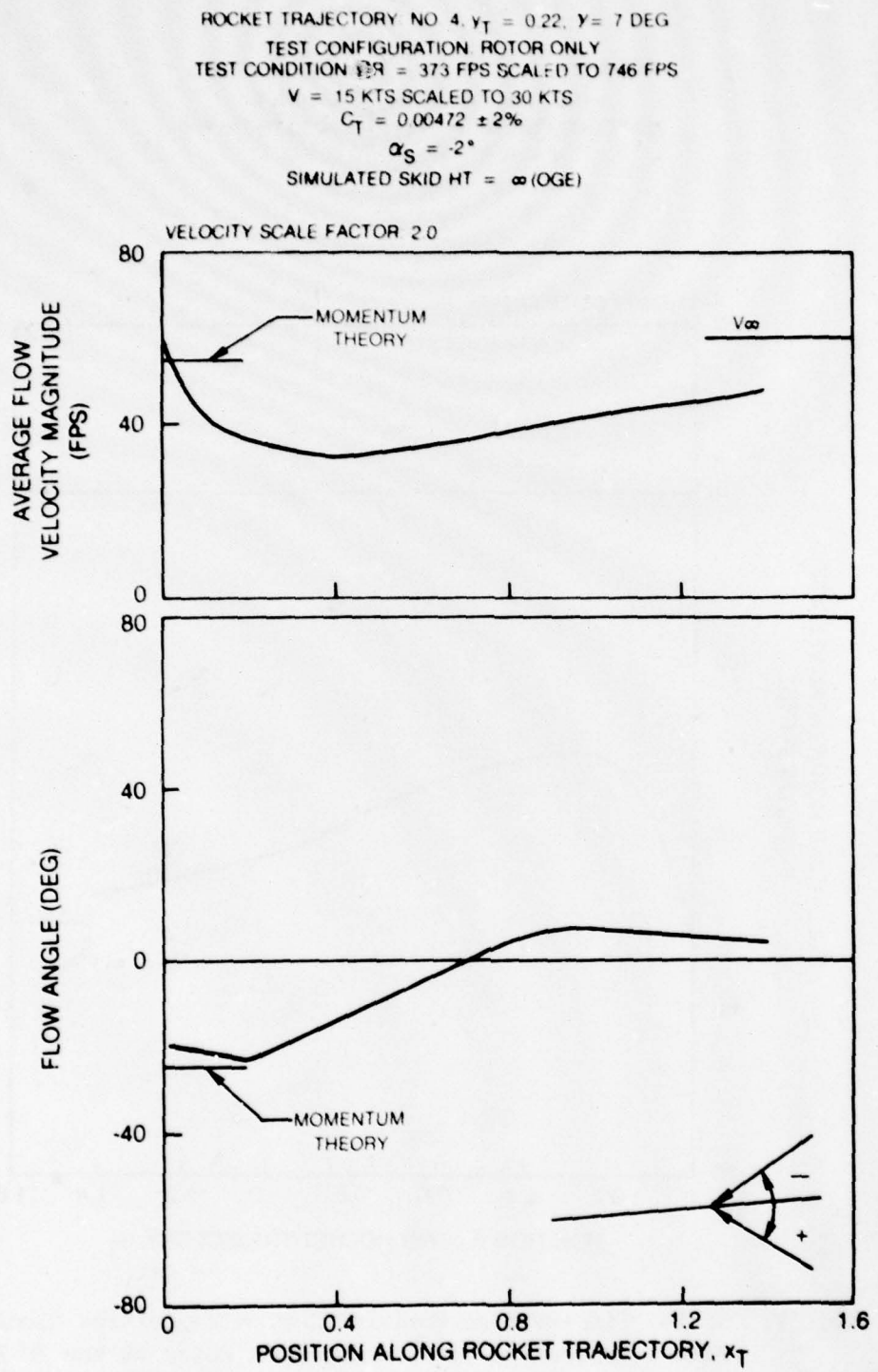

Figure 38. Scaled Time-Average Flow Velocity Magnitude and Flow Angle Along the Rocket Trajectory for the Isolated Rotor at the 30 kt Reference Condition.

79-09-33-62

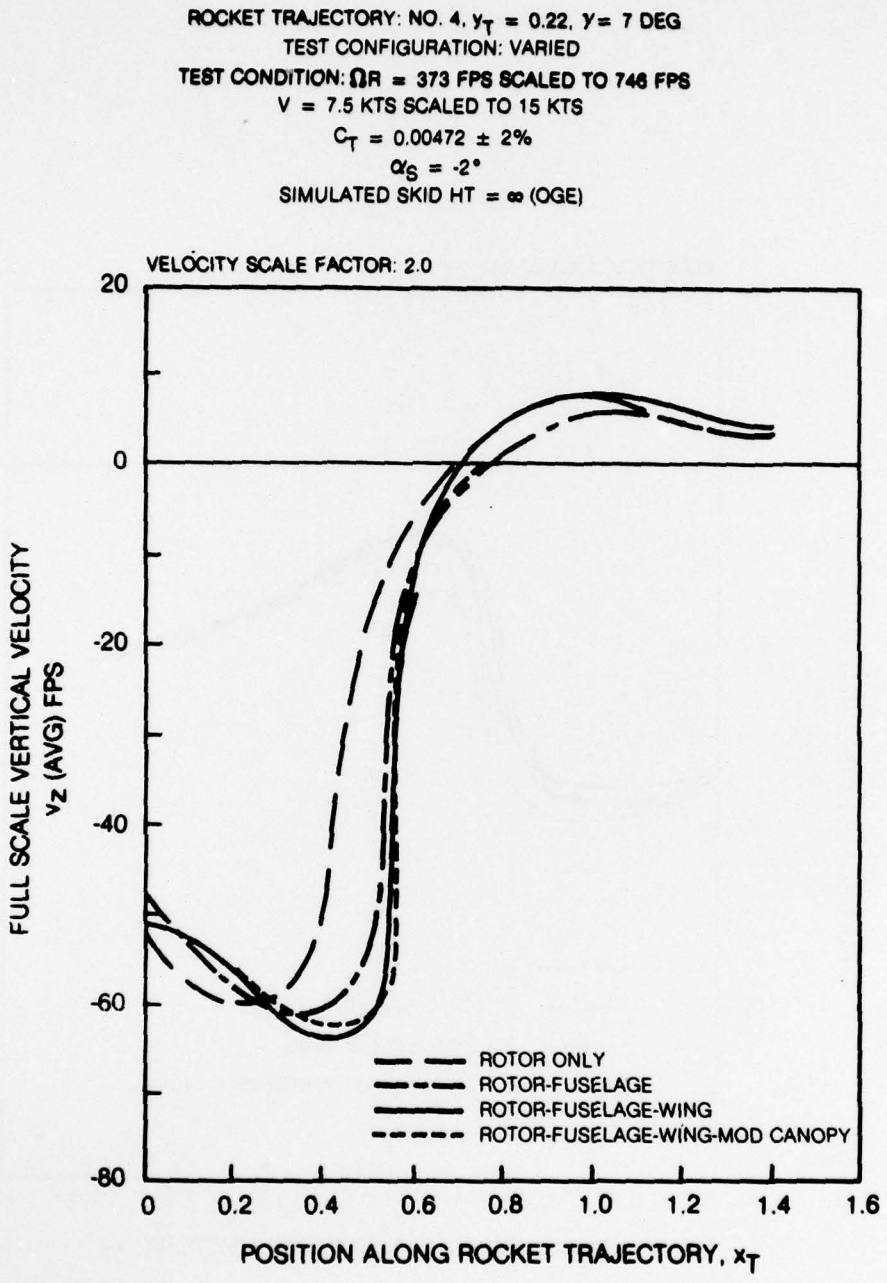

Figure 39. Effect of Model Configuration on the Scaled Time-Average Vertical Flow Velocities Along the Rocket Trajectory for the 15 kt Reference Condition.

79-09-33-51

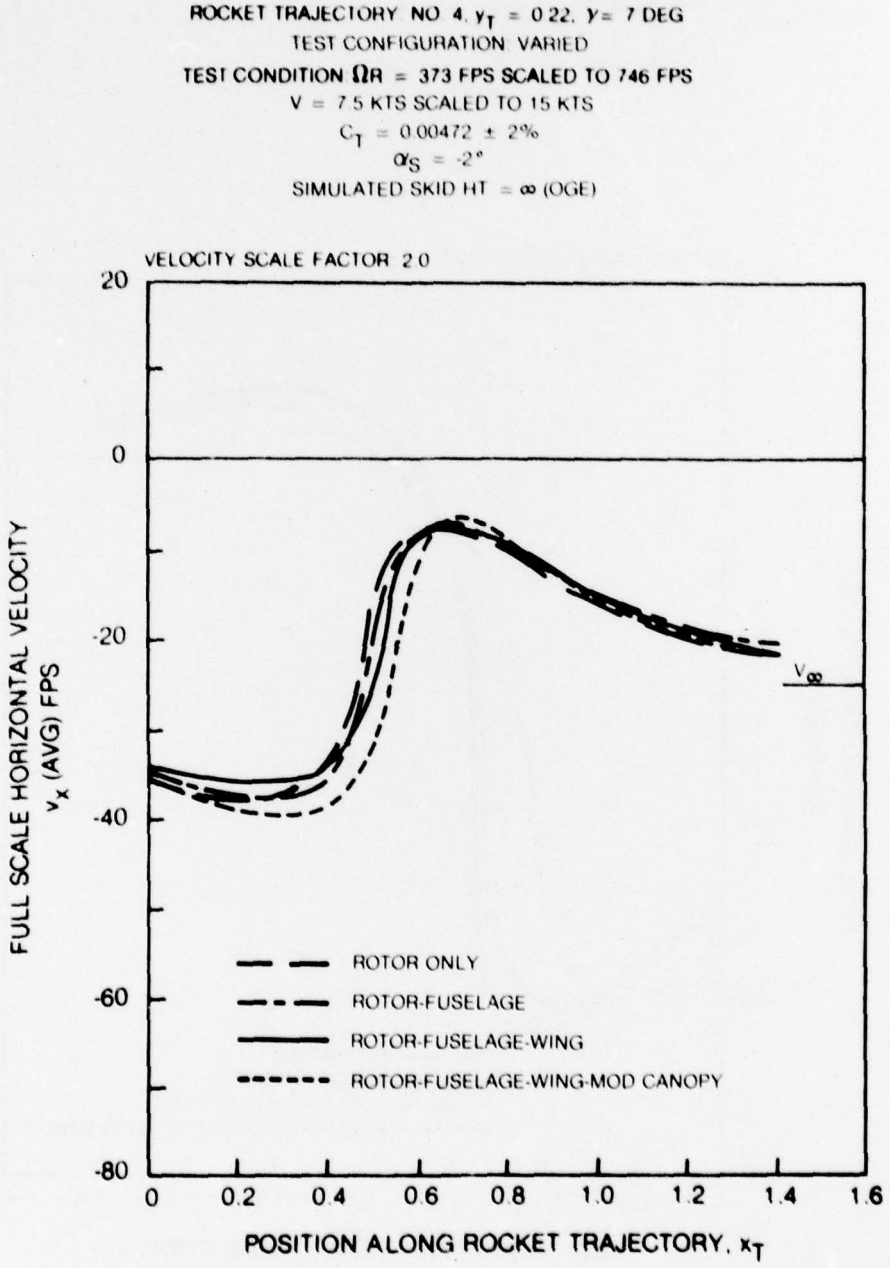

Figure 40. Effect of Model Configuration on the Scaled Time-Average Horizontal Flow Velocities Along the Rocket Trajectory for the 15 kt Reference Condition.

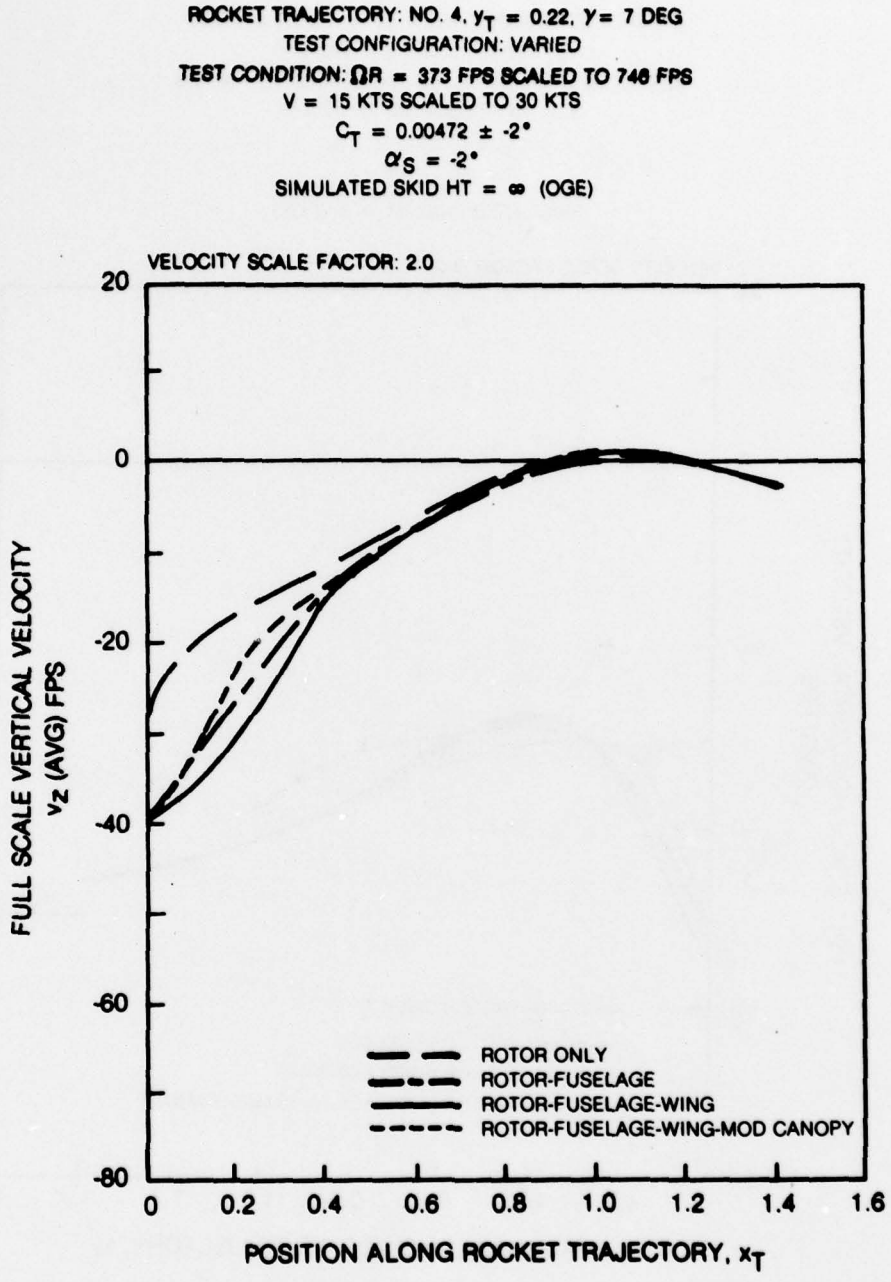

Figure 41. Effect of Model Configuration on the Scaled Time-Average Vertical Flow Velocities Along the Rocket Trajectory for the 30 kt Reference Condition.

79-09-33-52

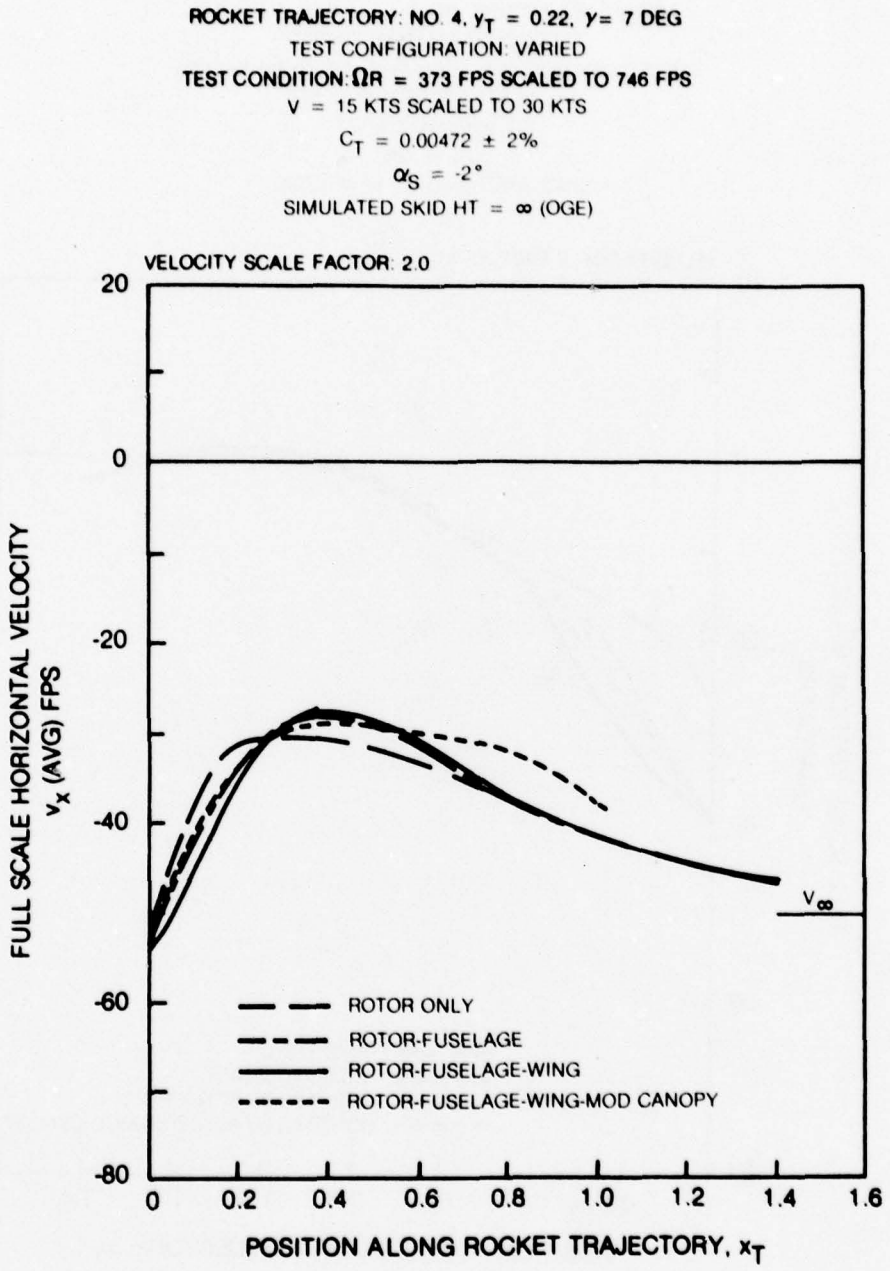

Figure 42. Effect of Model Configuration on the Scaled Time-Average Horizontal Flow Velocities Along the Rocket Trajectory for the 30 kt Reference Condition.

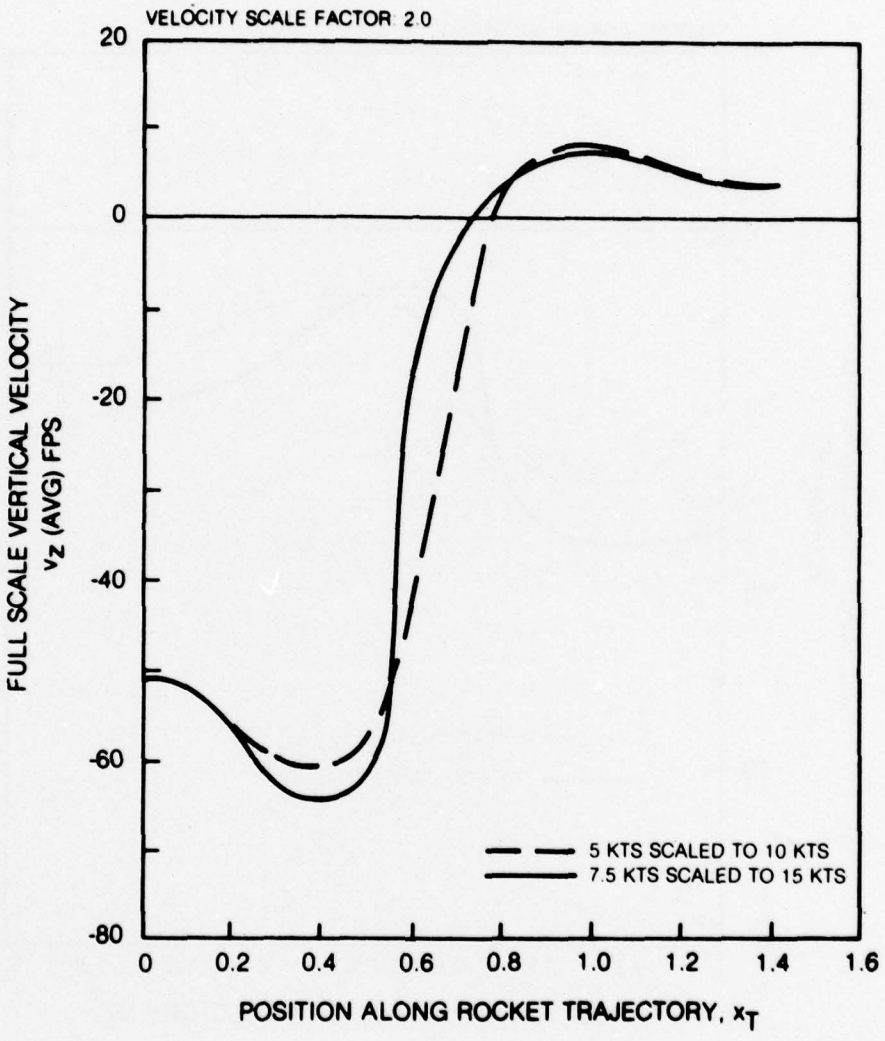

Figure 43. Comparison Between Scaled Time-Average Vertical Flow Velocities Along the Rocket Trajectory for the Reference Configuration at 10 kts and 15 kts.

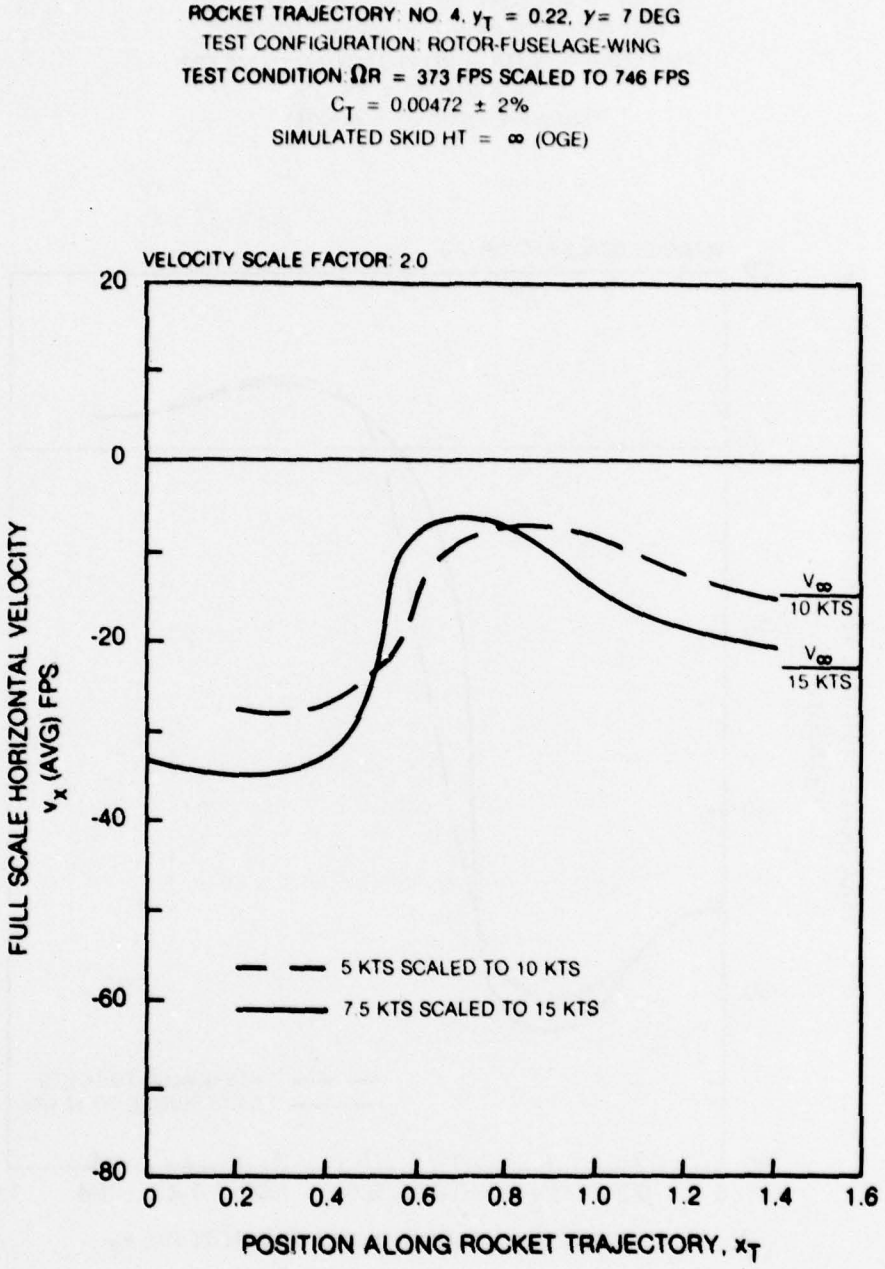

Figure 44. Comparison Between Scaled Time-Average Horizontal Flow Velocities Along the Rocket Trajectory for the Reference Configuration at 10 kts and 15 kts.

79-09-33-41

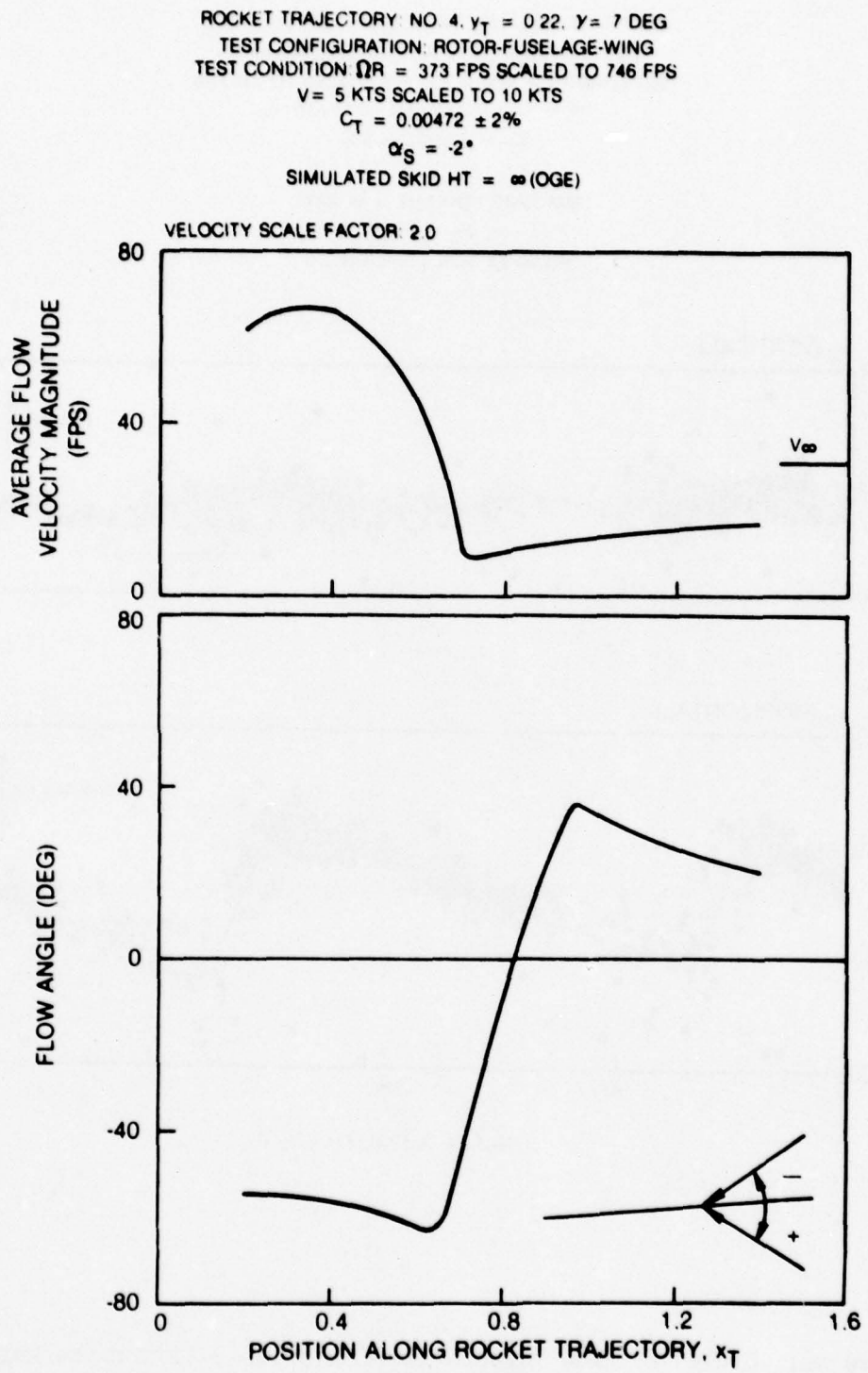

Figure 45. Scaled Time-Average Flow Velocity Magnitude and Flow Angle Along the Rocket Trajectory for the Reference Configuration at 10 kts.

79-09-33-63

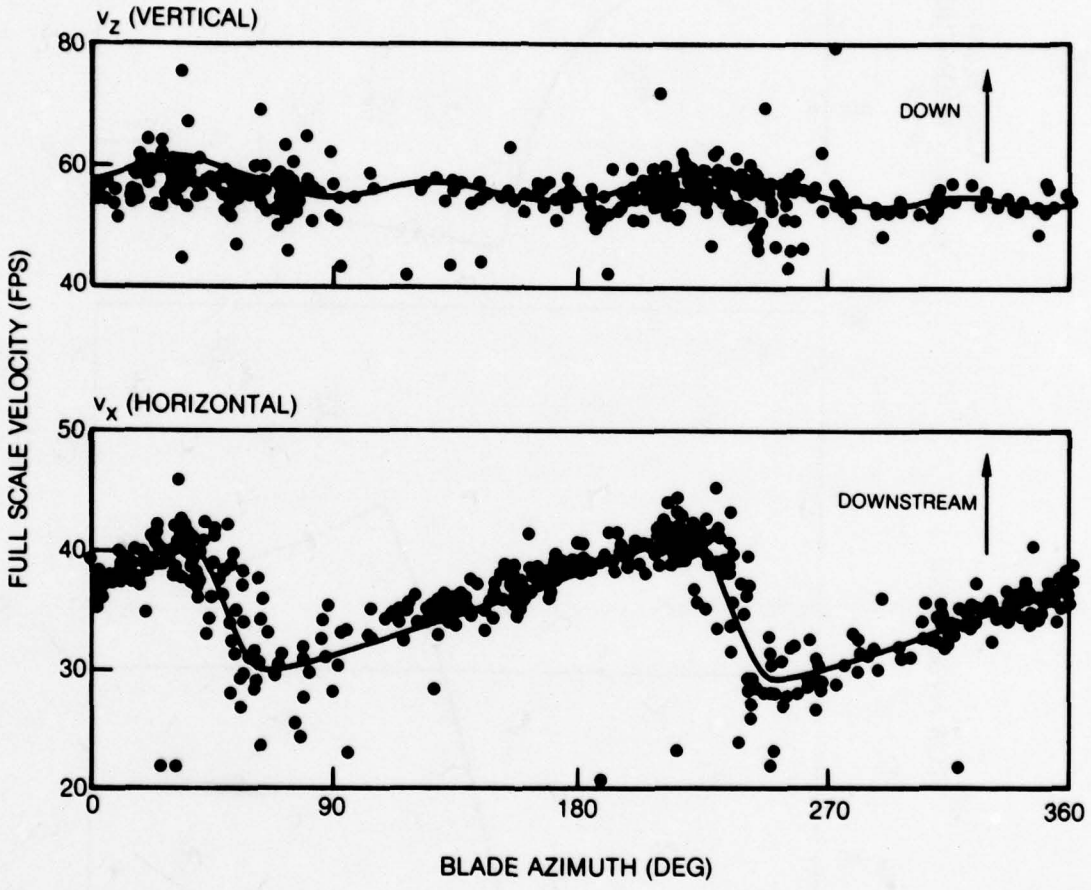

Figure 46. Scaled LV Flow Velocity Results at x_T = .2 for the Reference Configuration at the 15 kt Reference Condition.

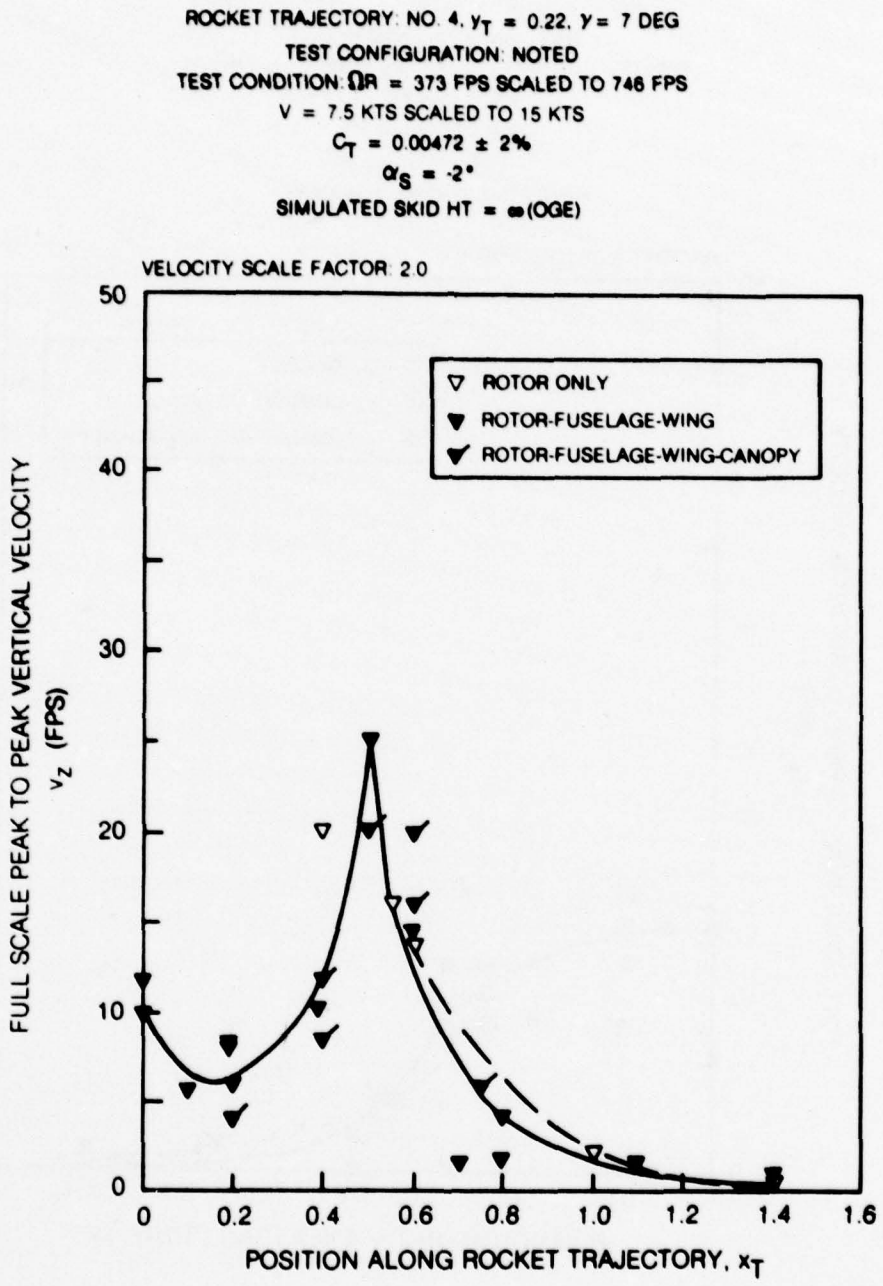

Figure 47. Scaled Peak-to-Peak Vertical Flow Velocities Along the Rocket Trajectory for the 15 kt Reference Condition.

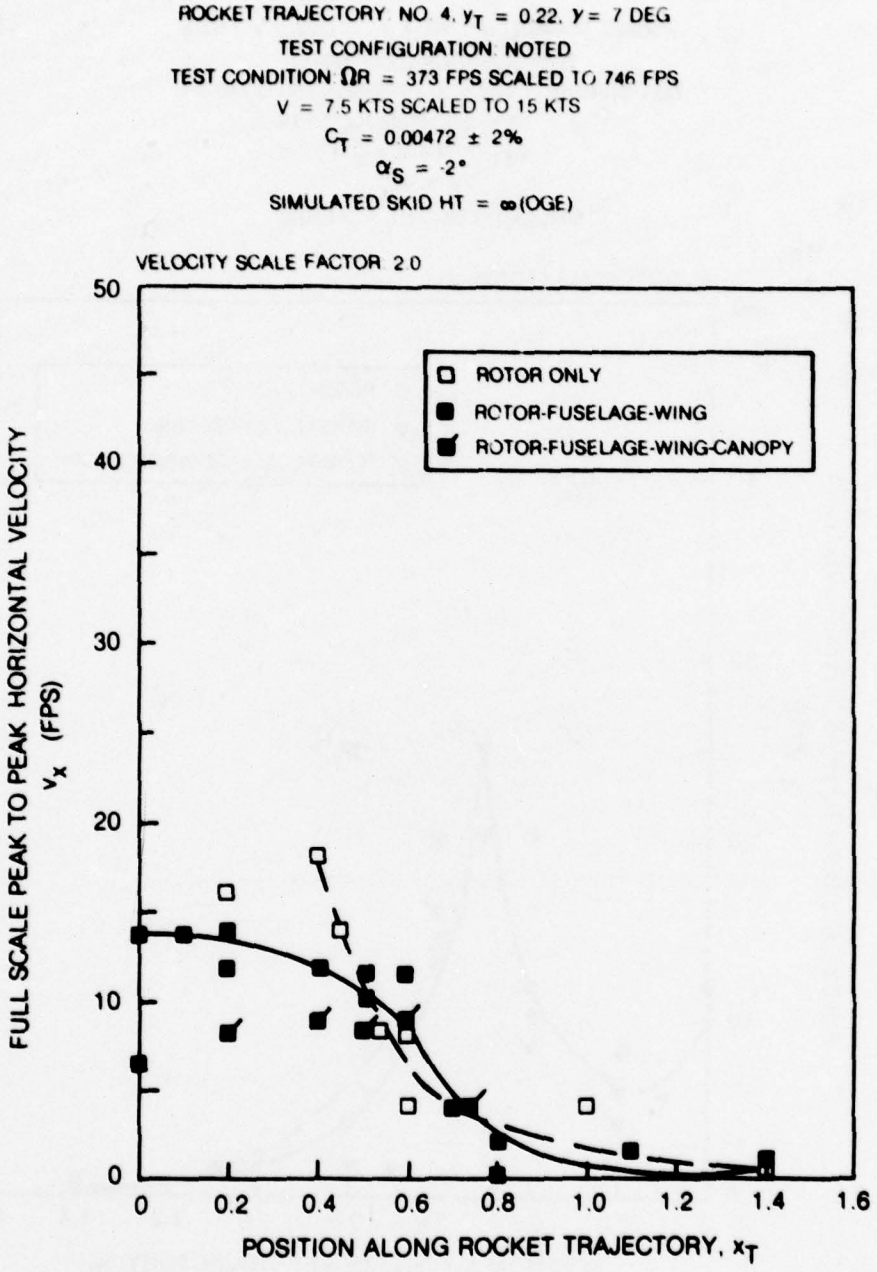

Figure 48. Scaled Peak-to-Peak Horizontal Flow Velocities Along the Rocket Trajectory for the 15 kt Reference Condition.

79-09-33-34

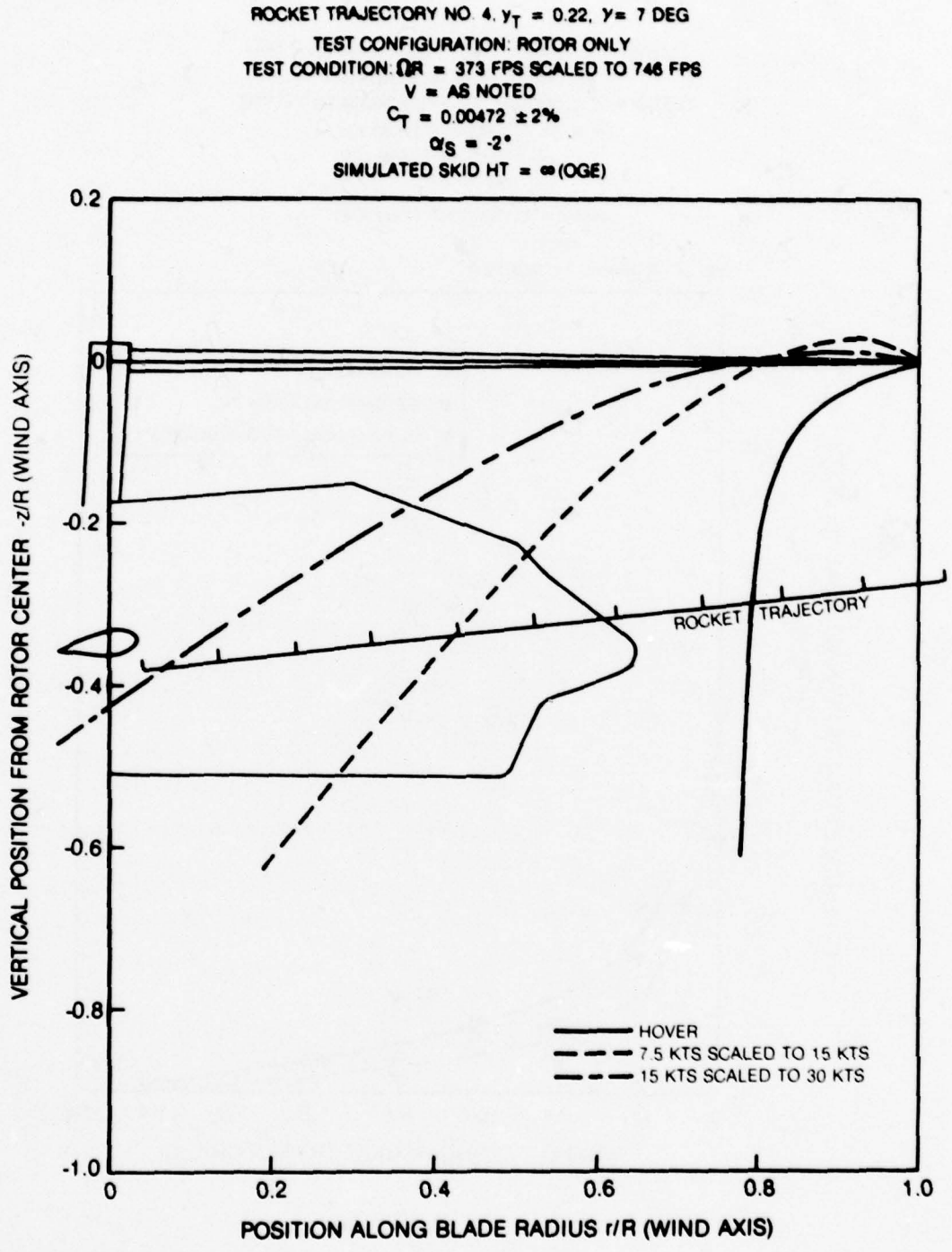

Figure 49. Comparison of the Rotor Wake Boundaries Determined from Smoke Flow Visualization for the Isolated Rotor in Hover and for the 15 kt and 30 kt Reference Conditions.

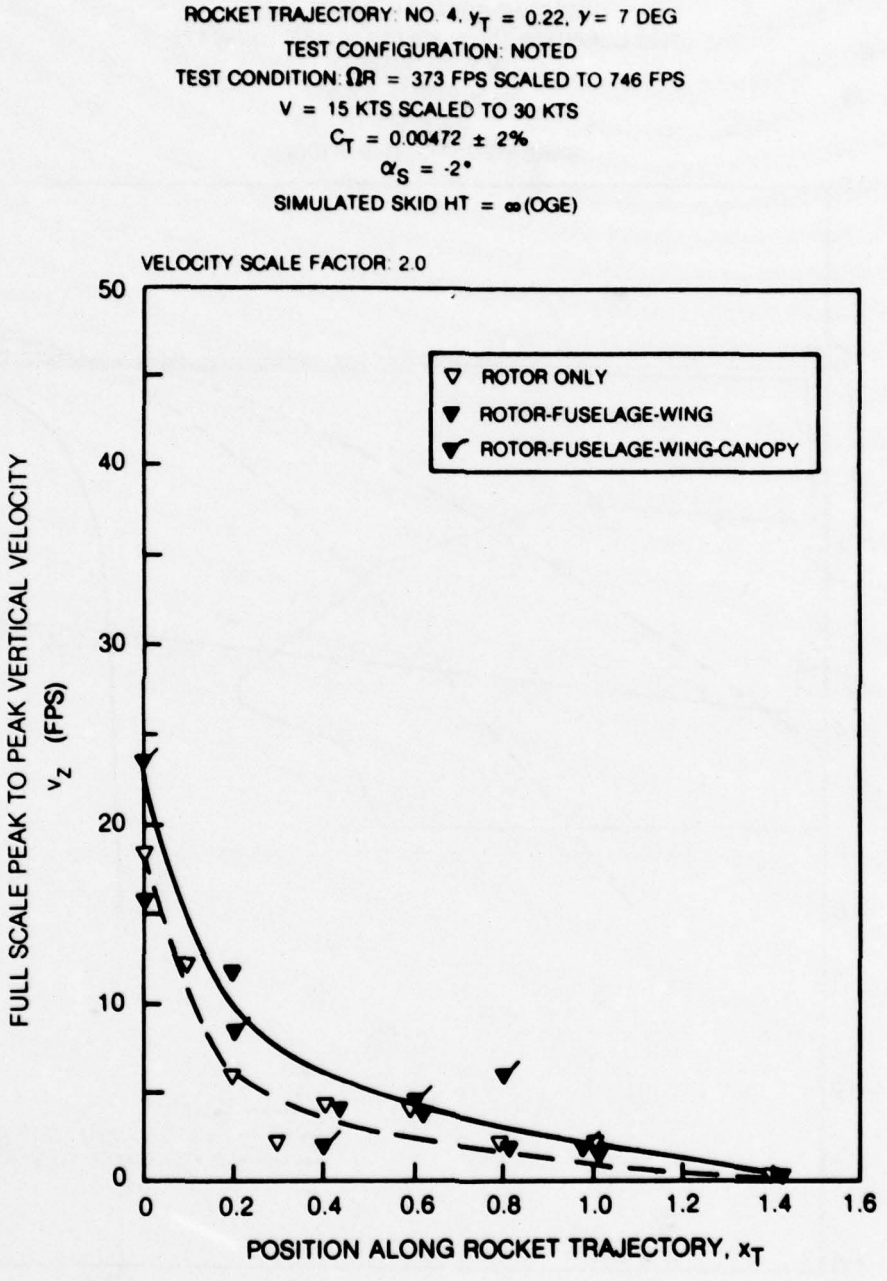

Figure 50. Scaled Peak-to-Peak Vertical Flow Velocities Along the Rocket Trajectory for the 30 kt Reference Condition.

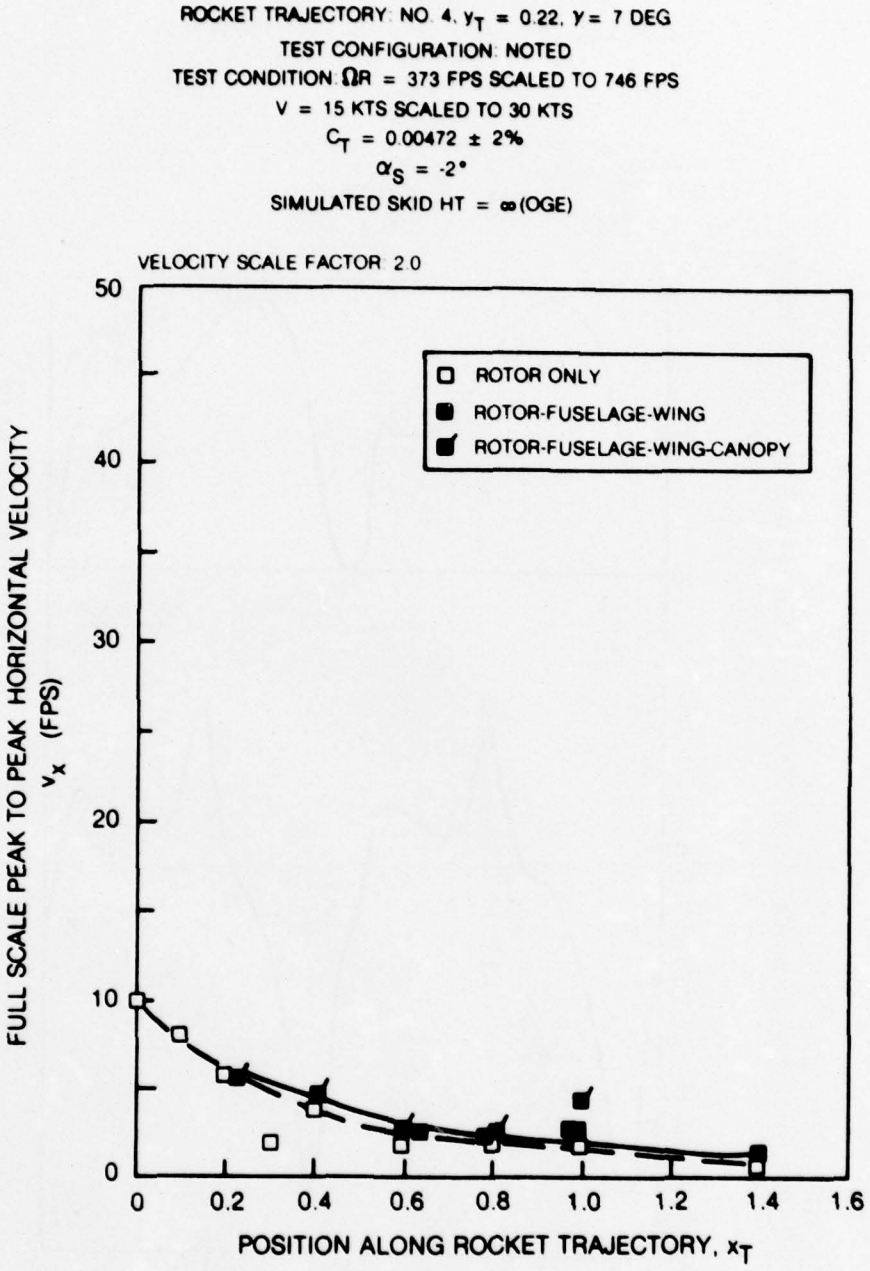

Figure 51. Scaled Peak-to-Peak Horizontal Flow Velocities Along the Rocket Trajectory for the 30 kt Reference Condition.

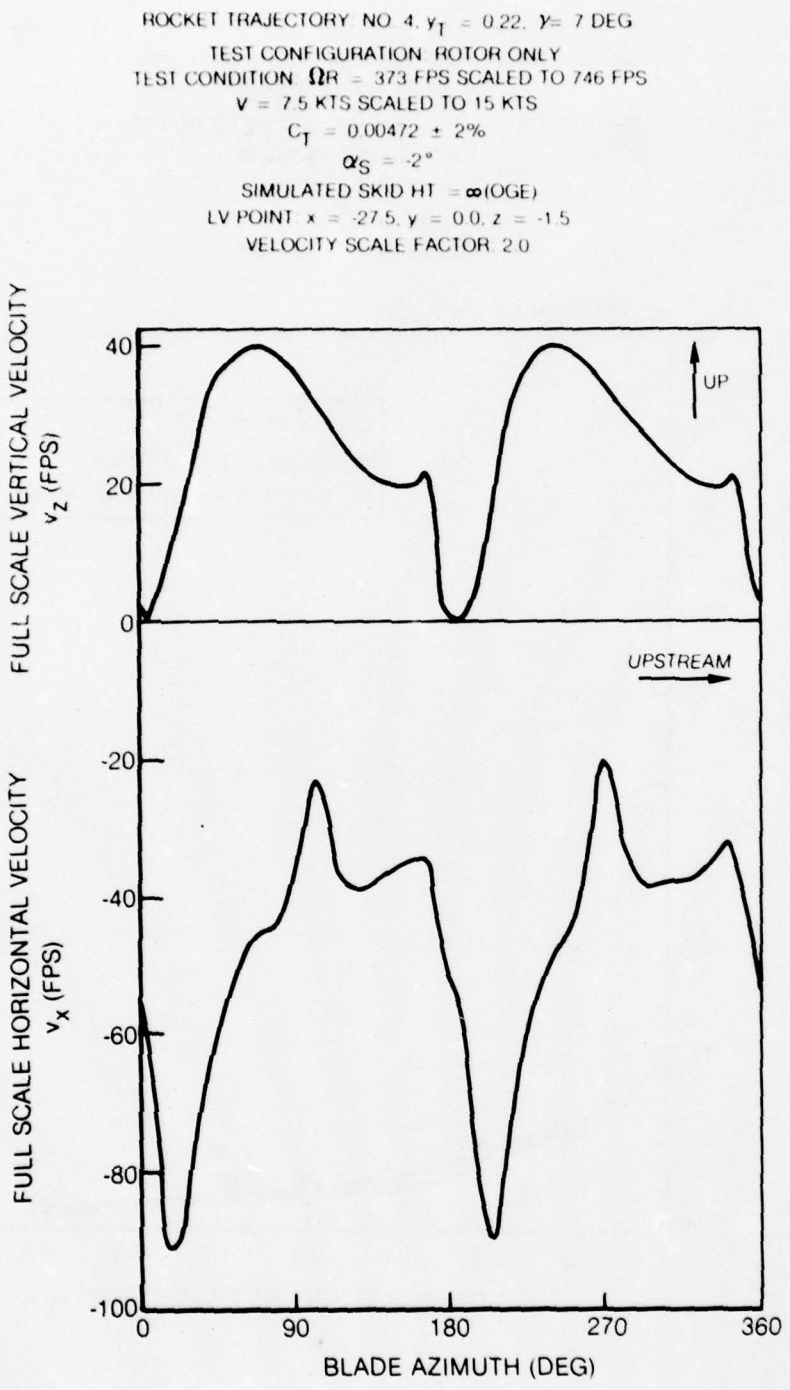

Figure 52. Time Variation of the Scaled LV Flow Velocity Results at a Point Above the Rotor and Near the Upstream Blade Tip for the 15 kt Reference Condition.

ROCKET TRAJECTORY: NO. 4 y_T = 0.22, γ = 7 DEG
TEST CONFIGURATION: ROTOR ONLY
TEST CONDITION: ΩR = 373 FPS SCALED TO 746 FPS
V = 7.5 KTS SCALED TO 15 KTS
C_T = 0.00472 ± 2%
α_S = -2°
SIMULATED SKID HT = ∞ (OGE)
LV POINT: x = NOTED, y = 0.0, z = -1.5
VELOCITY SCALE FACTOR: 2.0

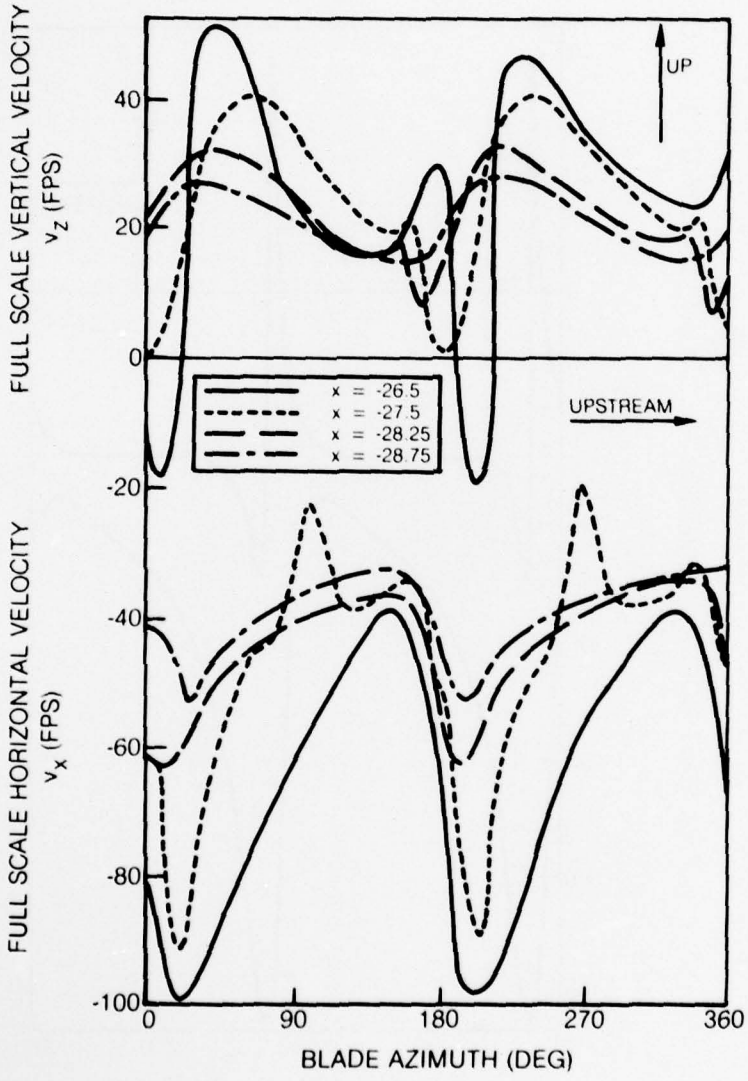

Figure 53. Time Variation of the Scaled LV Flow Velocity Results for Several Points Above the Rotor and Near the Upstream Blade Tip for the 15 kt Reference Condition.

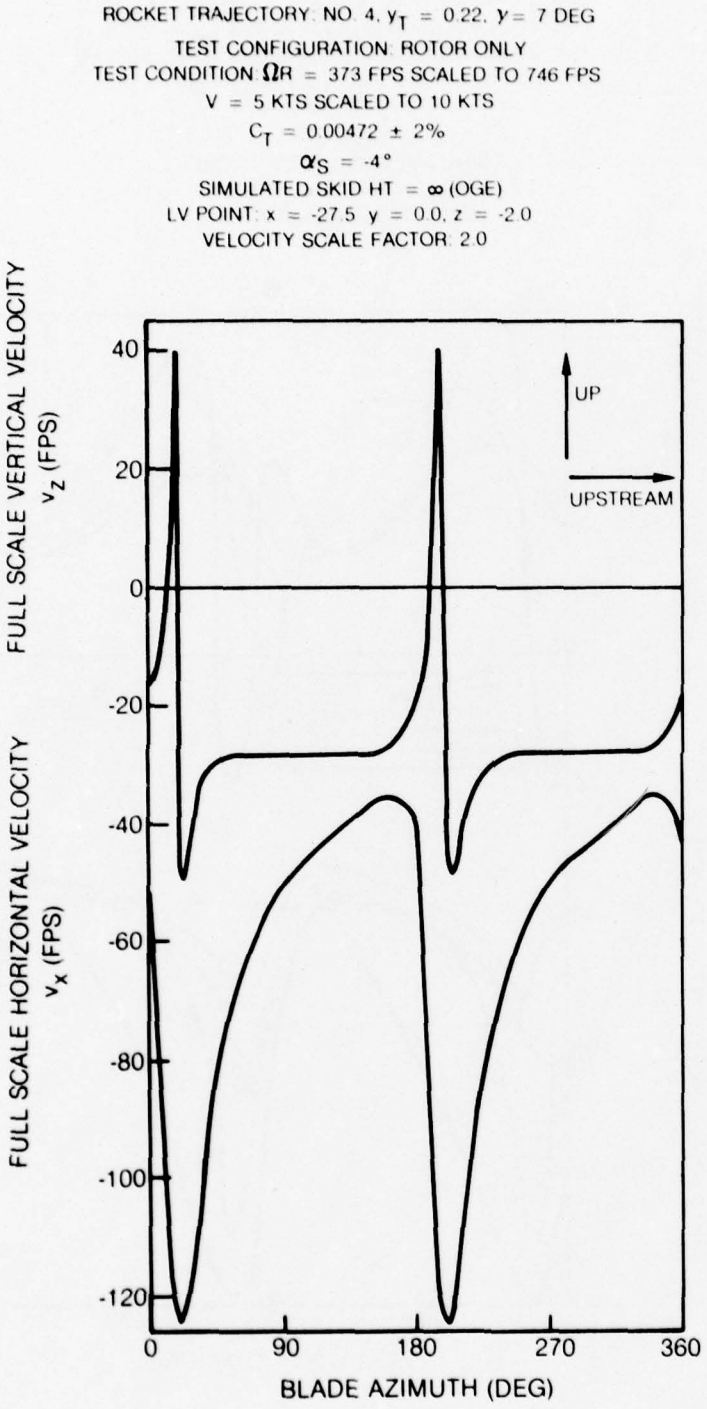

Figure 54. Time Variation of the Scaled LV Flow Velocity Results for a Point Close to the Tip Vortex Above the Blade at 10 kts.

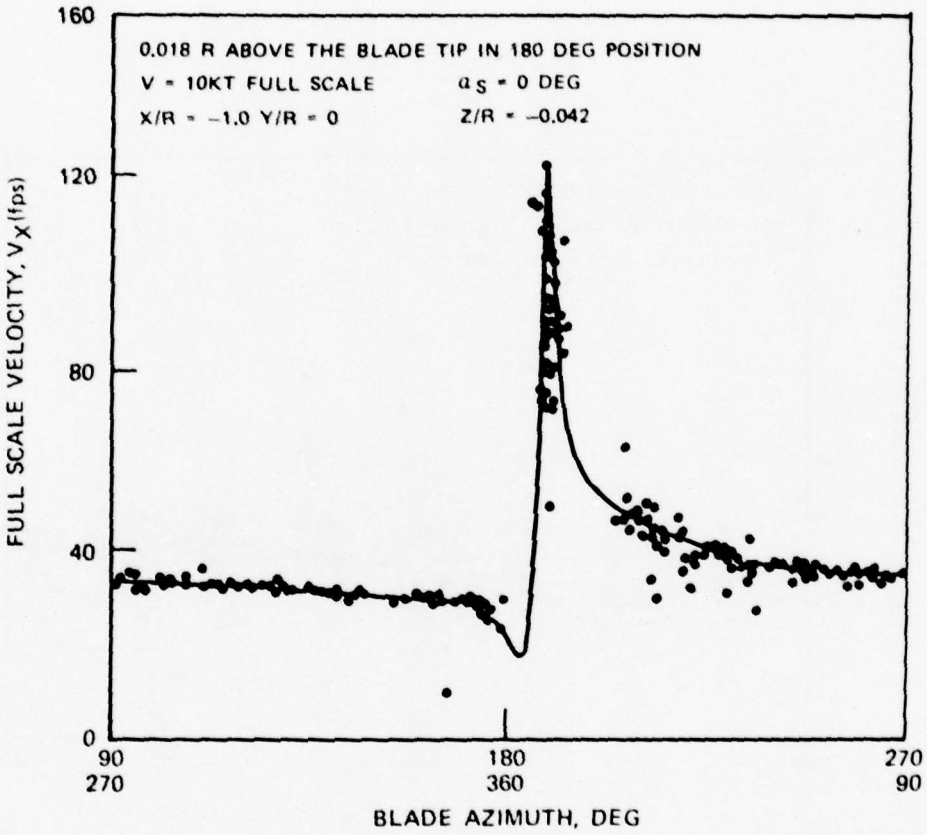

Figure 55. Time Variation of the Horizontal Flow Velocity Component at a Point Near the Up Stream Blade Tip for a Zero Shaft Tilt 10 kt Condition.

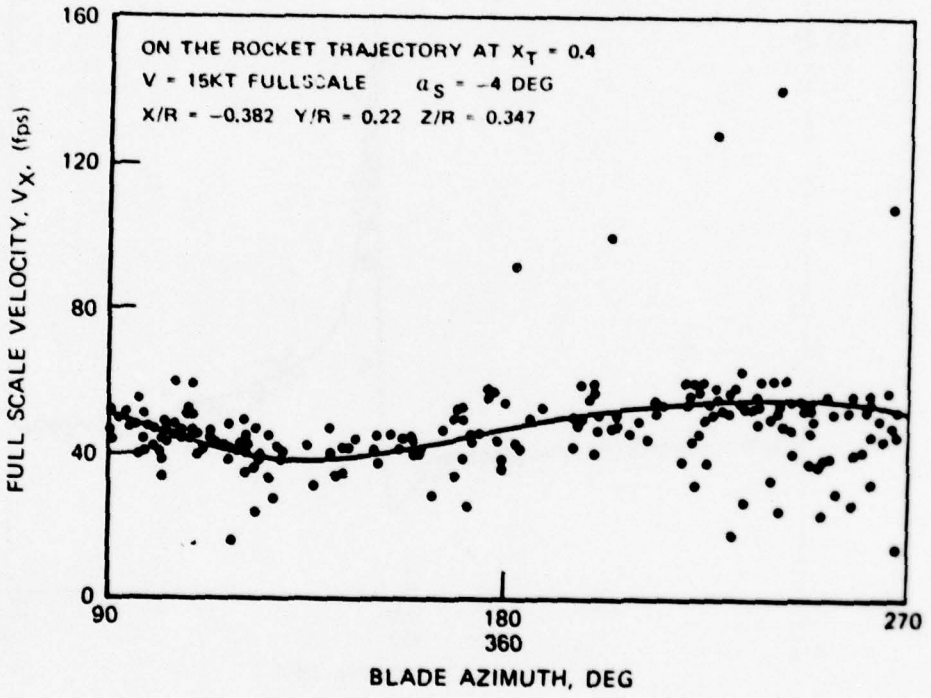

Figure 56. Time Variation of the Horizontal Flow Velocity Component at a Point on the Rocket Trajectory Near the Wake Boundary for a 4 Degree Shaft Tilt 15 kt Condition.

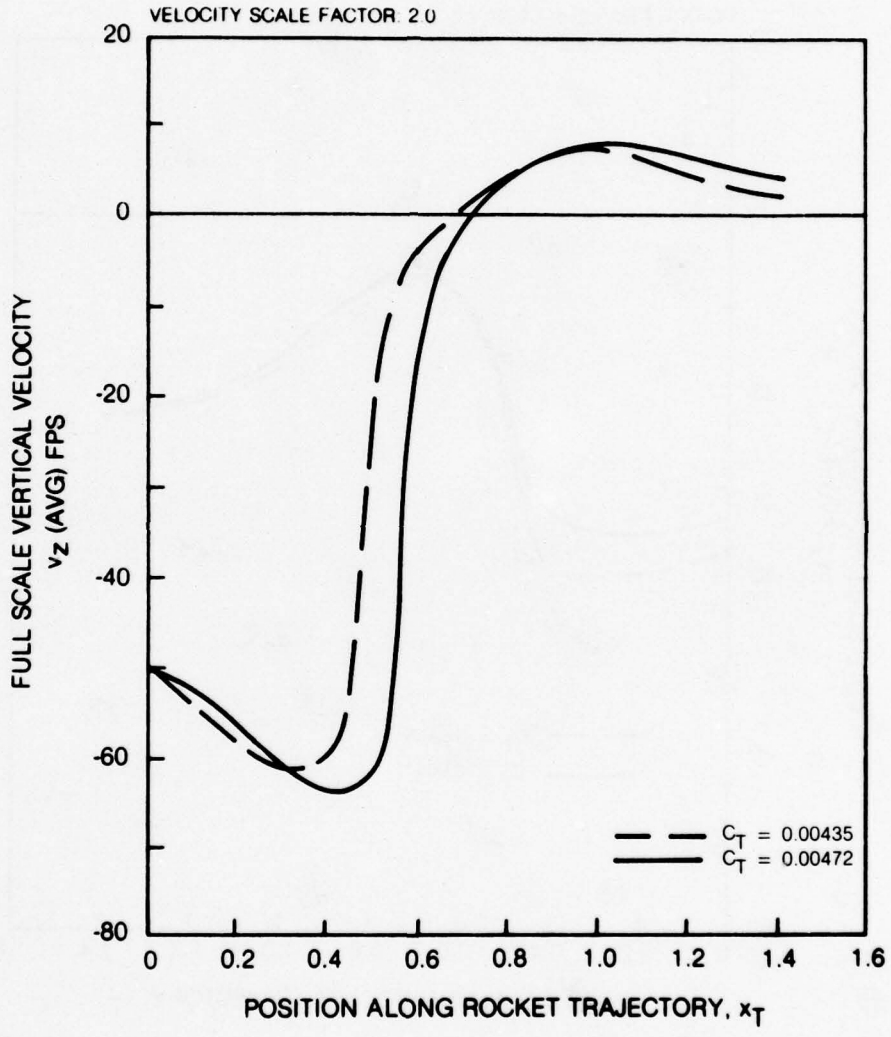

Figure 57. Effect of Rotor Thrust on the Scaled Time-Average Vertical Flow Velocities Along the Rocket Trajectory for the Reference Configuration at the 15 kt Reference Condition.

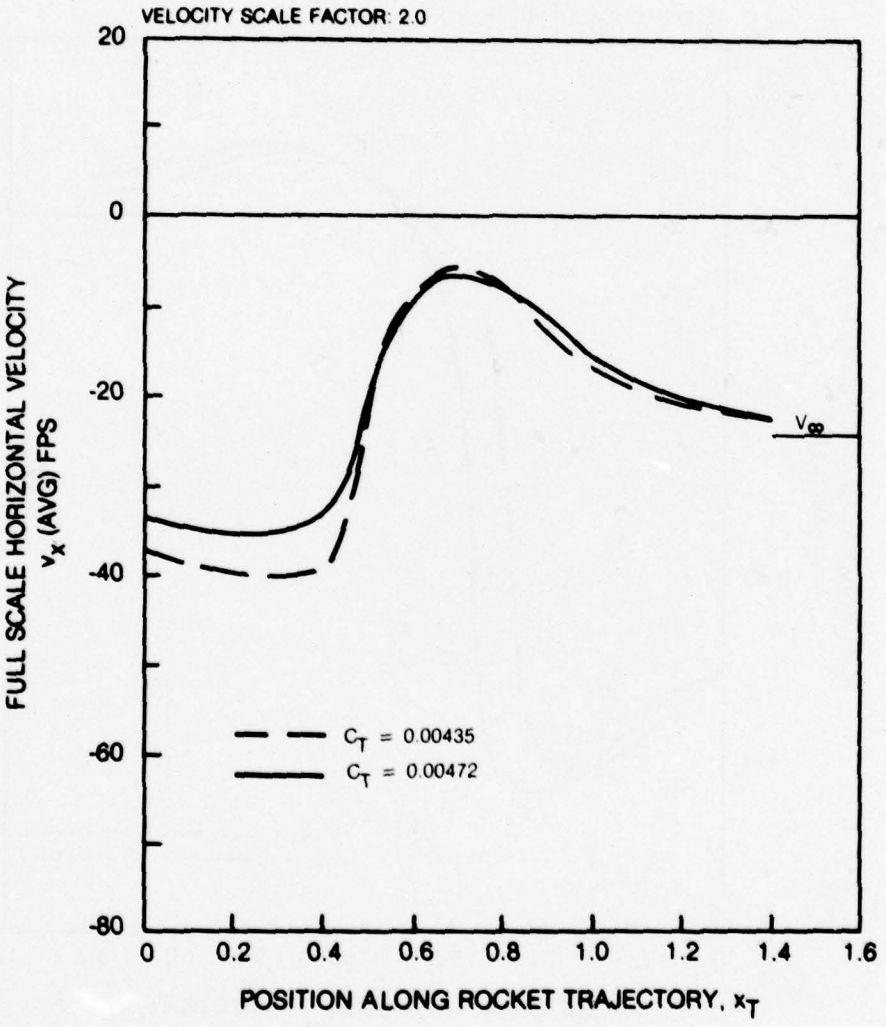

Figure 58, Effect of Rotor Thrust on the Scaled Time-Average Horizontal Flow Velocities Along the Rocket Trajectory for the Reference Configuration at the 15 kt Reference Condition.

79-09-33-42

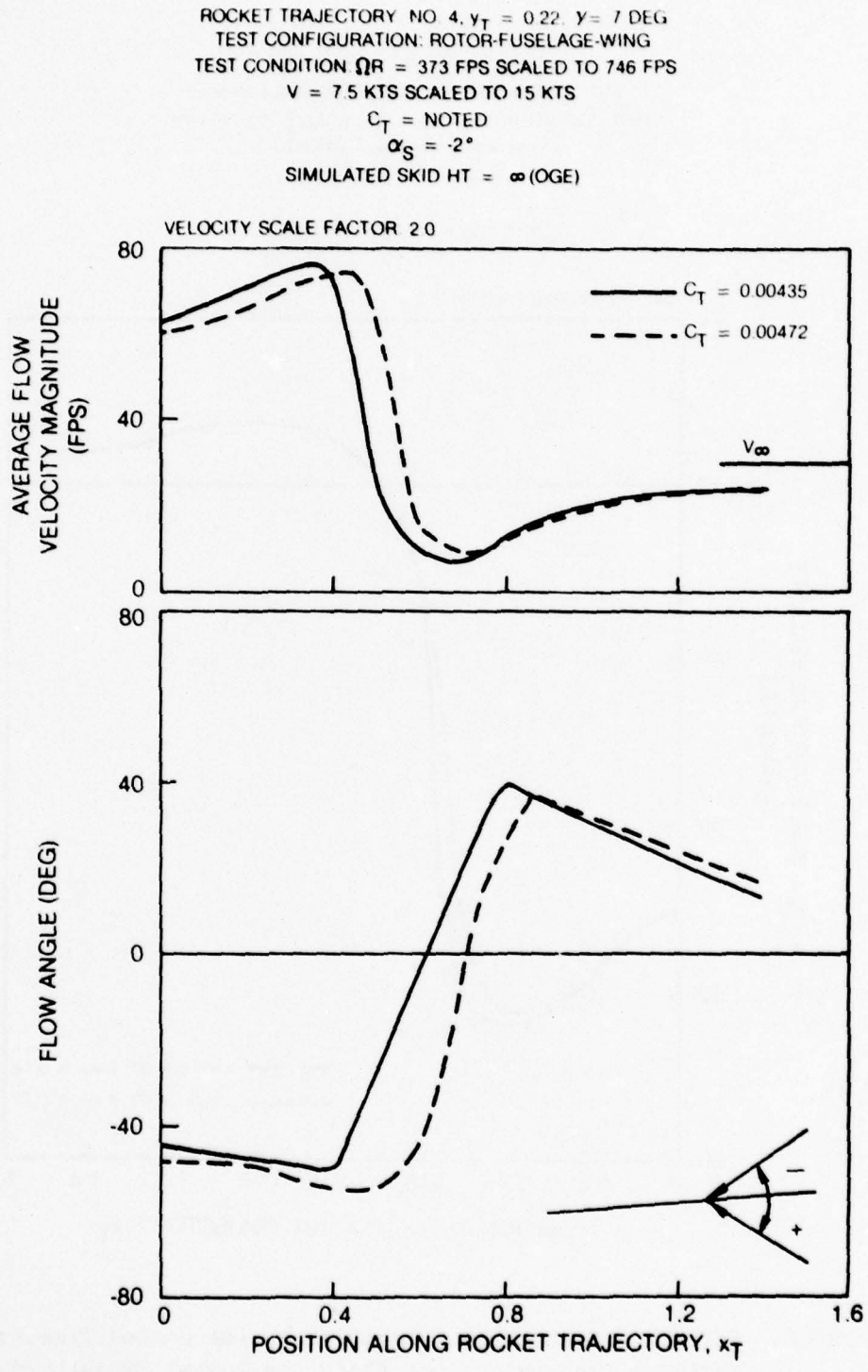

Figure 59. Effect of Rotor Thrust on the Scaled Time-Average Flow Velocity Magnitude and Flow Angle Along the Rocket Trajectory for the Reference Configuration at the 15 kt Reference Condition.

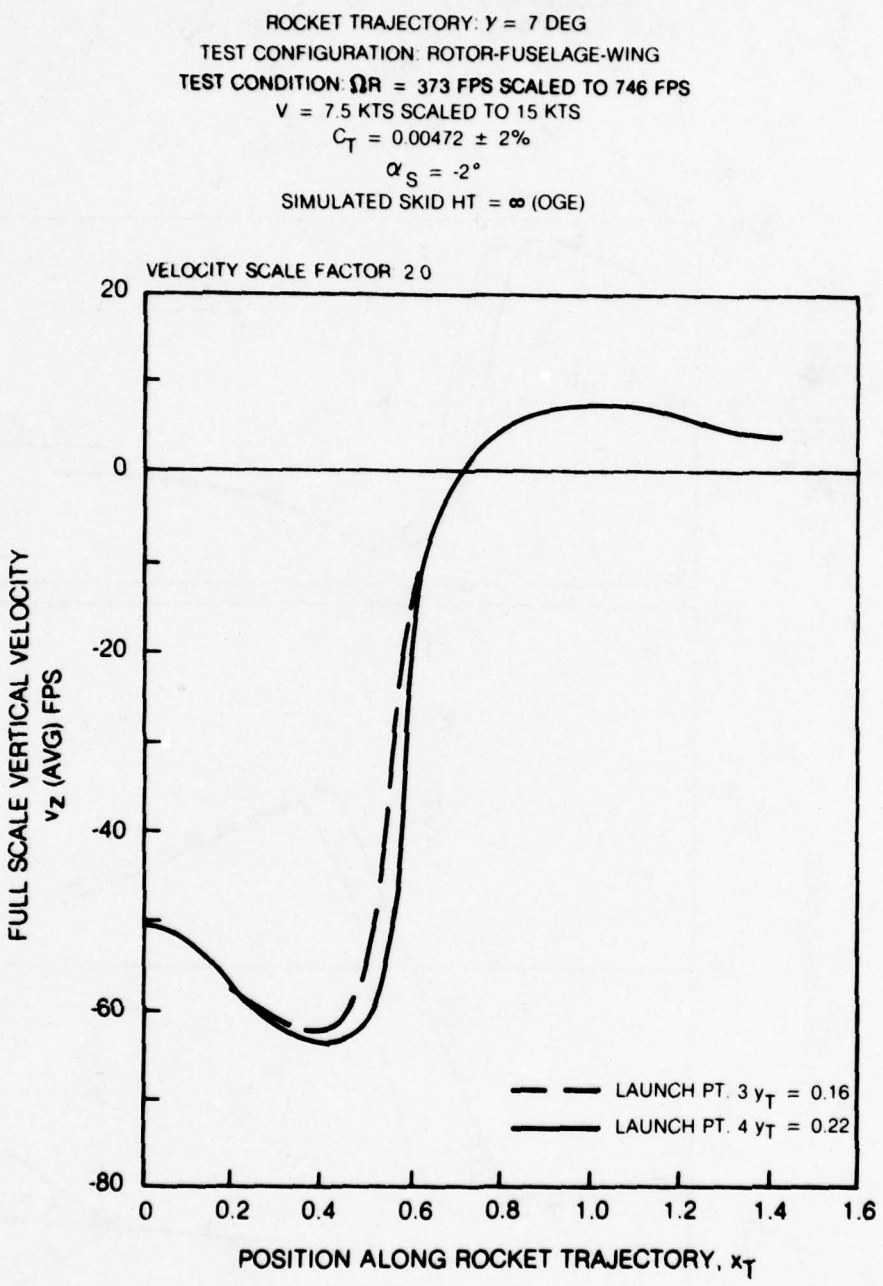

Figure 60. Effect of Launch Point Location on the Scaled Time-Average Vertical Flow Velocities Along the Rocket Trajectory for the Reference Configuration at the 15 kt Reference Condition.

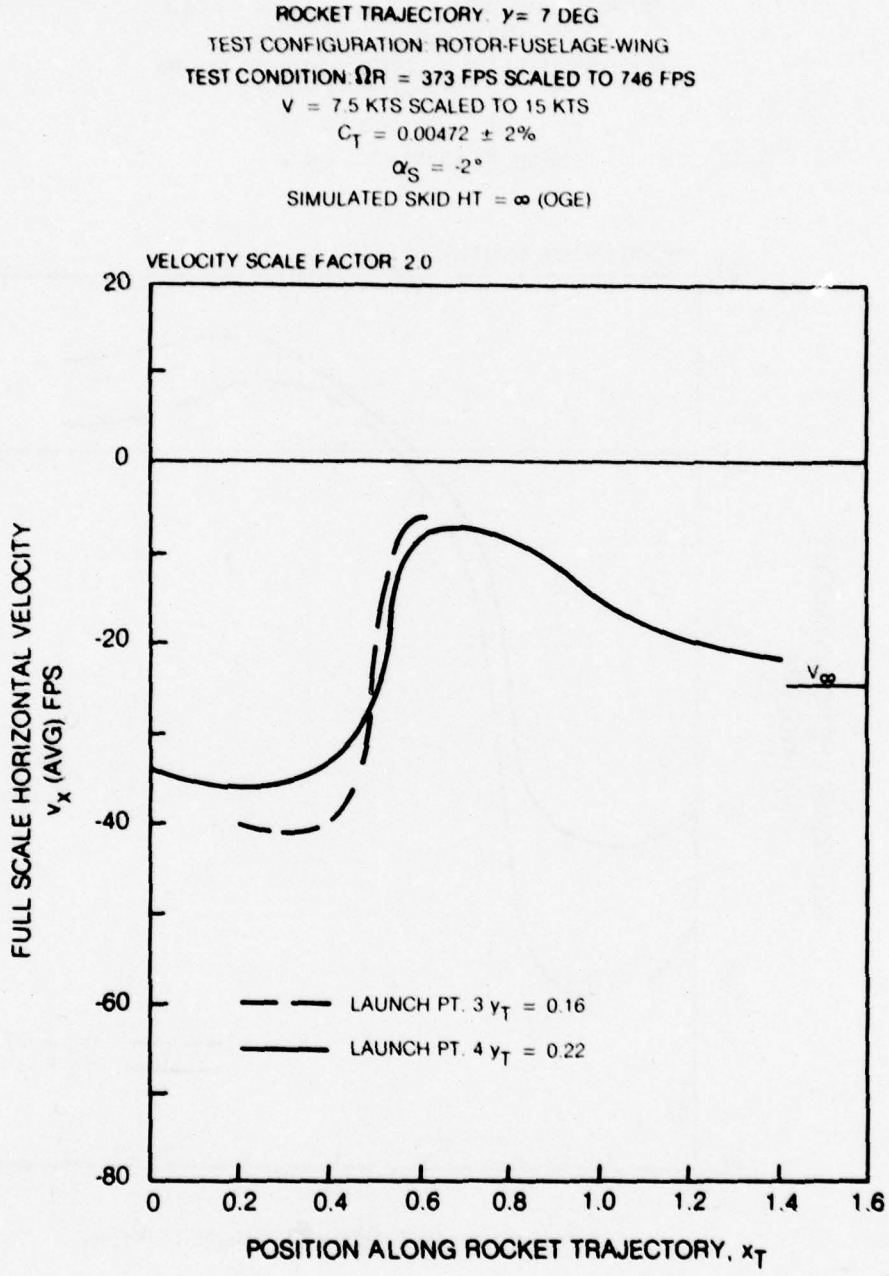

Figure 61. Effect of Launch Point Location on the Scaled Time-Average Horizontal Flow Velocities Along the Rocket Trajectory for the Reference Configuration at the 15 kt Reference Condition.

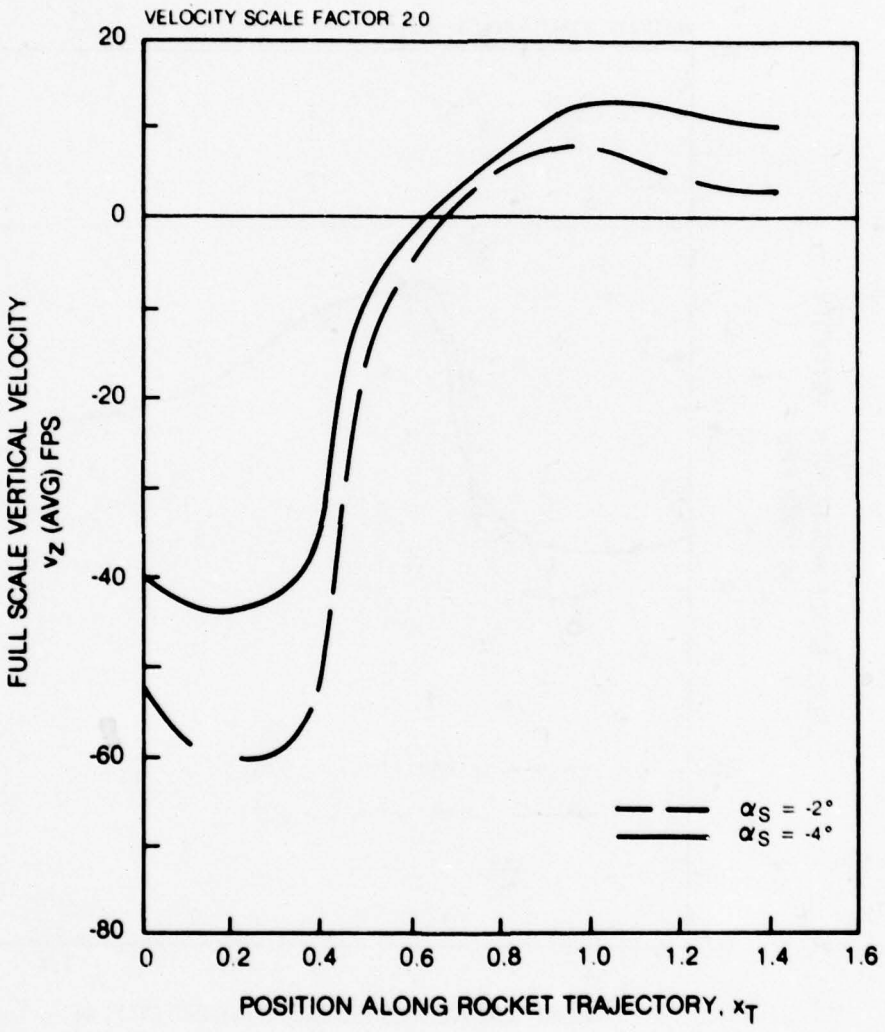

Figure 62. Effect of Simulated Change in Trajectory Angle on the Scaled Time-Average Vertical Flow Velocities Along the Rocket Trajectory for the Isolated Rotor at the 15 kt Reference Condition.

79-09-33-56

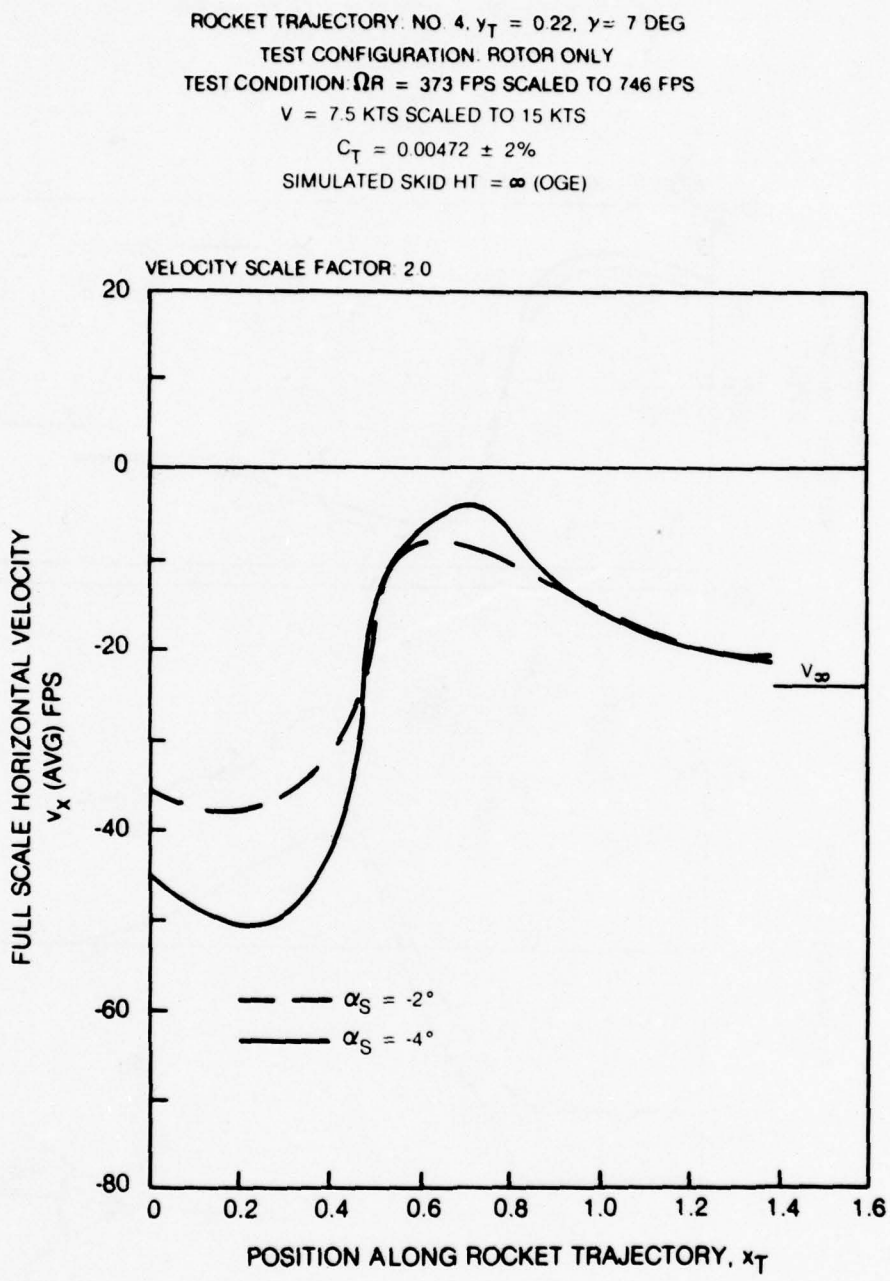

Figure 63. Effect of Simulated Change in Trajectory Angle on the Scaled Time-Average Horizontal Flow Velocities Along the Rocket Trajectory for the Isolated Rotor at the 15 kt Reference Condition.

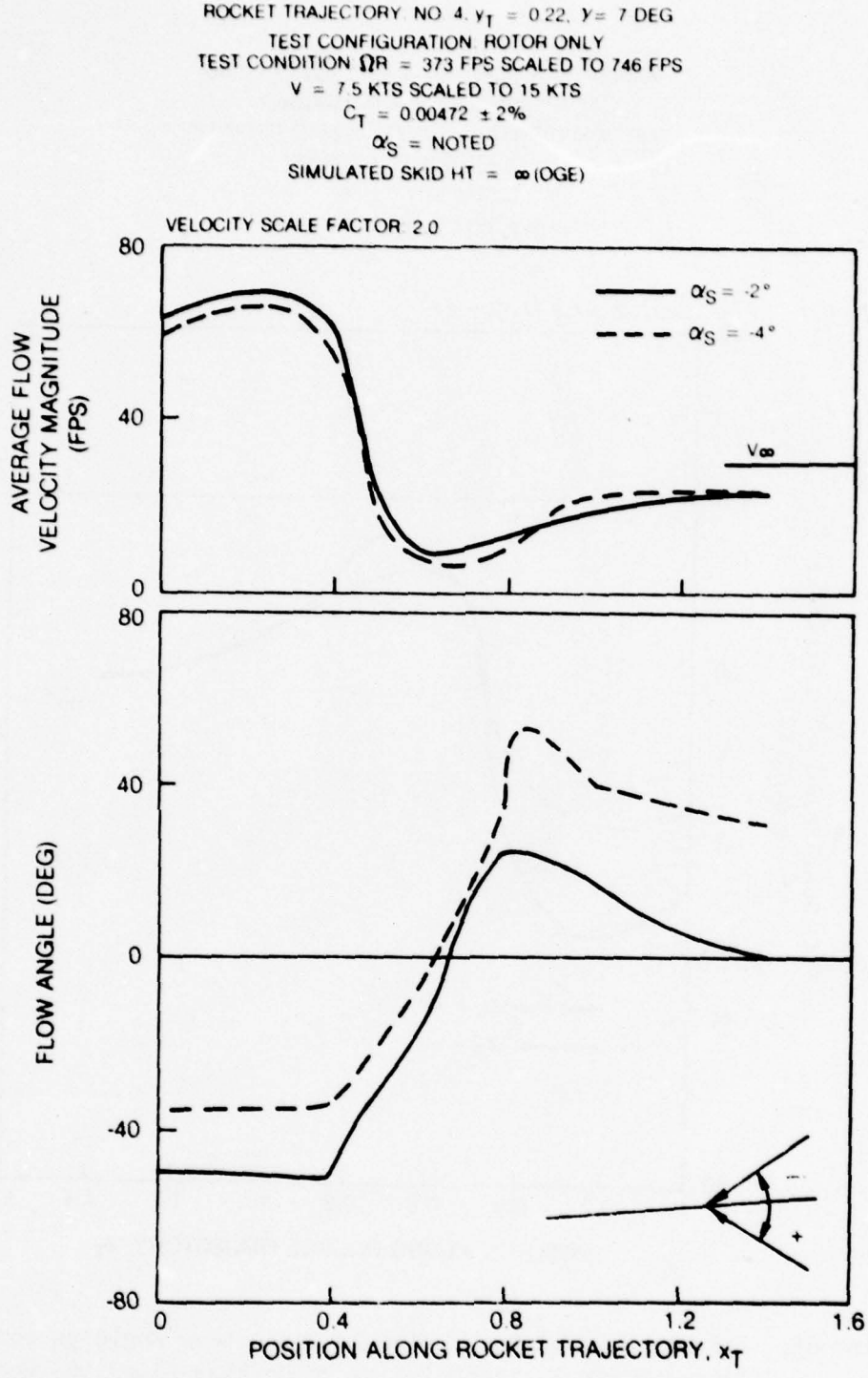

Figure 64. Effect of Simulated Change in Trajectory Angle on the Scaled Time-Average Flow Velocity Magnitude and Flow Angle Along the Rocket Trajectory for the Isolated Rotor at the 15 kt Reference Condition.

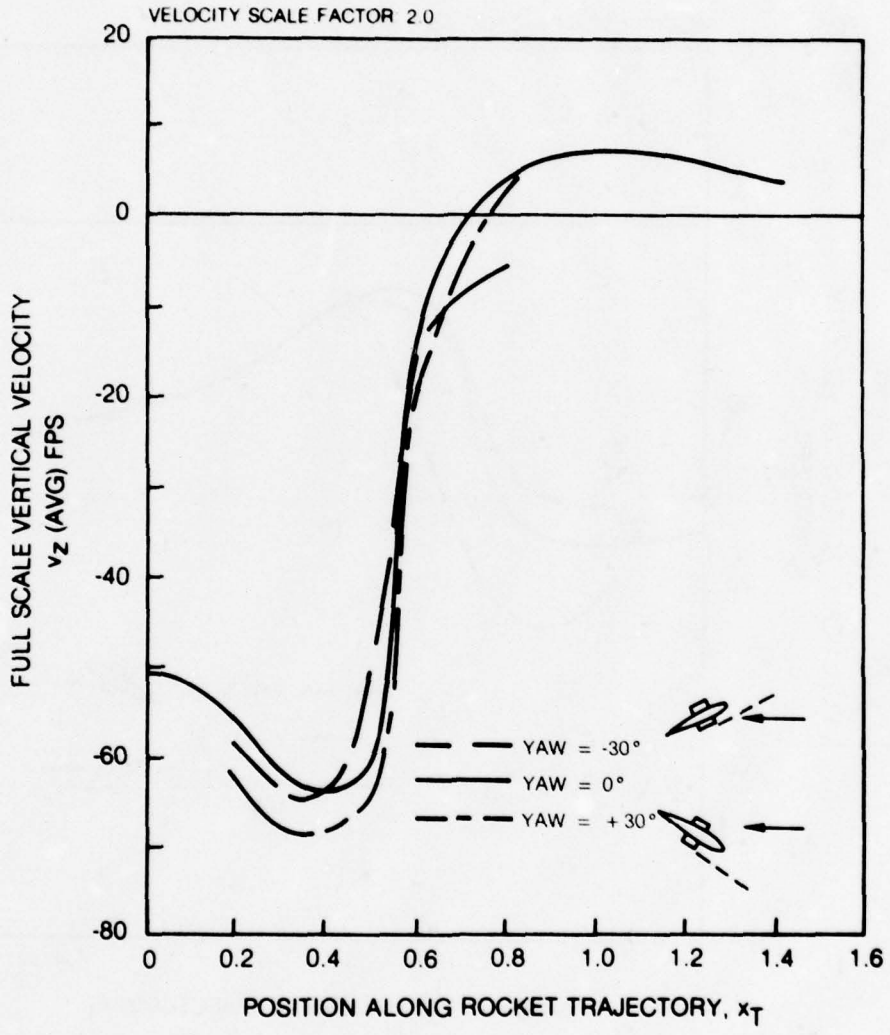

Figure 65. Effect of Sidewind on the Scaled Time-Average Vertical Flow Velocities Along the Rocket Trajectory for the Reference Configuration at the 15 kt Reference Condition.

79-09-33-57

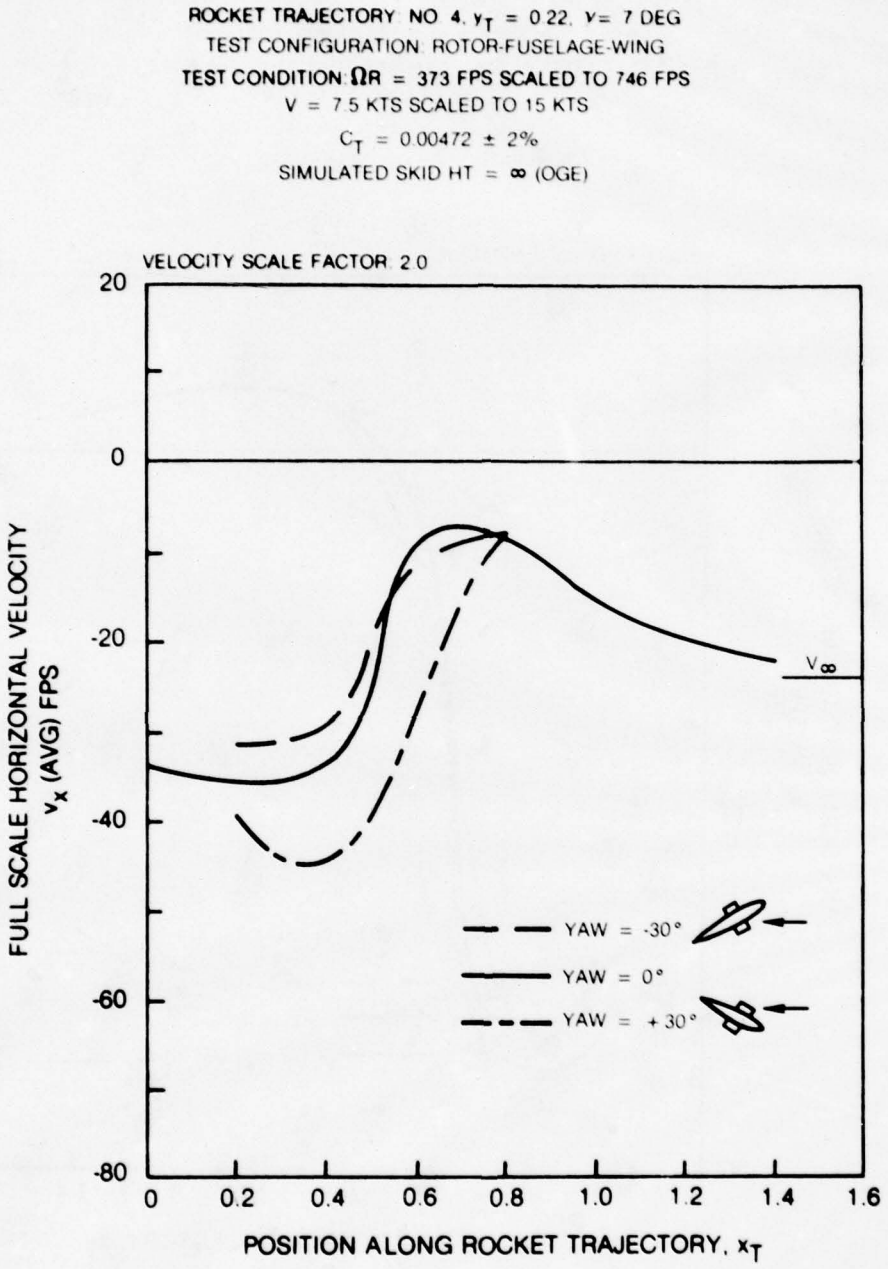

Figure 66. Effect of Sidewind on the Scaled Time-Average Horizontal Flow Velocities Along the Rocket Trajectory for the Reference Configuration at the 15 kt Reference Condition.

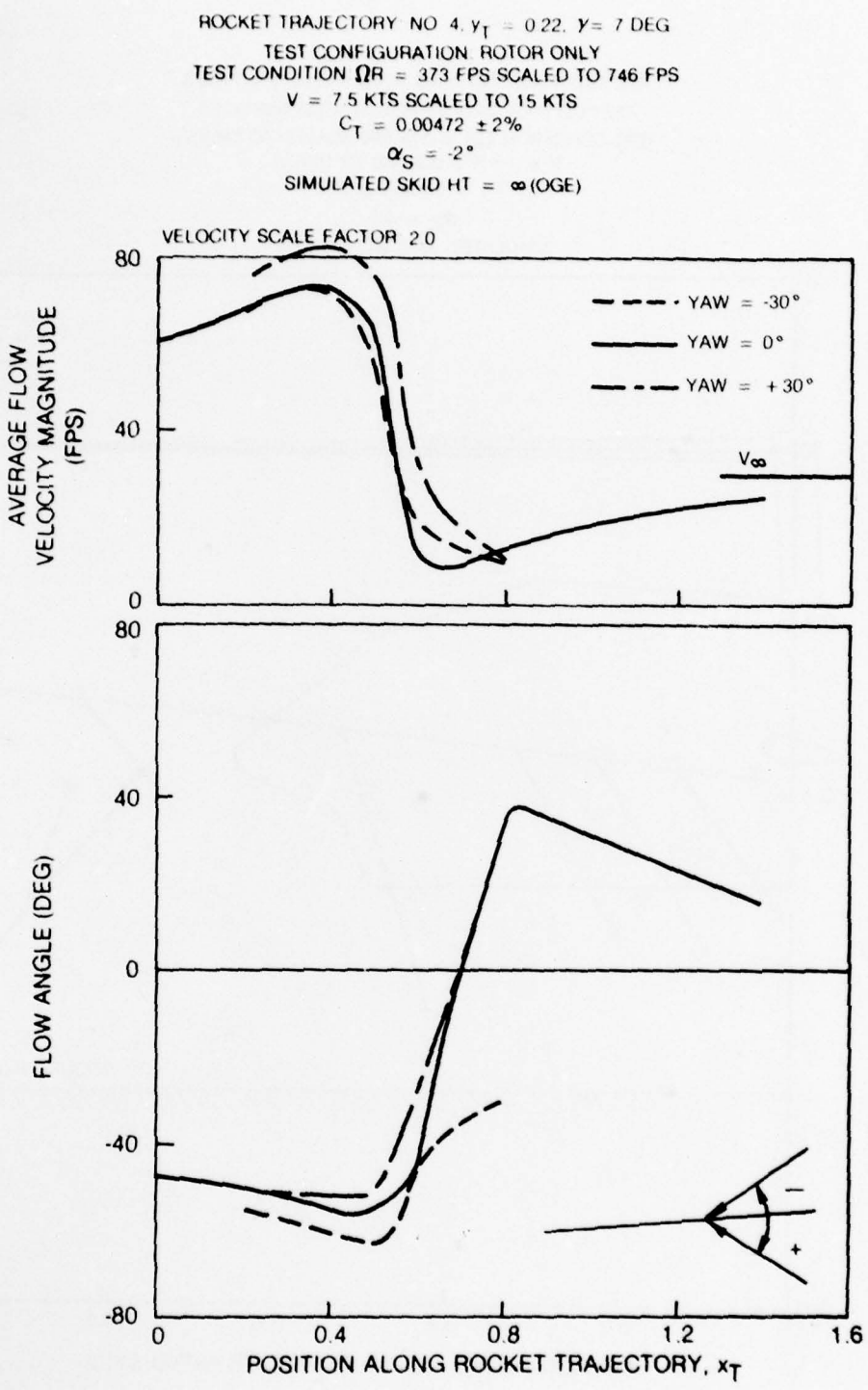

Figure 67. Effect of Sidewind on the Scaled Time-Average Flow Velocity Magnitude and Flow Angle Along the Rocket Trajectory for the Reference Configuration at the 15 kt Reference Condition.

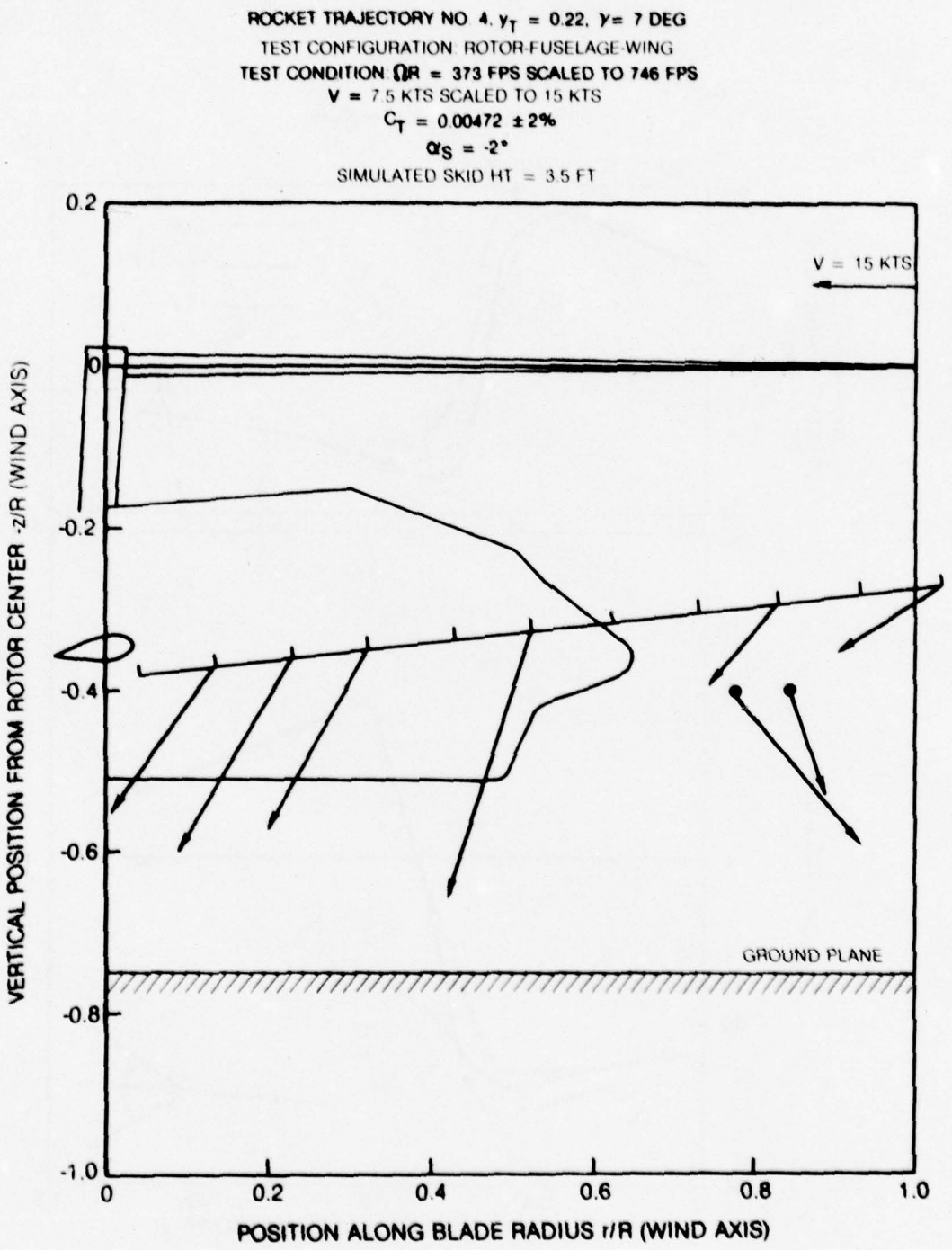

Figure 68. Scaled Time-Average Flow Velocity Vectors Along the Rocket Trajectory for the Isolated Rotor at the 15 kt Reference Condition In-Ground-Effect (IGE).

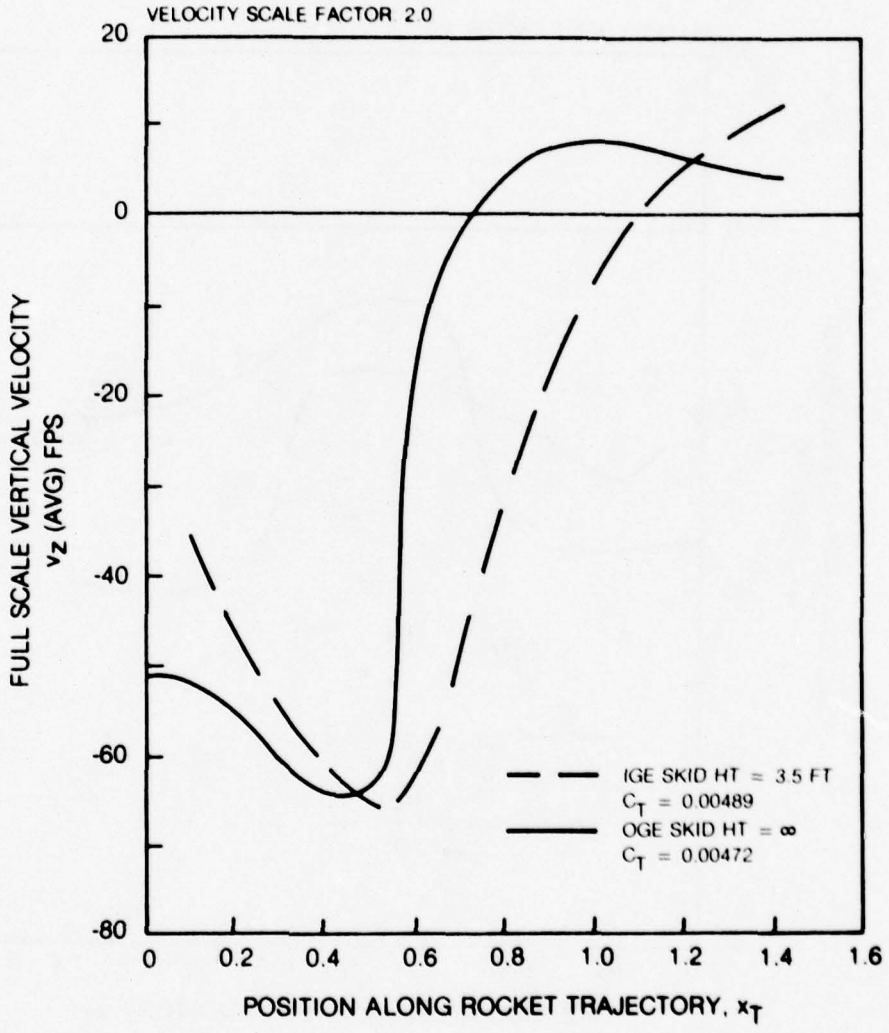

Figure 69. Ground Effect on the Scaled Time-Average Vertical Flow Velocities Along the Rocket Trajectory for the Reference Configuration at the 15 kt Reference Condition.

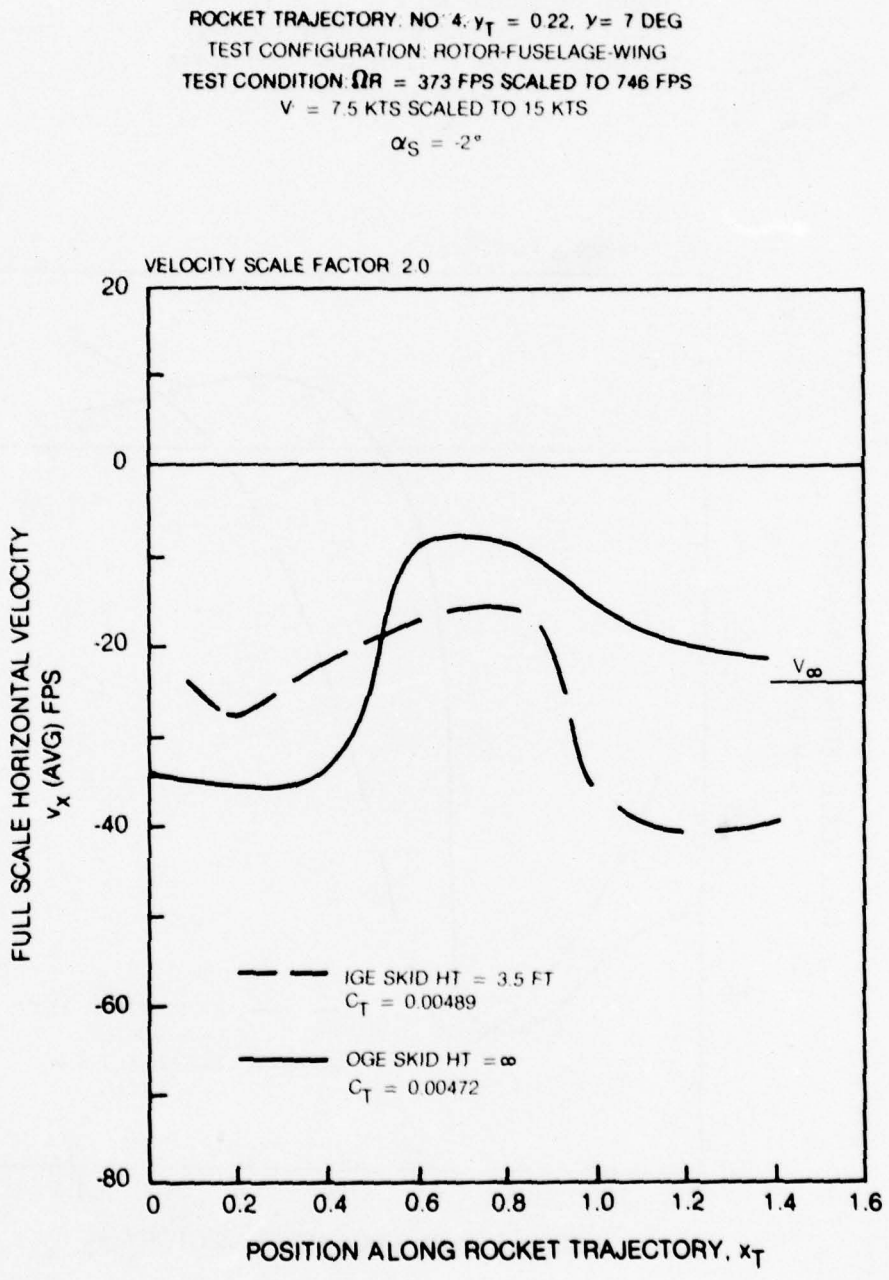

Figure 70. Ground Effect on the Scaled Time-Average Horizontal Flow Velocities Along the Rocket Trajectory for the Reference Configuration at the 15 kt Reference Condition.

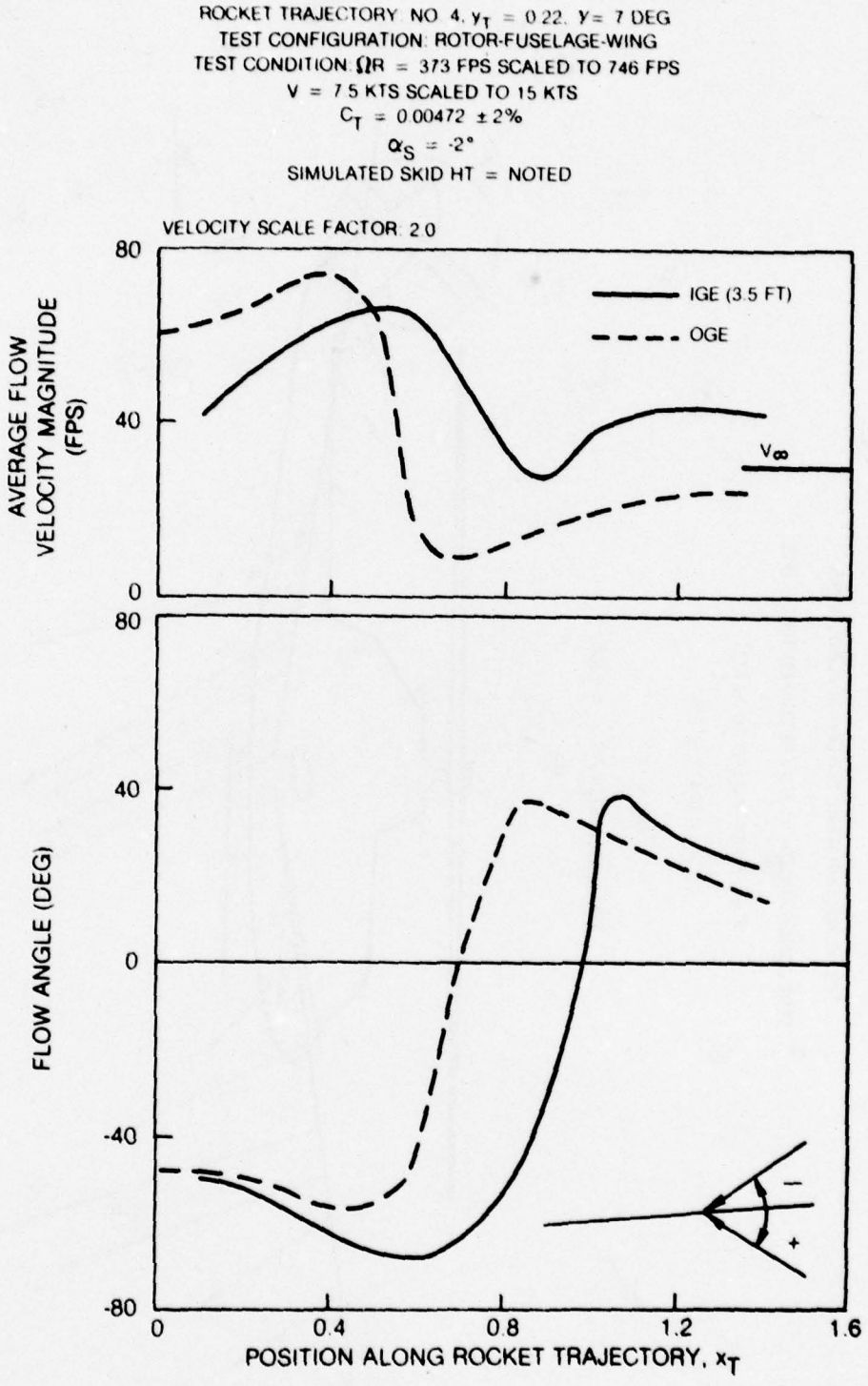

Figure 71. Ground Effect on the Scaled Time-Average Flow Velocity Magnitude and Flow Angle Along the Rocket Trajectory for the Reference Configuration at the 15 kt Reference Condition.

ROCKET TRAJECTORY: NO. 4, γ_T = 0.22, γ = 7 DEG

TEST CONFIGURATION: ROTOR-FUSELAGE-WING

TEST CONDITION: ΩR = 373 FPS SCALED TO 746 FPS

V = 7.5 KTS SCALED TO 15 KTS

C_T = 0.00472 ± 2%

α_S = -2°

SIMULATED SKID HT = ∞ (OGE)

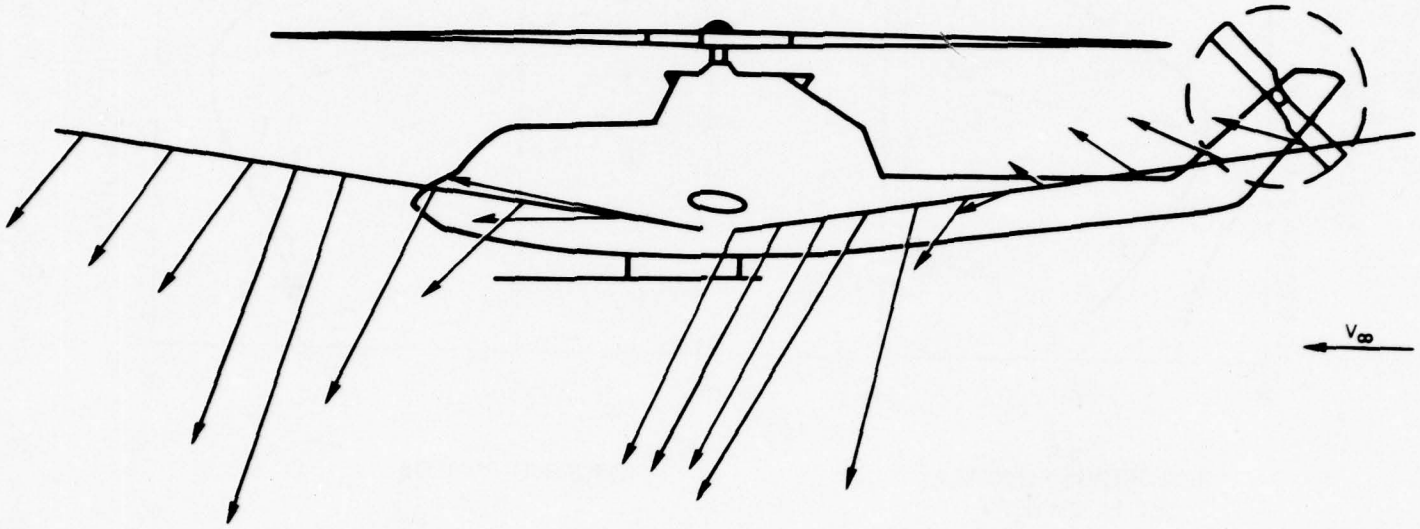

Figure 72. Scaled Time-Average Flow Velocity Vectors Along and Behind the Rocket Trajectory for the 15 kt Tailwind/Rearward Flight Condition Out-of-Ground Effect (OGE).

79-09-33-68

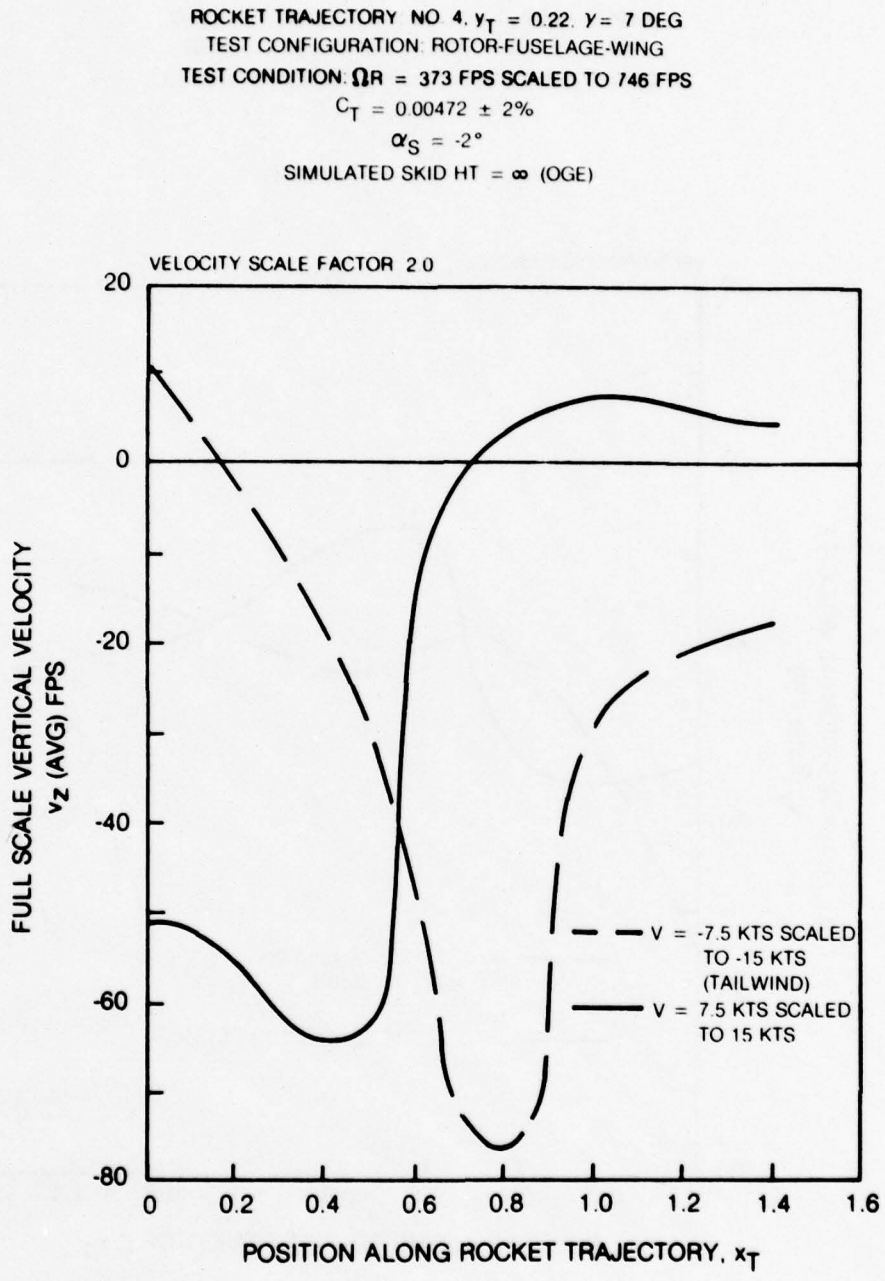

Figure 73. Effect of a Simulated 15 kt Tailwind on the Scaled Time-Average Vertical Flow Velocities Along the Rocket Trajectory for the Reference Configuration.

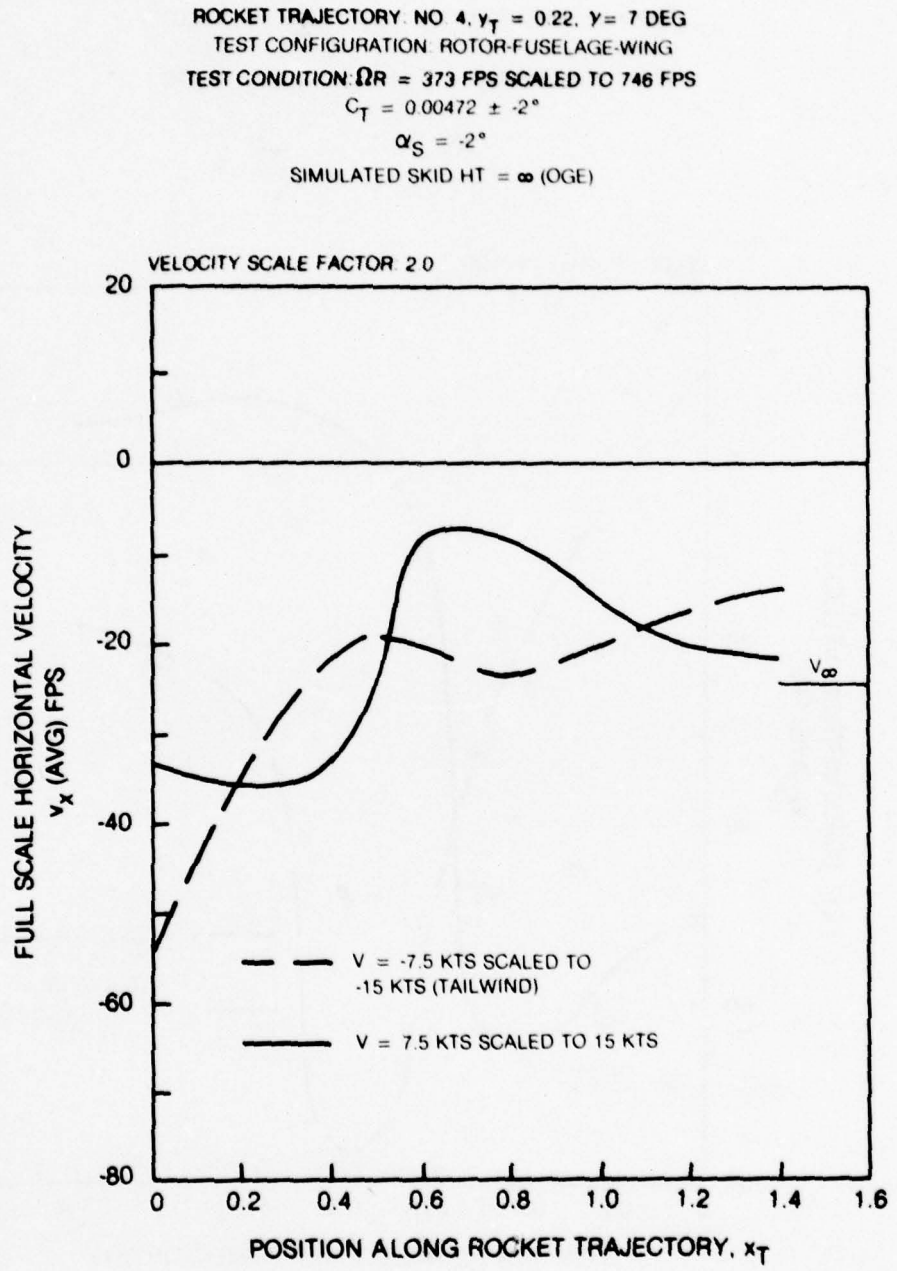

Figure 74. Effect of a Simulated 15 kt Tailwind on the Scaled Time-Average Horizontal Flow Velocities Along the Rocket Trajectory for the Reference Configuration.

ROCKET TRAJECTORY: NO. 4, y_T = 0.22, γ = 7 DEG

TEST CONFIGURATION: ROTOR-FUSELAGE-WING

TEST CONDITION: ΩR = 373 FPS SCALED TO 746 FPS

V = 7.5 KTS SCALED TO 15 KTS

C_T = 0.00472 ± 2%

α_S = -2°

SIMULATED SKID HT = 3.5 FT

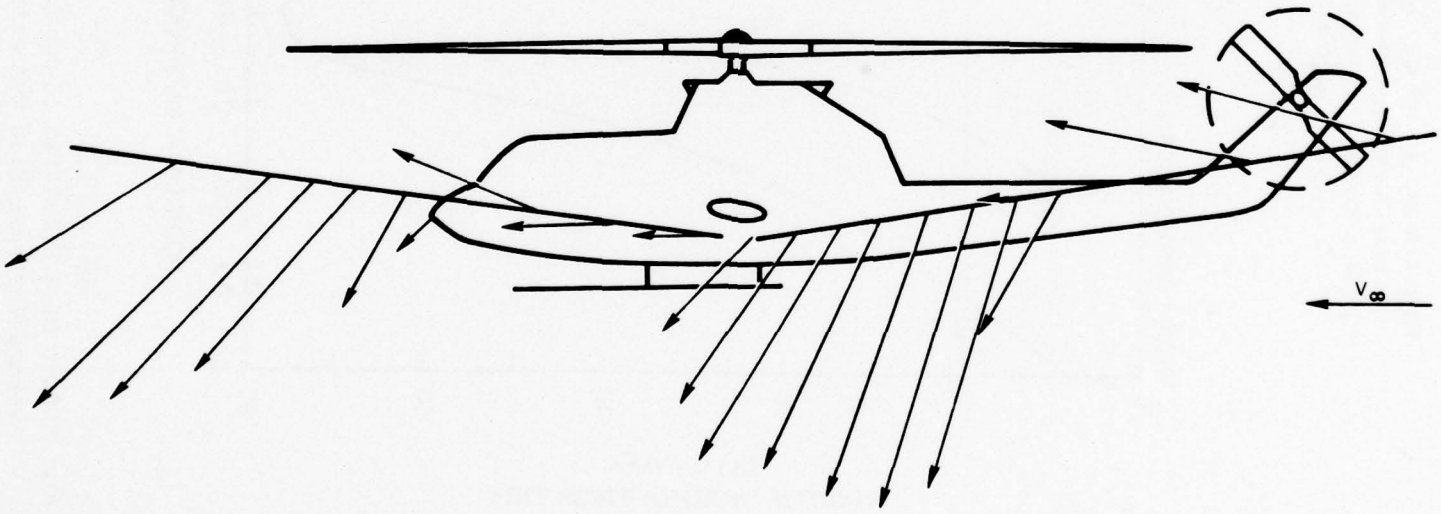

Figure 75. Scaled Time-Average Flow Velocity Vectors Along and Behind the Rocket Trajectory for the 15 kt Tailwind/Rearward Flight Condition In-Ground-Effect (IGE).

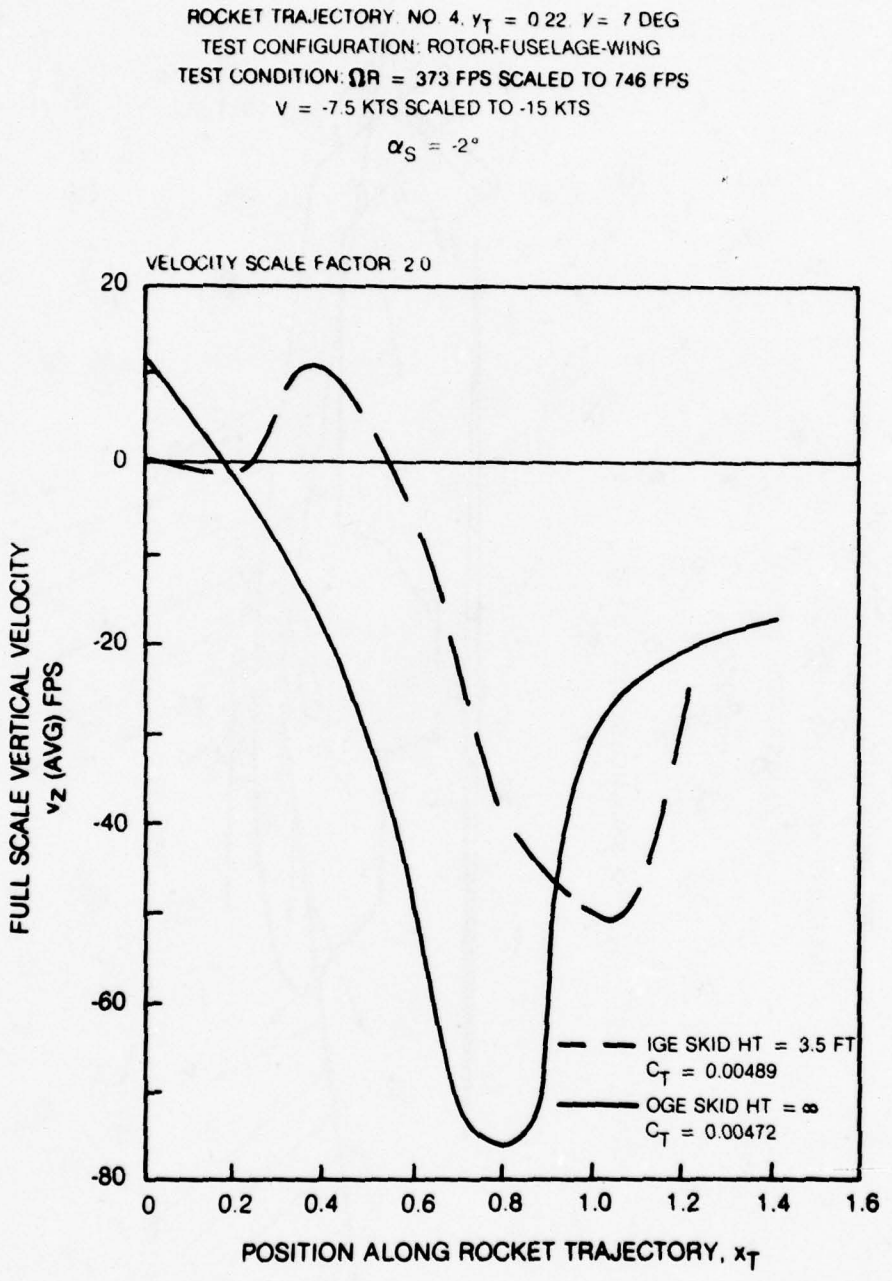

Figure 76. Effect of a Simulated 15 kt Tailwind on the Scaled Time-Average Vertical Flow Velocities Along the Rocket Trajectory for the Reference Configuration In-Ground-Effect (IGE).

79-09-33-60

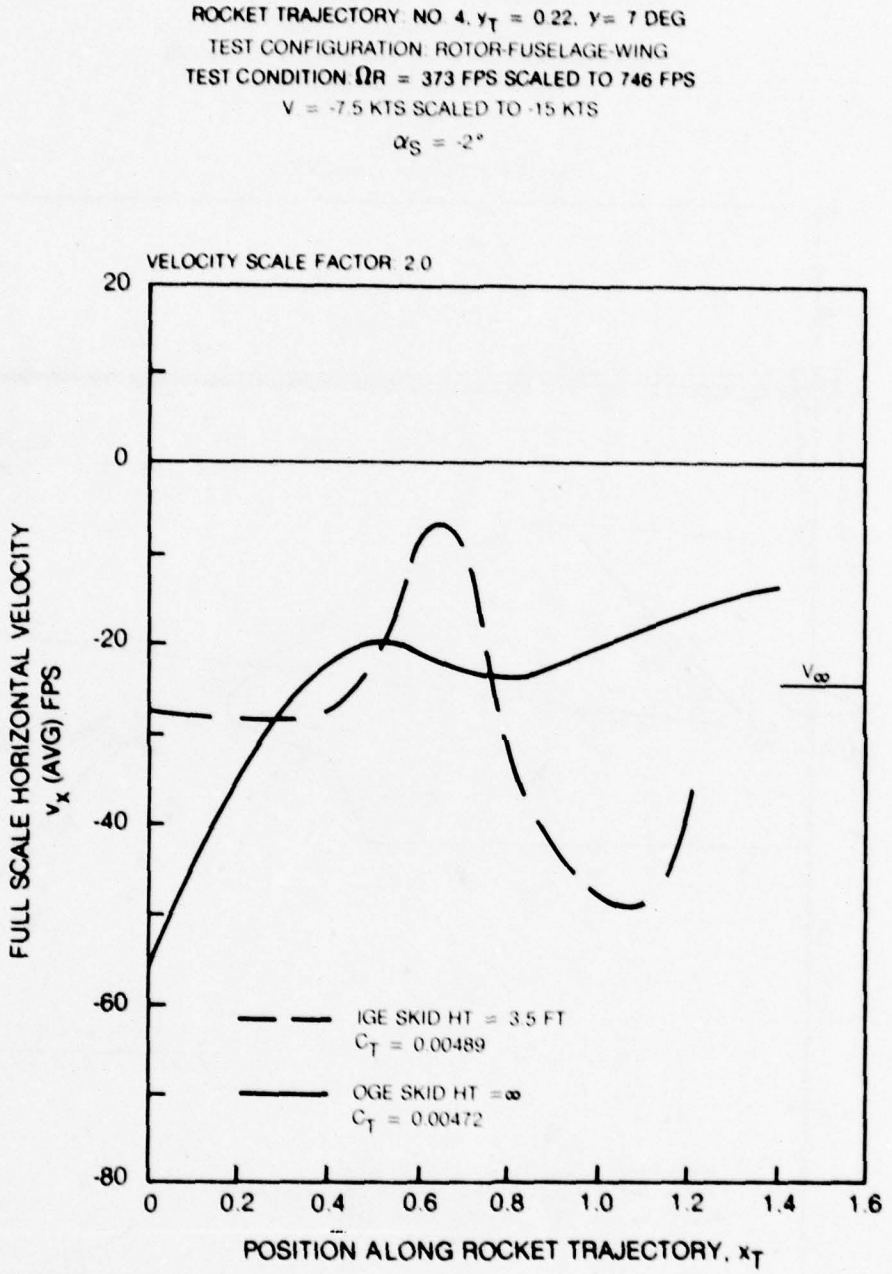

Figure 77. Effect of a Simulated 15 kt Tailwind on the Scaled Time-Average Horizontal Flow Velocities Along the Rocket Trajectory for the Reference Configuration In-Ground-Effect (IGE).

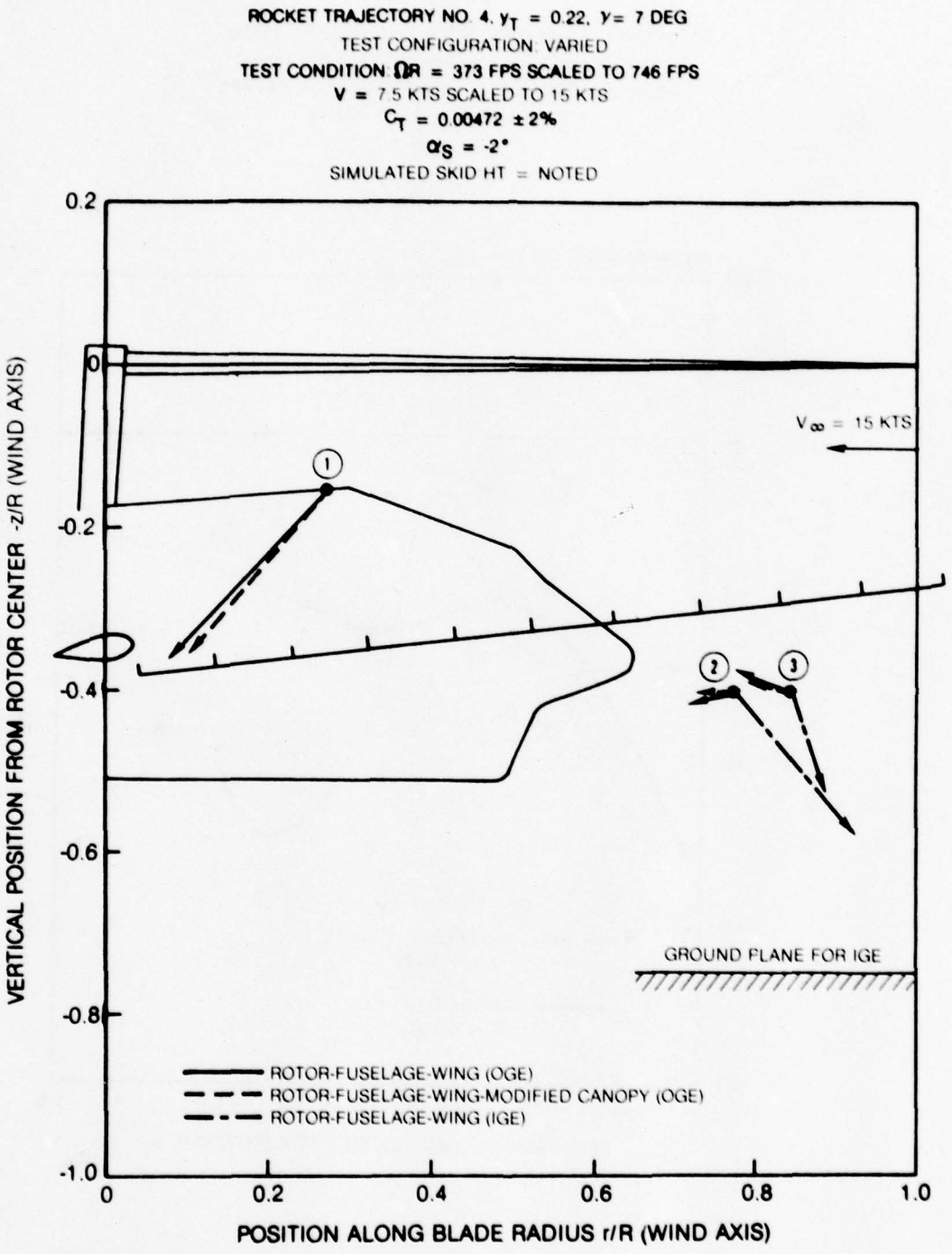

Figure 78. Scaled Time-Average Flow Velocity Vectors at Three Wind Sensor Locations for the 15 kt Reference Condition.

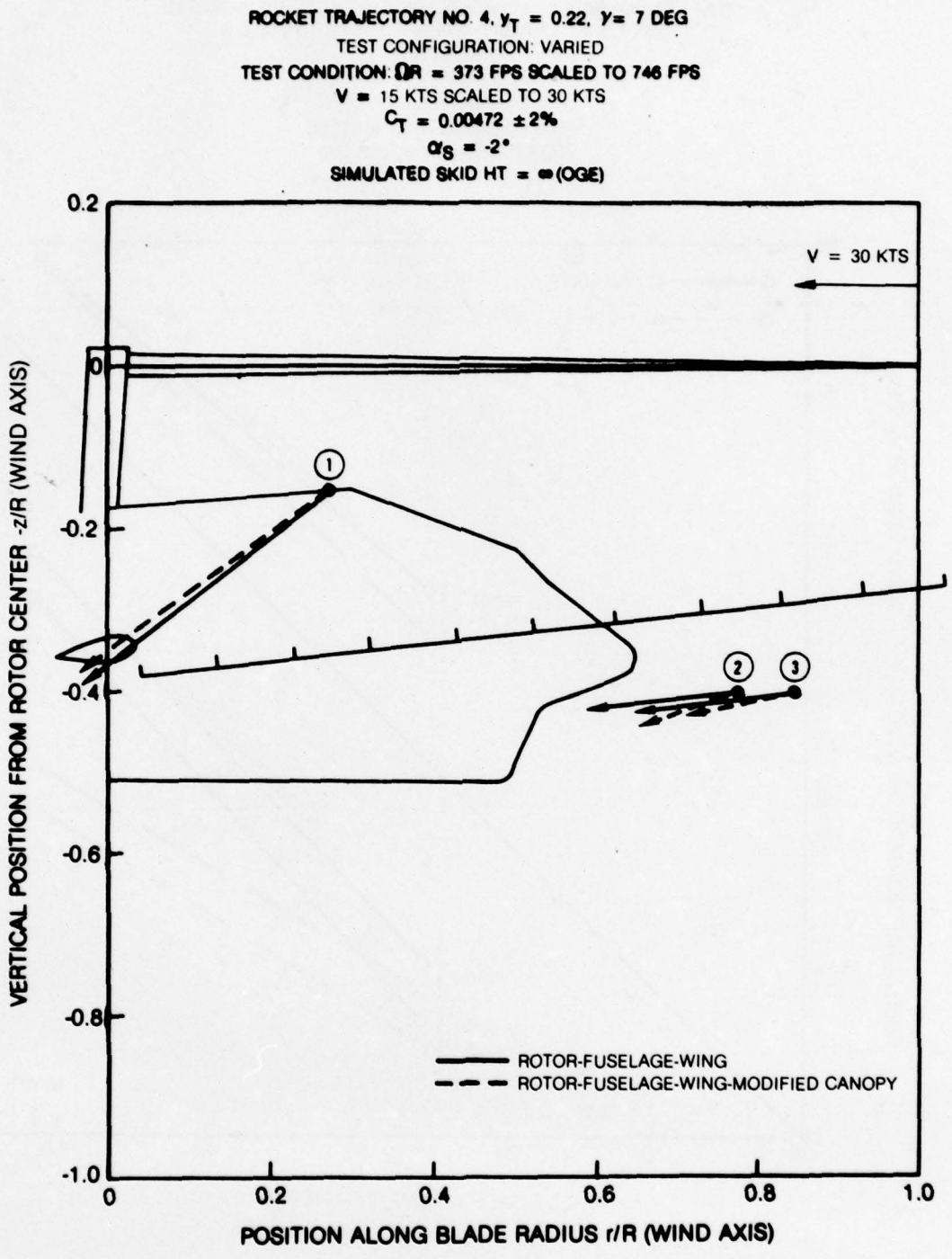

Figure 79. Scaled Time-Average Flow Velocity Vectors at Three Wind Sensor Locations for the 30 kt Reference Condition.

TEST CONFIGURATION: FUSELAGE-WING WITH CANOPY AS NOTED
TEST CONDITION: ΩR = 373 FPS SCALED TO 746 FPS
V = NOTED
C_T = 0.00472 ± 2%
α_S = -2°
SIMULATED SKID HT = ∞ (OGE)
VELOCITY SCALE FACTOR: 2.0

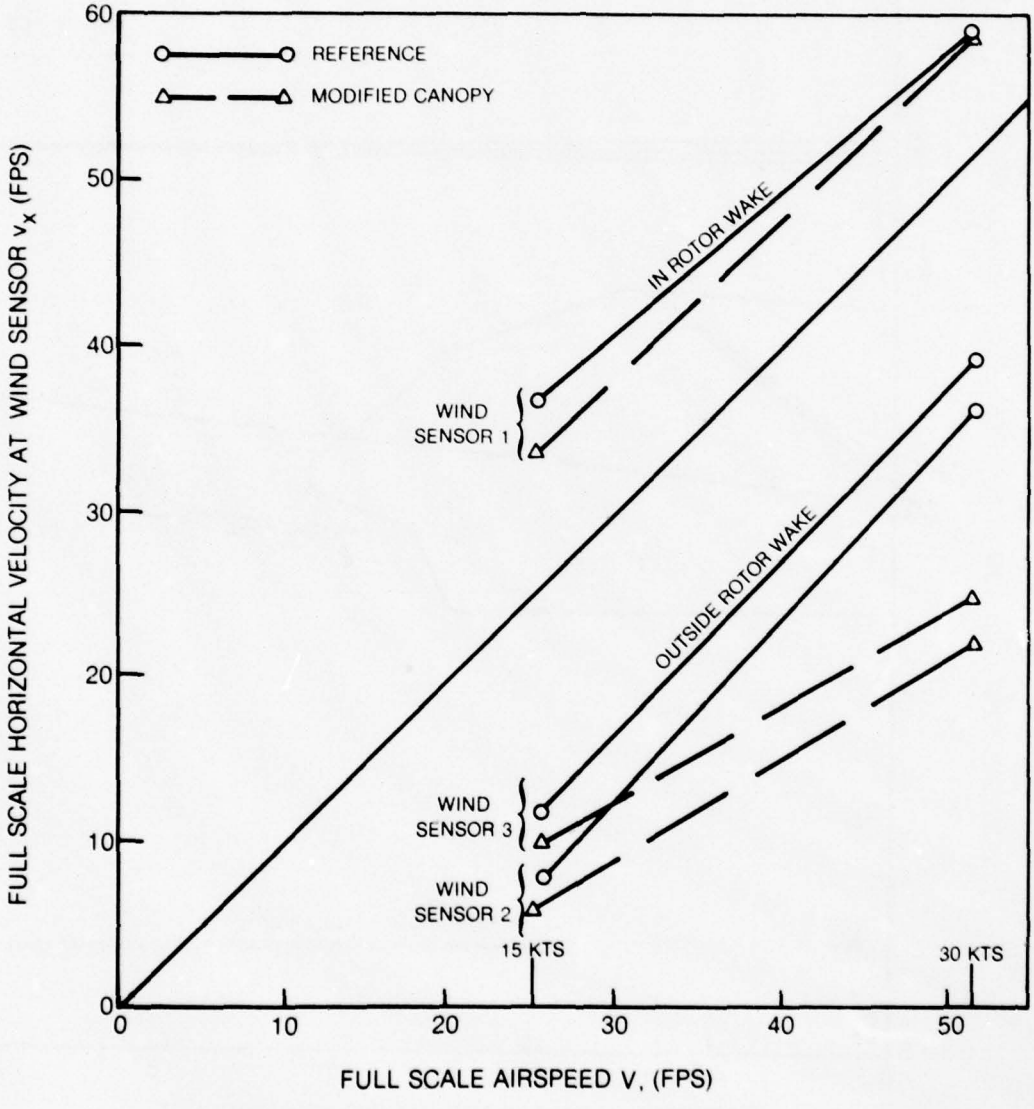

Figure 80. Comparison Between Actual and Sensed Flight Speed for Three Wind Sensor Locations for the Reference and Modified Canopy Configurations.

APPENDIX A

MICOM MEMO

DEPARTMENT OF THE ARMY

HEADQUARTERS UNITED STATES ARMY MISSILE COMMAND

REDSTONE ARSENAL, ALABAMA 35809

APR 21 1975

MEMO FOR RECORD

SUBJECT: Helicopter Air Flow Analysis at Hover and Low Air Speeds

1. Reference is made to United Aircraft Research Laboratories[1] Final Report "Prediction of Rotor Wake Induced Flow Velocities Along the Rocket Trajectories of an Army AH-1G Helicopter," dated March 1975.

2. The US Army Training and Doctrine Command (TRADOC) has determined that the appropriate attack helicopter tactic for the mid-intensity or mid-east battle scenarios will be low level flight, known as "Terrain Flying." The need to engage targets with sophisticated air defense elements results in a major concern with aircraft survivability. Maximum survivability is achieved by engaging targets at the maximum effective range of the helicopter weapon, while minimizing closure on the target during the engagement. These tactical requirements have been instrumental in formulating aircraft/weapon specifications which place major emphasis on firing rockets, cannon, and missiles from a hover as a worst case condition. The most stringent hover technique involves the capability to start from a low level hover behind a masking terrain feature, "pop-up" with some minimum vertical rate of climb, engage the target, and retain sufficient aircraft performance to recover from a vertical rate of descent just in case no portion of the ordnance load is expended.

3. Ordnance which can be fired with initial high velocities, such as cannon rounds, or which can be given terminal guidance, such as a missile, are the least affected by local air flow in the hover, pop-up or low air speed regimes. Since the free aerial rocket has a relatively low initial velocity and receives no terminal guidance, it is significantly affected by the helicopters rotor down wash during these maneuvers. The Advanced Attack Helicopter (AAH) specifications call for a major portion of the mission time to be conducted at the hover. However, the AAH Primary weapons are considered at this time, to be the TOW missile and 30 mm cannon; therefore, the 2.75 Inch Rocket System performance at the hover has not been a major concern.[2] The performance of helicopters during these maneuvers has been the main concern of the aeronautical laboratories and major research is being pursued to determine the parameters of hover dynamics. Relatively little emphasis has been placed on the effects on weapon performance during these same maneuvers. Although the AAH and the AH-1 helicopters are expected to have at least some of the major components of rocket fire control, very little

applied research is being pursued to develop a solution to the user requirement for an effective aircraft/weapon system at low air speed.

4. This Office sponsored the 2.75 Inch Rocket/AH-1G System Baseline Accuracy Test which was a detailed analysis of the helicopter/rocket system performance at airspeeds of 90 and 120 knots. The major conclusion of the test was that helicopter rocket fire control was needed to accomplish a significant improvement in system effectiveness. The lack of appropriate instrumentation was a prime factor in not acquiring the same type of data for hover and low forward air speeds. Currently, instrumentation has still not advanced sufficiently to provide adequate experimental data on airflow under the Cobra rotor disc throughout the weapon launch envelope at low airspeeds. Discussions with the aeronautical laboratories revealed that no definitive data existed on the area of interest. Rocket ballistic simulations had to be performed utilizing assumed data generated with standard momentum theory based on the size of the rotor and gross helicopter weight. Airflow perturbations within the rotor down wash were unknown.

5. After determining that there existed a large gap in data on airflow in the rocket launch envelope at low airspeeds, the 2.75 Inch Rocket Project Manager's Office took advantage of a proposal from United Aircraft Research Laboratories (UARL) to acquire basic information utilizing computer simulation. Mr. Jack Landgrebe and his associates at UARL have exhibited considerable expertise and dedication in deriving the degree of data presented in the reference report, particularly when one considers the size of the Picatinny Arsenal contract. The computer simulation techniques developed by UARL are unique in the capability to provide instantaneous and time-averaged airflow vectors in both distorted and undistorted rotor wakes.

6. Mr. Saul Wasserman[3] of the Aeroballistics section at Picatinny Arsenal is currently following through with the data presented in the report to calculate the effects of the airflow on the rocket ballistic trajectory. The rocket will normally be influenced by the passage of approximately two rotor blades during its exit from the weapon launch envelope. During preliminary simulations with a six degree of freedom rocket ballistic simulation, it was found that at ranges below 2000 meters, a variation in impact distance could be detected as a function of the blade position and instantaneous velocities depicted in Fig. 15 of the reference report. At ranges greater than 2000 meters, the rocket was not influenced sufficently by variation in firing time to be detected in changes in the simulated ground impact. In actual hover firing tests at Yuma Proving Ground in 1974, the 2.75 Inch Rocket achieved a mean point of impact at 4500 meters while at 30 feet above target with a three degree nose-up angle. Firings from 90 knots at 300 feet required a 7 degree climb to achieve 4000 meters. The rocket is highly stable and weathervanes up into the rotor down wash, therefore, the effect on the trajectory of the rocket is significant.

7. As mentioned in the report, a number of the assumed variables have yet to be confirmed and refinement will probably have some effect on the performance characteristics of the helicopter/rocket system. It must be noted that these simulations are conducted at specific airspeeds of 0, 15 and 30 knots, without representation of fuselage effects. A review of the report will result in the impression that the airflow under rotor is very dynamic and velocity predictions at any one point are not necessarily representative of the total launch envelope. An additional consideration is that in the tactical situation the helicopter will rarely be in a stationary hover without a velocity vector in some direction.

8. New techniques of airflow measurements, such as Laser Doppler Velocimeter (LDV) have been developed in recent years. United Aircraft is capable of LDV measurement, both on a hover stand and in wind tunnels. The advantage of the LDV technique is the ability to measure airflow from a remote position, thereby, eliminating the disturbance effects normally involved with mounting a sensing device directly in the airflow. Ultimately, the LDV may become a tool for helicopter instrumentation and be flight qualified for full scale flight research.

9. The reference report is viewed as only the initial step in achieving data to properly evaluate the characteristics of helicopter/rocket systems when fired at a hover. A number of recommended tasks to continue development of airflow simulation and data acquisition techniques are as follows:

a. An AH-1G flight test to accurately determine the rotor control, flapping and disc angles assumed in Table I of the reference report.

b. A Laser Doppler Velocimeter (LDV) survey of a scale model of each helicopter gunship to determine the optimum location for an operational fire control relative wind sensor on each aircraft.

c. A LDV survey of the weapon launch envelope of each helicopter gunship at hover and forward airspeeds to provide experimental data and analysis to support the findings of the reference report.

d. Determine the feasibility of packaging the LDV concept so that it can be used as instrumentation on-board a gunship for detection of airflow characteristics under actual flight conditions.

e. Further development of airflow simulation techniques to include fuselage configuration effects and the resultant effect in the weapon launch area.

f. Adaptation of the airflow simulation to determine flight dynamics during the pop-up maneuver.

g. Initiation of 6.2 and 6.3 research into instrumentation and operational air data sensor devices.

h. Funding for aeroballistics analysis of the airflow effects on weapon performance and evaluation of courses of action to compensate for airflow effects.

10. Helicopter stability must be improved during hover in order to provide an effective weapons platform. This is particularly true when a large number of rockets are to be fired in the shortest possible time. It is expected that helicopter control systems will eventually provide this characteristic. Parallel research efforts are necessary so that a combination of platform stability, fire control, and rocket design can accomplish accurate rocket delivery during hover, pop-up and low speed flight as the helicopter transitions. These integrated tasks must be performed in order that the user can be provided with the effective helicopter system he desires.

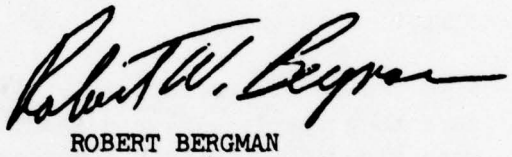

ROBERT BERGMAN
AMCPM-RK2[4]

1977 Updates:

[1] United Aircraft Research Laboratories (UARL) is now United Technologies Research Center (UTRC)

[2] The AAH primary weapon system is the Hellfire system. The 2.75 Inch Rocket and 30 mm cannon are secondary weapons systems.

[3] Mr. Saul Wasserman is now with U. S. Army Armament R&D Command.

[4] Mr. Robert Bergman is now at DRCPM-RK, MIRADCOM, Redstone Arsenal.

APPENDIX B
PAPER PRESENTED AT THE CONFERENCE ON
THE EFFECTS OF HELICOPTER DOWNWASH
ON FREE PROJECTILES

Rotor Wake Induced Flow Along Helicopter Rocket Trajectories

Anton J. Landgrebe
Supervisor, Rotary Wing Technology
and
T. Alan Egolf
Associate Research Engineer

United Technologies Research Center
East Hartford, Connecticut

SUMMARY

An analytical investigation was conducted to predict the rotor wake induced flow velocities along the trajectories of rockets fired from an Army AH-1G helicopter. The three components of both the time-averaged and instantaneous induced velocities were predicted at selected points along the trajectories of rockets fired from four wing locations. Three flight conditions with helicopter flight speeds of 0, 15, and 30 knots were investigated. The sensitivity of the predicted induced velocities to rotor wake model, rocket launch attitude, and rocket launch position was also investigated. Velocities induced by tip vortices near the intersections of the rocket trajectories with the wake boundary were found to be similar in magnitude to the launch velocity of the 2.75 in. rocket currently in use on AH-1G aircraft. Values of the downward induced velocity component as high as 70 fps (time-averaged) and 130 fps (instantaneous) were predicted for the hover condition, and the velocities decrease with increasing flight speed. For flight speeds greater than approximately 30 kts, the rotor wake passes behind the rocket launch position which significantly reduces the wake induced effects. The location of the rotor wake boundary relative to the rocket trajectories is a major determinant of the induced velocity distribution along the trajectories. Thus, the use of an accurate wake geometry was found to be important for accurate calculations of the induced velocities at the rocket.

The results of this analytical investigation were published in March 1975 in U.S. Army Picatinny Arsenal Technical Report 4797, "Prediction of Rotor Wake Induced Flow Velocities Along the Rocket Trajectories of an Army AH-1G Helicopter." This paper, presented on August 12, 1975 at the Conference on the Effects of Helicopter Downwash on Free Projectiles sponsored by the U.S. Army Aviation Systems Command, is a condensation of that report.

NOTATION

R	rotor radius, ft
V	forward flight velocity, fps
v_{x_T}, v_{y_T}, v_{z_T}	instantaneous induced velocity components in rocket trajectory coordinate system (x_T, y_T, z_T); sign convention is consistent with coordinate definition, fps
$v_{x_{T_{AVG}}}$, $v_{y_{T_{AVG}}}$, $v_{z_{T_{AVG}}}$	time averaged induced velocity components in rocket trajectory coordinate system (x_T, y_T, z_T); same sign convention as v_{x_T}, v_{y_T}, v_{z_T}, fps
x, y, z	hub centered axis system coordinates nondimensionalized by R, x-y plane parallel to rotor tip path plane, right handed coordinate system with positive x downstream (see Fig. 5)
x_T, y_T, z_T	rocket trajectory axis system coordinates nondimensionalized by R, centered at intersection of axis of rocket launch positions and fuselage centerline, left handed coordinate system with positive x_T in direction of rocket travel (see Fig. 1)
μ	rotor advance ratio, component of V parallel to rotor tip path plane nondimensionalized by rotor tip speed
ψ	blade azimuth angle measured from x axis (see Fig. 1), positive in the direction of rotation, deg

INTRODUCTION

The accurate determination of the flow field around a helicopter is required when the helicopter is used as a weapons platform. Since a free-flight projectile such as a rocket, when fired from a helicopter, may initially be travelling at a speed which is of the same order of magnitude as the flow velocities, the flow field induced by the rotor wake system can have a significant effect on the rocket trajectory. This may necessitate some form of aiming compensation or special firing techniques -- particularly at the low helicopter flight speeds at which rockets are to be fired in accordance with current Army tactical concepts.

To assess the influence of the rotor/wake flow field on the flight path of a rocket fired from the Army AH-1G helicopter when hovering or flying at low forward speeds, computer analyses developed at the United Technologies Research Center, UTRC (formerly the United Aircraft Research Laboratories) were used to predict the induced flow velocities along the rocket trajectories. The four rocket trajectories of the AH-1G helicopter (commonly referred to as the Cobra) are shown in Fig. 1. The results of the Army sponsored investigation have been presented in Ref. 1, and this paper is a condensation of that reference report. The induced velocity results from this investigation have recently been used in Army trajectory analyses to assess the influence of the aerodynamic interference of the rotor wake on rocket trajectories (Ref. 2).

Included herein are (1) a brief description of the computer analyses used, (2) a description of the flight conditions and wake models used in the analyses, (3) presentation of selected induced velocity results for the three flight conditions analyzed, and (4) conclusions and recommendations.

BRIEF DESCRIPTION OF THEORETICAL METHODS

The basic components of the UTRC Rotor Analysis are shown in Fig. 2. Brief descriptions of the Prescribed Wake Rotor Inflow Analysis and the Wake Geometry Analysis are presented below.* More detailed information on the contents, assumptions and applications of the methods is contained in Refs. 3 through 8.

Prescribed Wake Rotor Inflow Analysis

The function of the UTRC Prescribed Wake Rotor Inflow Analysis is to compute the time varying circulation and induced velocity distributions along the rotor blades

---

* Blade motions and control settings were provided by the Bell Helicopter Company. Thus, the blade response analysis in Fig. 2 was not used for this study.

and in the wake that are compatible with a prescribed set of blade section operating conditions and a prescribed wake geometry. Each blade is represented by a segmented lifting line, and the wake is represented by a finite number of segmented vortex filaments trailing from the blade segment boundaries. The fundamental relations of blade circulation to lift coefficient, angle of attack, blade motions, control settings, induced velocity, and wake geometry are used in this analysis. Once the circulations are computed, the velocities induced at and away (e.g., at rocket trajectories) from the rotor disc by the bound and trailing vorticity of the rotor are determined through application of the Biot-Savart law which relates the induced velocity at a point in space to the circulations and wake geometry. The induced velocity is proportional to the summation of the products of the circulation strength and the geometric influence coefficient of each element of vorticity in the rotor-wake system. The geometric coefficient is related only to the relative geometry between a wake element and the point at which the induced velocity is being computed. Since the wake geometry is prescribed, the wake may vary from an undistorted wake model to a complex experimental or distorted analytical wake model with tip vortex roll-up and vortex core effects mathematically modeled.

Wake Geometry Analysis

The Rotor Inflow Analysis requires that the rotor wake geometry be specified in order for circulations and induced velocities to be determined. There are several alternatives for rotor wake geometry. Appropriate experimental wake data is certainly most desirable, but, except for hover, is not currently available for most rotor configurations and forward flight conditions.

In its simplest form, the wake from each blade can be assumed to be a classical undistorted skewed helical sheet of vorticity defined from momentum considerations (hereafter referred to as the undistorted wake). Sample undistorted wake representations are shown in Figs. 3(b) and 4 for hovering and forward flight conditions, respectively.

To eliminate the necessity for prescribing an undistorted wake geometry, an analytical method for computing more realistic wake geometries was developed at UTRC. The basic approach of this method, entitled the UTRC Rotor Wake Geometry Analysis, involves the following. First, an undistorted wake model is defined along with the distribution of circulation strengths of the various vortex elements comprising the wake. The classical Biot-Savart law is then applied to determine the velocities induced by each vortex wake element at numerous points in the wake. These distorting velocities are then numerically integrated over a small time increment to obtain new wake element positions. The process of alternately computing new velocities and positions is continued until a converged, periodic distorted wake geometry is attained.

For hovering conditions, systematic model rotor wake geometry data have been acquired experimentally at UTRC. The data have been generalized in Ref. 3 to facilitate the rapid estimation of wake geometry for a wide range of rotor designs and operating conditions and have been used to accurately predict the hover performance for a wide range of full-scale helicopters. A special computer subroutine has been prepared to model the hovering rotor wake in accordance with the generalized data. A comparison of the experimental hovering wake representation with the undistorted wake representation is presented in Fig. 3.

DESCRIPTION OF WAKE GEOMETRIES USED IN THE ANALYSES

For this investigation, the wake geometry analysis was used to generate wakes for the forward flight conditions, and the generalized experimental wake geometry was used for the hover condition.

The wake representation used in the analyses consisted of 10 finite vortex filaments trailing from each blade. These vortex filaments were divided into straight vortex elements at azimuth intervals corresponding to 15 degrees of blade rotation. The extent of the filament geometry was prescribed by 6 wake revolutions from the rotor except for the hover condition for which it was 8 revolutions. The five outer vortex filaments were combined beyond a 15 degree azimuth distance from the blade to simulate the roll-up of the tip vortex. Both undistorted and distorted wake models, described previously, were used to show the sensitivity of the results to wake geometry. For the undistorted vortex filaments, the vortex elements were positioned in a direction normal to the rotor disc in accordance with the mean induced velocity as determined from momentum theory at the rotor disc. The values of this momentum induced velocity for the 0, 15, and 30 kt flight conditions are -36.3, -31.6, and -22.9 fps, respectively. For the distorted wake representations, only distortions of the tip vortices were calculated for the two forward flight conditions and an undistorted inboard wake model was assumed. The latter assumption may be justified considering the relatively higher circulation strength of the rolled up tip vortices compared to that of the inboard vortex filaments.

The undistorted and experimental distorted tip vortex geometries for the hover condition are presented in Figs. 5 and 6. The analytical distorted tip vortex geometries for the 15 and 30 kt conditions are presented in Figs. 7 and 8. The primary difference between the undistorted and distorted wakes (Figs. 5 and 6) for the hover condition is the wake contraction. In addition, as shown Fig. 3, the inboard wake is transported downward with a nonuniform radially varying axial velocity which causes the outer portion to travel faster than the inner portion. At 15 and 30 kts, the tip vortex distortions result in a contraction of the forward boundary of the wake. This contraction of the wake has a predominant effect on the induced velocity distribution along the rocket trajectories in that it moves the intersection point of each trajectory with the wake boundary rearward, and thus decreases the duration of time that the rocket is inside the rotor wake.

DESCRIPTION OF FLIGHT CONDITIONS AND AIRCRAFT CONFIGURATION USED IN THE ANALYSES

Induced velocities were calculated for the Army AH-1G helicopter, commonly referred to as the Cobra. A schematic of the AH-1G helicopter is shown in Fig. 1. The teetering type rotor of this helicopter has a radius of 22 ft. Each of its two blades has a nominal chord of 2.25 ft, a linear twist of -10 deg, a modified 0009 airfoil section, and a preconing of 2.75 deg.

The calculations were performed for a helicopter gross weight of 9500 lbs and a center-of-gravity position at 198.5 in. from the nose of the aircraft. Three flight conditions were investigated corresponding to flight speeds of 0 (hover), 15, and 30 kts. Considering the rotor tip speed of 746 fps, these flight speeds result in rotor advance ratios, μ, of 0, 0.034, and 0.068, respectively. The respective rotor control, flapping, and disc angles used in the analyses are presented in Ref. 1.

Induced velocity calculations were performed for the four rockets mounted at 0.39 R below and 0.034 R foward of the rotor hub, and lateral positions of 0.16 R and 0.22 R on both sides of the fuselage centerline. The rocket launch attitudes were all specified at an elevation of 126 mils (7 degrees) relative to the fuselage waterline except in a sensitivity study where 160 and 195 mils were used. It is noted that each rocket was assumed to be concentrated at a point (center-of-gravity) when determining the launch point. Induced velocities were calculated at increments of 0.1 R along the rocket trajectories from the launch point. The trajectories from the launch point to a distance of one rotor diameter (extent of calculation) were assumed to be straight lines. The coordinate system (x_T, y_T, z_T) used for the predicted induced velocities is referenced to the rocket launch point and the axes are parallel and normal to the rocket trajectories as shown in Fig. 1. Positive directions are also shown in Fig. 1.

DISCUSSION OF INDUCED VELOCITY RESULTS

The three components of induced velocty, v_{x_T}, v_{y_T}, and v_{z_T}, were calculated along each rocket trajectory numbered 1 through 4, as shown in Fig. 1. Since the orientation of the rotor blades and wake relative to a point on a rocket trajectory varies with time, the instantaneous velocity components induced at that point also vary with time. Since steady flight conditions were selected for this investigation, the positions of the blade and wake and the resulting velocities are periodic. The period is the time corresponding to the blade passage interval, which for the 2-bladed AH-1G rotor is the time required for a blade to travel 180 degrees. Thus, time was expressed in terms of increments of rotor rotation designated by rotor position and the corresponding azimuth angles of the two blades. The calculations were performed using an azimuth increment of 15 degrees, which resulted in 12 rotor positions per blade passage interval.* In addition to the instantaneous velocities at each rotor position, the time-averaged velocities were calculated.

The major variables for this investigation and the notation to be used for the plotted results are summarized below:

Major Variables

Flight Conditions	V = 0, 15, 30 kt
Wake Models	Distorted, Undistorted
Instantaneous Velocity Components	v_{x_T}, v_{y_T}, v_{z_T}
Time-Averaged Velocity Components	$v_{x_{T_{AVG}}}$, $v_{y_{T_{AVG}}}$, $v_{z_{T_{AVG}}}$
Rotor Positions (Time Step)	1, 2, 3, ..., 12
Blade Azimuths, ψ, deg	0, 180; 15, 195; 30, 210; ... 165, 345
Rocket Number	1, 2, 3, 4
Rocket Lateral Position	y_T = -0.22, -0.16, 0.16, 0.22
Position Along Rocket Trajectory	x_T = 0, 0.1, 0.2, ..., 2.0

In addition to all combinations of these variables, a few computer cases were run to investigate the sensitivity of the results to rocket launch attitude and launch position.

In total, six base cases (3 flight conditions x 2 wake models) plus three sensitivity variations were run. Considering the 3 velocity components, 4 rockets, 21 rocket trajectory points and the 12 rotor positions plus the time-average velocities, a total of 3276 velocity values were computed for each of the 9 cases. Tabulations of these values have been provided separately to the Army. In Ref. 1 a judicious selection was made of combinations of variables for which velocity data comprising 40 figures

* For the AH-1G, and a rocket speed of 100 fps, a rocket travels a distance of 0.42 R during a blade passage interval (one-half rotor revolution).

were presented. A sampling of these figures, selected to convey the primary results for the hover and forward flight conditions, are presented and discussed below.

Hover Condition (V = 0)

The variation of the time-average v_{z_T} velocity along the rocket trajectories of all four rockets, based on the distorted wake model, is presented in Fig. 9. This velocity component normal to each trajectory, increases from approximately 30 to 70 fps (downward) going from the rocket launch position ($x_T = 0$) to the intersection of each trajectory with the wake boundary shown in the top view in Fig. 6, (e.g., at $x_T = 0.77$ for rocket 4). Moving from inside to outside of the wake boundary an abrupt change in velocity occurs in both magnitude and direction (downflow to upflow). The upflow is not as severe as the downflow because the contributions of the tip vortices and the inboard wake are opposing outside of the wake, whereas they are additive just inside the wake. As the rocket moves away from the wake, the velocity decreases as expected. It is also shown in Fig. 9 that the influence of the different lateral positions of the four rocket trajectories on this average velocity component is small.

In Fig. 10, the instantaneous v_{z_T} velocity component is presented for rocket 4 and four selected rotor positions. Near the wake boundary the instantaneous velocities vary significantly with rotor position. This time variation is clearly shown in Fig. 11 where the v_{z_T} velocity is plotted versus rotor position for selected trajectory points both near and far from the wake boundary. For the rocket launch point ($x_T = 0$), the variation with rotor position is relatively small. At the farthest point calculated ($x_T = 2.0$), the 2 fps velocity is negligible, considering its effect on the rocket. The variation is generally small for points in the wake up to the region of $x_T = 0.7$ as shown by the abrupt change in the peak-to-peak values between $x_T = 0.6$ and 0.7. At $x_T = 0.7$, the velocity component ranges from 36 to 130 fps in the downward direction. It is noted that the 130 fps flow velocity exceeds the initial rocket launch velocity which is approximately 100 fps. The cyclic nature of the induced flow at a frequency of once-per-blade passage is a direct result of the passage of the tip vortex, and to a lesser extent the inboard vortex sheet, past the trajectory point. The peak downward velocity of 130 fps occurs when the tip vortex is closest to the point. The magnitude of the velocity is low (36 fps) at rotor position 1, because as shown in Fig. 6, the trajectory passes approximately mid-way between the tip vortices at this rotor position. Similar results were generally predicted for the other three rocket trajectories.

Results for the v_{x_T} and v_{y_T} velocities are included in Ref. 1. The time-averaged v_{x_T} velocity was predicted to be in a direction opposite to that of the rocket travel, and the peak value of 23 fps predicted near the wake boundary is significantly less than the 70 fps of the v_{z_T} velocity component. Instantaneous values as high as 60 fps were predicted. The v_{y_T} velocity component, which is in a direction to influence the lateral motion of the rockets, was predicted to have the lowest magnitude of the three components. The predicted time-average velocity did not exceed 10 fps, and the instantaneous velocity did not exceed 25 fps.

Two primary effects of wake model, distorted versus undistorted, on the induced velocity components were noted. The predominant difference observed from the time-average velocity results in Ref. 1 is the outward shift of the point at which the velocity components change abruptly, caused by the outward shift of the uncontracted wake boundary of the undistorted wake evident in a comparison of Fig. 5 with Fig. 6.

The predominant effect of wake model on the instantaneous velocity components also occurs in the region of the wake boundary, and consists of a shift in the time (rotor position) at which the peak velocities occur at rocket trajectory points in this region. This is evident in a comparison of Fig. 12 with Fig. 11. These differences indicate the importance of accurately representing the wake when predicting induced velocities at rocket trajectories.

In order to show the sensitivity of the induced velocity component to small variations in rocket launch attitude, the launch attitude relative to the fuselage waterline was changed in 2 degree increments for the hovering flight condition. That is, the launch attitude was changed from 7 degrees (126 mils elevation) to 9 and 11 degrees (160 and 195 mils). Since the flight condition and distorted wake geometry were unchanged, the time-averaged velocity components did not change significantly with the small reorientation of the rocket to the time-averaged wake geometry. However, the instantaneous velocity components in the vicinity of the wake boundary experienced a phase shift with rotor position due to the reorientation of the rocket trajectory to the tip vortices at a specific rotor position. This phase shift is shown in Fig. 13.

15 Kt Flight Condition

At the 15 kt flight condition, the wake boundary is skewed back toward the rocket launch point as shown in Fig. 7. The rocket trajectory intersects the distorted wake boundary between an x_T of 0.3 and 0.4. This results in the occurrence of the maximum downward velocity component (v_{z_T}) in that region as shown in Figs. 14 and 15. Thus, the rapid change in the skew angle of the wake with the small change in flight speed from 0 to 15 kts leads to a significant decrease in the distance from the launch point that the rocket is inside the rotor wake ($x_T \approx 0.35$ at 15 kts vs. 0.77 at 0 kt). The maximum time-average downward velocity ($v_{z_{T_{AVG}}}$) at the four rocket trajectories ranges between approximately 40 and 60 fps (Fig. 14) compared to the 70 fps at 0 kts (Fig. 9). A representative variation of the instantaneous v_{z_T} velocity component for selected rotor positions is shown in Fig. 15.

30 Kt Flight Condition

It is shown in Fig. 8 that the predicted distorted wake is skewed just enough at 30 kt for the tip vortices to pass behind the rocket launch point. This placement of the rocket trajectories outside of the wake results in relatively low magnitudes (less than $\pm$ 10 fps) of all velocity components. This was true for both time-averaged

and instantaneous velocities. (Time-averaged velocities are presented in Fig. 16; instantaneous velocities are similar.) Also, only minor variations of the velocity components were predicted between the four rocket trajectories and the various rotor positions. It thus appears that beyond a flight speed of approximatly 30 kt the AH-1G rotor wake is swept behind the rocket trajectories, and the wake induced effects at the rockets are probably insignificant.

Use of an undistorted wake model, for comparison, placed the rocket launch point right at the wake boundary. The resulting close proximity of the tip vortices to the launch point resulted in large instantaneous velocities at certain rotor positions. To show the sensitivity of the induced velocity components to a change in rocket launch position, the launch position was moved forward and down by 0.05 R for the 30 kt flight condition. The selection of this example was based on the intent to show the potential for significantly reducing the induced effects at the rocket by moving the launch point outside the wake. As shown in Fig. 17, moving the launch point outside the undistorted wake by the 0.05 R movements mentioned above, results in a significant decrease in interference similar to that attained through use of the distorted wake model. This emphasizes the importance of accurately locating the wake boundary relative to the rocket launch point. The placement of the launch point inside, at, or outside the wake boundary results in an extreme difference in the predicted induced velocities. Changes in the relative position of the rocket launch point to the wake boundary can be produced by changes in any of the factors determining the wake skew angle (flight speed, aircraft gross weight, and rotor attitude as determined by the aircraft center of gravity location or maneuver condition).

CONCLUSIONS

The following conclusions apply to the AH-1G helicopter operating at hover and low speed flight conditions:

1. The magnitudes of the predicted induced velocity components at the trajectories can exceed the rocket launch velocity. Values of the downward induced velocity component as high as 70 fps (time-averaged) and 130 fps (instantaneous) were predicted.

2. Of the three velocity components, the greatest induced velocities were predicted for the downward component normal to the rocket trajectory. The component along the rocket trajectory was generally next in order of magnitude, and the smallest velocity magnitudes were predicted for the lateral component.

3. As the rocket moves from its launch position, the downward velocity component increases as the wake boundary is approached. As the rocket moves to the outside of the rotor wake the magnitude of the downward velocity decreases abruptly, and becomes insignificant within a distance of one rotor diameter from the launch position.

4. The position of the intersection of a rocket trajectory with the wake boundary is most influential for it determines the length of time that the rocket remains in the higher induced velocity region inside the wake. It also determines the location where the close proximity to a tip vortex can result in a high induced velocity. The importance of the wake boundary location establishes the importance of accurately determining the items which establish the wake skew angle -- flight speed, rotor and aircraft attitude, and aircraft gross weight (rotor thrust).

5. Considering the variation of the predicted induced velocities with flight speed, the influence of the wake aerodynamic interference on the rocket trajectories is expected to decrease with increasing flight speed. In hover, the predicted velocities are the highest, and the rocket remains in the wake for the longest period of time. For flight speeds greater than approximately 30 kts, the rotor wake generally passes behind the rocket launch position which significantly reduces the wake induced effects.

6. Large impulsive type, induced velocity variations with time occur at points on the rocket trajectory near the wake boundary. These variations are caused by the passage of the tip vortices. If the high impulsive type velocities induced by the close passage of a tip vortex are found to significantly alter the flight path of the rocket, a mechanism for synchronizing the rocket firing time with the rotor position for minimum tip vortex interference could be considered.

7. The variation of the predicted time-averaged induced velocity components between the four rockets of the AH-1G helicopter is within ±10 fps at similar points along the trajectories.

8. It is necessary to use an accurate rotor wake model in calculations directed toward predicting induced velocities at rocket trajectories. The use of an undistorted wake model rather than a realistic distorted wake model results in significant differences in predicted induced velocities.

9. Small variations (4 degrees) in rocket launch attitude produce small induced velocity changes at the rocket trajectories except near the wake boundary where the variations produce a difference in the phasing of the velocities associated with the relation between rotor position and the passage of a tip vortex. This is generally also true for small variations in rocket launch point. However, vertical and/or longitudinal variations in launch point produce significant variations in induced velocities near the launch point at approximately 30 kts due to the movement of the point from inside to outside of the rotor wake or vice versa. The relative position of the rocket launch point to the wake boundary could also be varied by changes in any of the factors which determine the wake boundary (flight speed, aircraft gross weight, and rotor/fuselage attitude).

RECOMMENDATIONS

1. Several factors which were approximated or neglected in the analytical calculations, should be considered. These are wake instability and dissipation, vortex core size, the selection of the finite spatial and temporal increments used in the analyses, and wing and fuselage interference effects. Also, the possible requirement for iterating between the induced velocities and the rocket trajectory should be considered.

2. Calculations of the effect of the rotor wake induced velocities determined in this investigation on the rocket trajectories should be continued.

3. The rotor wake effects for flight conditions other than the three discussed herein should be determined. In particular, calculations for specific flight conditions for which flight test rocket trajectory data become available should be performed for correlation purposes. Also, the sensitivity of the results to variations of the significant parameters in actual aircraft operation which influence the wake strength and wake/rocket positioning should be investigated, and procedures for generalizing the results should be determined.

4. Model helicopter tests should be conducted to acquire systematic experimental data on this rocket aerodynamic interference problem. Model hovering and wind tunnel facilities and experimental flow measurement and visualization techniques should be used to measure the wake boundaries and flow velocities in the regions of the rocket trajectories. Combined model rotor-fuselage-wing testing, application of flow visualization techniques, and application of laser velocimeter techniques (as reported in Reference 9) to measure flow velocities, should be conducted. The results of such an experimental program would provide data for correlation with theory and for a systematic determination of the total and separate influence of each of the aircraft components (rotor, fuselage and wing) and significant parameters (flight speed, gross weight, aircraft attitude, etc.). In addition, the determination of the velocity field at potential locations for wind sensors mounted on the aircraft would assist in solving the problem of accurately measuring flow velocities at the low aircraft flight speeds required in accordance with current rocket firing tactics.

REFERENCES

1. Landgrebe, A. J. and T. A. Egolf: Prediction of Rotor Wake Induced Flow Velocities Along the Rocket Trajectories of an Army AH-1G Helicopter, Picatinny Arsenal Technical Report 4797, Prepared by the United Aircraft Research Laboratories (presently United Technologies Research Center) for U. S. Army Picatinny Arsenal, Dover, New Jersey, March 1975.

2. Wasserman, S.: Preliminary Analysis of the Effects of Calculated Downwash Distribution on Flight Performance of the 2.75" Rocket, Picatinny Arsenal, Proceedings of the USAAVSCOM Conference on the Effects of Helicopter Downwash on Free Projectiles, 1975.

3. Landgrebe, A. J.: An Analytical and Experimental Investigation of Helicopter Rotor Hover Performance and Wake Geometry Characteristics, USAAMRDL Technical Report 71-24, Prepared by the United Aircraft Research Laboratories for the Eustis Directorate, U. S. Army Air Mobility Research and Development Laboratory, Fort Eustis, Va., June 1971.

4. Landgrebe, A. J.: The Wake Geometry of a Hovering Helicopter Rotor and Its Influence on Rotor Performance, Jl. American Helicopter Society, Vol. 17, No. 4, October 1972.

5. Landgrebe, A. J. and E. D. Bellinger: An Investigation of the Quantitative Applicability of Model Helicopter Wake Patterns Obtained from a Water Tunnel, USAAMRDL Technical Report 71-69, Prepared by the United Aircraft Research Laboratories for the Eustis Directorate, U. S. Army Air Mobility Research and Development Laboratory, Fort Eustis, Va., December 1971.

6. Landgrebe, A. J.: An Analytical Method for Predicting Rotor Wake Geometry, Jl. American Helicopter Society, Vol. 14, No. 4, October 1969.

7. Landgrebe, A. J. and M. C. Cheney: Rotor Wakes - Key to Performance Prediction, AGARD-CP-111, AGARD Conference Proceedings No. 111 on Aerodynamics of Rotary Wings, Fluid Dynamics Panel Specialists Meeting, September 1972. (Also, paper presented at the Symposium on Status of Testing and Modeling Techniques for V-STOL Aircraft, Mideast Region of the American Helicopter Society, October 1972.)

8. Landgrebe, A. J. and T. A. Egolf: Rotorcraft Wake Analysis for the Prediction of Induced Velocities, USAAMRDL Technical Report 75-45, Prepared by the United Technologies Research Center for the Eustis Directorate, U. S. Army Air Mobility Research and Development Laboratory, Fort Eustis, Va., to be published.

9. Landgrebe, A. J. and B. V. Johnson: Measurement of Model Helicopter Rotor Flow Velocities with a Laser Doppler Velocimeter, Jl. American Helicopter Society, Vol. 19, No. 3, July 1974.

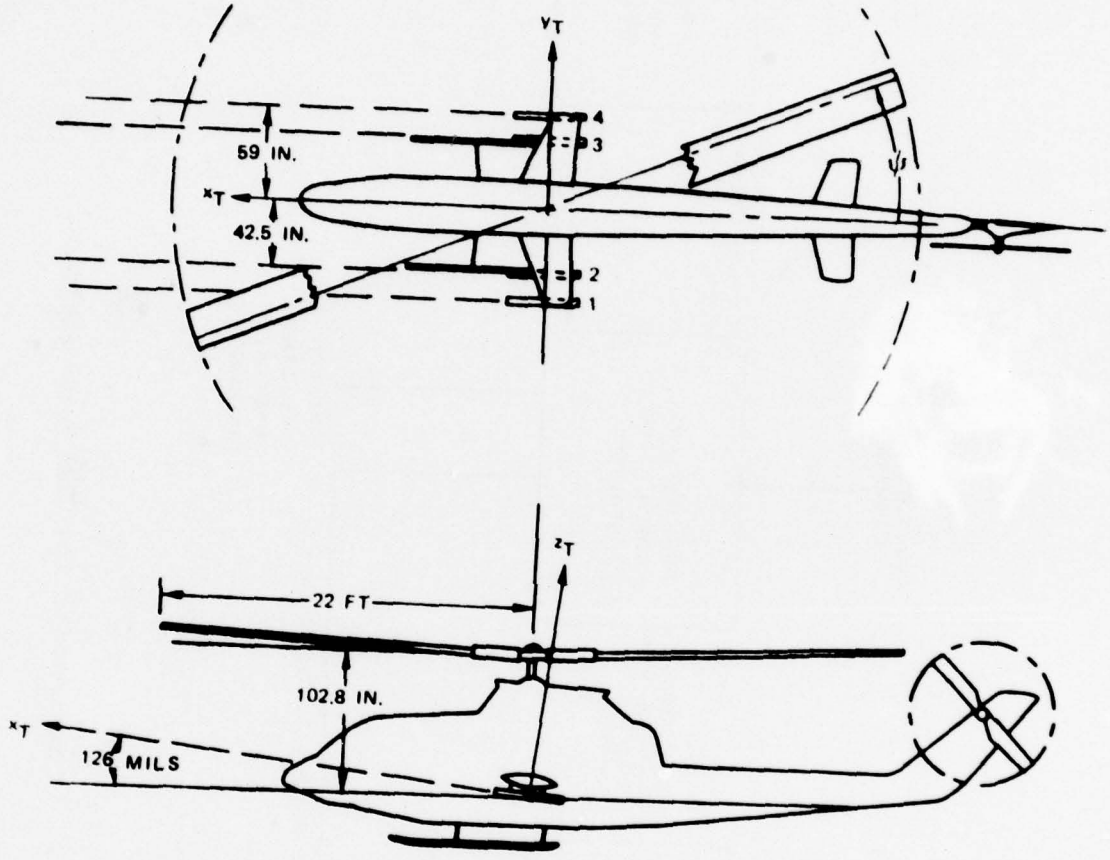

Figure 1. Schematic of AH-1G Helicopter Showing Assumed Rocket Trajectories and Coordinate System.

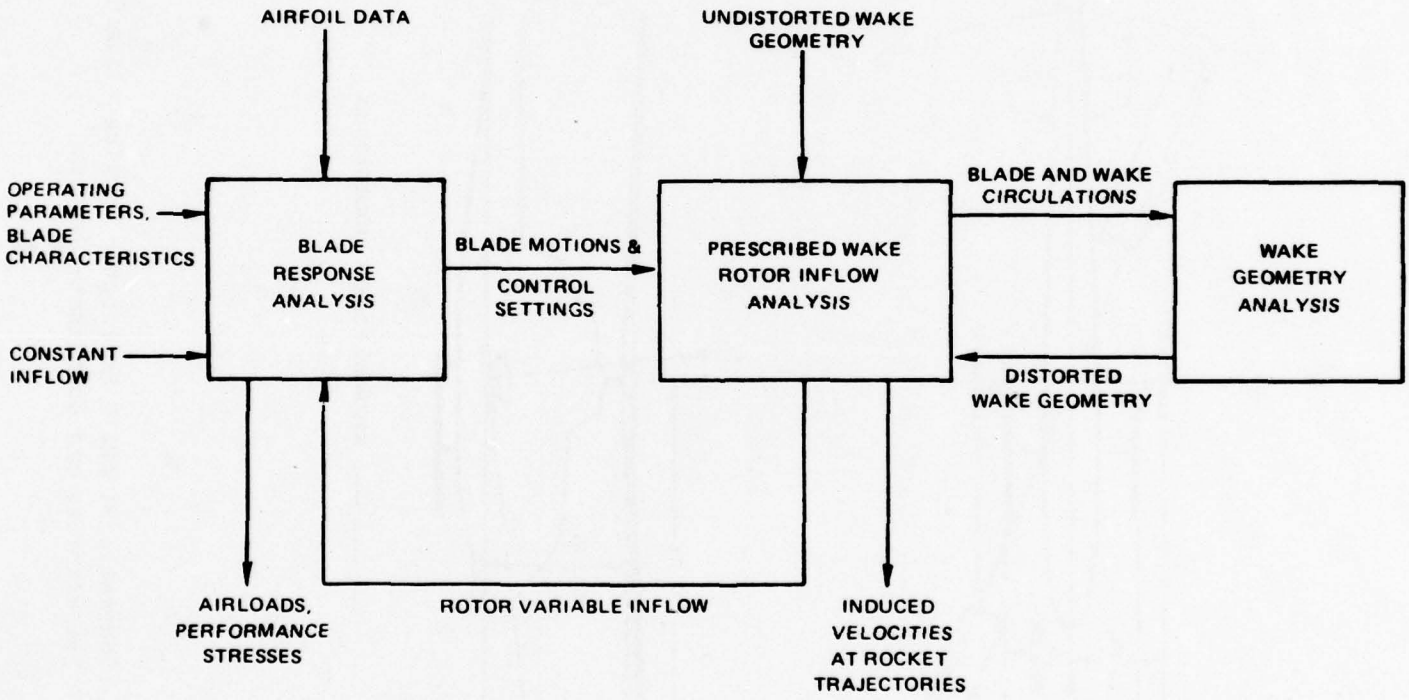

Figure 2. Components of the UTRC Rotor Analysis.

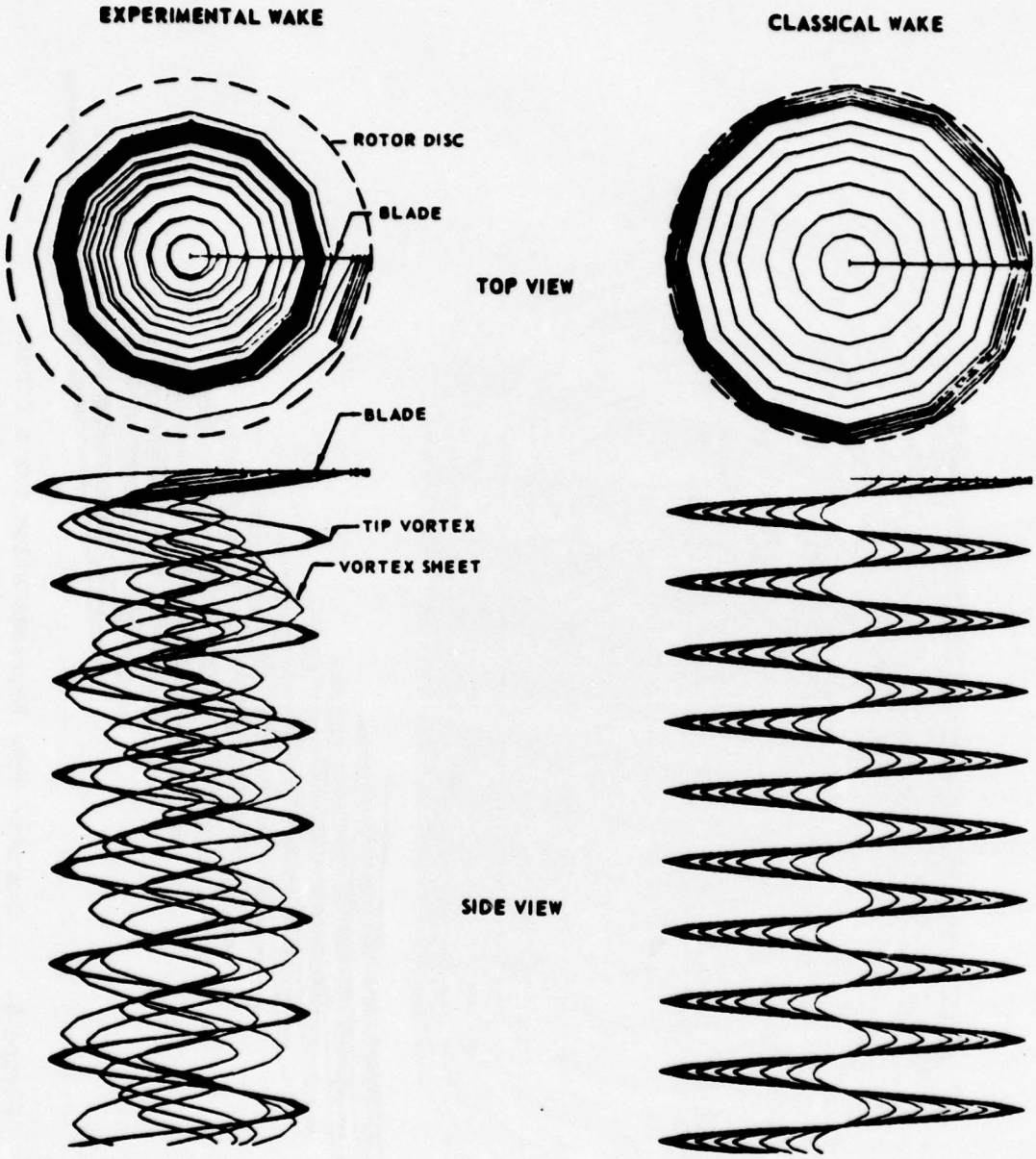

Figure 3. Computer Wake Trajectories For One Blade of a Hovering Rotor.

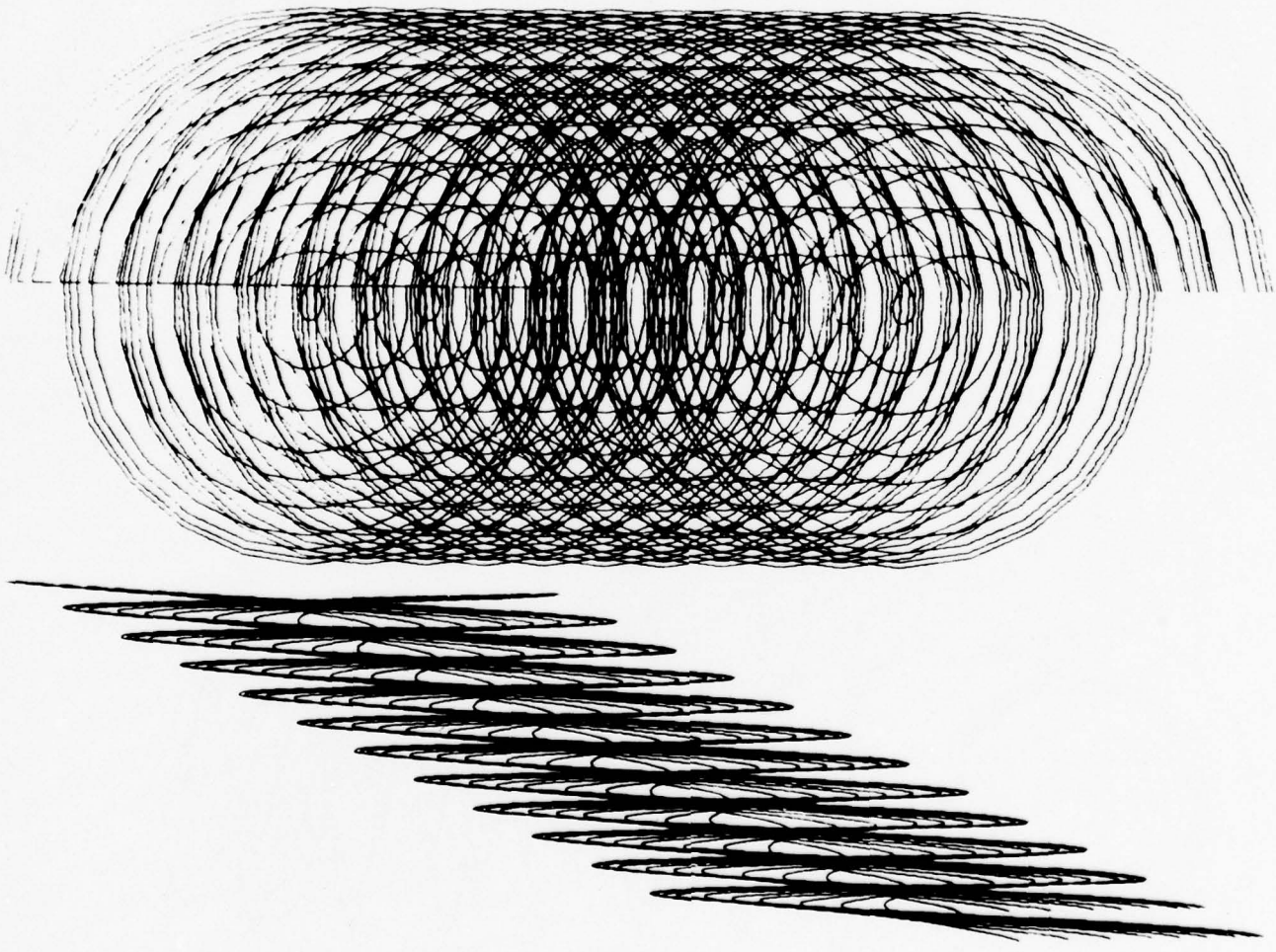

Figure 4. Computer Wake Representation for a Forward Flight Condition -- Undistorted Wake Model, All Filaments Shown.

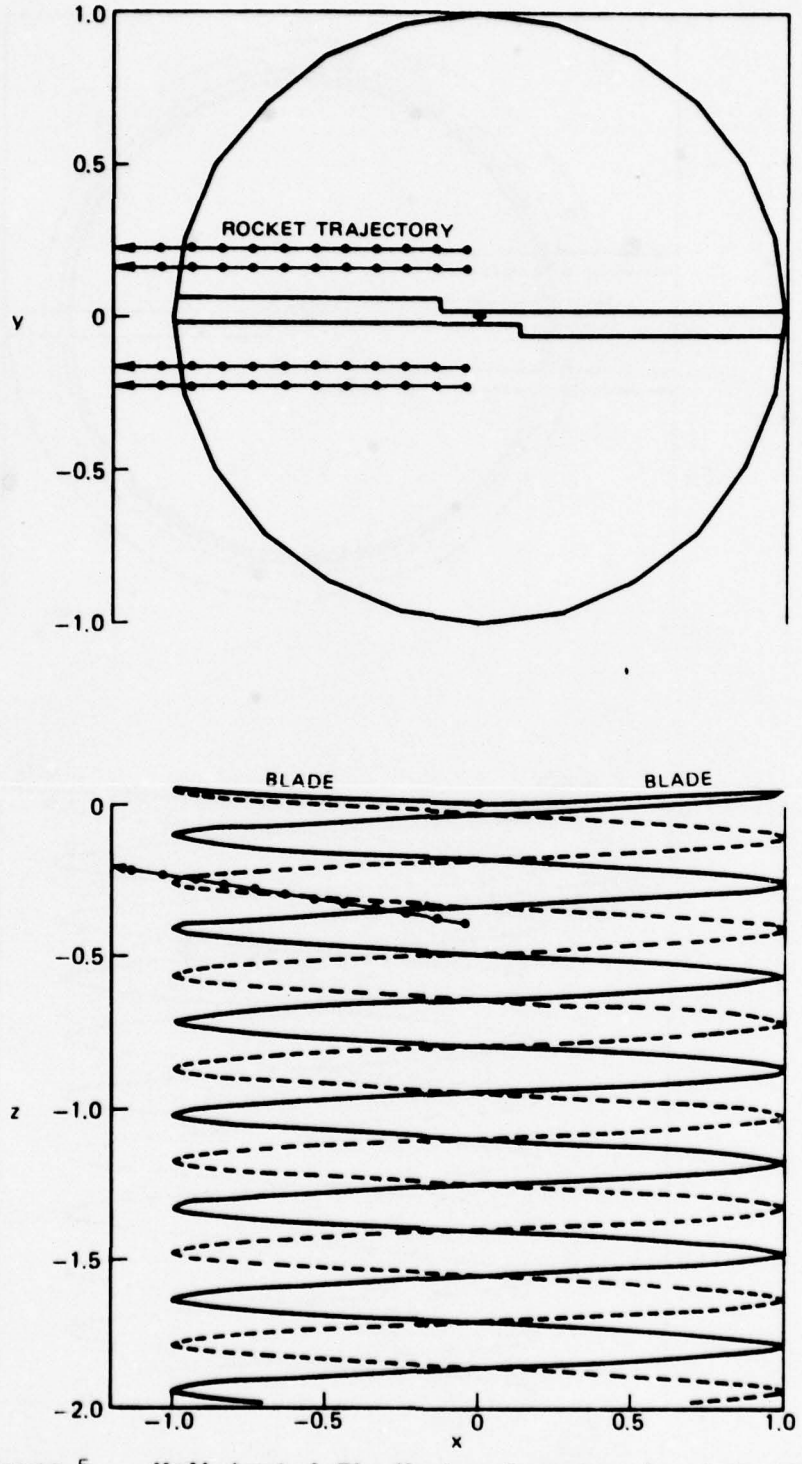

Figure 5. Undistorted Tip Vortex Geometry for 0 Kt Flight Condition and Rotor Position 1.

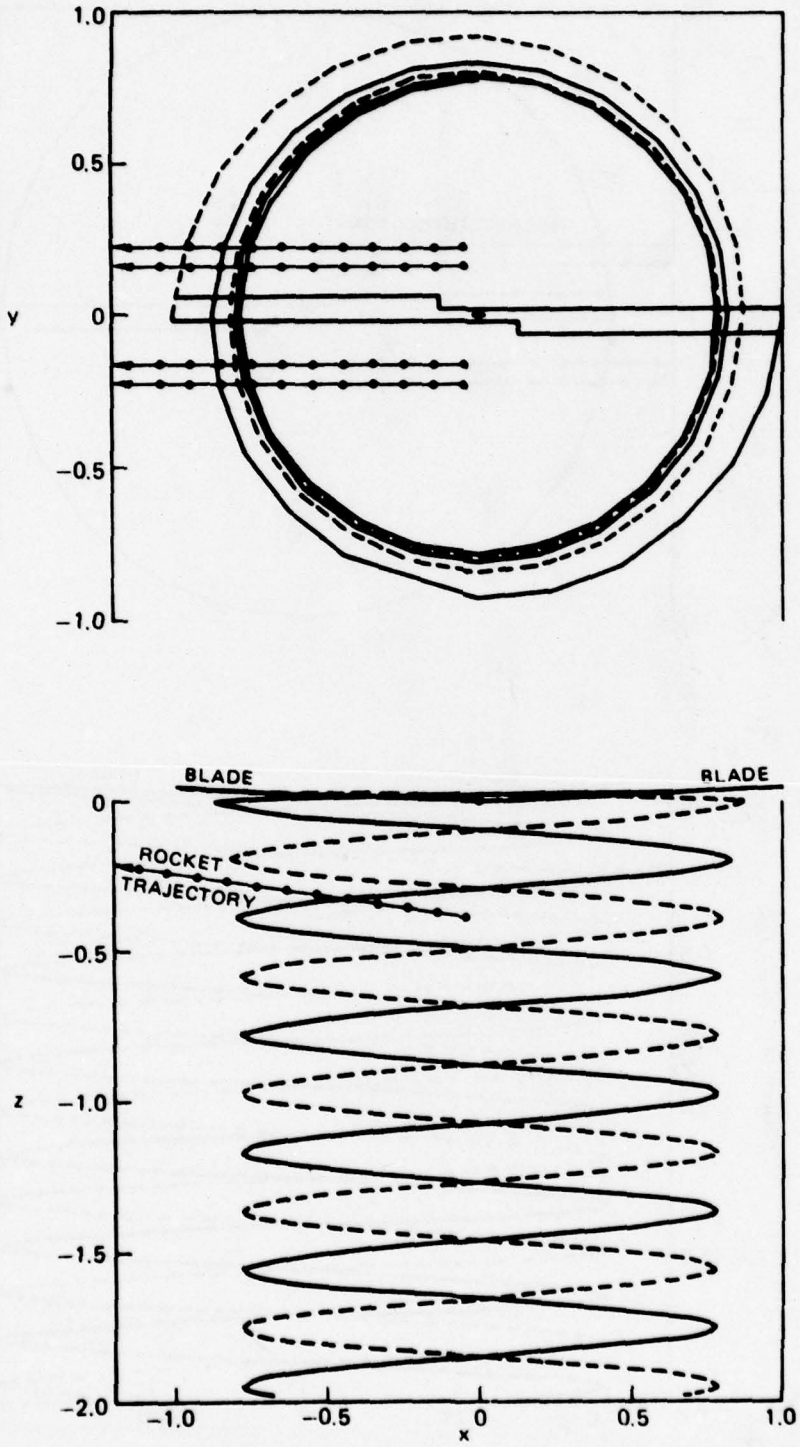

Figure 6. Distorted Tip Vortex Geometry (Experimental) for 0 Kt Flight Condition and Rotor Position 1.

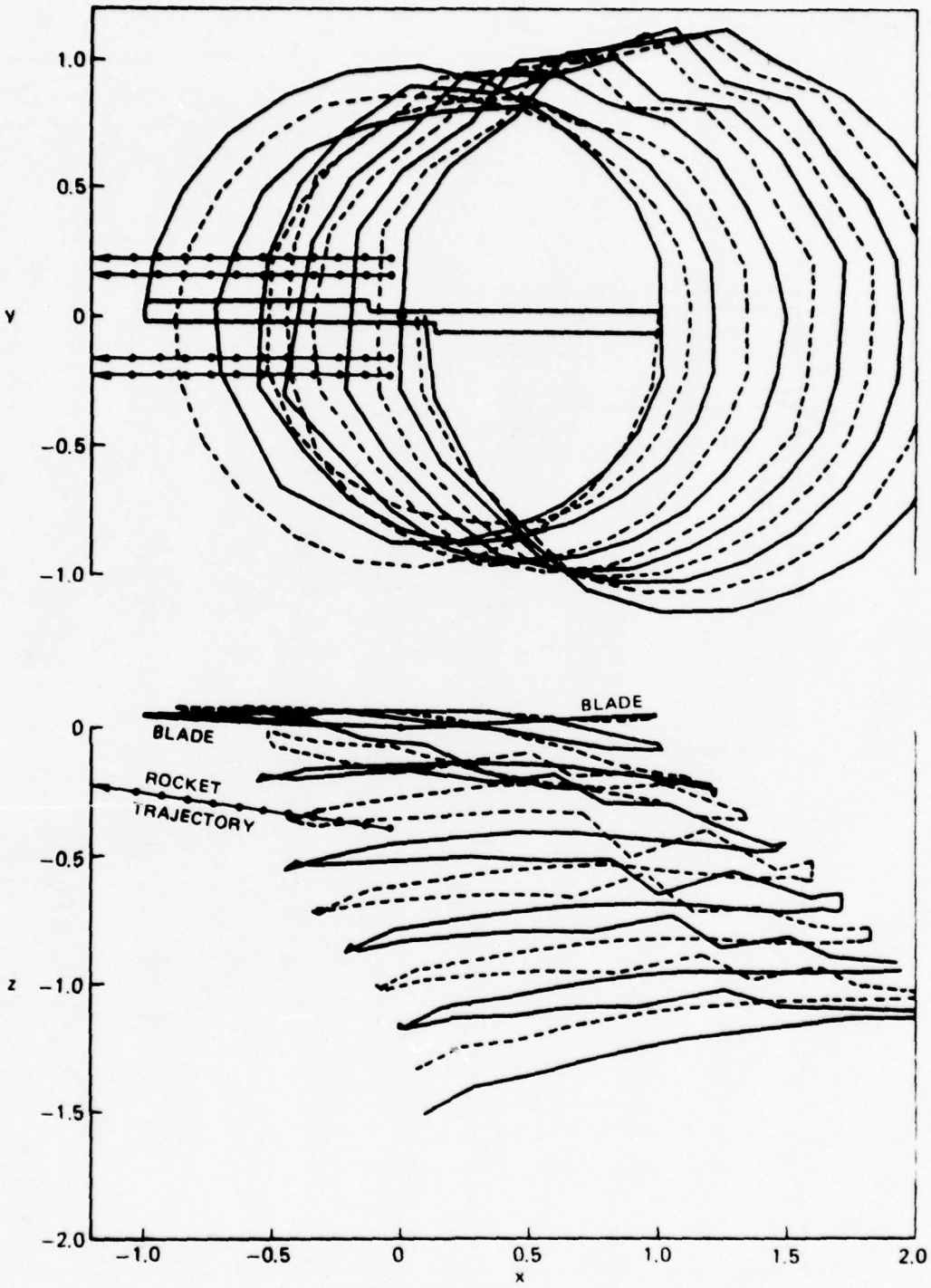

Figure 7. Distorted Tip Vortex Geometry (Analytical) for 15 Kt Flight Condition and Rotor Position 1.

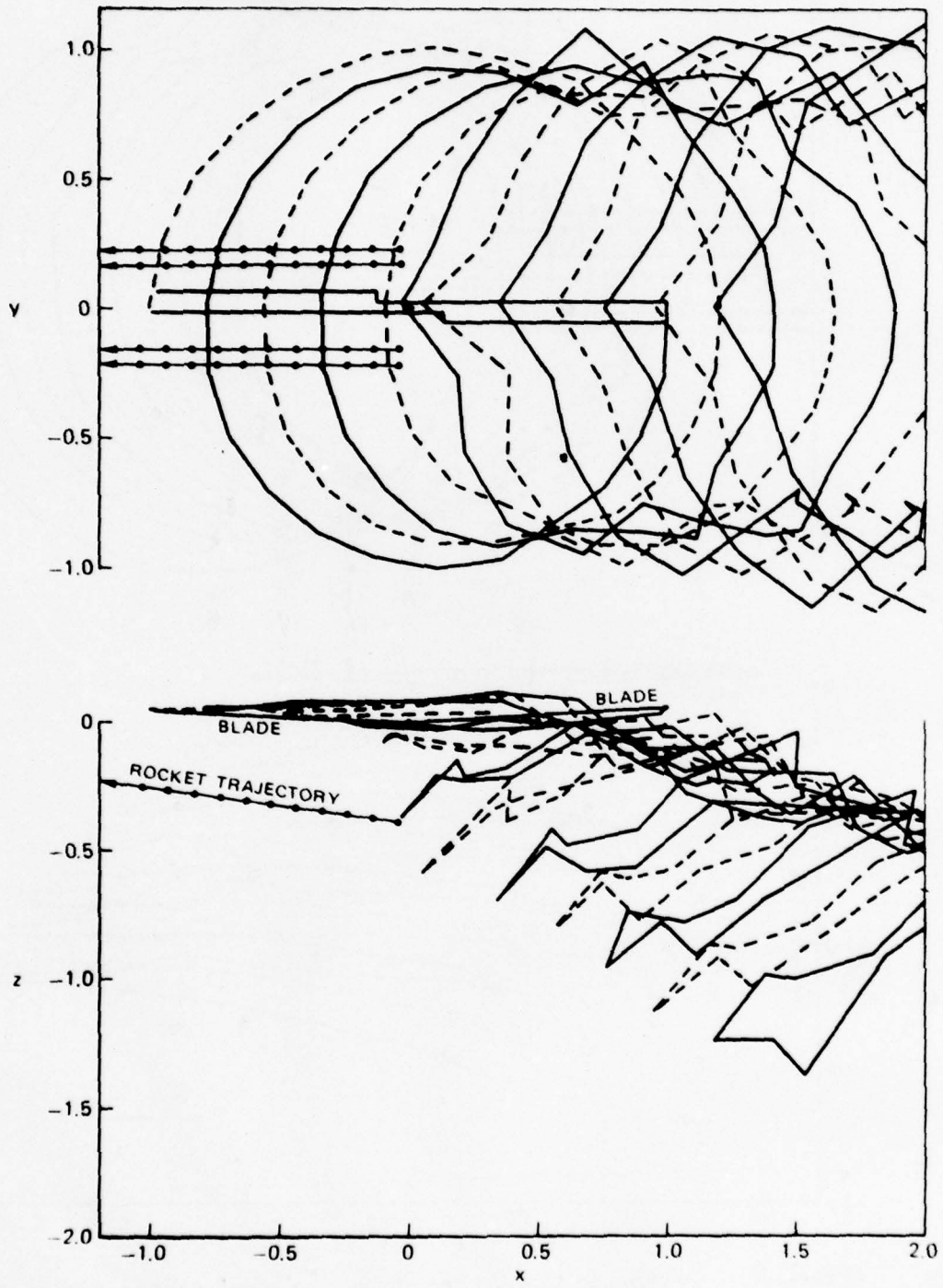

Figure 8. Distorted Tip Vortex Geometry (Analytical) for 30 Kt Flight Condition and Rotor Position 1.

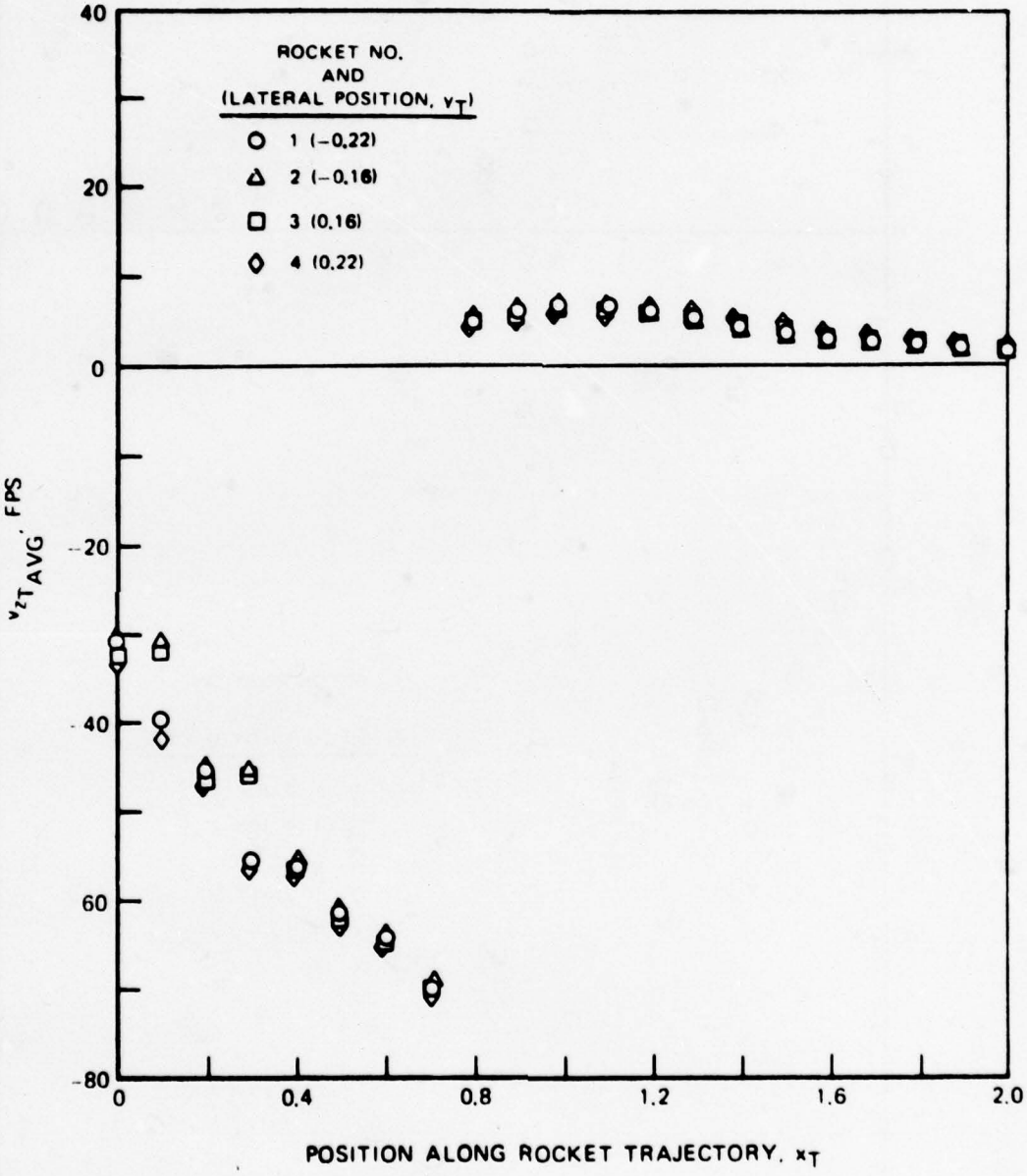

Figure 9. Variation of Time-Averaged v_{z_T} Velocity Component Along the Four Rocket Trajectories -- 0 Kt, Distorted Wake.

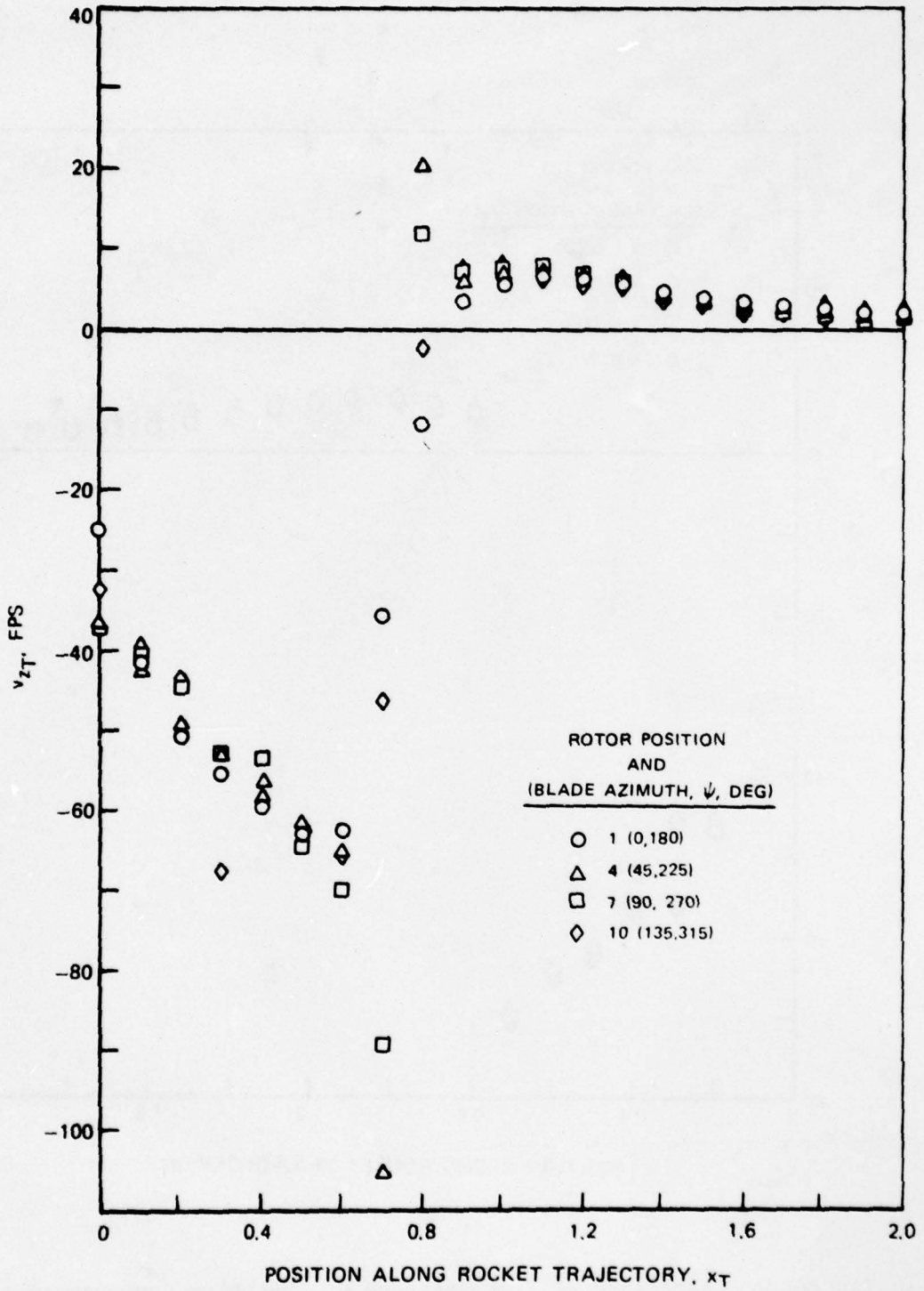

Figure 10. Variation of Instantaneous v_{zT} Velocity Component Along One Rocket Trajectory for Selected Rotor Positions -- 0 Kt, Distorted Wake, Rocket No. 4 (y_T = 0.22).

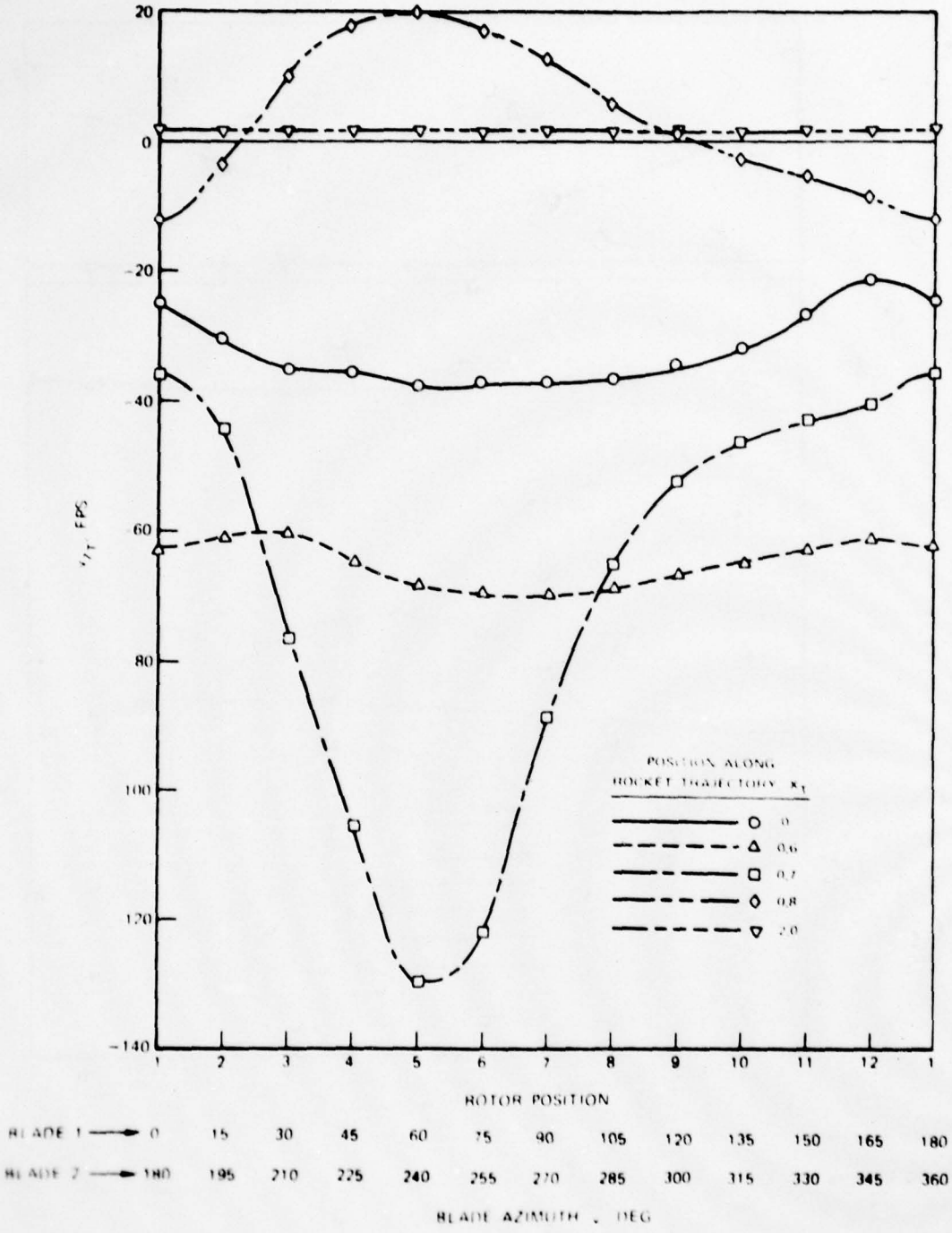

Figure 11. Variation of Instantaneous v_{zT} Velocity Component With Rotor Position for Selected Points on One Rocket Trajectory -- 0 Kt, Distorted Wake, Rocket No. 4 (γ_T = 0.22).

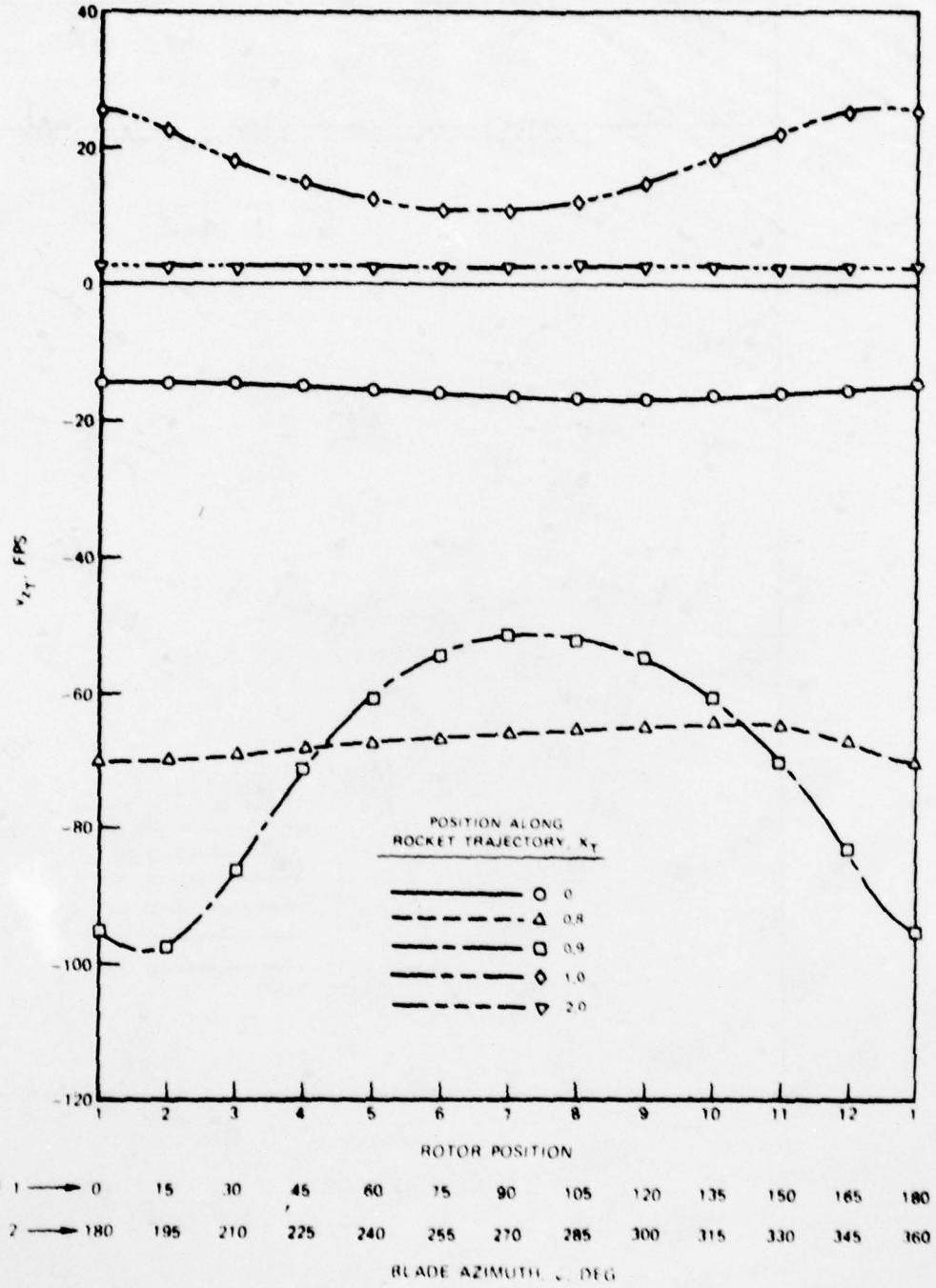

Figure 12. Variation of Instantaneous v_{zT} Velocity Component With Rotor Position for Selected Points on One Rocket Trajectory -- 0 Kt, Undistorted Wake, Rocket No. 4 (y_T = 0.22).

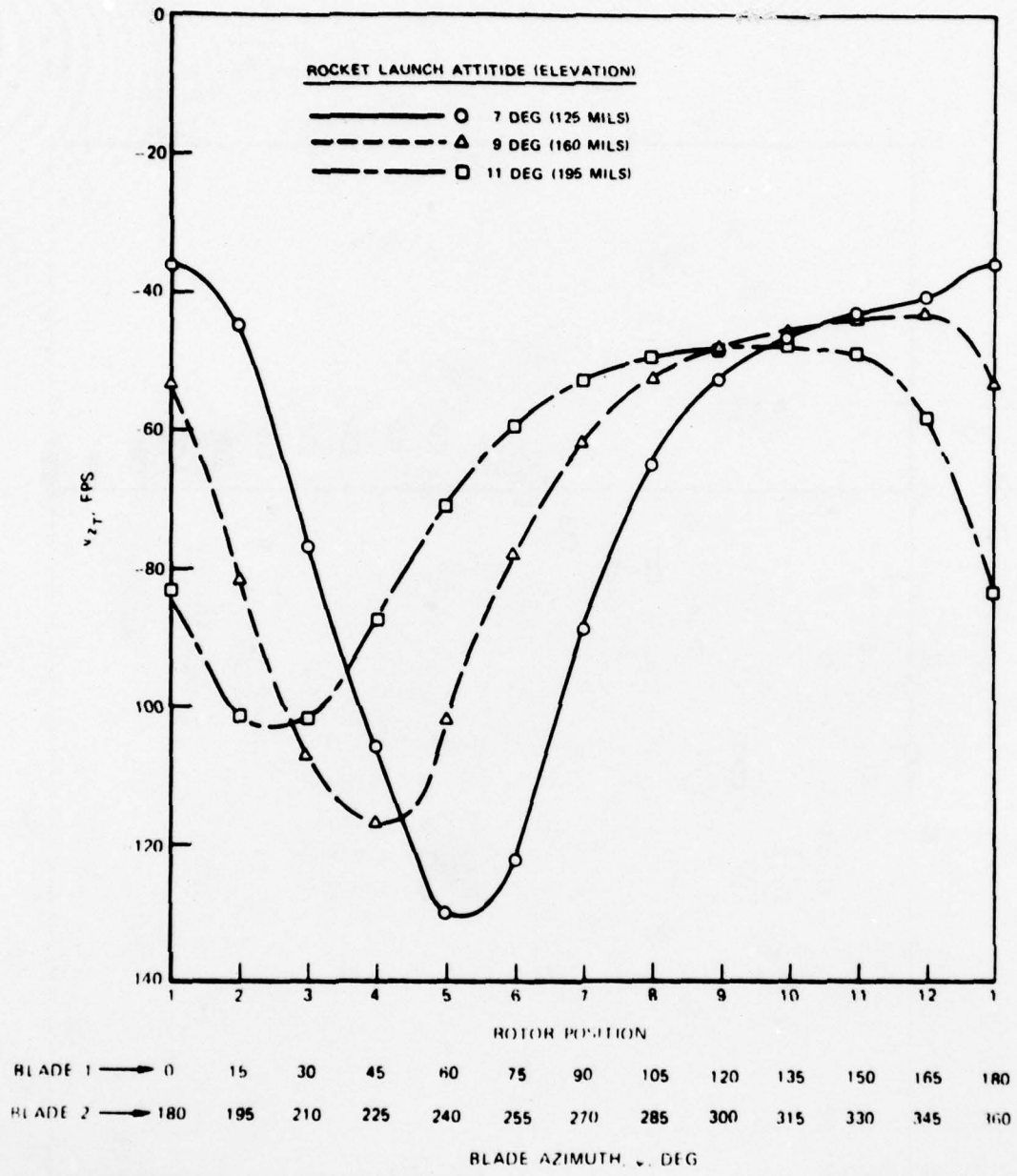

Figure 13. Effect of Variation of Rocket Launch Attitude on Instantaneous v_{z_T} Velocity Component Near the Wake Boundary -- 0 Kt, Distorted Wake, Rocket No. 4 ($x_T = 0.7$).

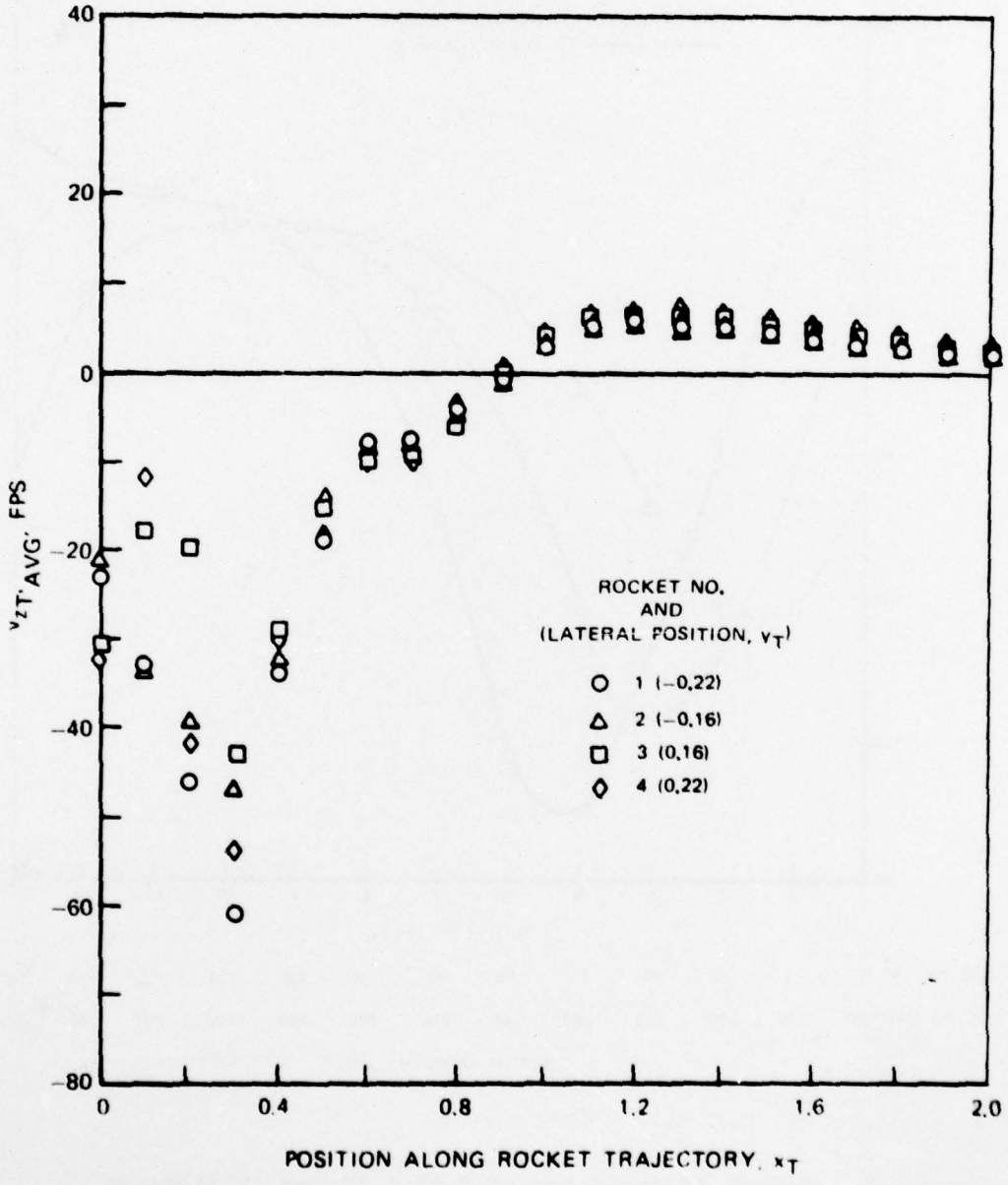

Figure 14. Variation of Time-Averaged v_{z_T} Velocity Component Along the Four Rocket Trajectories -- 15 Kt, Distorted Wake.

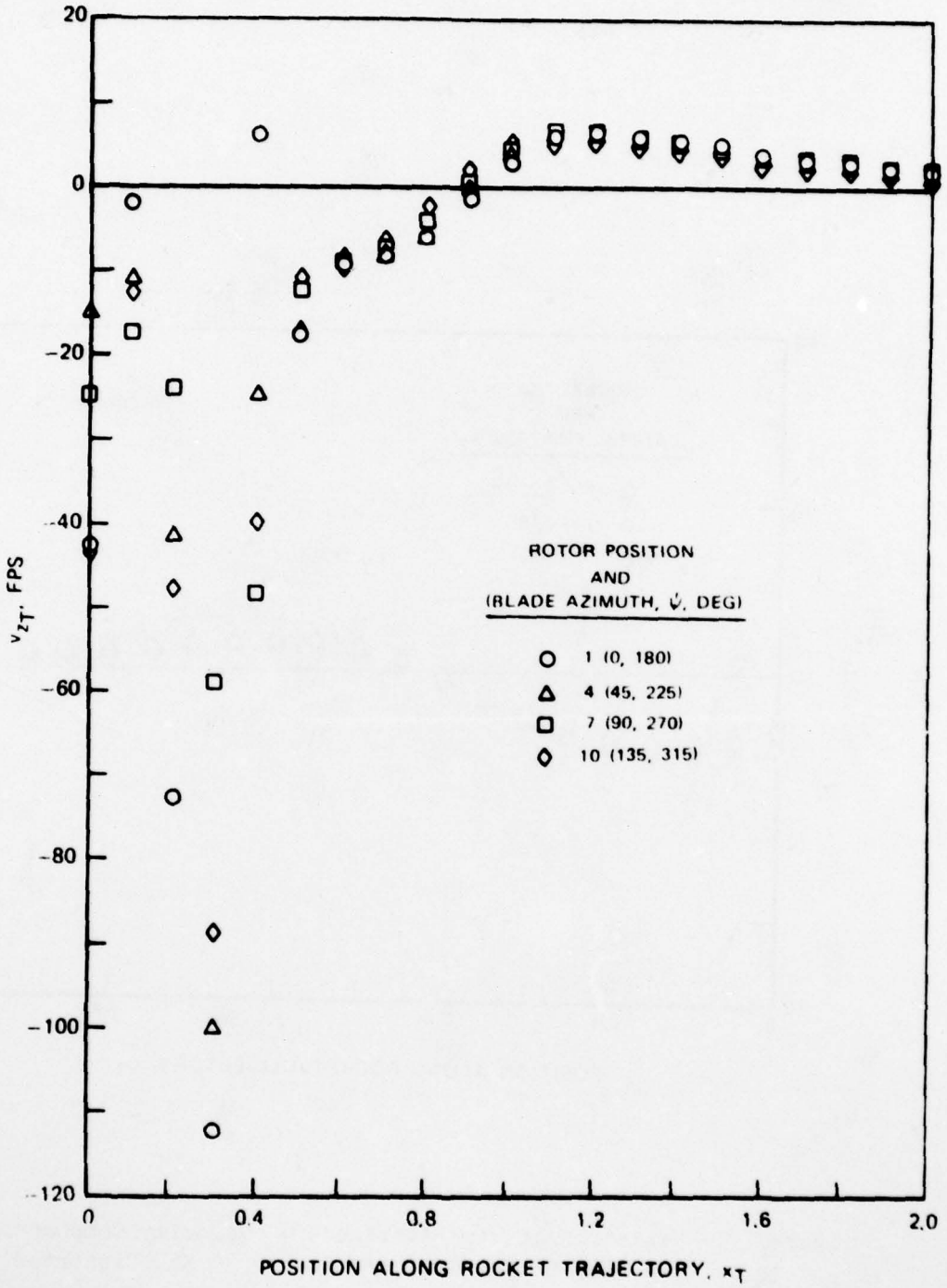

Figure 15. Variation of Instantaneous z_T Velocity Component Along One Rocket Trajectory for Selected Rotor Positions -- 15 Kt, Distorted Wake, Rocket No. 4 (v_T = 0.22).

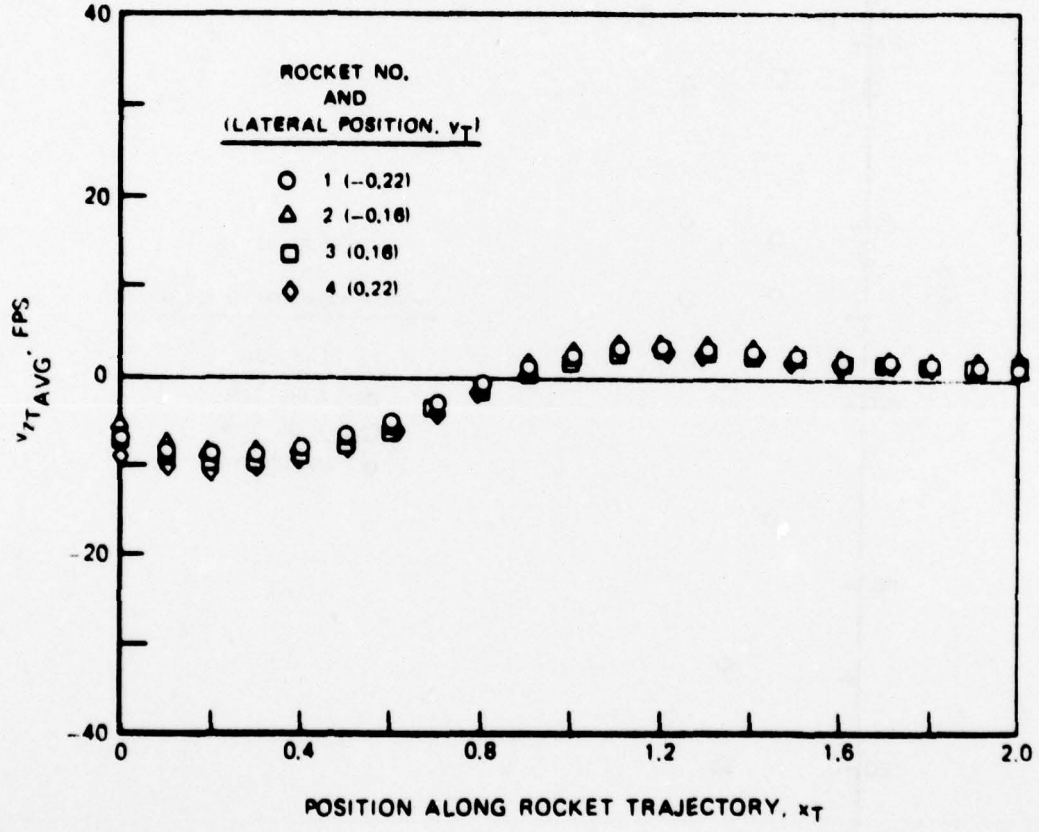

Figure 1c. Variation of Time-Averaged v_{zT} Velocity Component Along the Four Rocket Trajectories -- 30 Kt, Distorted Wake.

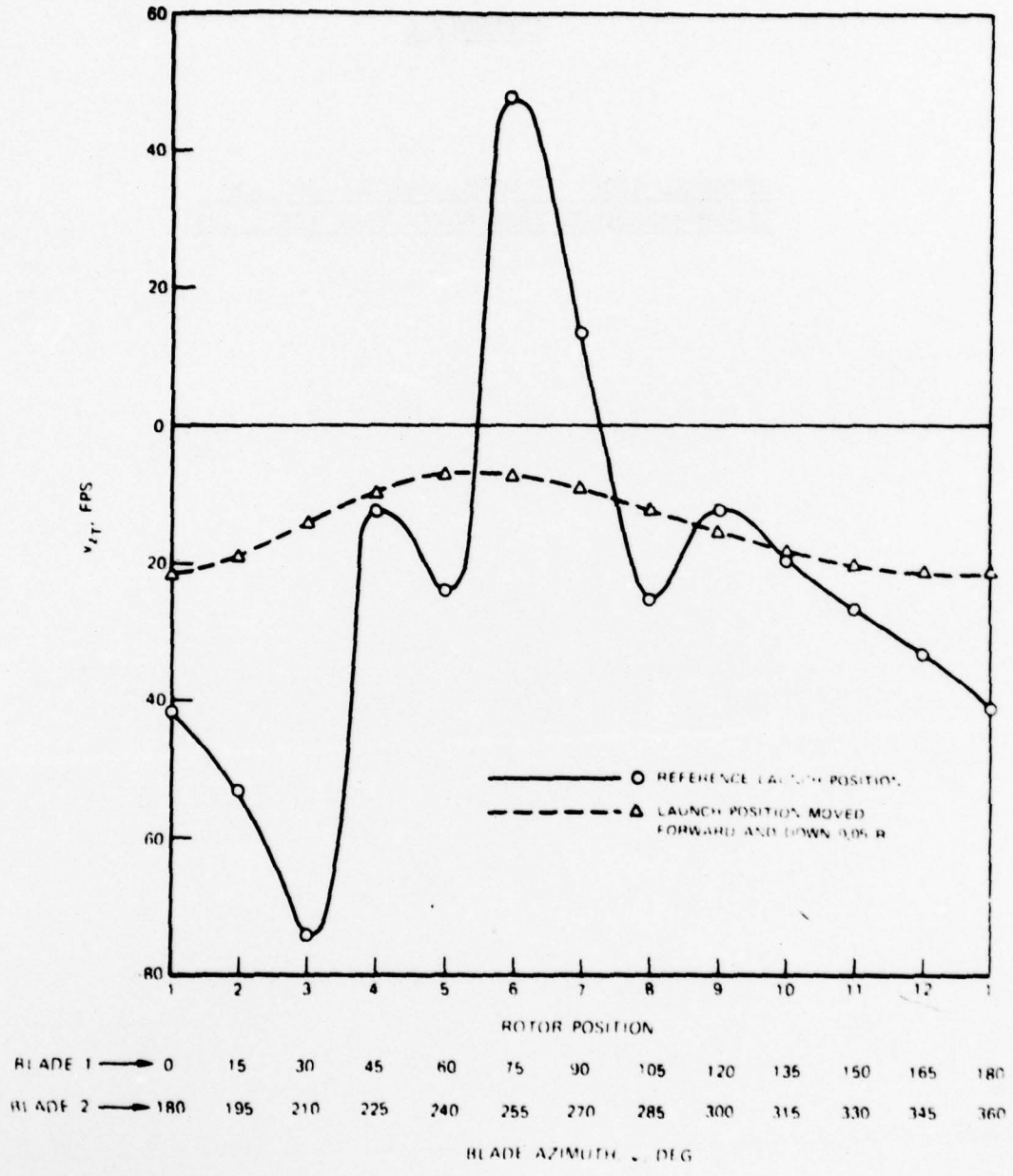

Figure 17. Effect of Variation of Rocket Launch Position on Instantaneous v_{2T} Velocity Component Near the Wake Boundary -- 30 Kt, Undistorted Wake, Rocket No. 4, ($x_T = 0$).

APPENDIX C

SUMMARY, SCOPE OF WORK, CONCLUSIONS AND RECOMMENDATIONS FROM HOVER TEST (REF. 23)

SUMMARY

(From Ref. 23)

As investigation was conducted to determine the airflow characteristics in the vicinity of a model helicopter to determine representative flow velocities at the rocket trajectory and wind sensor locations of a hovering Army AH-1G "Cobra" helicopter. Laser velocimetry and flow visualization techniques were applied to provide flow velocity and wake geometry data for correlation with theory and for a systematic determination of the total and separate influence of each of the aircraft components (rotor, fuselage, and wing), and significant operating condition parameters (rotor thrust, tip speed, and ground effect) on the airflow influencing rocket trajectories. In addition, the flow velocities at potential locations for a fire control system wind sensor, mounted on the aircraft, were determined to assist in identifying wind sensor locations for accurately measuring flow velocities at hover.

Time-averaged and peak-to-peak values of flow velocity components, measured with a laser velocimeter (LV), are presented and compared for the model test configurations and conditions. Also, the cyclic time-variant flow velocities, related to blade azimuth position, are presented for points on a rocket trajectory for the reference model AH-1G configuration and condition. The measured model flow velocities are scaled to representative full-scale values, and the applicability of scaling procedures to rotor thrust and tip speed variations is demonstrated. Rotor wake theory was applied to selected model and full-scale configurations and conditions. The predicted flow velocities are compared with LV test data and used in combination with wake geometry data for interpretation of the airflow results. The location of the rotor wake (particularly the tip vortices at the wake boundary) relative to the rocket trajectories and wind sensors is shown to be a major determinant of their flow velocities. The presence of either the fuselage, modified canopy, or ground is shown to produce significant flow velocity increments; however, the influence on the rocket flight trajectory and resulting aim bias requirements remain to be determined from a separate aeroballistics investigation.

SCOPE OF WORK FOR CONTRACT DAAA21-76-C-0151
(From Ref. 23)
INVESTIGATION OF THE AIRFLOW OF A MODEL HELICOPTER FOR THE DETERMINATION OF AERODYNAMIC INTERFERENCE AT ROCKET TRAJECTORY AND WIND SENSOR LOCATIONS (HOVER TEST)

I. Objective:

a. The objective of the study proposed by the Contractor is to determine, through an experimental program, the air flow characteristics in the vicinity of a model of the AH-1G "Cobra" helicopter at zero forward air velocity. The results of the experimental program shall provide flow velocity and wake geometry data for correlation with theory and for a systematic determination of the total and separate influence of each of the aircraft components (rotor, fuselage and wing), ground effect, and significant parameters (gross weight, and aircraft attitude) on the airflow influencing rocket trajectories. In addition, the flow velocities at potential locations for a fire control system wind sensor mounted on the aircraft shall be determined to assist in identifying potential wind sensor locations for accurately measuring flow velocities at hover. The data will also be used to determine the aim bias necessary for rocket firings at hover.

II. Background:

a. The accurate determination of the flow field in the vicinity of a helicopter is required when a helicopter is used as a weapons platform. Since a free flight projectile such as a rocket, when fired from a hovering helicopter, initially travels at a speed which is the same order of magnitude as the flow velocities, the flow field induced by the rotor wake system can have a significant effect on the rocket trajectory. This can necessitate some form of aiming compensation, particularly at the low helicopter flight speeds being considered for tactical use. It was concluded that model helicopter testing should be conducted to provide systematic experimental data for correlation, investigation of neglected interference effects and determination of wind sensor locations required for a fire control system. It was therefore suggested by UTRC that the UTRC model hovering facilities be used to measure the flow velocities and wake boundaries in the regions of the rocket trajectories and potential wind sensor locations.

III. Procedure:

a. The program described herein is directed to the experimental determination of rotor induced air velocities in the vicinity of an AH-1G Helicopter model along a 2.75 inch Rocket trajectory and in various potential wind sensor locations.

b. The Contractor shall apply his personnel and facilities for a period of 11 months towards the measurement, data analysis and reporting of rotor induced velocities along the 2.75 inch Rocket flight path and at potential wind sensor locations.

IV. Requirements:

a. The Contractor shall run an experimental program to acquire hover flow data. The test will be run using a 1/8th scale AH-1G fuselage model which will be borrowed from the Bell Helicopter Company by the Government and furnished to the Contractor. The Contractor shall provide two existing model rotor blades and an existing hub system to approximate the AH1-G rotor. The Contractor shall use suitable model helicopter test rigs, flow visualization and measurement equipment.

b. Hover Test

(1) The hover test program shall be conducted at the Contractor's model helicopter hover test facility. A laser velocimeter system should be used to measure the two components of flow velocity in the plane normal to the axis of the emitted laser beams. A configuration consisting of the rotor, fuselage and wing shall be selected as the reference configuration. A nominal thrust coefficient representative of the AH1-G gross weight (9500 lbs) and a nominal tip speed of approximately 500 feet per second shall be selected in combination with out-of-ground-effect operation as the reference operating condition. In addition to testing the reference configuration and operating condition, the influence of the fuselage and wing on the flow velocities and wake patterns shall be measured by testing the isolated rotor and the rotor fuselage combination without the wing at the reference operating condition. An independent variation of each of the operating condition parameters (a single increment of thrust coefficient, tip speed and ground effect) shall then be tested for the reference configuration The fuselage of the reference configuration shall be modified to represent a flat sided canopy and tested at the reference operating condition.

(2) Flow velocity and flow visualization data shall be acquired for all test conditions. Velocity data shall be acquired at selected points along the two rocket trajectories on one side of the model helicopter. Velocity measurements at selected points for a rocket trajectory attitude variation and a rocket trajectory on the opposite side of the fuselage shall be taken for the reference configuration and condition. At least eight points along the trajectory lines ranging from the launch point to a point outside the wake shall be selected for the reference configuration and condition. Points for other configurations and conditions shall be selected to provide comparative data at trajectory points of primary interest (i.e., near the launch point and wake boundary). The velocity component in the vertical plane and normal to the rocket trajectory shall be measured at all selected points.

Also, the velocity components in the lateral direction and the direction of the rocket trajectory shall be measured for the reference configuration and condition at a few selected points.

(3) In addition to rocket trajectory points, velocity measurements should be taken at several potential wind sensor locations. The vertical component of velocity should be measured at five points in the region of the nose and cabin of the model fuselage for the reference configuration and condition, reference configuration and thrust variation condition, and isolated rotor and reference condition. For the modified canopy configuration, vertical velocity data shall be required at rocket trajectory points and five (5) wind sensor points.

(4) Measured data should consist of rotor thrust, torque, flow visualization photographic data, velocity measurement point locations, and velocity component data. The rotor thrust and torque data should be reduced to coefficient form. The flow visualization data should be analyzed to determine the tip vortex coordinates. All velocity data shall be reduced to time-averaged form. Selected velocity data shall be reduced to provide time - histories of velocity with rotor azimuth position as averaged over several rotor revolutions.

c. Analysis

(1) The wake geometry and flow velocity results should be prepared in graphical form and then compared and analyzed to assess the influence of the model helicopter components (fuselage and wing) and the experimental variations of the operating condition parameters. The experimental wake and velocity results for the model should be scaled and compared with those of the full-scale AH1-G predicted in the analytical study reported in Picatinny Arsenal Report TR 4797. In addition, the Contractor shall use the UTRC "Prescribed Wake Hover Performance Analysis" to predict the velocity components at the measured rocket trajectory points for the hovering model configuration at the two thrust levels tested. This shall permit a direct comparison of the predicted and measured velocities to be made for the same configuration. The most desirable locations for wind sensor locations should be identified from the data at the measured locations.

V. Progress Reports:

Periodic progress reports shall be prepared and submitted in accordance with the requirements set forth in the DD Form 1423. The contracted effort should culminate with the submittal of a final summary report in which the test program shall be described and the results documented. The results should also be summarized in an oral presentation.

CONCLUSIONS

(From Ref. 23)

The following conclusions are based on the application of model test results to a full-scale hovering helicopter. Where values or locations are indicated, they are representative of the full-scale AH-1G helicopter.

1. The flow velocities of the hovering helicopter simulation model, measured with the laser velocimeter, substantiated the general airflow characteristics at rocket trajectories of the AH-1G helicopter predicted in the previous theoretical investigation.*

2. The application of laser velocimetry to measure hovering rotor airflow was successful. LV proved to be a valuable technique for acquiring both the time-average and time variation of flow velocity components at rocket trajectory and wind sensor locations inside and outside of the rotor wake.

3. Flow visualization techniques (smoke and Schlieren) were valuable to identify wake geometry, wake stability, and vortex core size in the vicinity of the rocket trajectory and wind sensor locations. The influence of the fuselage, modified canopy, thrust level, tip speed, and ground effect on wake geometry, determined from analysis of the flow visualization data, were useful for interpretation of the flow velocity data.

4. The total and separate influence of each of the aircraft components (rotor, fuselage, modified canopy, and wing), and significant operating condition parameters (rotor thrust, tip speed, and ground effect) on the airflow influencing rocket trajectories were successfully measured.

5. The presence of the fuselage produces a small but possibly significant effect on rocket trajectory airflow. On the starboard side of the aircraft, the fuselage effect is most noteworthy in the vicinity of the rocket launch points where it contributes additional downflow. A possible fuselage produced flow dissymmetry, which requires further verification, was indicated in a comparison of LV data from opposite sides of the fuselage. The presence of the stub-wing does not significantly add to the aerodynamic interference of the fuselage at rocket trajectories. The modified flat-sided canopy of the AH-1G produces an additional downflow increment along the portion of the rocket trajectories aside of the fuselage.

*Primary airflow characteristics are listed in the conclusions from the theoretical investigation in Appendix B.

6. The effects of rotor thrust and tip speed increments on the rocket trajectory airflow are scalable using momentum induced velocity as the scaling parameter. For large tip speed increments, a possible deviation from the scaling procedure at points near the fuselage remains to be substantiated through further investigation.

7. Operation near the ground results in a significant reduction in the magnitude of the downflow along the extent of rocket trajectories in the rotor wake. For simulated AH-1G skid heights above ground of less than approximately 20 ft, time-averaged upflow was measured in the vicinity of the launch point of an inboard rocket trajectory.

8. In the rotor wake, consistent with rotor hovering downflow patterns, the downflow at the outboard rocket trajectory is generally greater than that of the inboard trajectory.

9. Of the three velocity components, the downward component normal to the rocket trajectory is substantially larger in magnitude than the others.

10. A rocket attitude variation of 2 deg does not significantly influence the time-averaged flow velocities at the rocket trajectory, but does result in a phase shift of the time variant velocities relative to rotor azimuth position.

11. The airflow inside the rotor wake is fairly steady; however, large induced velocity variations with small increments of distance and time occur at points on a rocket trajectory near a wake boundary. These variations are caused by the close passage of the tip vortices. The magnitude of the mean time-variant downflow associated with each rotor azimuth position is generally within approximately $\pm$10 fps of the time-average value for points on the rocket trajectories within the rotor wake. This peak-to-peak variation increases substantially (e.g., $\pm$30 fps) in the vicinity of the wake boundary. The RMS deviations from the mean downflow values for specific rocket trajectory points and rotor azimuth positions, representative of flow unsteadiness, are generally within 10 fps, away from the wake boundary.

12. Of the tested wind sensor locations, a location aside and removed from the fuselage canopy by 18 percent of the rotor radius, was found to be most favorable for avoiding fuselage aerodynamic interference and the wake boundary. If the distance must be compromised, based on forward flight drag considerations, placement ahead of the wing tip may be preferable.

AD-A075 378 UNITED TECHNOLOGIES RESEARCH CENTER EAST HARTFORD CONN F/G 1/3
INVESTIGATION OF THE AIRFLOW AT ROCKET TRAJECTORY AND WIND SENS--ETC(U)
SEP 79 R B TAYLOR, A J LANDGREBE DAAG29-77-C-0013
UNCLASSIFIED UTRC-R79-912985-5 ARO-14277.1-E NL

3 OF 3
AD A075378

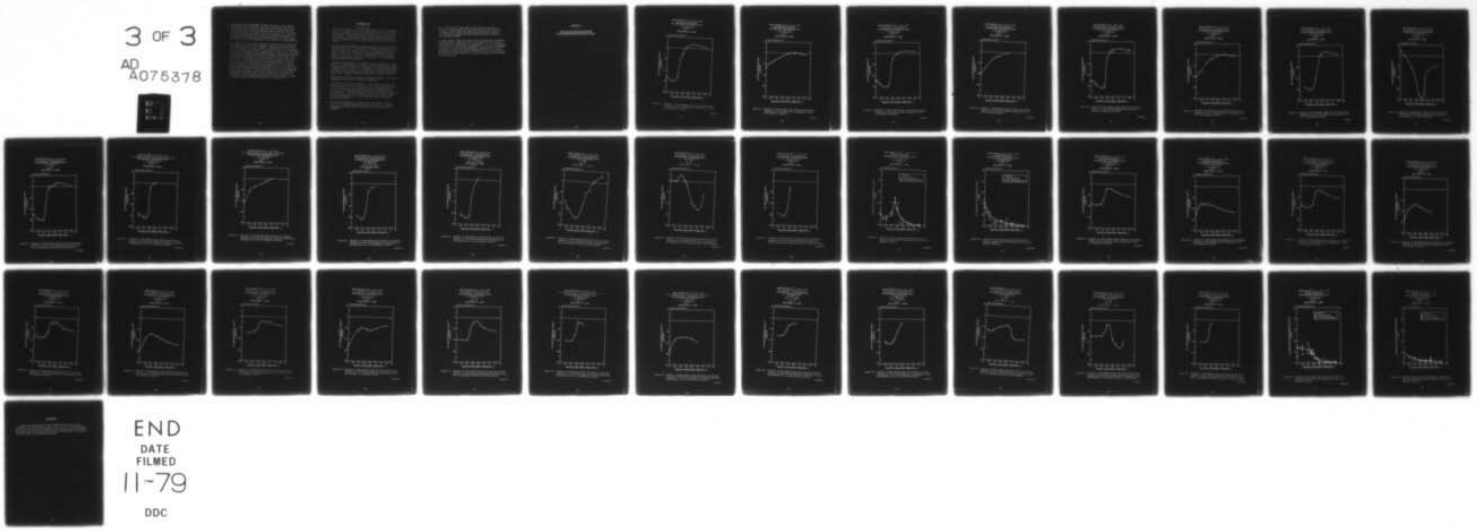

END
DATE FILMED
11-79
DDC

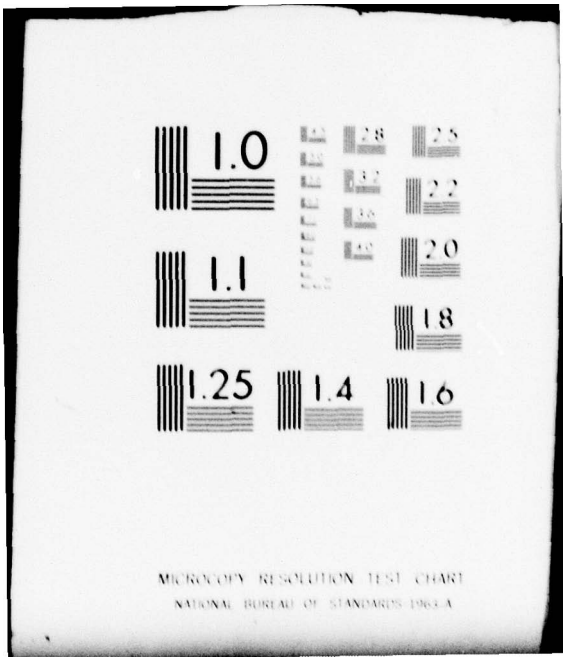
1.0
1.1
1.25
1.4
1.6
2.8
3.2
3.6
4.0
2.5
2.2
2.0
1.8
MICROCOPY RESOLUTION TEST CHART
NATIONAL BUREAU OF STANDARDS 1963-A

13. Neglecting fuselage interference effects, the results of the limited correlation study indicate that the UTRC Prescribed Wake Hover Performance Analysis can accurately predict the airflow characteristics at rocket trajectories. The time-averaged downflow within the rotor wake was generally predicted within 5 fps for the isolated rotor. (Fuselage aerodynamic interference is not currently included in the analysis.) The capability of the analysis to accurately predict the time-variation of the flow velocities is dependent on the accuracy of the wake geometry.

14. The model test data for rocket trajectory and wind sensor flow velocities can be appropriately scaled to represent full-scale aircraft operating conditions (thrust level and tip speed). Refinements for the full-scale AH-1G representation, to account for remaining differences in configuration design, airfoil characteristics (Reynolds number, Mach number), and coning angle can be determined using predicted increments between model and full-scale theoretical results as a guide. Theoretical indications are that the effects of the latter scaling differences are generally small, particularly for time-averaged velocities and the magnitudes of the time variant velocities. Any influence on the positioning and/or timing of the tip vortices, such as blade coning differences or aircraft and wake motions associated with full-scale helicopter operation, would result in a phase shift in the flow velocity time variation at a rocket trajectory or wind sensor location. Corrections for phase shifts associated with coning angle can be determined. The determination of corrections for random shifts associated with ambient winds, helicopter motion, or wake unsteadiness would be much more difficult, if not impractical.

RECOMMENDATIONS

(From Ref. 23)

1. As planned, the effect of the rotor wake induced velocities determined in this investigation on the rocket trajectories should be calculated using the Army rocket dynamic response analysis and the procedures described herein. Using these procedures, the deviations of the rocket trajectories can be determined, and the degree of accuracy required of the induced effects for rocket trajectory calculations would be established.

2. Analysis of the time-variant flow velocity data to present and interpret the results for all configurations and conditions relative to rotor azimuth position was beyond the scope of the investigation reported herein. The results of the above recommended aeroballistics investigation should be used to assess the requirement for additional data analysis in the time history format (in addition to the time-averaged and peak-to-peak format presented).

3. Considering the demonstrated usefulness of laser velocimetry for rocket trajectory flow measurements, the model helicopter experimental program is being extended to apply the LV technique to low speed forward flight conditions in a wind tunnel. It is suggested that several tasks beyond the scope of the planned program be considered, such as the testing of yawed flight, sideward flight, in-ground-effect, and gust conditions.

4. Additional hover testing to further investigate the extent of the flow dissymmetry produced by the fuselage is recommended.

5. Considering the favorable correlation of the hovering wake theory for the isolated rotor, and the usefulness of the theory for interpretation of the model data for full-scale aircraft, it is recommended that analytical refinements be included to improve the scope and accuracy of the analysis. Recommended refinements include provisions for ground effect, vertical climb, and fuselage aerodynamic interference. Wake modeling refinements should be incorporated as guiding experimental data become available.

6. Application and evaluation of hovering rotor wake theory for other aircraft (for example, AAH and UTTAS) over a wide range of operating conditions, and generalization of the predicted flow velocities is recommended.

7. Flow velocity data for full-scale aircraft should be acquired, at least for a limited number of flow field points and test conditions, to compare with the model test data and to determine the relative flow unsteadiness between full-scale operation and model testing in a controlled environment.

8. The model testing, laser velocimetry, and flow visualization techniques, as demonstrated in combination in this investigation for the specific rocket/wind sensor application, are recommended for use in a more general investigation of hovering rotor aerodynamics and associated performance. In addition to further defining fundamental characteristics, such an experimental program would provide comprehensive data for validation of theory and the further generalization of the aerodynamics and performance of hovering rotors.

APPENDIX D

PLOTS OF FLOW VELOCITY DATA POINTS FOR TIME-AVERAGE AND PEAK-TO-PEAK LV DATA

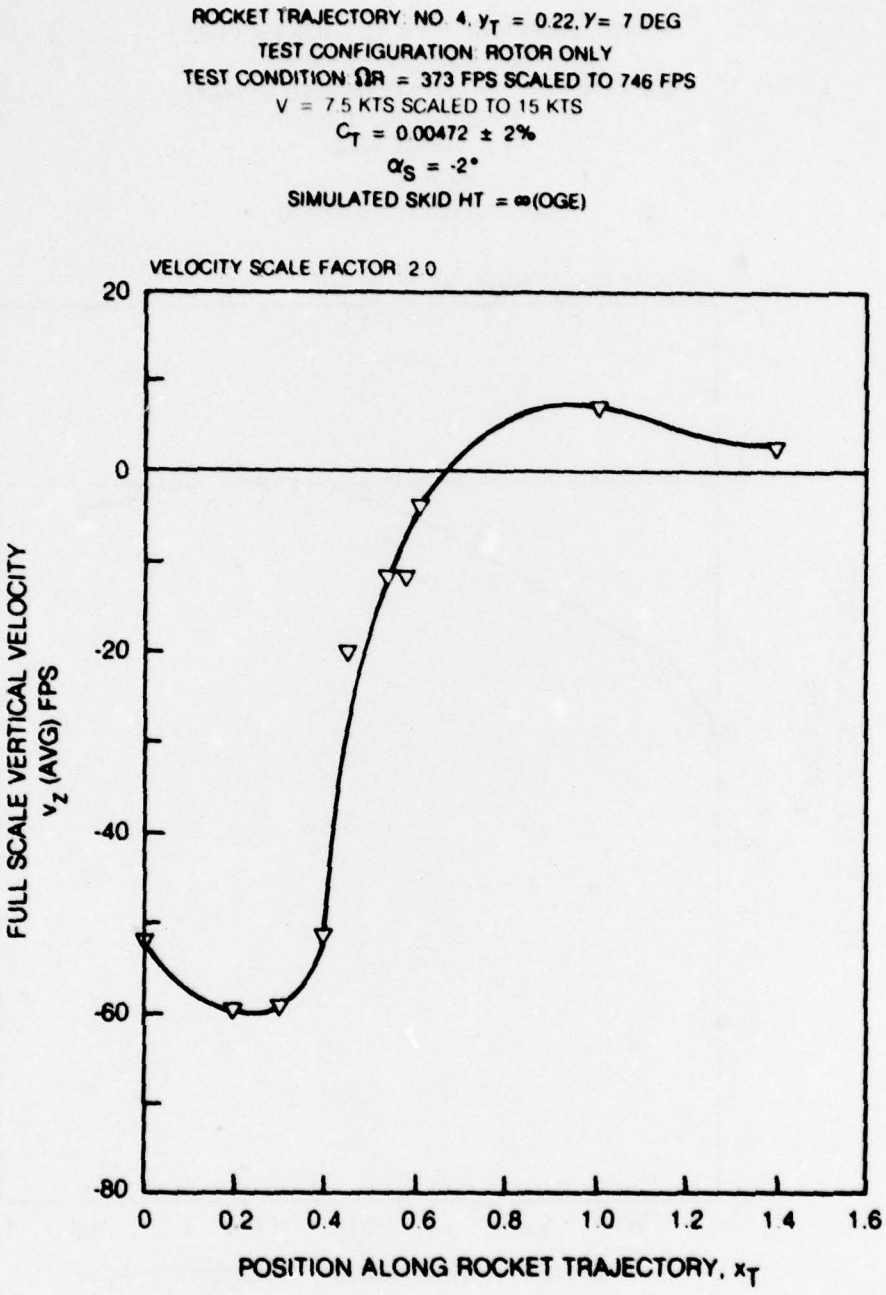

Figure D1. Variation of Time-Average Scaled Vertical Flow Velocity Component for the Isolated Rotor Configuration at the 15 kt Reference Condition.

79-09-33-1

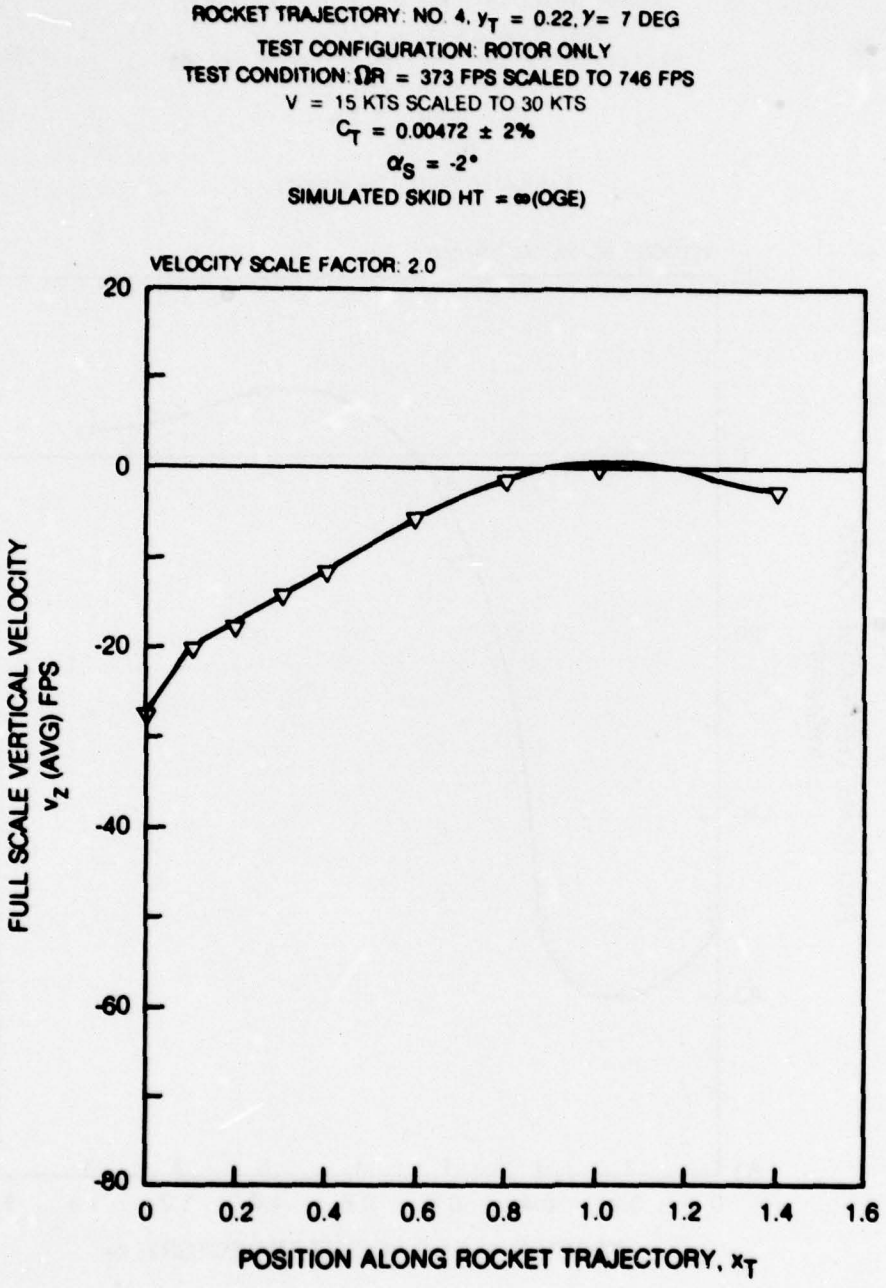

Figure D2. Variation of Time-Average Scaled Vertical Flow Velocity Component for the Isolated Rotor Configuration at the 30 kt Reference Condition.

79-09-33-2

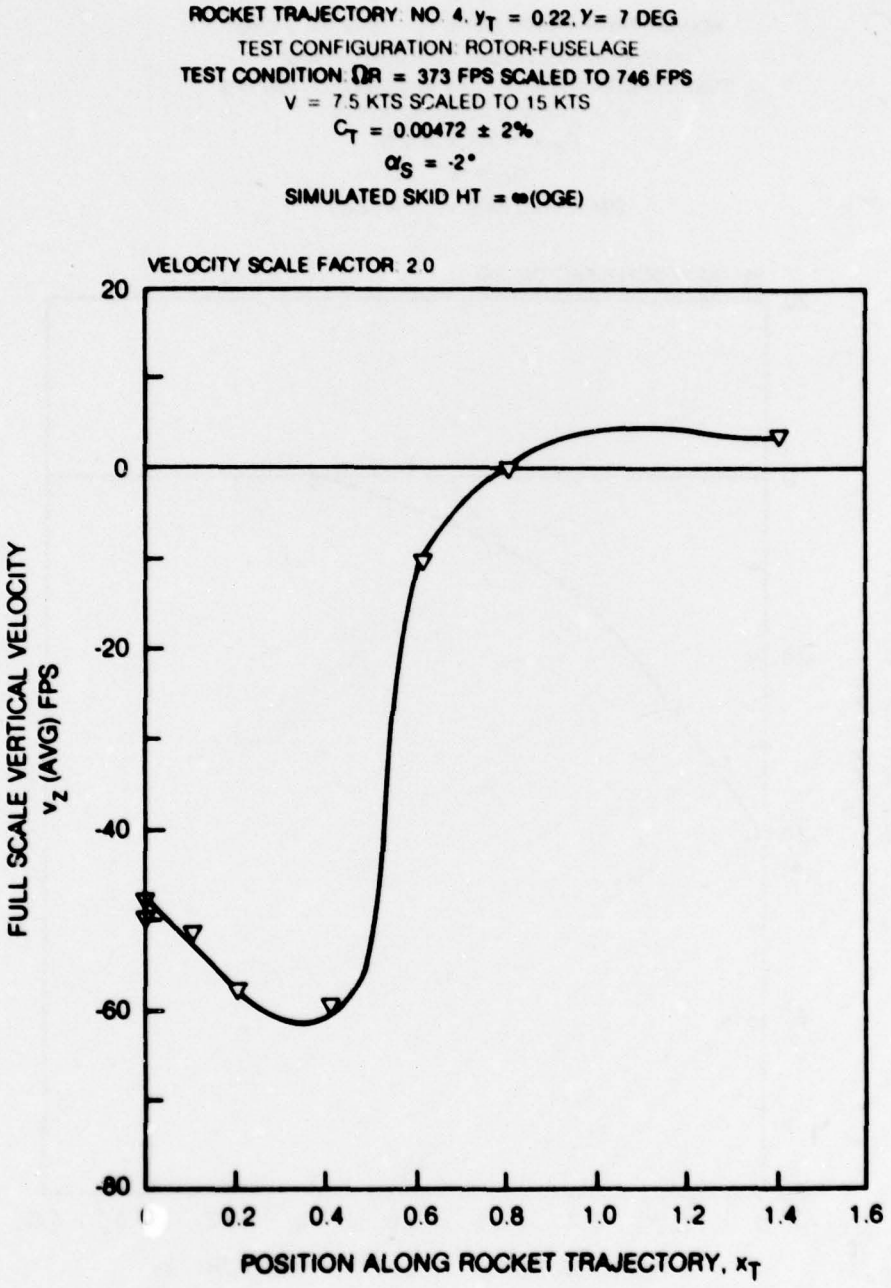

Figure D3. Variation of Time-Average Scaled Vertical Flow Velocity Component for the Rotor-Fuselage Configuration at the 15 kt Reference Condition.

79-09-33-3

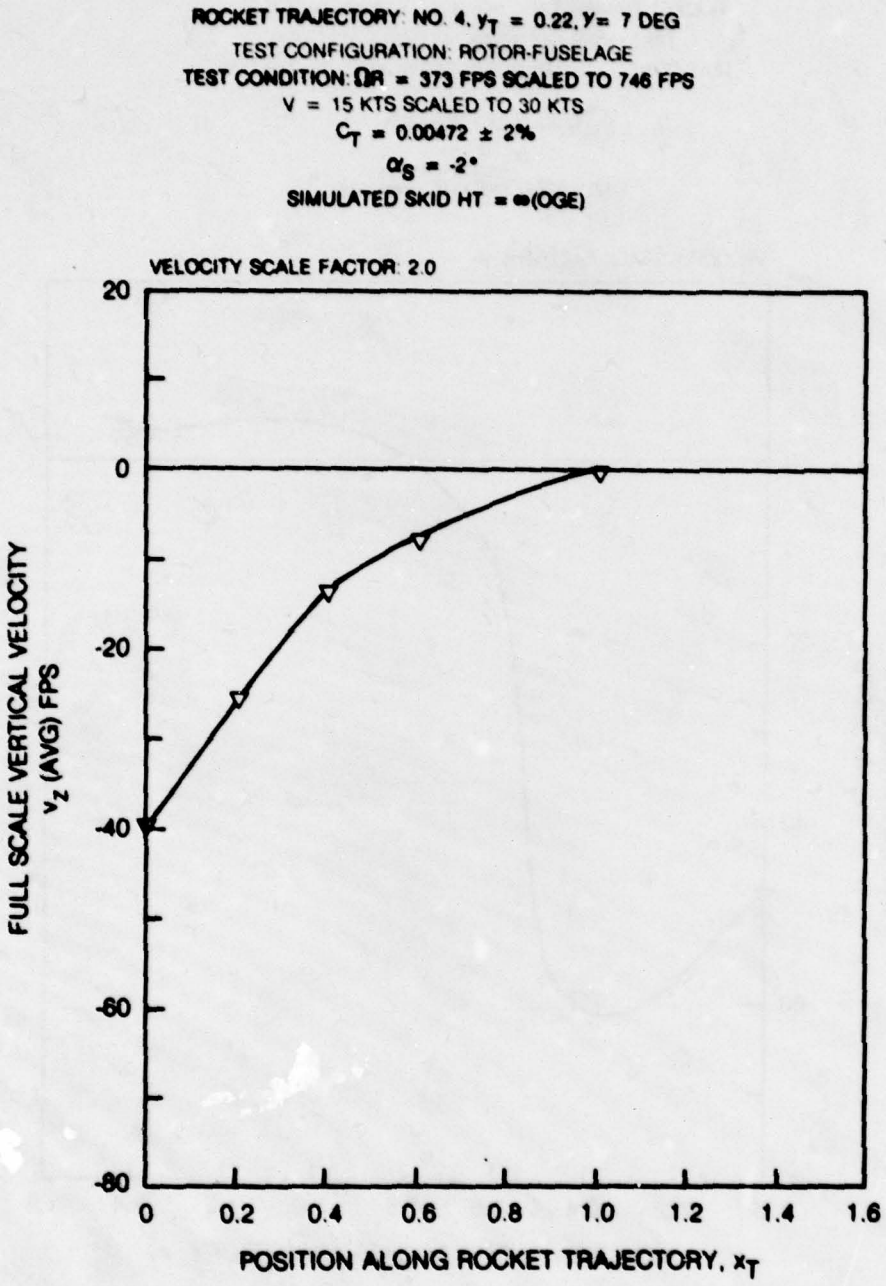

Figure D4. Variation of Time-Average Scaled Vertical Flow Velocity Component for the Rotor-Fuselage Configuration at the 30 kt Reference Condition.

79-09-33-4

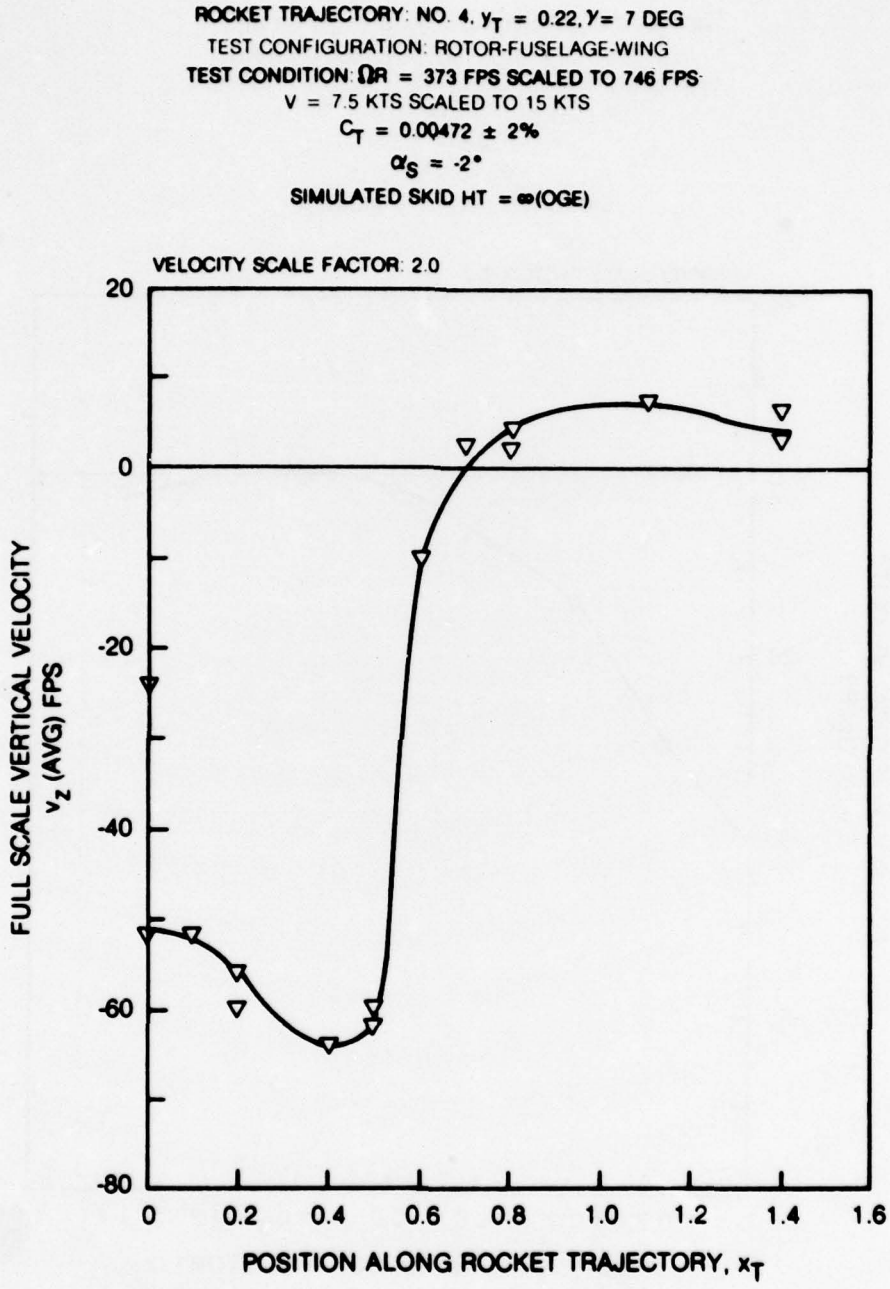

Figure D5. Variation of Time Average Scaled Vertical Flow Velocity Component for the Rotor-Fuselage-Wing Configuration at the 15 kt Reference Condition.

79-09-33-5

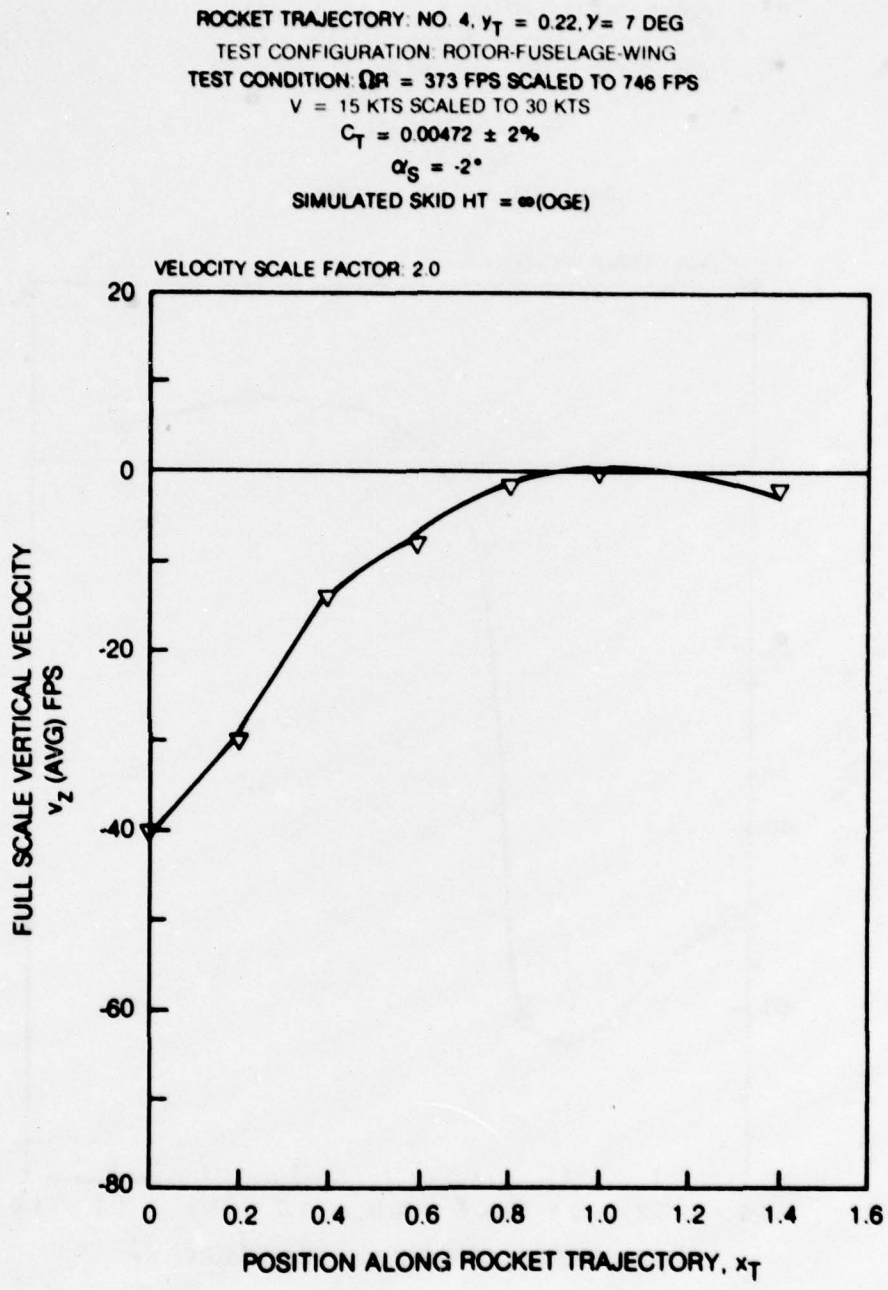

Figure 15. Variation of Time-Average Scaled Vertical Flow Velocity Component for the Rotor-Fuselage-Wing Configuration at the 30 kt Reference Condition.

79-09-33-6

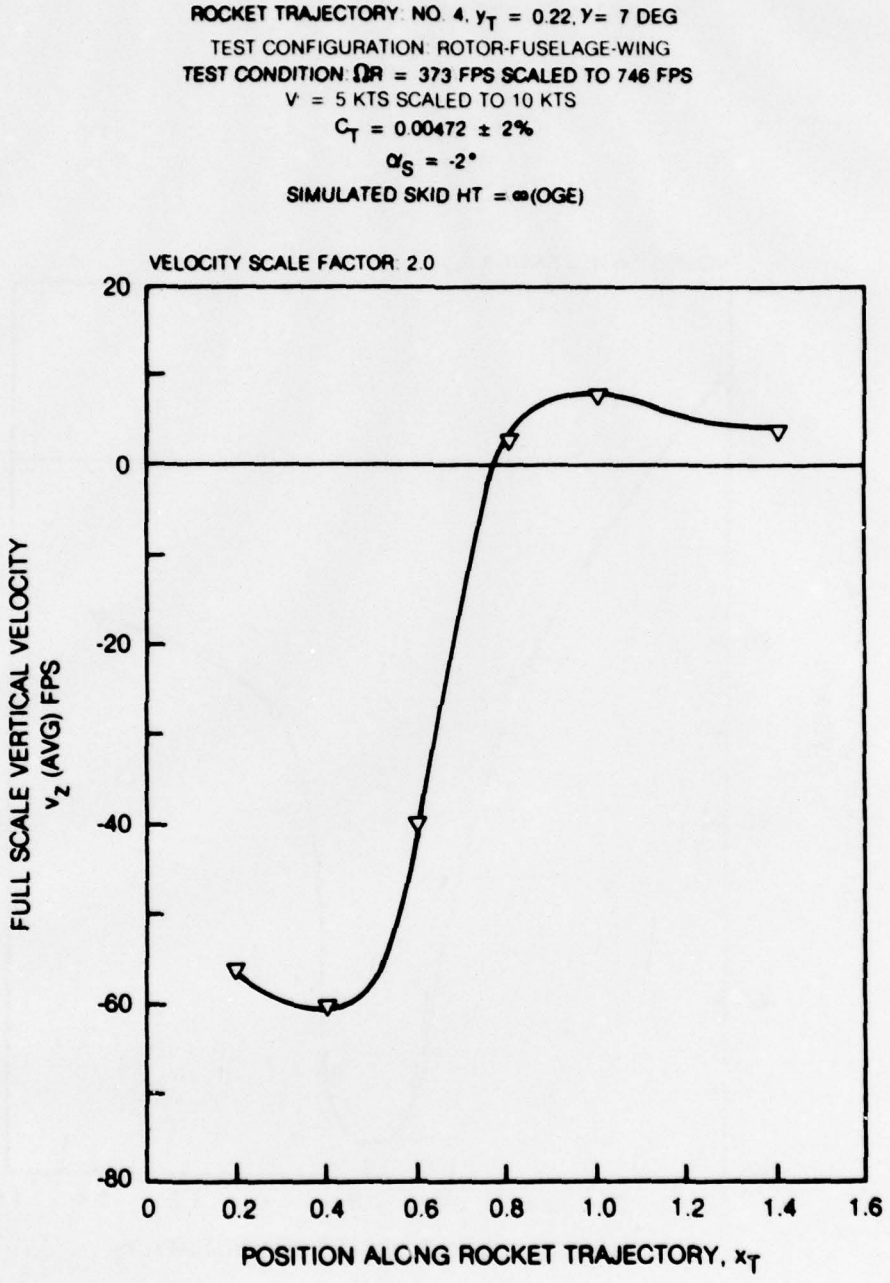

Figure D7. Variation of Time-Average Scaled Vertical Flow Velocity Component for the Rotor-Fuselage-Wing Configuration at the 10 kt Reference Condition.

79-09-33-7

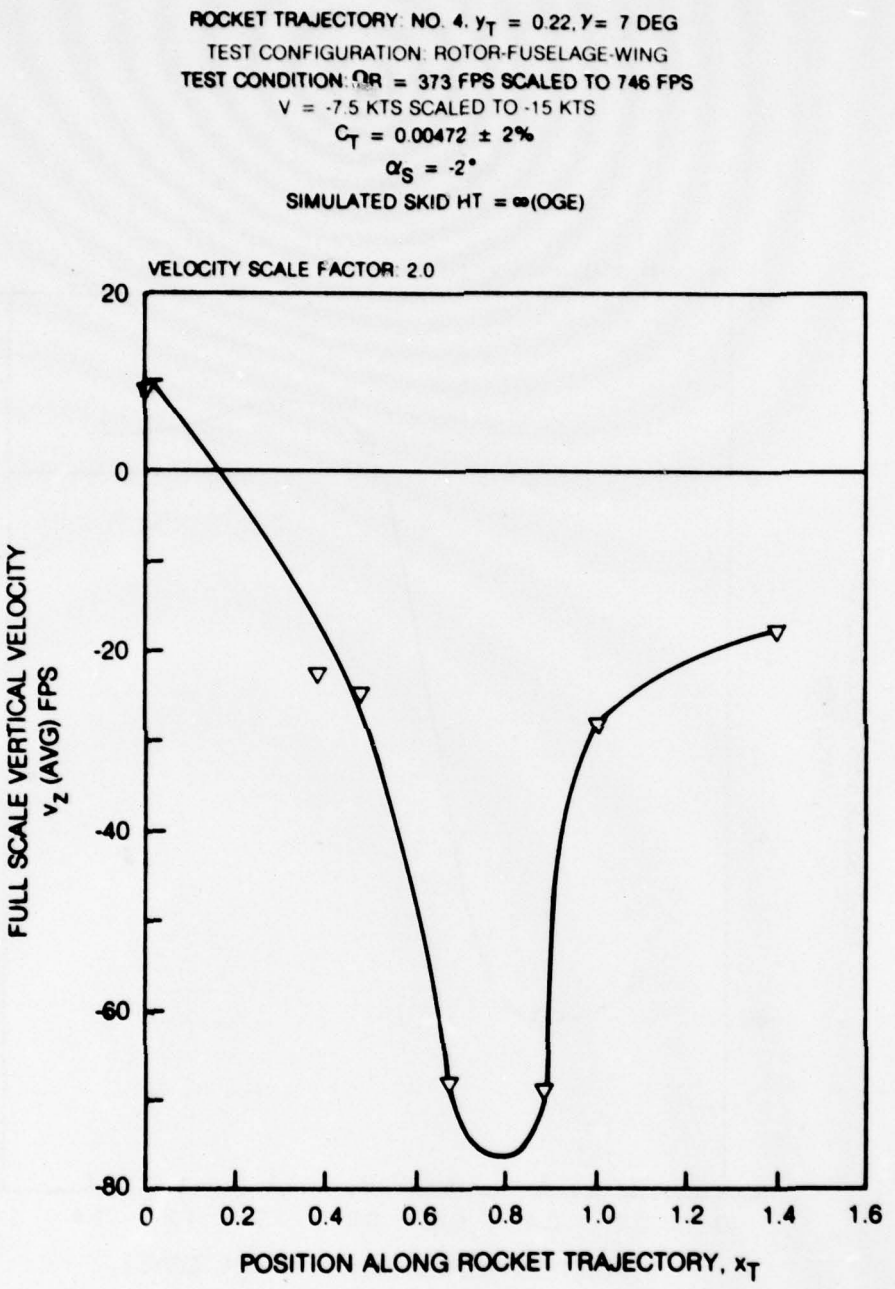

Figure D8. Variation of Time-Average Scaled Vertical Flow Velocity Component for the Rotor-Fuselage-Wing Configuration at the Simulated 15 kt Tailwind Condition.

79-09-33-8

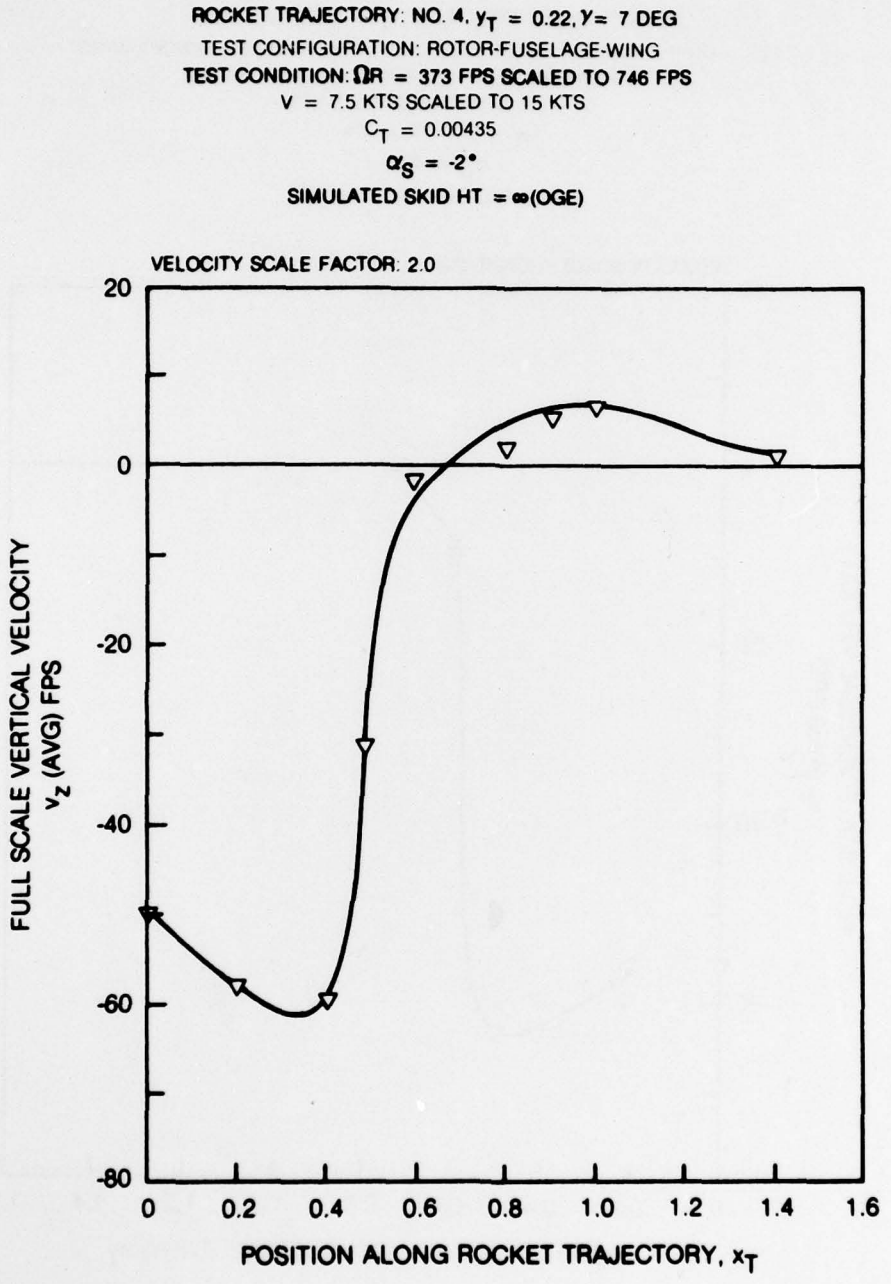

Figure D9. Variation of Time-Average Scaled Vertical Flow Velocity Component for the Rotor-Fuselage-Wing Configuration at the 15 kt Reference Condition with Reduced Thrust.

79-09-33-9

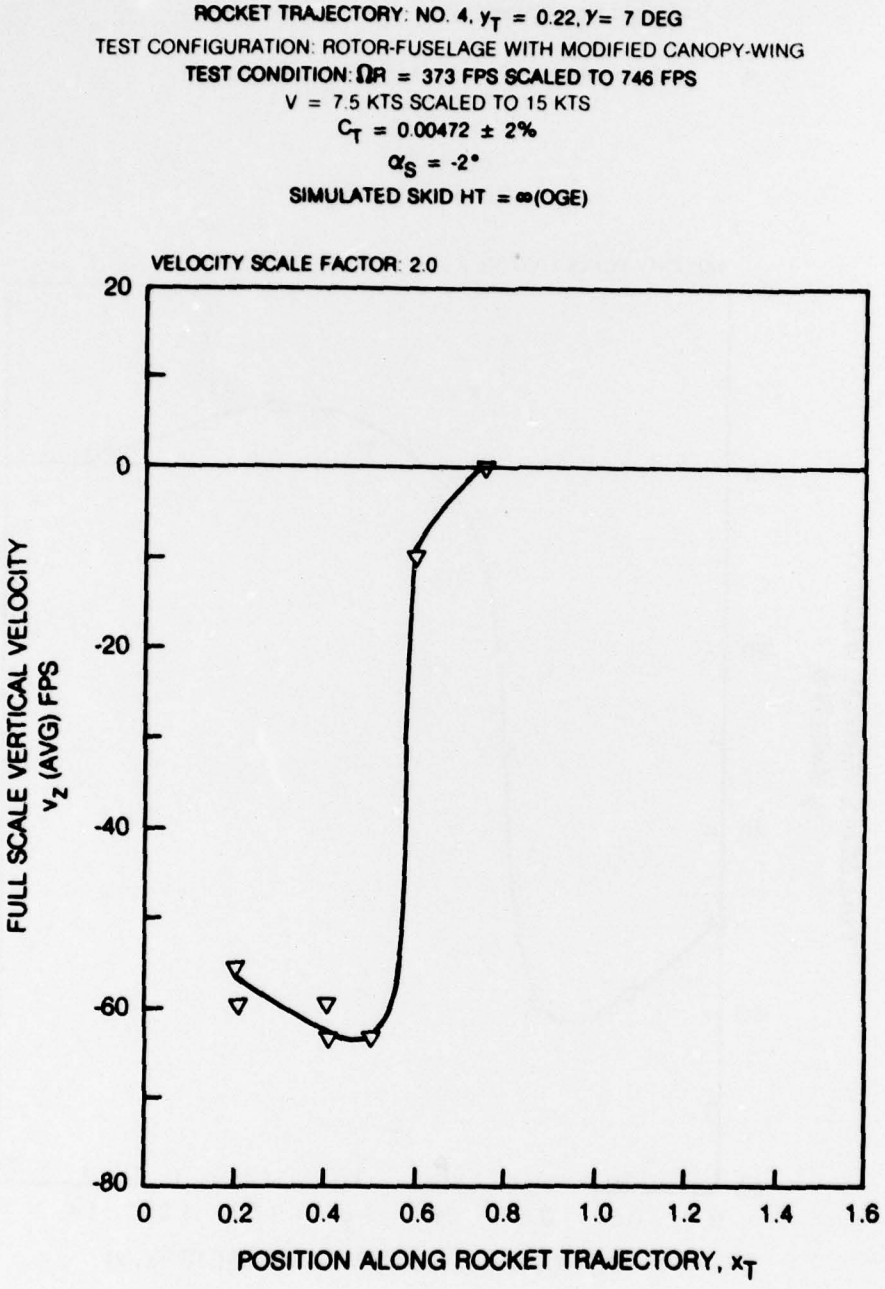

Figure D10. Variation of Time-Average Scaled Vertical Flow Velocity Component for the Rotor-Fuselage with Modified Canopy-Wing Configuration at the 15 kt Reference Condition.

79-09-33-10

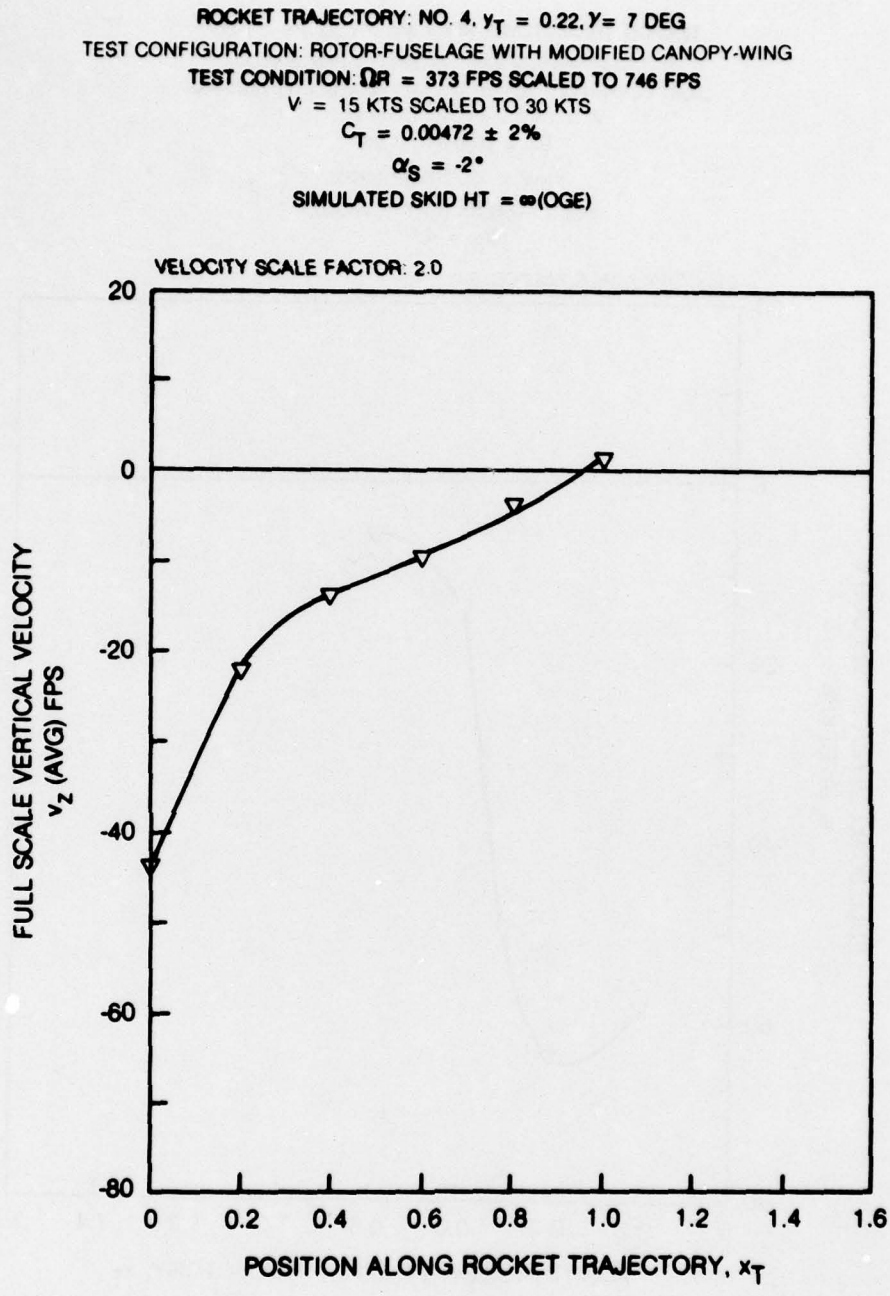

Figure D11. Variation of Time-Average Scaled Vertical Flow Velocity Component for the Rotor-Fuselage with Modified Canopy-Wing Configuration at the 30 kt Reference Condition.

79-09-33-11

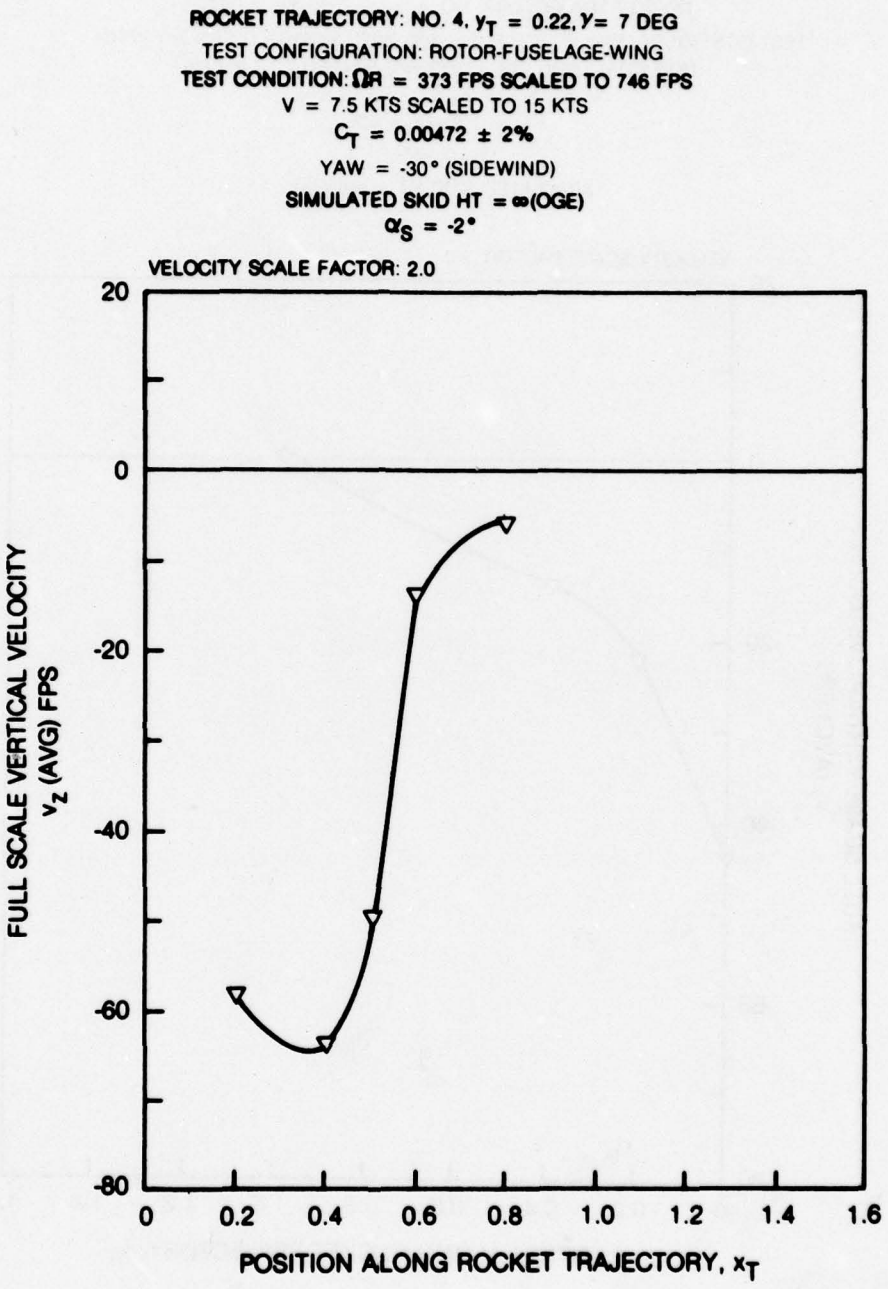

Figure D12. Variation of Time-Average Scaled Vertical Flow Velocity Component for the Rotor-Fuselage-Wing Configuration at the Simulated 15 kt -30 Deg Sidewind Condition.

79-09-33-12

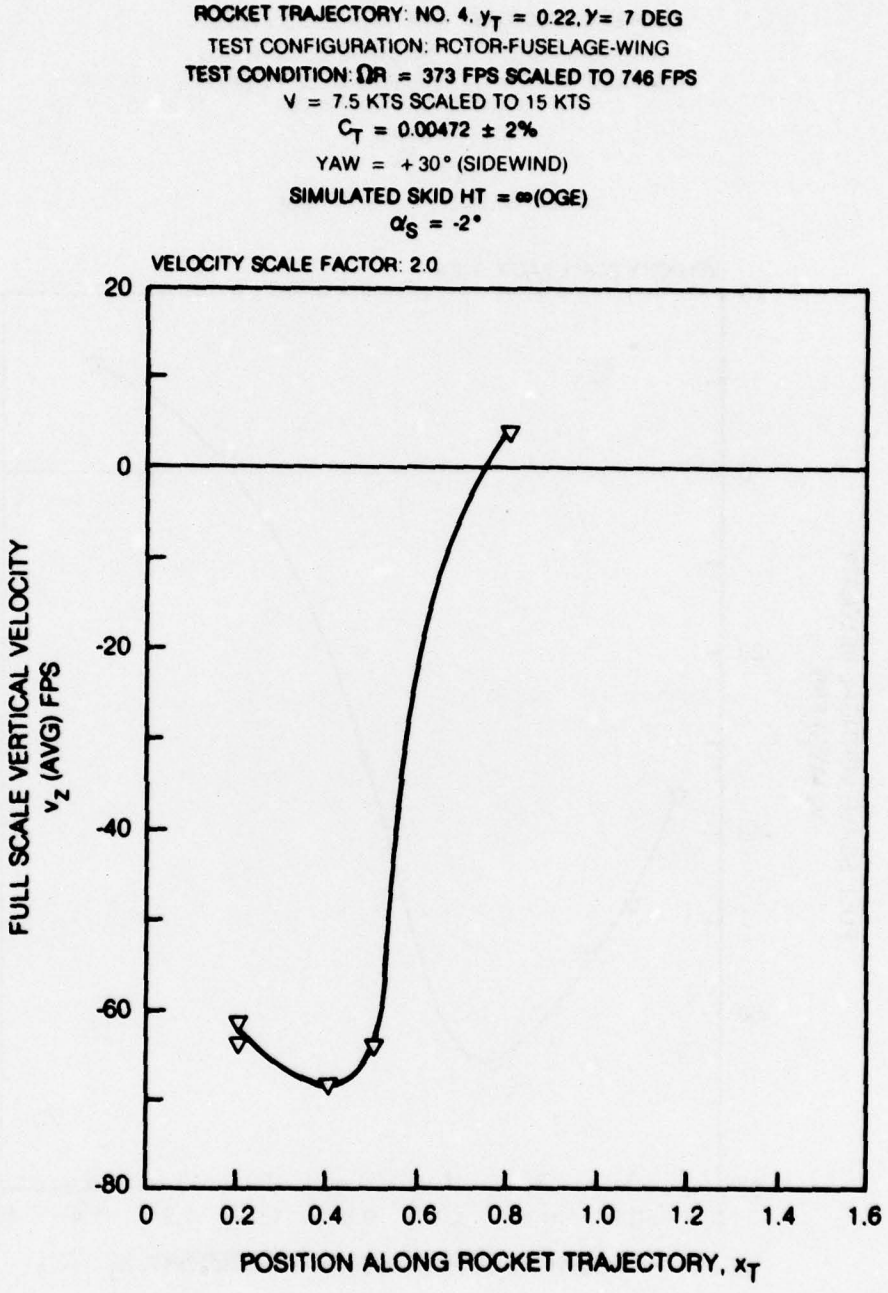

Figure D13. Variation of Time-Average Scaled Vertical Flow Velocity Component for the Rotor-Fuselage-Wing Configuration at the Simulated 15 kt +30 Deg Sidewind Condition.

79-09-33-13

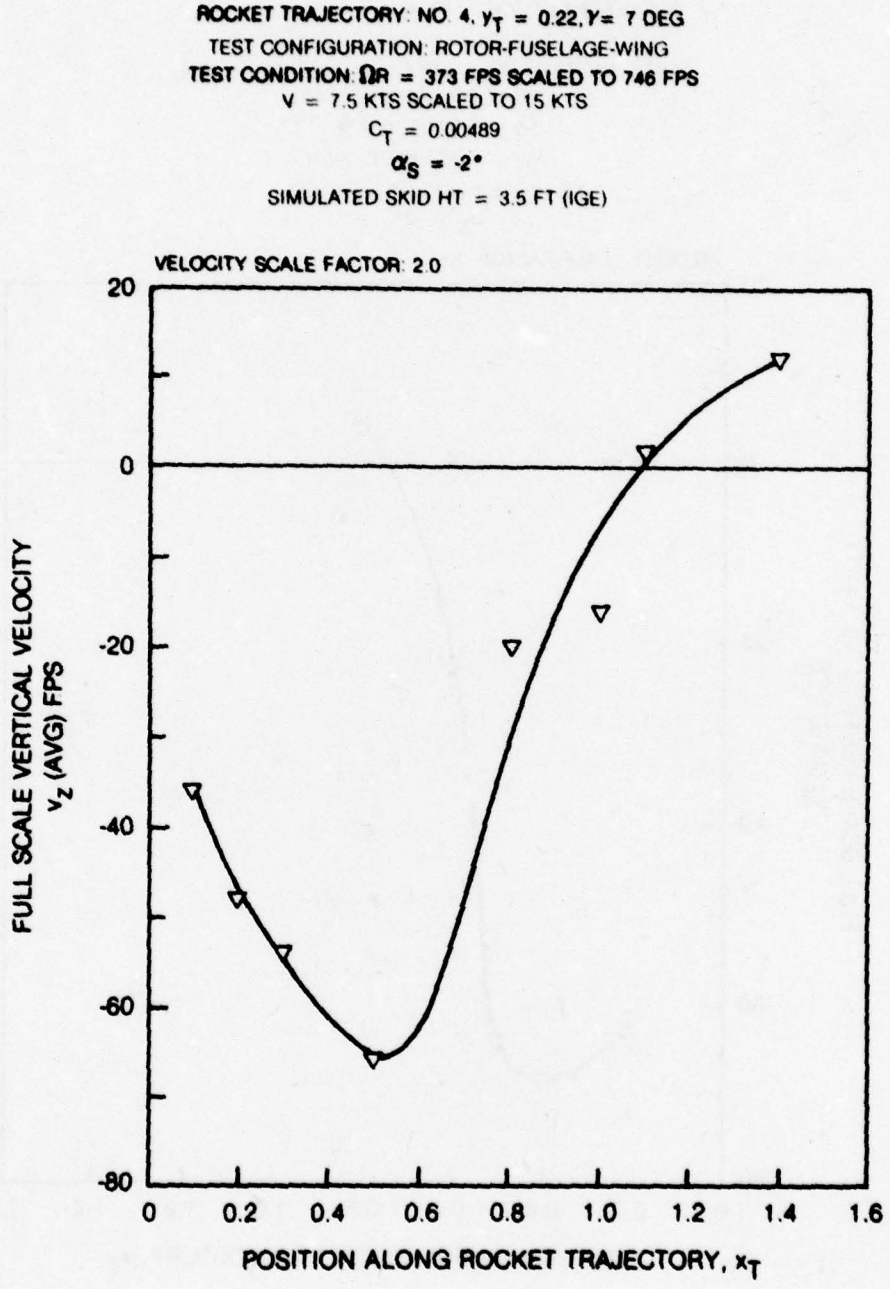

Figure D14. Variation of Time-Average Scaled Vertical Flow Velocity Component for the Rotor-Fuselage-Wing Configuration at the 15 kt Reference Condition In-Ground-Effect.

79-09-33-14

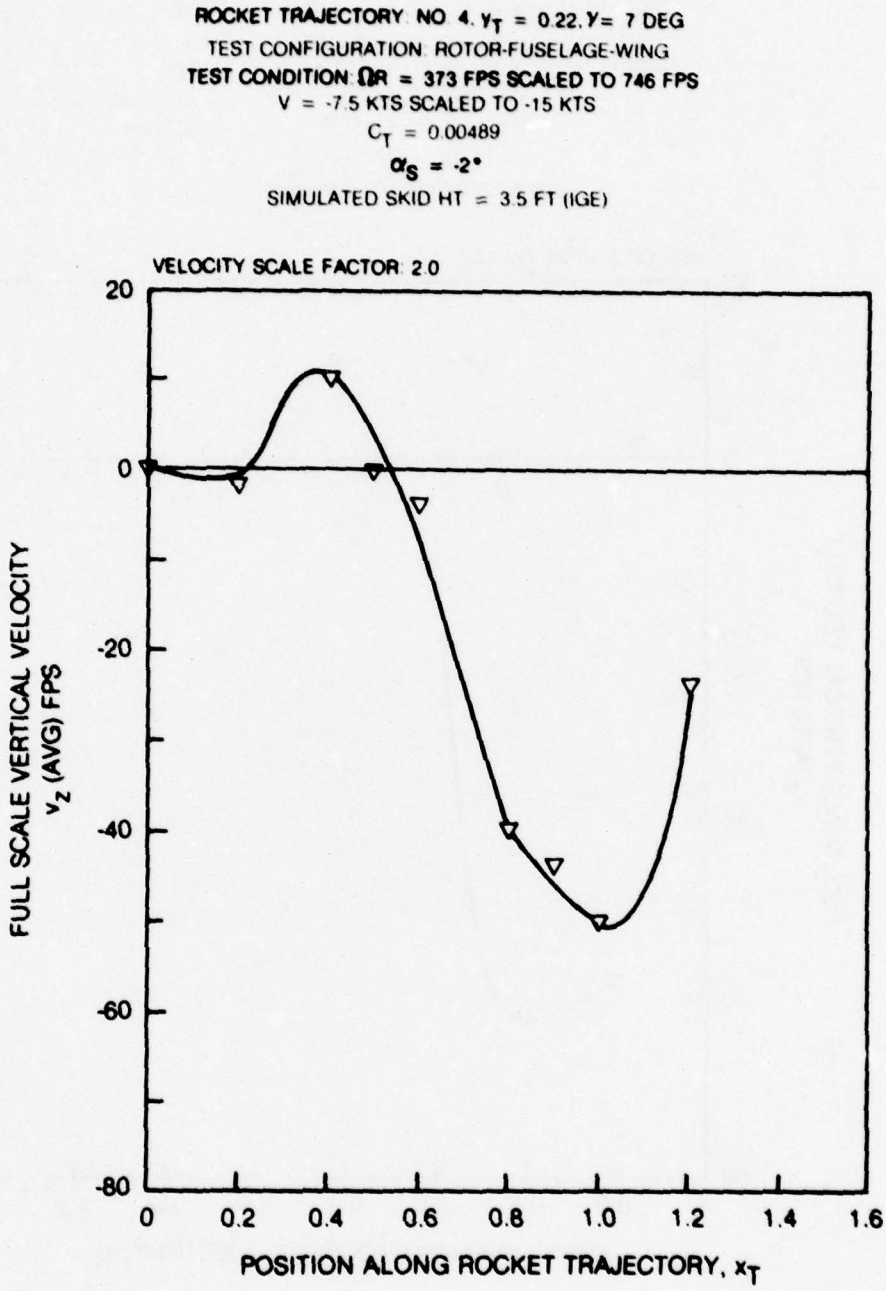

Figure D15. Variation of Time-Average Scaled Vertical Flow Velocity Component for the Rotor-Fuselage-Wing Configuration at the Simulated 15 kt Tailwind Condition In-Ground-Effect.

79-09-33-15

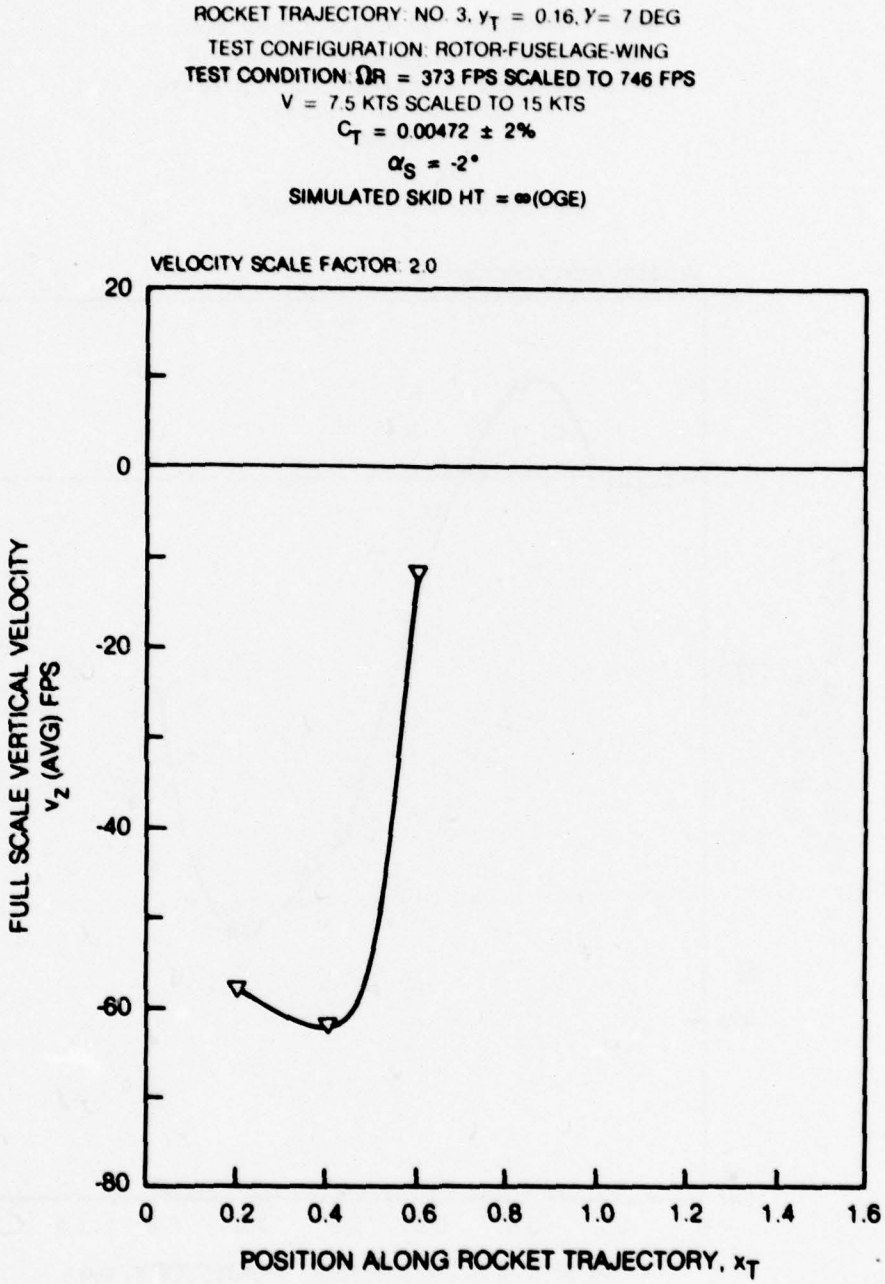

Figure D16. Variation of Time-Average Scaled Vertical Flow Velocity Component for the Rotor-Fuselage-Wing Configuration at the 15 kt Reference Condition for the No. 3 Launch Position.

79-09-33-16

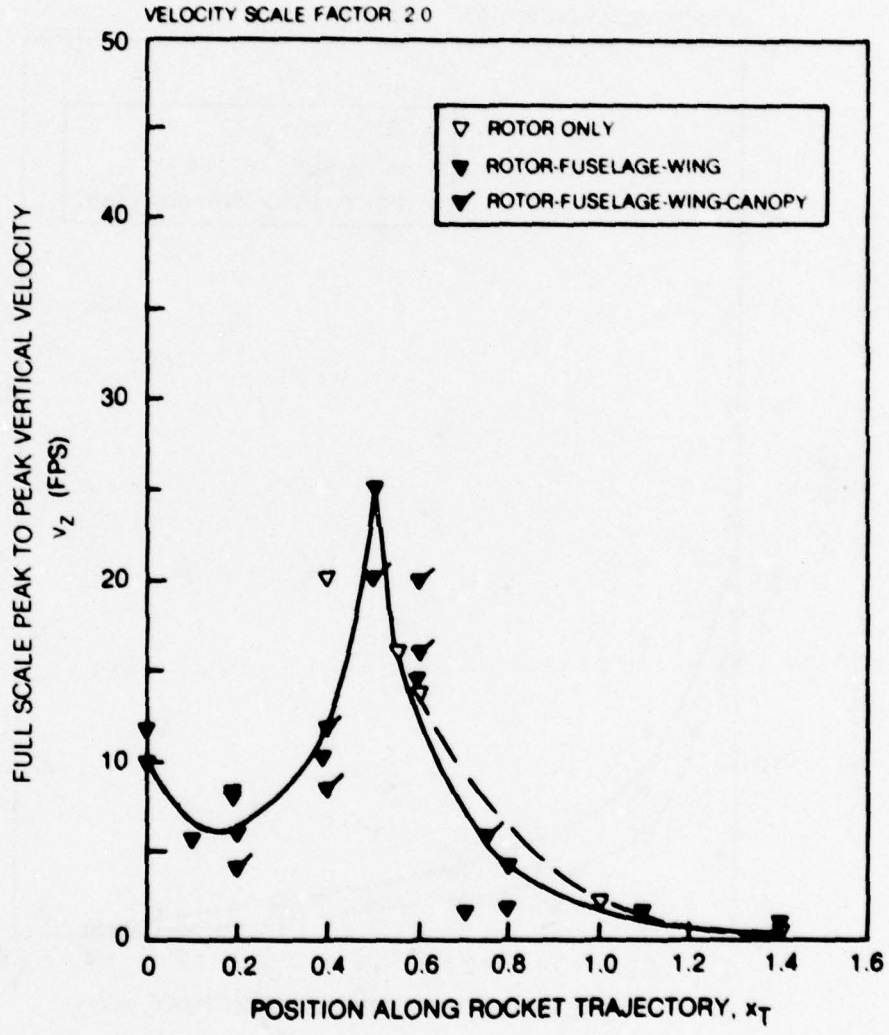

Figure D17. Variation of the Scaled Peak-to-Peak Vertical Flow Velocity Component Along the Trajectory for the 15 kt Reference Condition.

79-09-33-38

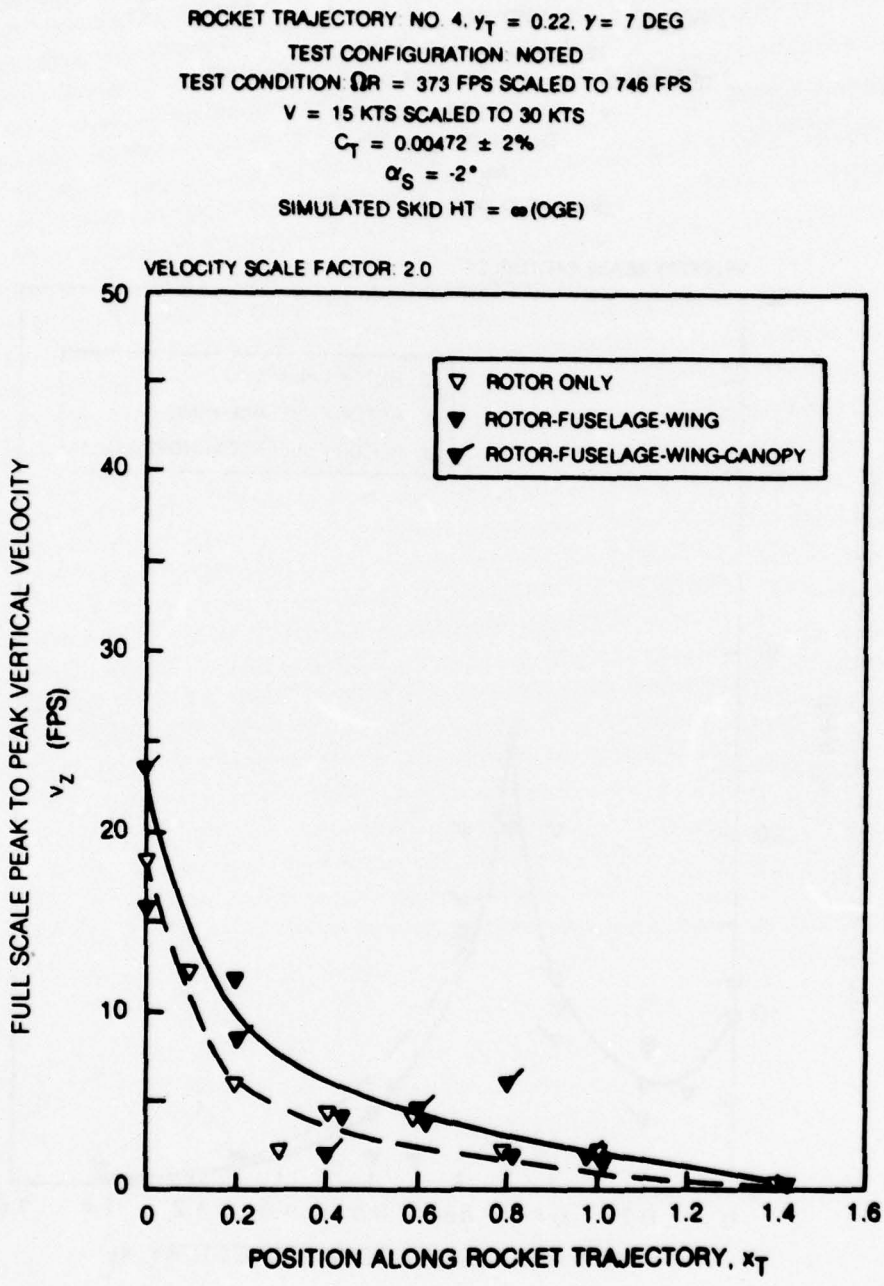

Figure D18. Variation of the Scaled Peak-to-Peak Vertical Flow Velocity Component Along the Trajectory for the 30 kt Reference Condition.

79-09-33-36

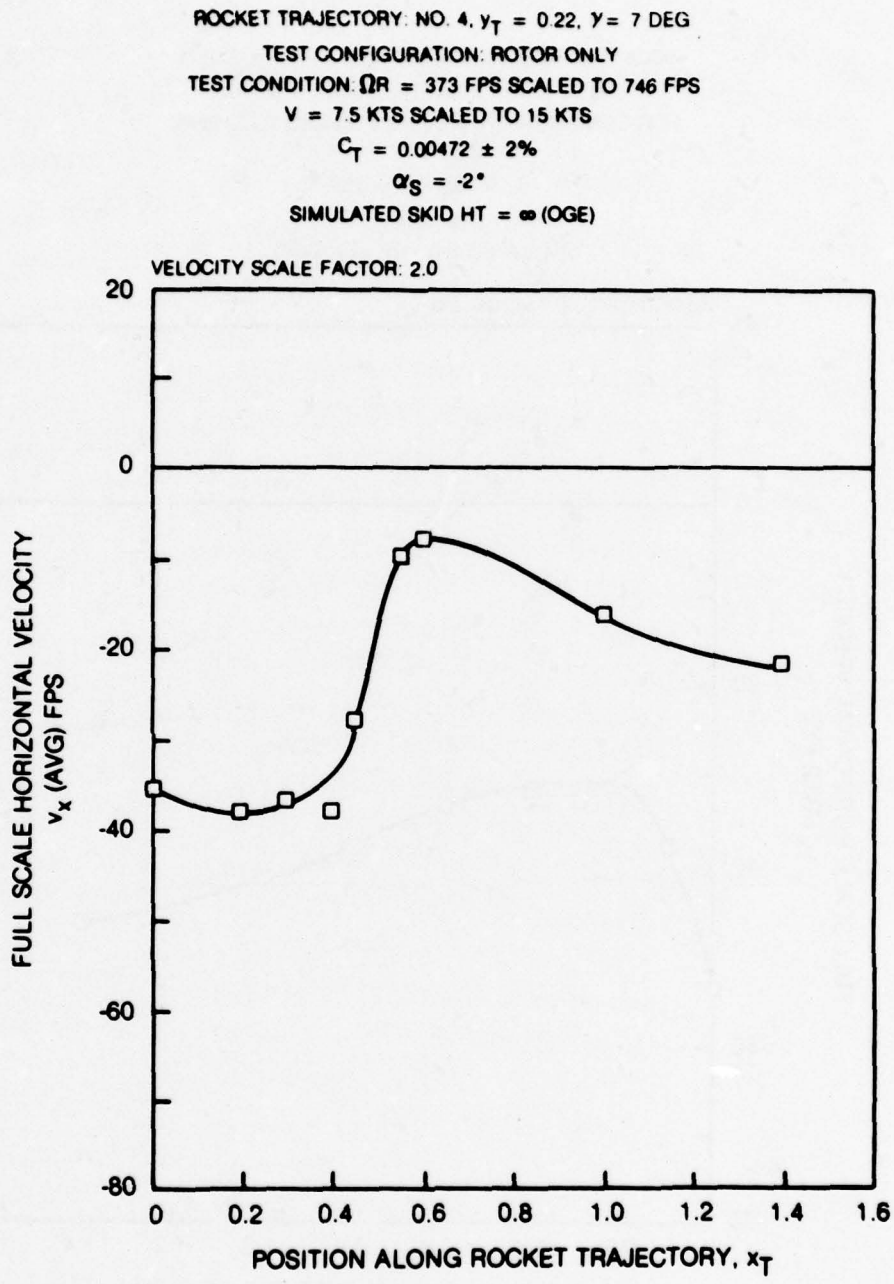

Figure D19. Variation of Time-Average Scaled Horizontal Flow Velocity Component for the Isolated Rotor Configuration at the 15 kt Reference Condition.

79-09-33-17

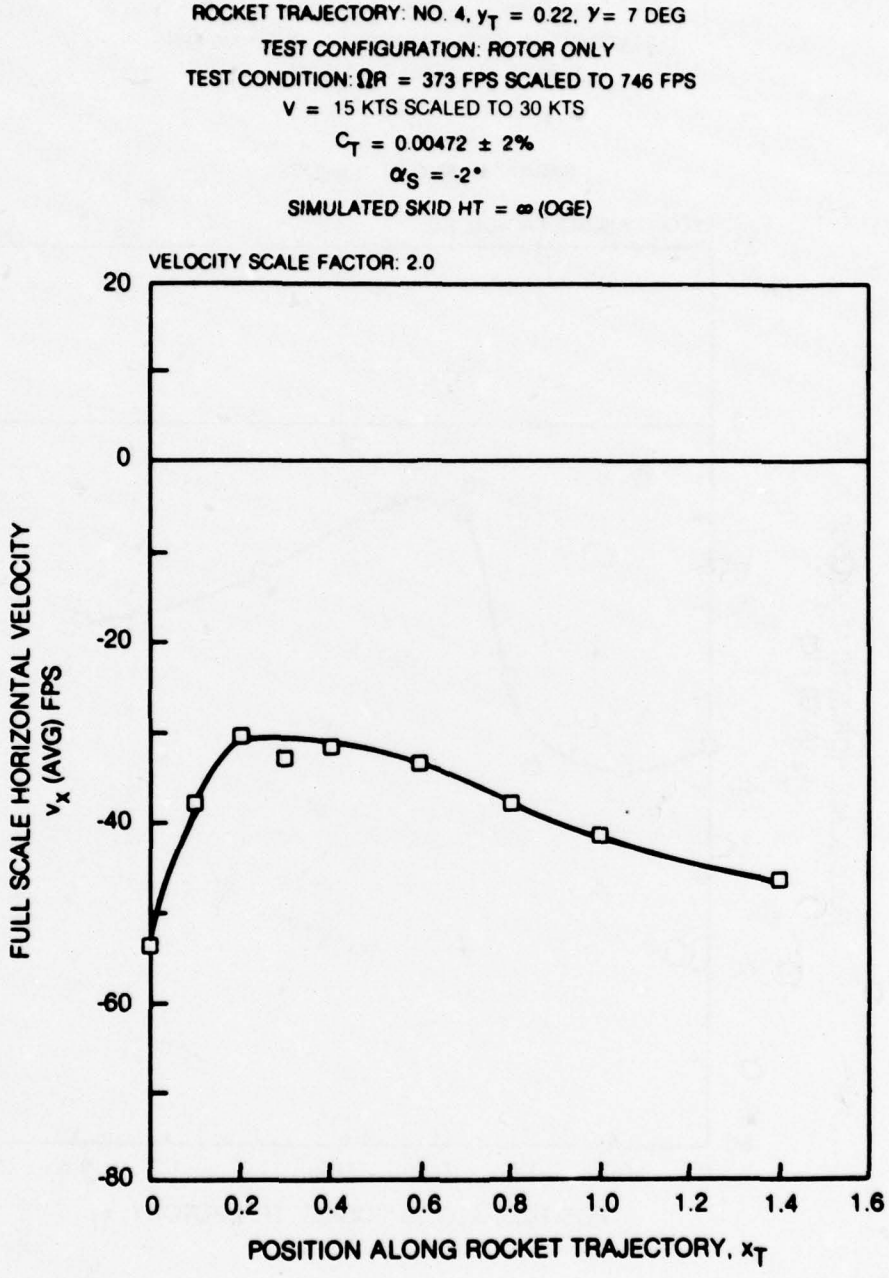

Figure D20. Variation of Time-Average Scaled Horizontal Flow Velocity Component for the Isolated Rotor Configuration at the 30 kt Reference Condition.

79-09-33-18

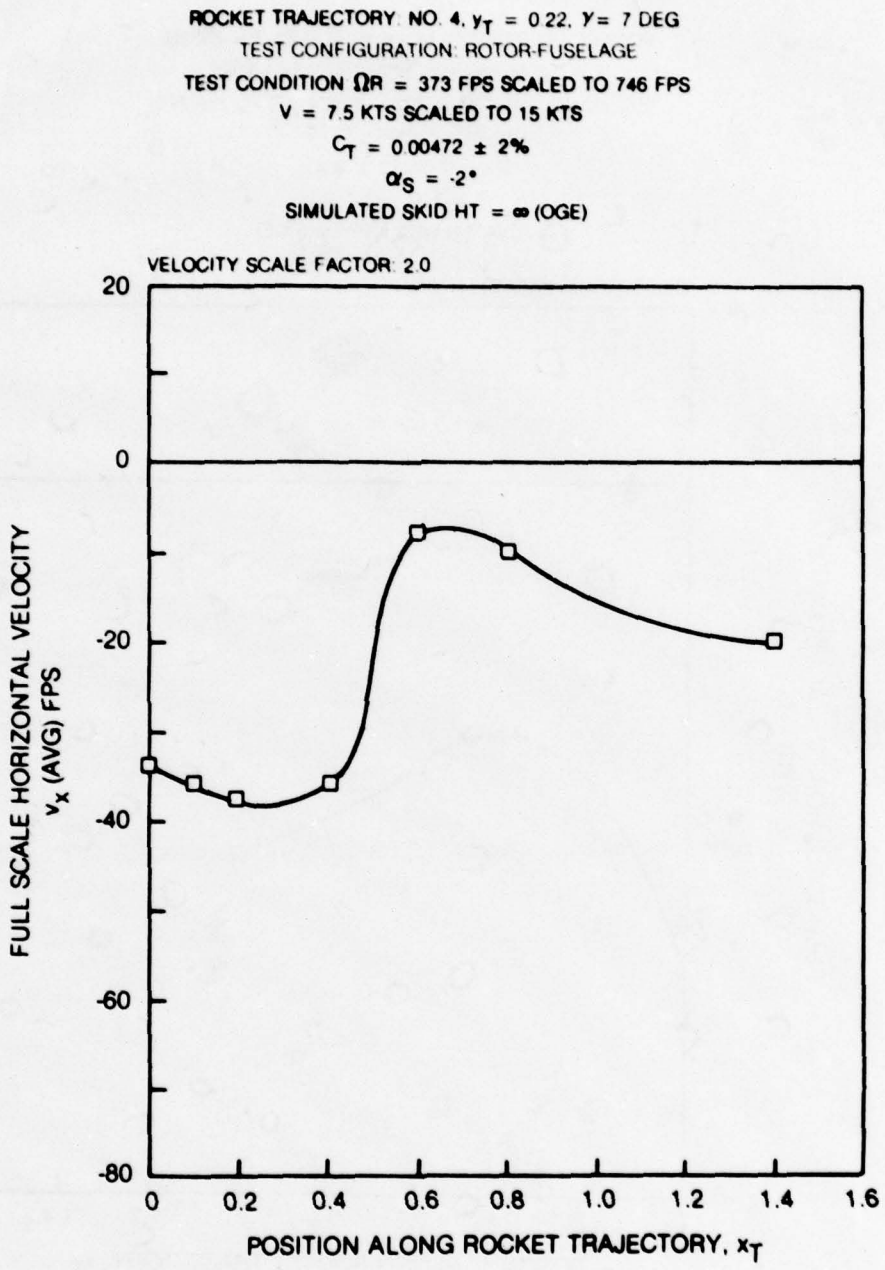

Figure D21. Variation of Time-Average Scaled Horizontal Flow Velocity Component for the Rotor-Fuselage Configuration at the 15 kt Reference Condition.

79-09-33-19

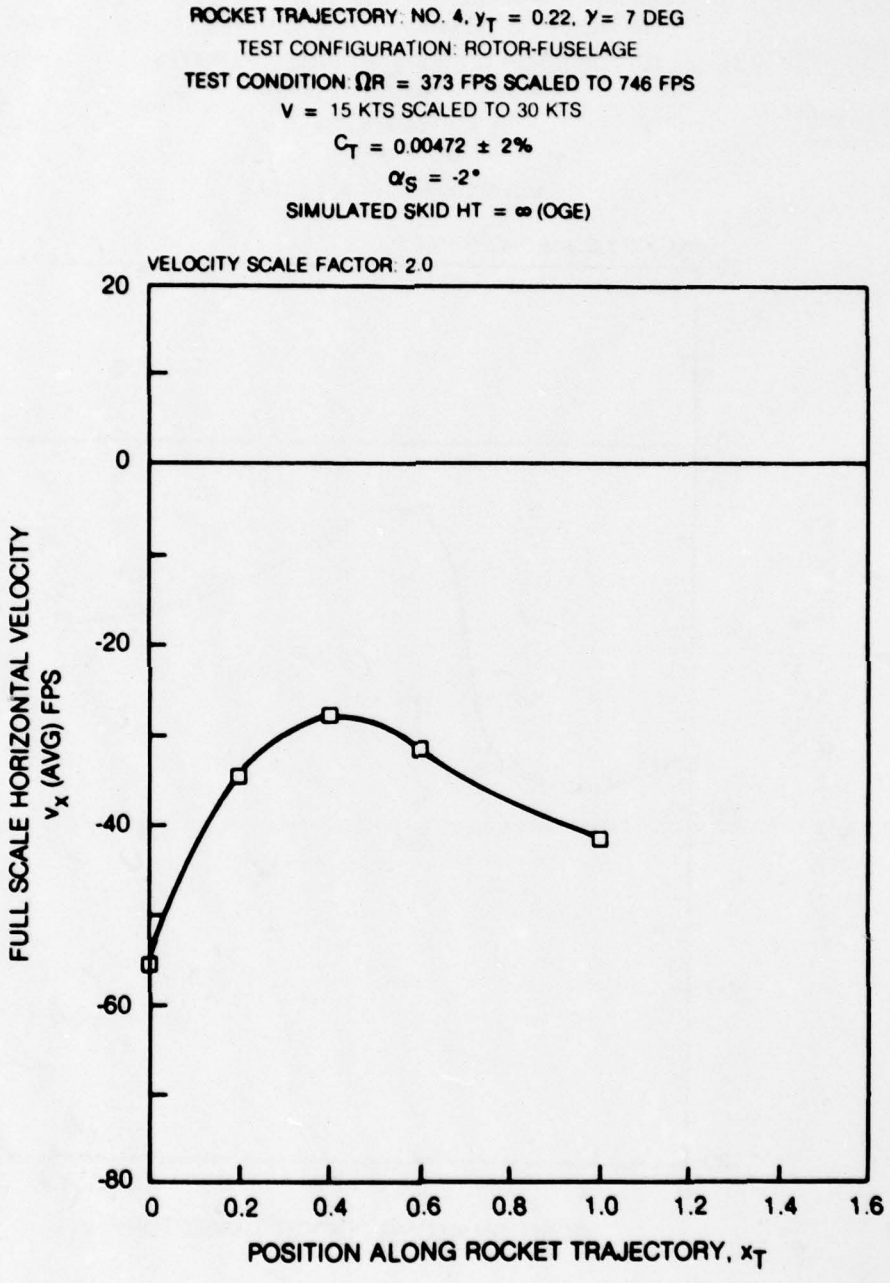

Figure D22. Variation of Time-Average Scaled Horizontal Flow Velocity Component for the Rotor-Fuselage Configuration at the 30 kt Reference Condition.

79-09-33-20

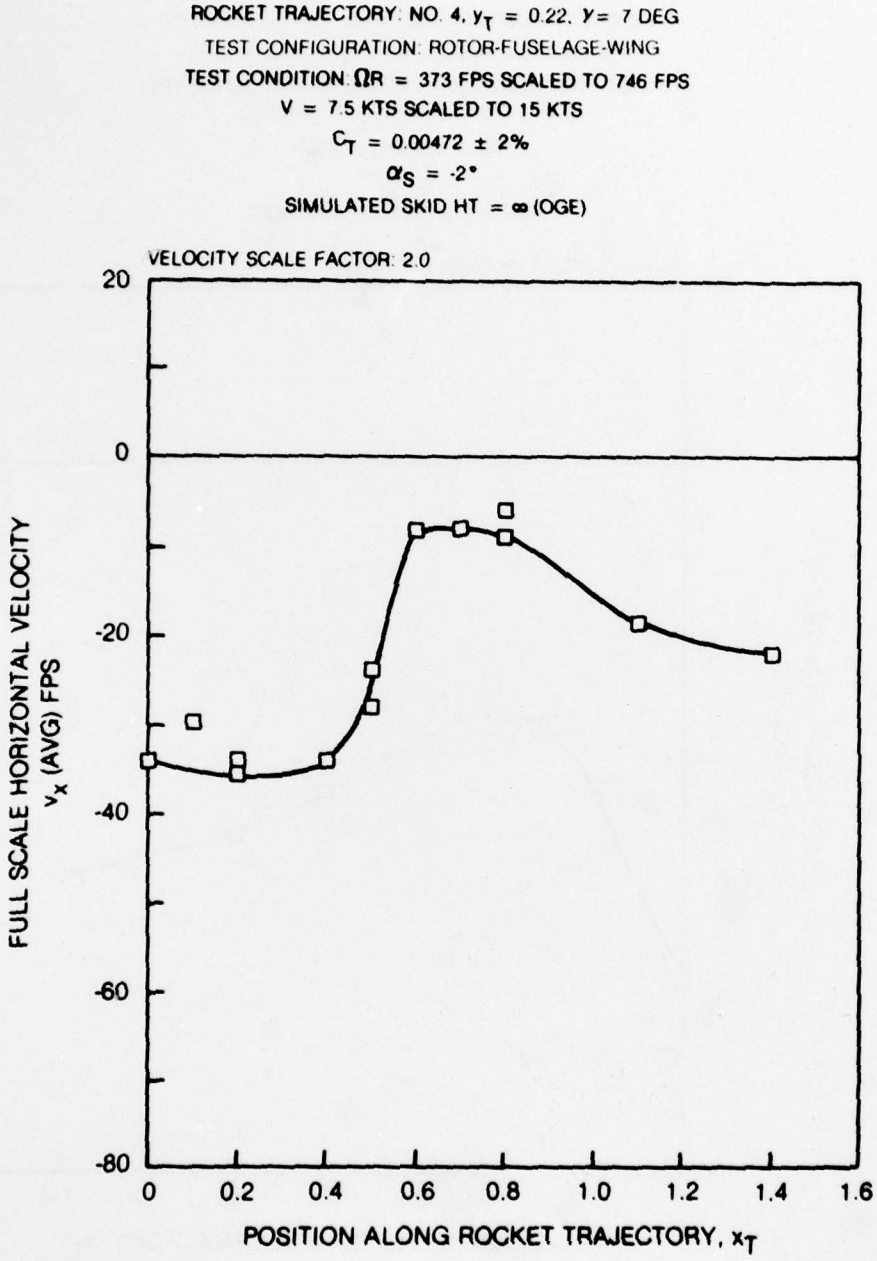

Figure D23. Variation of Time-Average Scaled Horizontal Flow Velocity Component for the Rotor-Fuselage-Wing Configuration at the 15 kt Reference Condition.

79-09-33-21

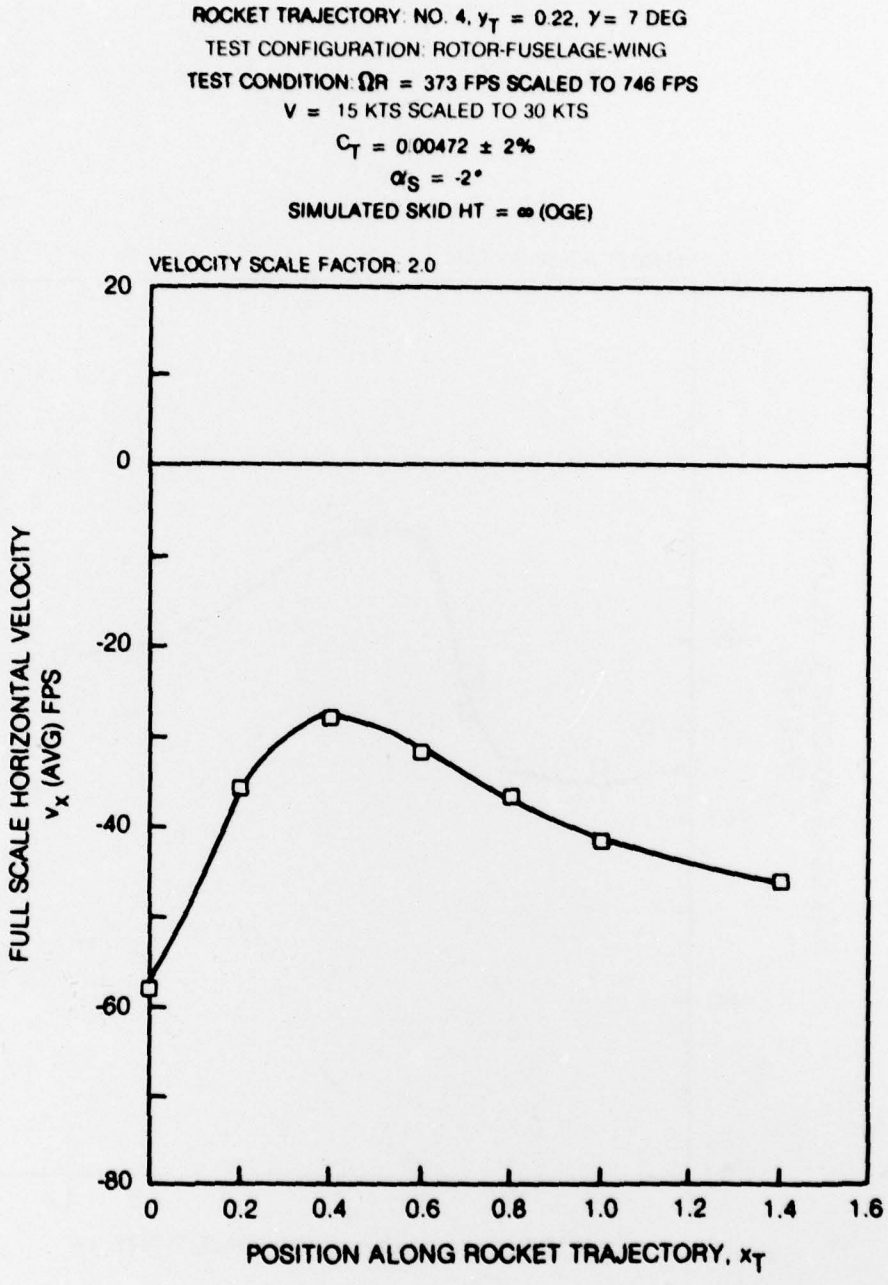

Figure D24. Variation of Time-Average Scaled Horizontal Flow Velocity Component for the Rotor-Fuselage-Wing Configuration at the 30 kt Reference Condition.

79-09-33-22

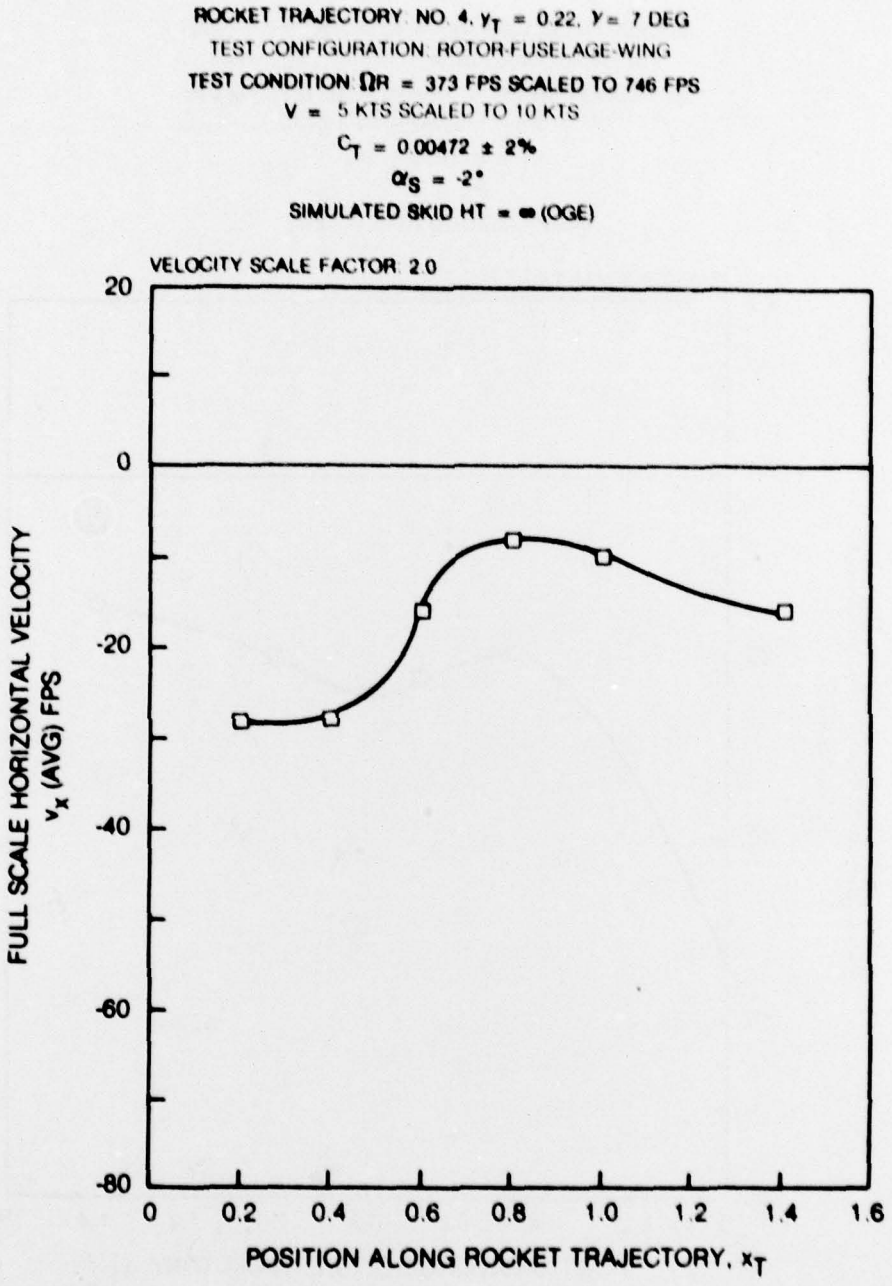

Figure D25. Variation of Time-Average Scaled Horizontal Flow Velocity Component for the Rotor-Fuselage-Wing Configuration at the 10 kt Reference Condition.

79-09-33-23

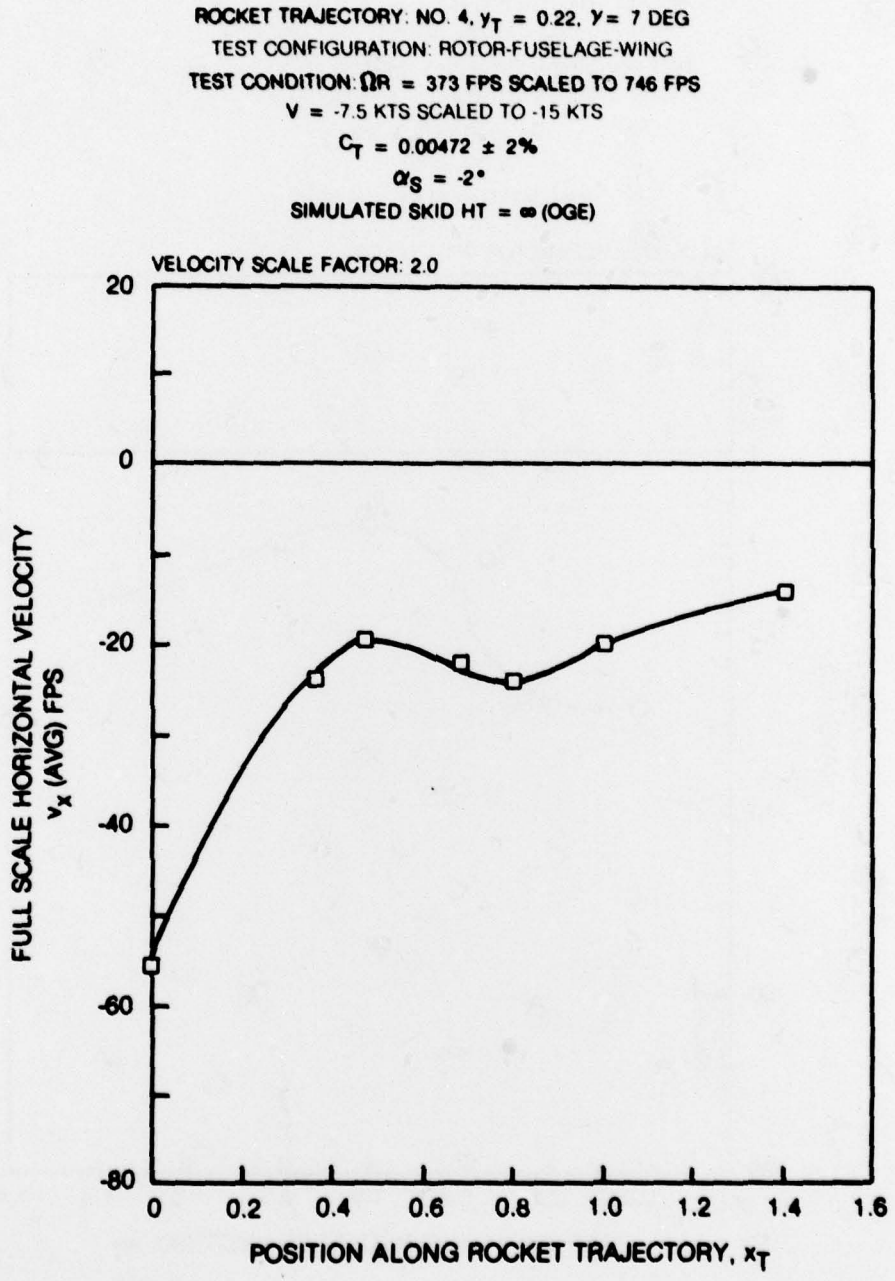

Figure D26. Variation of Time-Average Scaled Horizontal Flow Velocity Component for the Rotor-Fuselage-Wing Configuration at the the Simulated 15 kt Tailwind Condition.

79-09-33-24

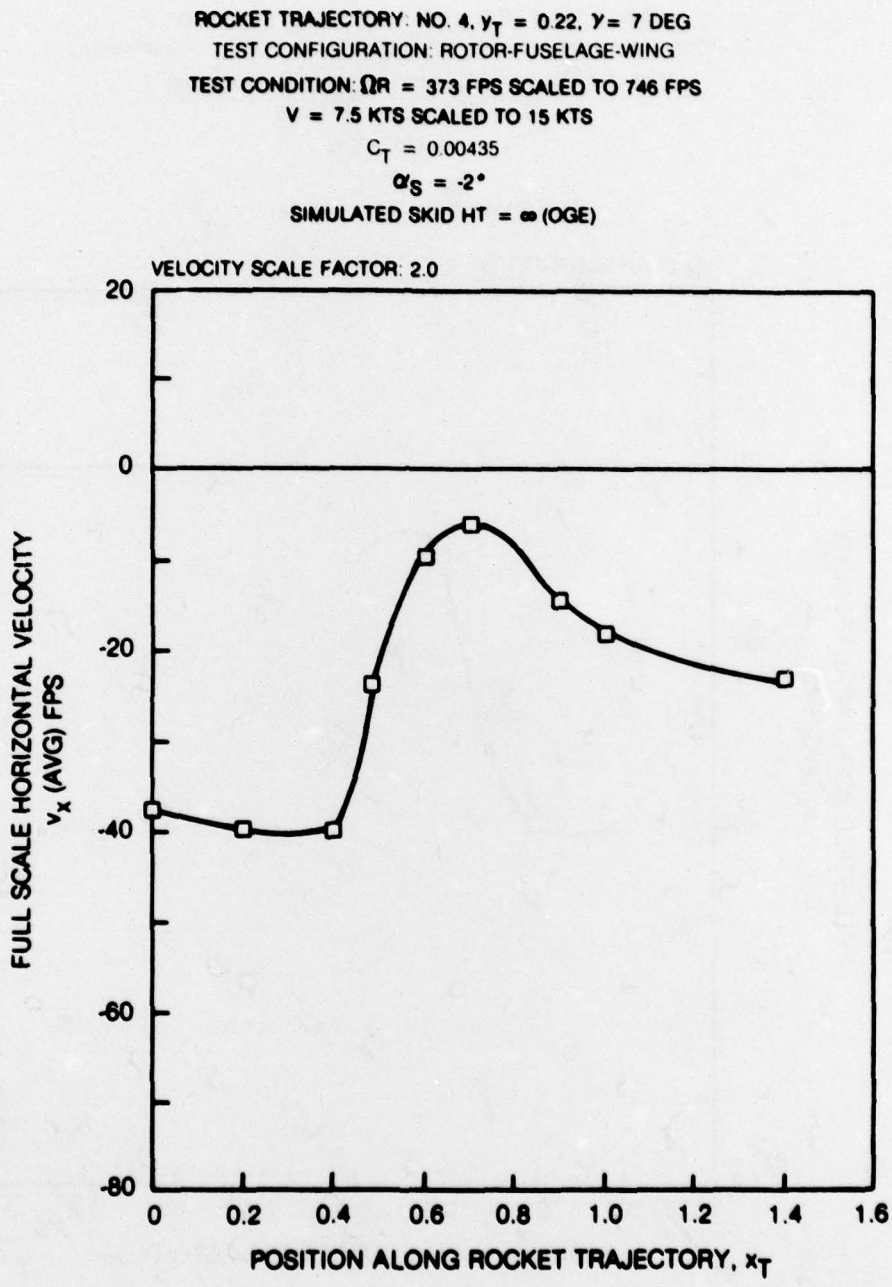

Figure D27. Variation of Time-Average Scaled Horizontal Flow Velocity Component for the Rotor-Fuselage-Wing Configuration at the the 15 kt Reference Condition with Reduced Thrust.

79-09-33-28

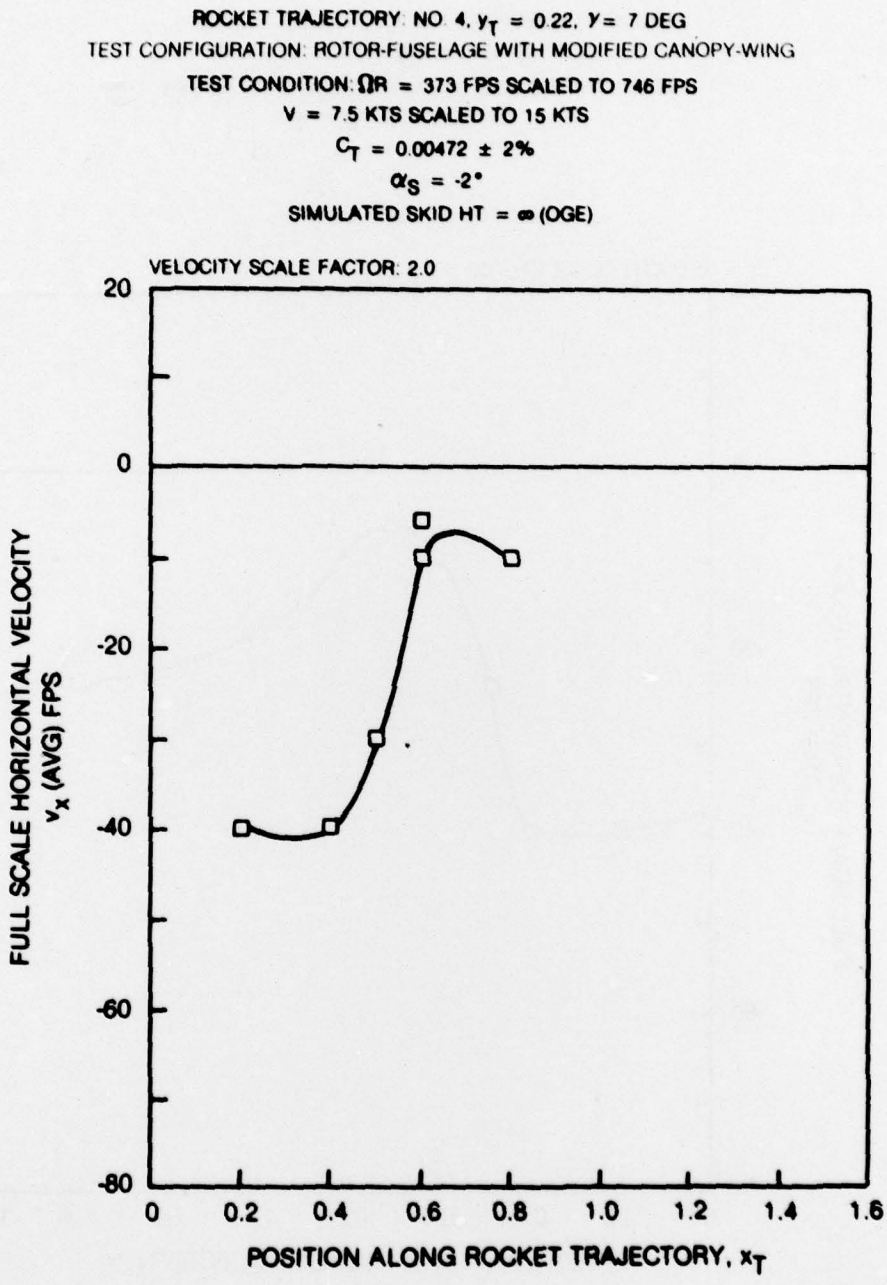

Figure D28. Variation of Time-Average Scaled Horizontal Flow Velocity Component for the Rotor-Fuselage with Modified Canopy-Wing Configuration at the 15 kt Reference Condition.

79-09-33-26

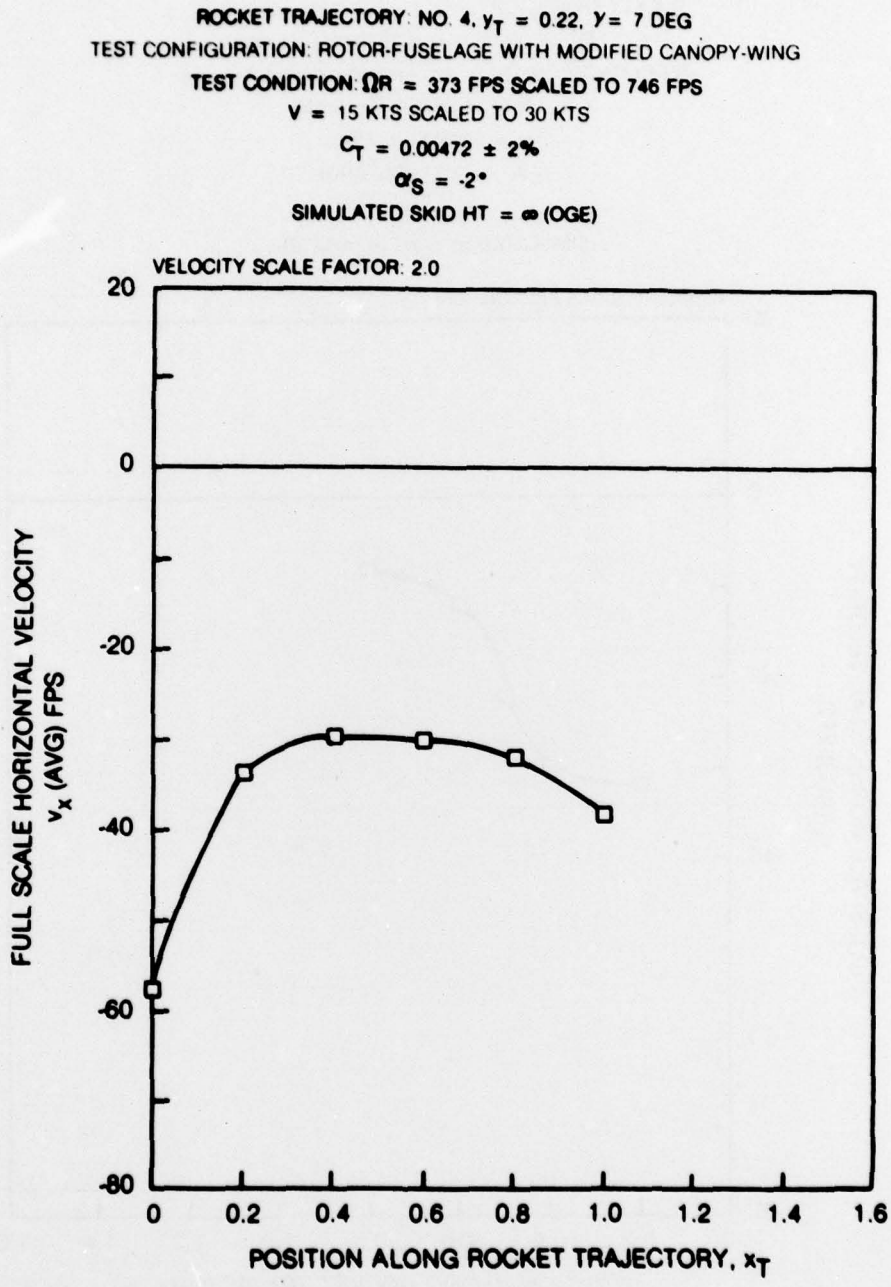

Figure D29. Variation of Time-Average Scaled Horizontal Flow Velocity Component for the Rotor-Fuselage with Modified Canopy-Wing Configuration at the 30 kt Reference Condition.

79-09-33-27

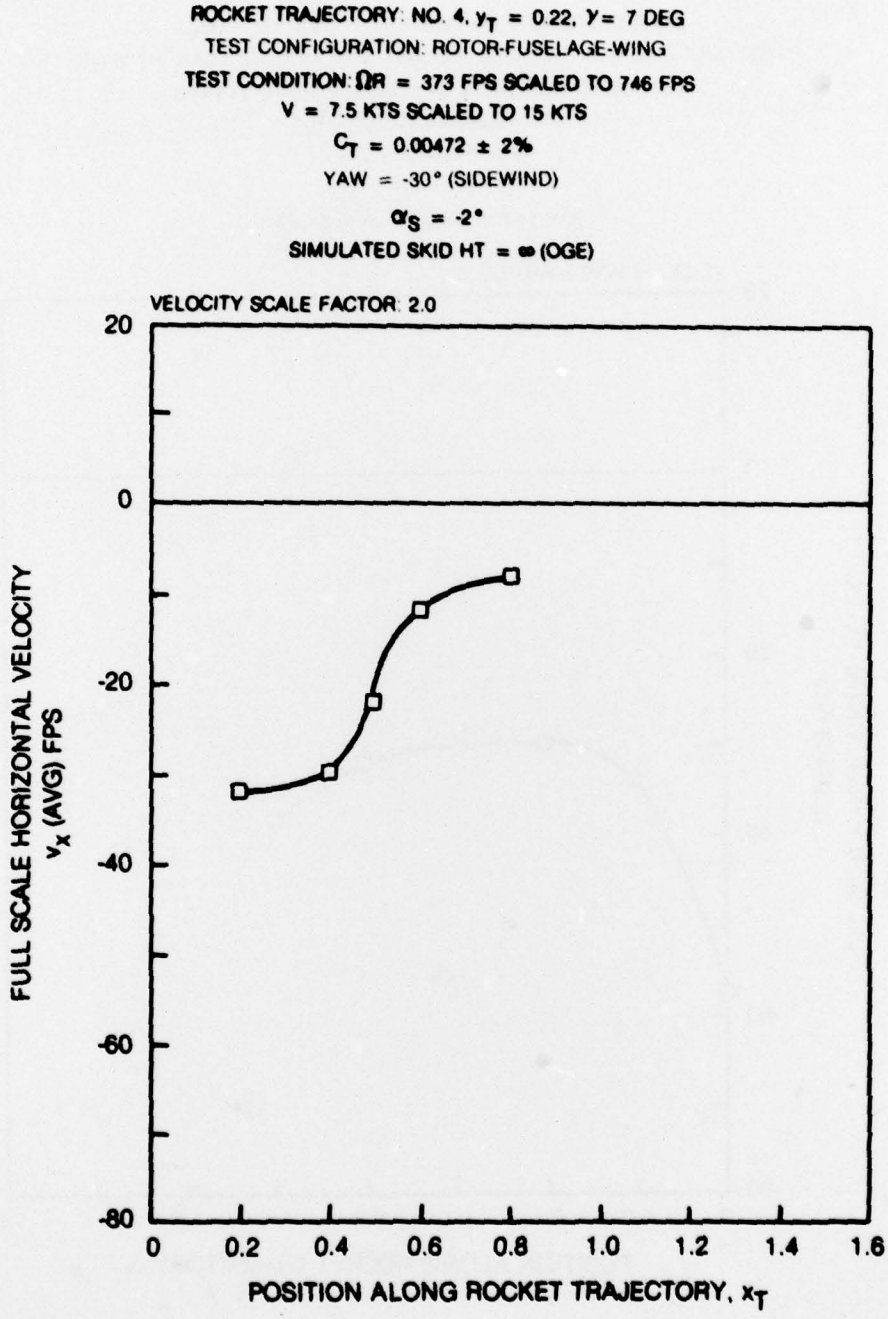

Figure D30. Variation of Time-Average Scaled Horizontal Flow Velocity Component for the Rotor-Fuselage-Wing Configuration at the the Simulated 15 kt -30 Deg Sidewind Condition.

79-09-33-28

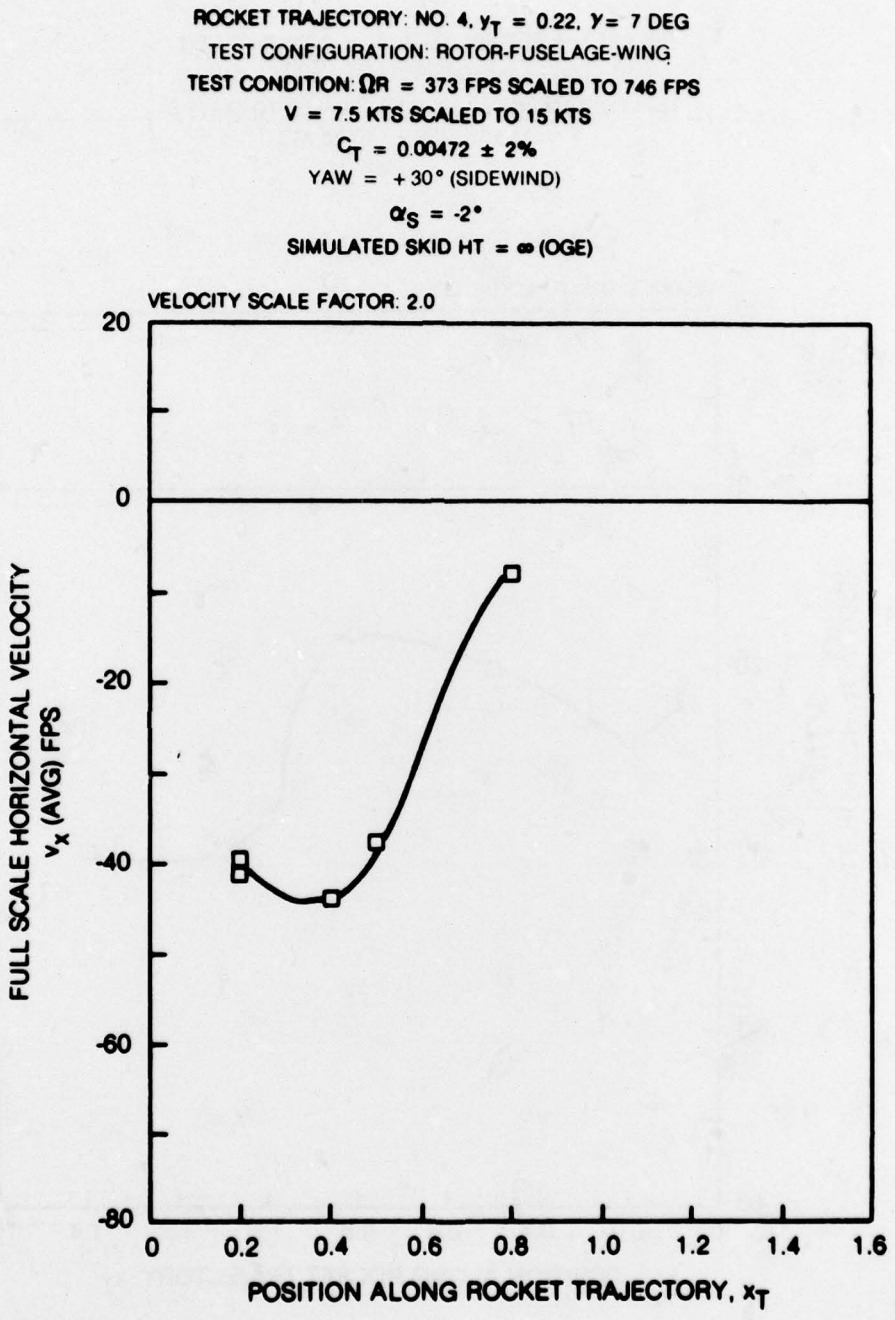

Figure D31. Variation of Time-Average Scaled Horizontal Flow Velocity Component for the Rotor-Fuselage-Wing Configuration at the the Simulated 15 kt +30 Deg Sidewind Condition.

79-09-33-29

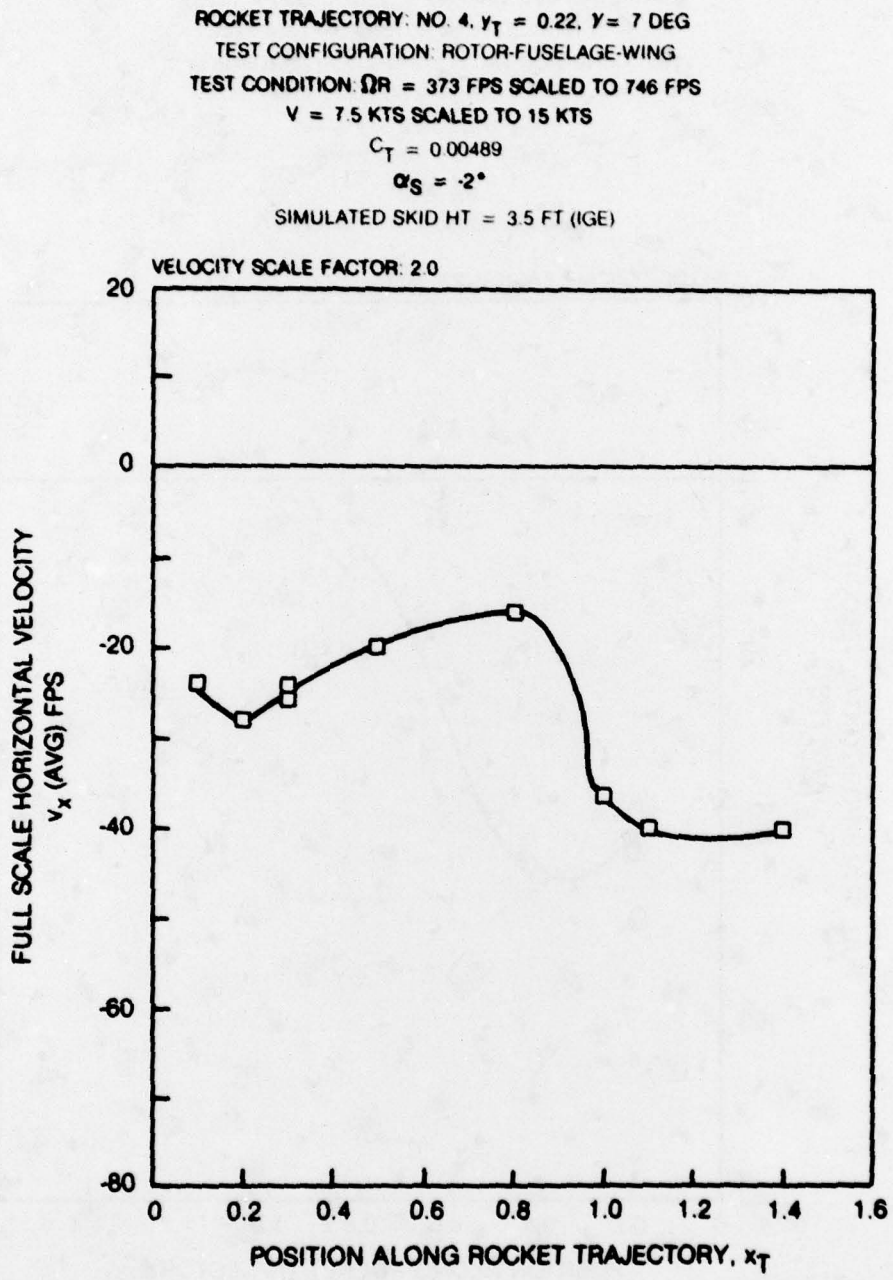

Figure D32. Variation of Time-Average Scaled Horizontal Flow Velocity Component for the Rotor-Fuselage-Wing Configuration at the the 15 kt Reference Condition In-Ground-Effect.

79-09-33-30

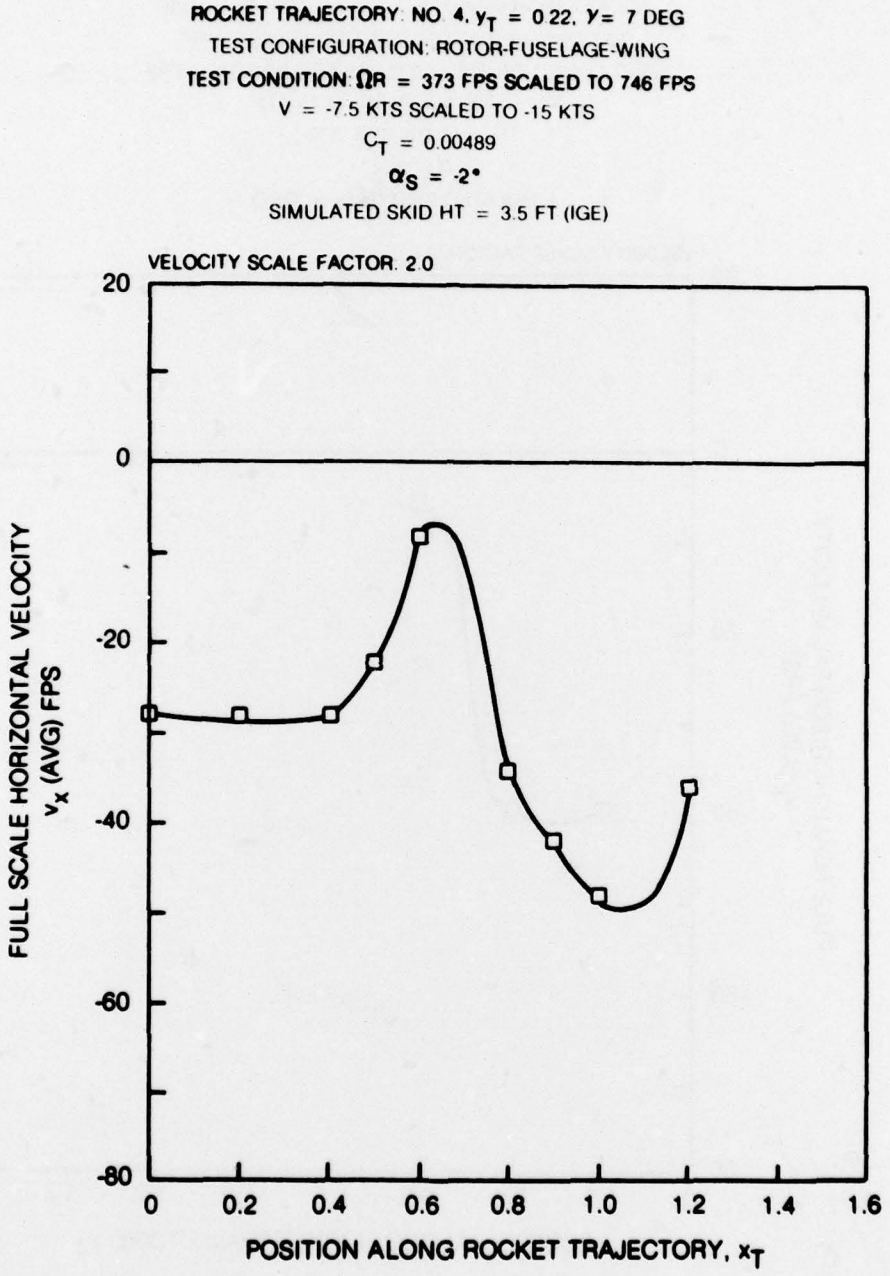

Figure D33. Variation of Time-Average Scaled Horizontal Flow Velocity Component for the Rotor-Fuselage-Wing Configuration at the the Simulated 15 kt Tailwind Condition In-Ground-Effect.

79-09-33-31

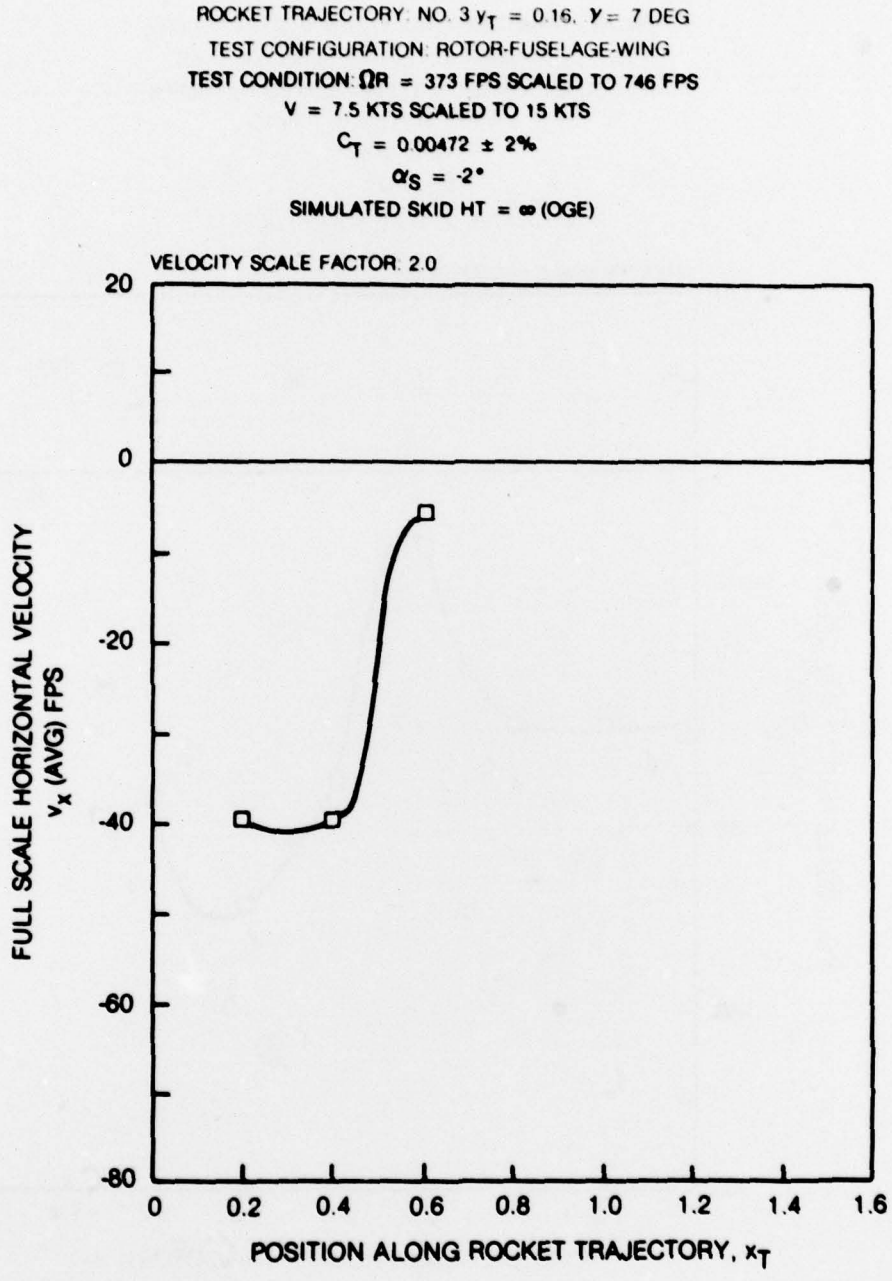

Figure D34. Variation of Time-Average Scaled Horizontal Flow Velocity Component for the Rotor-Fuselage-Wing Configuration at the the 15 kt Reference Condition for the No. 3 Launch Position.

79-09-33-32

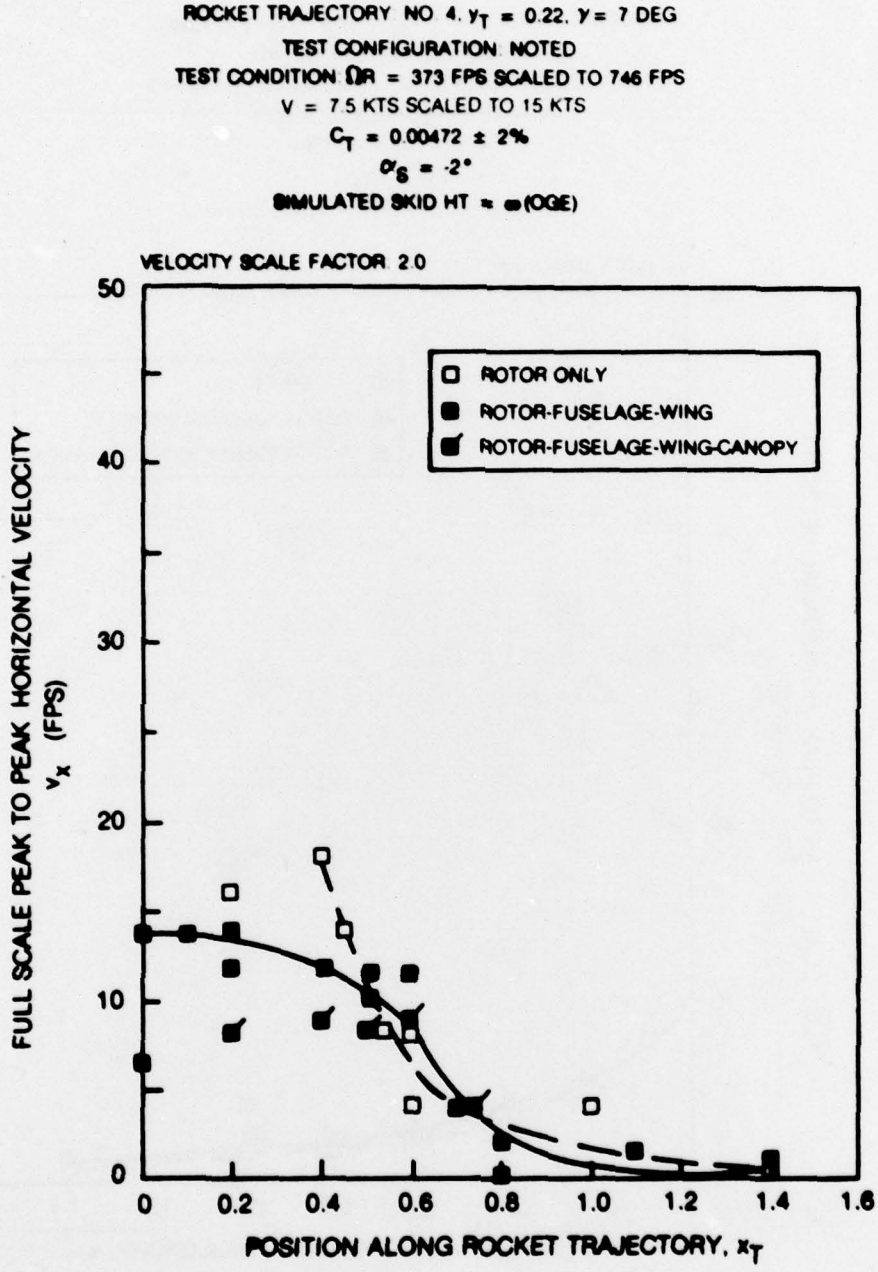

Figure D35. Variation of the Scaled Peak-to-Peak Horizontal Flow Velocity Component Along the Trajectory for the 15 kt Reference Condition.

78-09-33-34

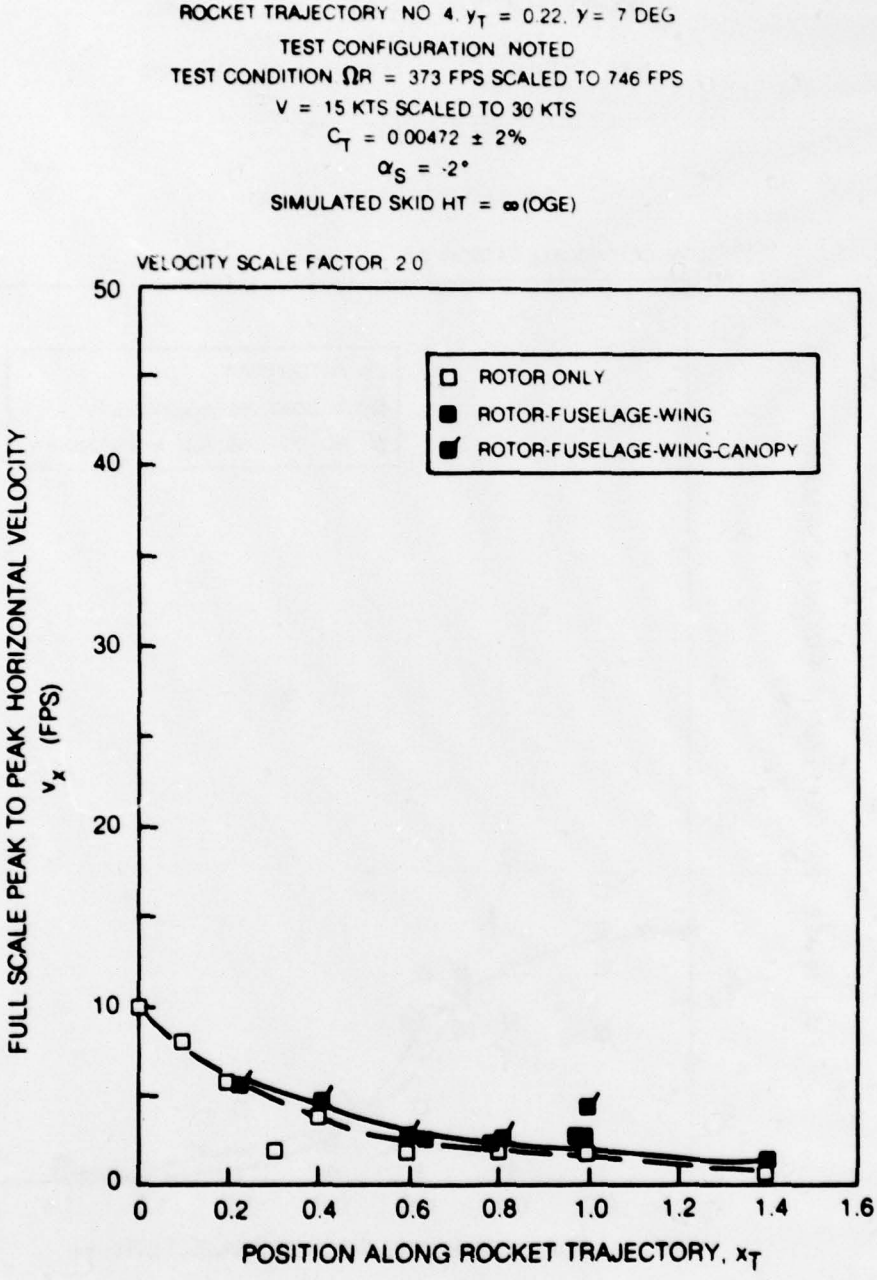

Figure D36. Variation of the Scaled Peak-to-Peak Horizontal Flow Velocity Component Along the Trajectory for the 30 kt Reference Condition.

79-09-33-33

DISTRIBUTION

As per the instructions for Contract DAA629-77-C-0013, the official distribution list for this final report will be compiled by the Army Research Office and will comprise those agencies, offices, contractors, and individuals who should receive the report in the interest of the Government. The distribution will be made by the Army Research Office.